The Serendipitous Discovery of Luminescent Liquid Crystalline and Photoconductive Triphenoxazoles

by

Gregory Calum O'Callaghan

A thesis submitted to

The University of Birmingham

For the degree of

DOCTOR OF PHILOSOPHY

School of Chemistry

University of Birmingham

College of Engineering and Physical Sciences

October 2017

Acknowledgements

First and foremost, I would like to acknowledge Professor Jon. A. Preece. As a supervisor, his guidance, humour and focus has aided me in no end to finish this thesis. As a co-supervisor, Dr Alex Robinson has been of great help, together with Jon in furthering the development of the triphenoxazoles.

To that end I would like to thank the triphenylene team: Owen Jones, Dennis Zhao and Karolis Virzbickas, Michael Butlin, Alex Wayman and Callum Duckworth for their contributions to the project. Furthermore, the Preece group in general has been a fruitful place of work and I am thankful for the experience gained from Dr Parvez Iqbal, Abduljabbar Rushdi, Toni-Bianca DiPaolo, Mariana Cardoso, Dorin Simionesie and Nina Simou.

I am indebted to the analytical team (past and present) at the University of Birmingham. Dr Neil Spencer for the help in characterising the first triphenoxazole, Dr Peter Ashton, Dr Chi Tsang, Dr Cecile Le Duff and Liane Hill, for the many mass spectrums, elemental analysis and other requests that they have always managed to fulfil.

Friends (both outside and inside the department) Dr Shani Osborne, Dr Ashleigh Danks, Johnathon Lilley, Nikhil Sahotra, Siobhan King, Francia Allabush, and Harriet Alford- thanks for putting up with me.

Finally, I would like to thank my mum and dad who are always there for me. Without them I wouldn't be here…

Table of Contents

Abbreviations

2,4,7-trinitrofluorenone	TNF
absorbance	A
acetate	Ac
aggregation induced emission enhancement	AIEE
alkoxy	C_n
alkyl emission	AlkEm
angstrom	Å
anthracenyl	ant
aryl	Ar
asymmetrical	asym
B-bromocatecholborane	BrBcat
bipyridine	bpy
bright-field	BF
carbazole	Cb
chemical amplification	CA
chemically amplified resist	CAR
columnar	Col
columnar hexagonal	Col_h
columnar hexagonal plastic	Col_{hp}
columnar oblique	Col_{ob}

columnar rectangular	Col_r
crystalline	Cr
deionised	DI
dielectric constant	ϵ_r
differential scanning calorimetry	DSC
dimethylformaldehyde	DMF
discotic liquid crystal	DLC
discotic nematic	N_D
dynamic light scattering	DLS
electron beam lithography	EB
electron beam lithography	EBL
electron impact mass spectrometry	EIMS
electrospray mass spectrometry	ES^+MS
emission area	D
epoxide	Ep
excited state intramolecular proton transfer	ESIPT
extreme ultraviolet	EUV
glass	g
helical	H
heteronuclear multiple-bond correlation	HMBC
heteronuclear single quantum coherence	HSQC
hexagonal	Hex

hexatic B	B_{hex}
hour	h
imidazole	Im
infrared	IR
isocratic	I
isopropyl	*i*-pr
isotropic	I
lifetime	τ
line edge roughness	LER
liquid crystal display	LCD
liquid crystalline	LC
lower unoccupied molecular orbital	LUMO
luminescent liquid crystal	LLC
matrix assisted laser desorption ionisation	MALDI
mesityl	Mes
meta	*m*
min	minute
molar absorption coefficient	ϵ
molarity	M
naphthyl	nap
nematic columnar	N_{col}
nuclear magnetic resonance	NMR

nuclear Overhauser effect spectroscopy	NOESY
number	No.
organic light emitting diodes	OLED
ortho	*o*
oxazole	Ox
para	*p*
parts per million	ppm
peak maxima	λ_{max}
pentoxy	C_5
phenyl	Ph
phenyl emission	PhEm
photoacid generator	PAG
photomultiplier tube	PMT
planar conjugated emission mechanism	PCEM
polarised optical microscopy	POM
poly(methylmethacrylate	PMMA
polyaromatic hydrocarbon	PAH
potassium *tert*-butoxide	KO*t*-Bu
pseudo stokes shift	pSS
quantum yield	Φ
refractive index	n
revolutions per minute	RPM

smectic	Sm
symmetrical	sym
tetrahydrofuran	THF
thin layer chromatography	TLC
time dependent density functional theory	TD-DFT
transition electron microscopy	TEM
trinitrofluorenone	TNF
triphenylene	Tp
triphenylsulfonium	TPS
tris(trifluoromethyl)phenyl	Fmes
twisted internal charge transfer	TICT
twisted non-conjugated emission mechanism	TnCEM
ultraviolet	UV
unknown	X
visible	vis
wavelength	λ
weight percent	w%
x-ray diffraction	XRD

1 Triphenylene and their Derivatives: Liquid Crystalline and Photophysical Properties

1.1 Thesis Outline

The hexaalkoxytriphenylene discotic liquid crystals (DLC) have been the subject of intense research since their discovery by Zann *et al.* in 1978,[1] during which time many exotic derivatives have been synthesised.[2] These derivatives are mainly synthesised through modifying chain length,[3] chain type,[4] addition of functionality to the triphenylene core,[5] as well as the alkyl tails,[6] and fusing moieties that increase the π area of the triphenylene core,[7] leading to a plethora of new material[7] and enhanced photophysical properties.[4]

As well as DLC properties, triphenylene has been shown to possess interesting luminescent properties, such as a large pseudo Stokes shift and an excellent molar absorptivity coefficient.[8]

The research described in this thesis aims to focus on the serendipitous discovery of the incorporation of an oxazole moiety to the triphenylene core of alkoxytriphenylenes, and the study of the properties of this new class of material – triphenoxazoles – which show them to be highly luminescent, photoconducting and liquid crystalline.

The first chapter focuses on introducing liquid crystals, in particular discotic liquid crystals (DLCs) and the alkoxytriphenylenes. The chapter describes (i) current methodologies of alkoxytriphenylene synthesis, (ii) the liquid crystal properties and structures of these materials,

(iii) the mechanism by which molecules like triphenylene fluoresce, and (iv) finally, examples are illustrated of materials possessing liquid crystal properties which are luminescent.

Chapter 2 presents discussions on the thermal analysis of liquid crystals employed throughout this research which include differential scanning calorimetry (DSC), polarised optical microscopy (POM) and X-Ray diffraction (XRD).

Chapter 3 describes the serendipitous discovery of the novel intramolecular annulation of hexaalkoxytriphenylene to create the new triphenoxazole core. This chapter goes into detail about the development of the synthesis of this novel species, allowing a synthetic strategy for a broad array of derivatives, leading to changes in liquid crystal and luminescence properties.

Chapter 4 describes a novel intermolecular annulation to create conjugated and functionalised triphenoxazoles. This chapter focuses upon the effect of *ortho*, *meta* and *para* fluorophenyl triphenoxazole derivatives. Showing that a change in position of the fluorine leads to significant alterations in the fluorescent and liquid crystal properties.

Chapter 5 displays the effect of increasing the aromatic area of the oxazole R group from phenyl to anthracyl on the fluorescent and liquid crystal properties, such that the emission is at longer wavelengths and the Col_h mesophase are in temperature windows >100 °C.

Chapter 6 aims to conclude the current results presented in this thesis and outline further work that could be done to extend the areas of study.

The appendix shows characterisation of all novel structures synthesised within this thesis.

1.2 Polycyclic Aromatic Hydrocarbons

Benzene is an iconic chemical structure and has been held in fascination by researchers since its discovery in 1825 by Michael Faraday.[9] Forty years later Augustus Kekulé showed the equivalency of each carbon atom and signalled the birth of aromaticity.[10] Fused benzene rings have been a large subject of study across many scientific fields.[11] Polycyclic aromatic hydrocarbons (PAHs) abundance in the universe [12] and fossil fuels, [13] as well as uses in light harvesting, [14] semiconductors,[15] and biolabels[16] are a few of the areas in which they are studied.

This chapter will focus on one particular PAH; triphenylene (Figure 1). Triphenylene has more resonance structures than its PAH isomers (tetracene, chrysene and benzanthracene and benzophenanthrene) and is much more resistant to hydrogenation.

Triphenylene is a fully benzenoid 18 electron delocalised system, and Figure 1.1 shows the nine resonance structures which contribute to its stability. Unlike benzene, where all carbons are equivalent, triphenylene has electron rich and electron deficient areas. Gaussian modelling of triphenylene[17] has shown the peripheral carbons of triphenylene to be electron rich and the central carbons of triphenylene to be electron deficient. This contrast can be seen by Clar's rules[18] whereby of the nine resonance structures seven have the full aromatic sextet of electrons in the three outer rings only two (presented in red) have the aromatic sextet in the centre ring.[19]

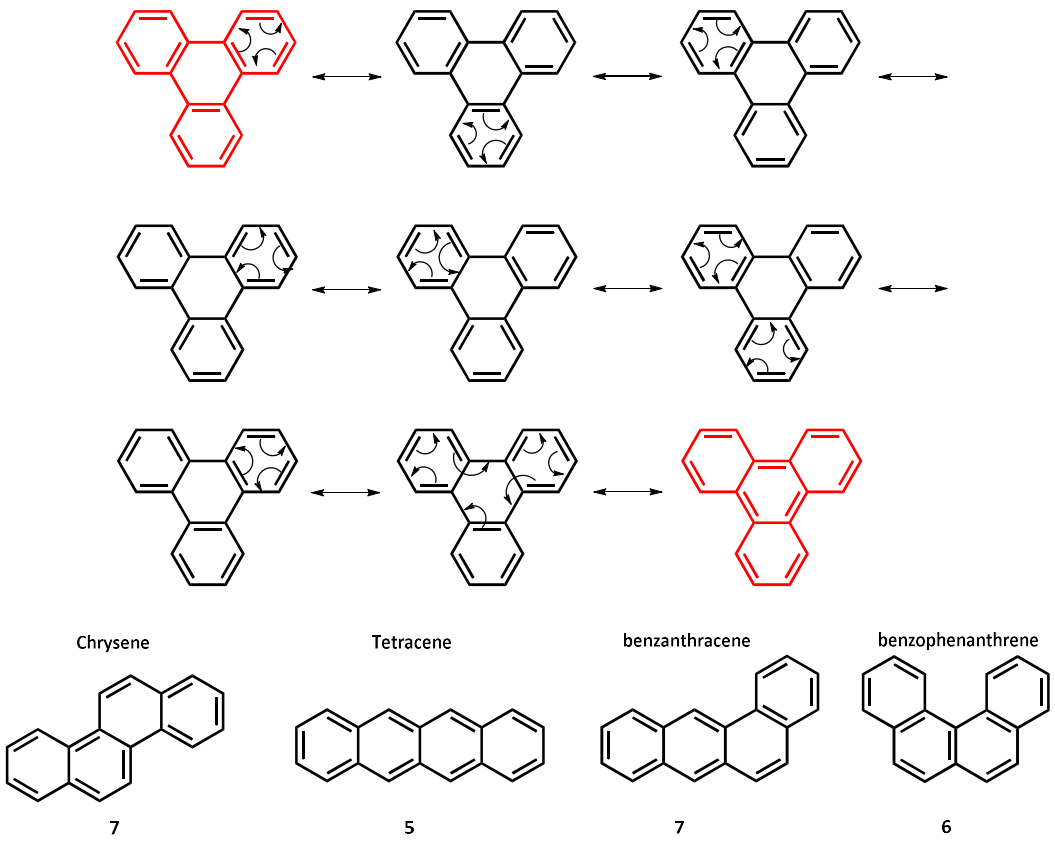

Figure 1.1: Triphenylene's resonance structures compared to its isomers shown below with their number of resonance structures

Triphenylene was first discovered in 1906 by Mannich,[20] but it was not until more than twenty years later interest grew with the first examples of functionalised derivatives.[21] These triphenylene derivatives had alkoxy chains appended to the periphery affording discotic liquid crystalline (DLC)[1] behaviour and materials with interesting photophysical properties.[22] The liquid crystalline behaviour and luminescence properties of functionalised triphenylenes will be key features of this introductory chapter.

1.3 Liquid Crystals

Liquid crystals (LCs), discovered in 1888,[23] are the fourth state of matter and are very broadly classified as anisotropic liquids, i.e. they are fluids (generally viscous) that have structural anisotropic order of the molecular entities which make up the fluid. Thus, these anisotropic liquids exhibit birefringence,[24] where as an isotropic liquid, e.g. water does not. This duality of fluidity and order has led to liquid crystals being used in various technologies, like self-healing structures, where defects can be formed and then removed by annealing (found use in solar technology; whereby donor-acceptor pair can be spontaneously reformed),[25-26] and magnetic alignment[27] as well as use in liquid crystal displays (LCDs).[28-29]

1.3.1 Characterisation of Liquid Crystals

There are three primary analytical techniques that are used to characterise liquid crystals: differential scanning calorimetry (DSC), polarised optical microscopy (POM) and X-Ray Diffraction (XRD). These are described in detail in Chapter 2. Below a brief description is given of these techniques:

1.3.1.1 Differential Scanning Calorimetry (DSC)

Differential Scanning Calorimetry is a thermoanalytical technique which measures as a function of temperature the difference in the amount of heat required to change the temperature of the sample compared to that of a reference. [30] DSC records endothermic or exothermic events.[30] Thus, the solid to liquid transition is endothermic, as is heating from one liquid crystalline phase to another. Conversely, cooling from one phase to another is exothermic. This technique provides

the user with information on the enthalpy associated with the phase change, as well as the onset temperature of the phase change;

1.3.1.2 Polarising Optical Microscopy (POM)

Polarising optical microscopy is a technique which observes a sample through crossed polarisers. If the material is anistropically ordered, which liquid crystals are, then the material will possess two refractive indices, and the birefringence will manifest itself as a tapestry of colours known as textures.[31] These textures can be used qualitatively to determine the type of liquid crystal phase.

1.3.1.3 X-Ray Diffraction (XRD)

X-Ray Diffraction is a powerful tool in quantitative phase identification. Unlike POM and DSC, XRD allows the user to elucidate the exact phase of a structure.[32] Different LC phases have given rise to XRD patterns as a result of various packing arrangements of the molecules making up the gross structure of the phase. This in turn leads to phase identification. As with POM a heating stage can be attached, allowing for signature XRD peaks to appear when the LC phase is apparent.[33] Table 1.1 summarises the information that can be gathered using POM, DSC and XRD, as can be seen the techniques are complementary and as such play a critical role in LC analysis.

Table 1.1: Summary of information gathered from POM, DSC and XRD

Technique	Phase Type	Temperature Range	Phase Energy	Cost	Comment
POM	Yes [a]	Yes	No	~£50k [34]	Qualitative [a]
DSC	No	Yes	Yes	~£25k [35]	Quantitative
XRD	Yes	No	No	~£500k [36]	Quantitative

1.3.2 Classification of Liquid Crystal Phases

The two broad categories of liquid crystals are thermotropic and lyotropic liquid crystals.[37] Thermotropic liquid crystal phases are temperature dependent, whilst lyotropic are concentration dependent.

Within the two broad categories there are further subcategories. For the purposes of this review only thermotropic LCs will be discussed.

1.3.2.1 Thermotropic Liquid Crystalline Materials

Various molecular structures can display liquid crystalline properties in the bulk phase. The two most common are rod-like (calamitic)[38] and disc-like (discotic),[39] but more recently banana,[40] bowl-shaped[41] and polycatenar[42] molecular structures have been shown to support liquid

crystalline phases. Below only calamitic and discotic molecular structures and their bulk mesophases will be considered.

1.3.2.2 Calamitic Liquid Crystals

Calamitic LCs are compounds which possess an elongated shape (hence rod-like), where the length is significantly longer than the width of the molecule Figure 1.2a.

Calamitic liquid crystals often have at least one flexible alkyl chain terminal unit attached to the core, such as MHPOBC which has two alkyl chain units (Figure 1.2b).

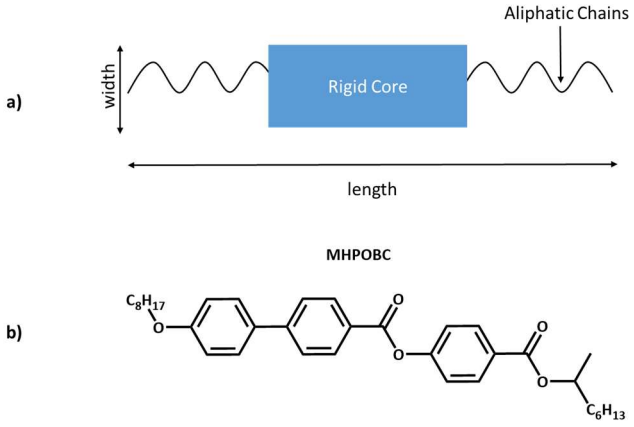

Figure 1.2: a) Cartoon representation of calamitic LCs, and b) molecular example MHPOBC[43]

Calamitic molecular structures generally support two types of liquid crystalline phase (mesophase): nematic (N) and smectic (S).

1.3.2.3 The Director

The director is a vector of no dimensions, defined as preferred orientation of the mesogens in a given domain (Figure 1.3).[44]

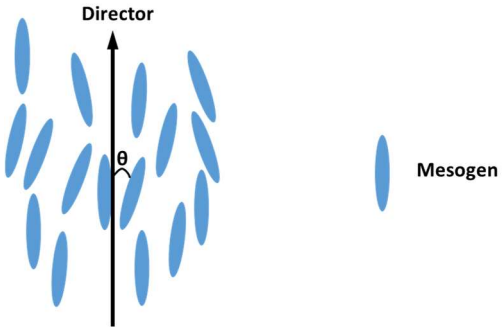

Figure 1.3: Liquid Crystalline alignment: where θ is the angle of displacement a given mesogen and the director

The average angle of displacement (θ) details the strength of the ordering. The smaller the average angle of displacement from the director, the more ordered the liquid crystal.[45]

This ordering is defined by the order parameter (S) (Equation 1.1). Where S=0 shows an isotropic phase, and S= 1 shows perfect alignment. Typical values for S range from 0.3-0.8.[46]

$$S = \langle \frac{3cos^2\theta - 1}{2} \rangle$$

Equation 1.1: The order parameter

1.3.2.3.1 Nematic Phase

Nematic liquid crystals are the least ordered phase where the molecules have no positional order, but self-align to have long range directional order with the long axes on average parallel with each other (Figure 1.4a).[47]

A further important subcategory of nematic liquid crystals is the cholesteric phase (Figure 1.4b).[48] Cholesteric liquid crystals are often formed by doping nematic liquid crystals such as **C_5BiPhCN** (Figure 1.4c)[49] with chiral dopants such as Merck S1011 (Figure 1.4d).[49] Cholesteric LC phases have a helical structure, induced by the molecular chirality, and are therefore chiral. The helical nature means that the cholesteric mesophase reflect one component of the polarised light, where the wavelength of reflection is determined by the distance over which a full rotation is completed - the pitch (depicted as the return of αβ in Figure 1.4b), resulting in the colour of light which is reflected varying as a function of the temperature of the phase. This colour invariably has led to many technological uses, such as medical thermometers,[50] low power devices- where colour can remain after switching the device off,[51] solar panels- where the LC component enlarges the interface area, which helps maximise charge separation[52-53] and extended into fashion as mood rings.[54]

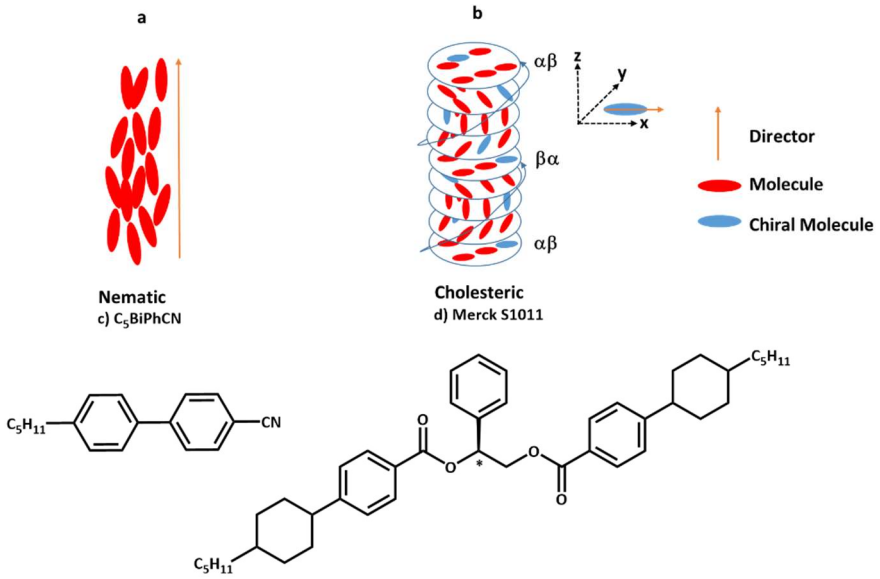

Figure 1.4: Exaggerated cartoon diagram of a) nematic liquid crystal, b) cholesteric liquid crystals where the director lies in the xy plane perpendicular to the direction of the helix (z). αβ refer to the pitch length. Where αβ is a full pitch, βα is half pitch. c) nematic liquid crystal C_5BiPhCN becomes cholesteric when doped with d) Merck S1011 at 16 %w/w[49]

1.3.2.3.2 Smectic phases

Smectic liquid crystals are more ordered than the nematic phase[55] and form layers which possess translational order enabling these sheets to flow past each other.[56] Though there are twelve different types of smectic LCs, by far the most common are Smectic A and C.[57] Smectic A (Figure 1.5a) and B have a loose positional order with the mesophases orientation with the director-perpendicular to the smectic plane. Smectic C has more order than A[58] and displays a general tilt of the mesogen in the same direction of the smectic plane (Figure 1.5c).[59]

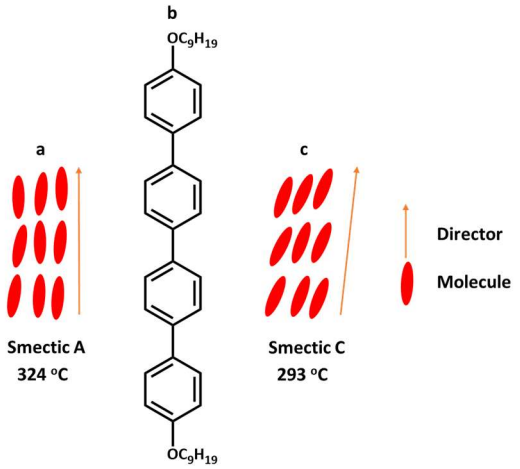

Figure 1.5: Exaggerated cartoon diagrams of smectic phases A and C (a and c) of quarterphenyl derivative (b). Where at 293 °C Smectic C phase is seen, when heated to 324 °C Smectic A is observed [59]

1.3.3 Discotic Liquid Crystals

Discotic liquid crystals (DLCs) were first reported by Chandrasekhar *et al.* in 1977,[60] and are flat molecules in which molecular chains (tails) radiate from the molecular core forming a disc-shaped structure. (Figure 1.6).

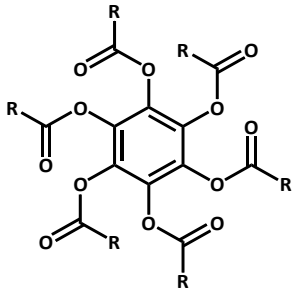

Figure 1.6: The first series of DLCs discovered by Chandrasekhar et al. Where R=C_4H_9 to C_9H_{19}.[60]

1.3.3.1 Nematic Discotic and Columnar Nematic

Nematic discotic (N_D) is the least ordered mesophase with full translational order of the constituent molecules. In the N_D there is no positional order, only orientational order, aligned on average with the director (Figure 1.7). [61-62]

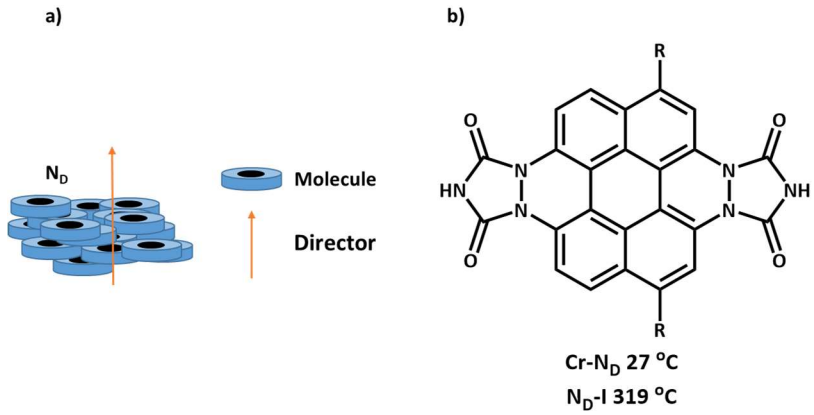

Figure 1.7: a) Cartoon diagram of N_D and b) molecular example from Spiess et al.[61] R=C_5H_{11}

Chiral forms of this phase exist and can be achieved by addition of a chiral dopant[63] or use of a chiral mesogen.[64] The core's position is rotated across the phase with the director field twisted continuously in a parallel direction to the stacks. Katz *et al.* have shown that the return to starting position (the pitch) can be modified by electric field, a feature which has potential use in optical devices.[65]

The Nematic columnar (N_{Col}) phase consists of short stacks lacking translational order. N_{Col} are often formed using dopants[66] or co-polymers (Figure 1.8).[67] The thermodynamic ordering of these systems is highlighted in Figure 1.8b, where N_{col} is more ordered than N_D.

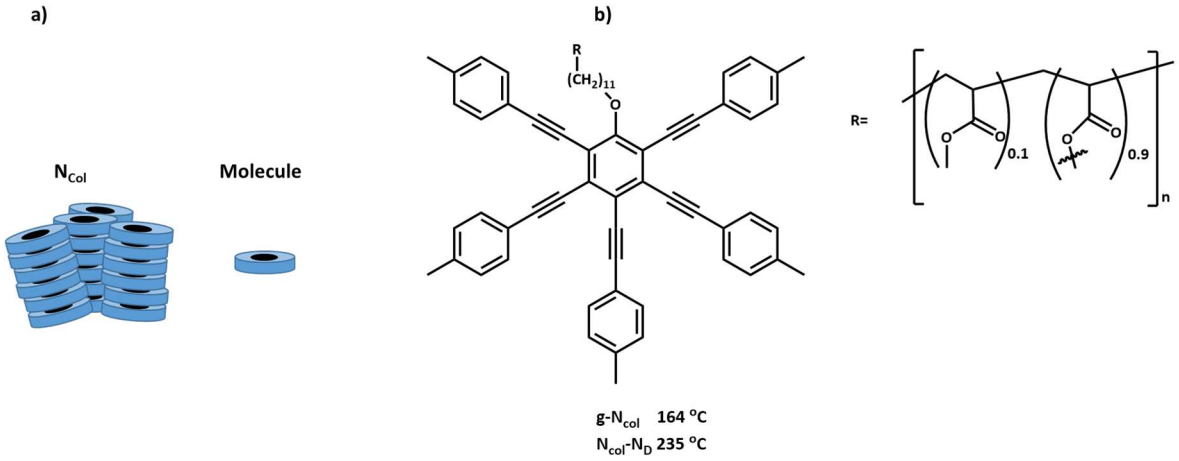

Figure 1.8: a) Cartoon diagram of N_{Col} and b) molecular example from Mijs et al. where they connected 90 % of a polyacrylate backbone of molecular weight 9000, to the pentakis(phenylethynyl)phenoxy moiety shown, g= glass [67]

N_{col} mesogens have shown promise in liquid crystalline displays (LCDs). When using N_{col} the viewing angle increases. However, the switching times are slower than nematic LCs and, therefore, to make these commercially viable faster switching times are needed.[67]

1.3.3.2 2D Discotic Liquid Crystals

Two dimensional (2D) [68] DLCs can be treated as ordering of the N_{col} phase, where the stacks are arranged into different lattice patterns.[69] The most common arrangements are:

1) Columnar hexagonal (Col_h) phase where the mesogens are non-tilted and the stacks are arranged hexagonally (Figure 1.9a);
2) Columnar rectangular (Col_r) phase where stronger core interactions cause the cores to tilt and the stacks are rhombohedrally arranged (Figure 1.9b). Due to stronger intermolecular interactions Col_r is more ordered than Col_h and so a transition from Col_r to Col_h is often observed with increasing temperature (Figure 1.9a and b) or increasing the chain length of the alkyl spacers; [32]

4) Col_{ob} is a rarer phase[70] with a higher degree of order than Col_r. The phase has four tilted stacks arranged as a square, interlaced with three stacks tilted the opposing direction of the square (Figure 1.9c). [71] Furthermore chiral versions of the 2D DLCs also exist.[72]

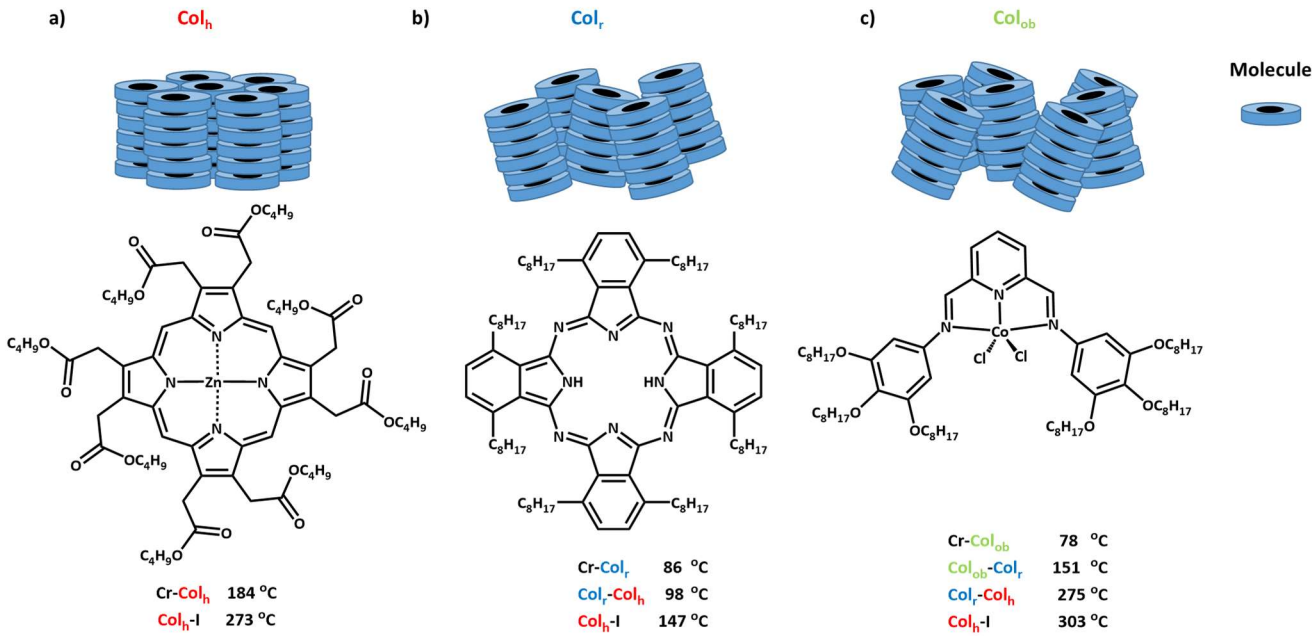

Figure 1.9: 2D DLCs arrangements a) Col_h phase displayed by a zinc porphyrin metallomesogen,[73] b) Col_r phase displayed by an phthalocyanine mesogen[74] and c) Col_{ob} phase displayed by cobalt phenylamine pyridine complex[71]

The examples in Figure 1.9 a and c show that inorganic complexes and smaller cores can also sustain DLCs.

The self-organisation into columns is reinforced by side chains which are long tails usually alkyl or alkoxy units often five atoms or more in length. Due to the disorder of the tails the formation of

a 3D crystal is hindered. [75] This leads to nanosegregation between cores and the tails resulting in the columns above (Figure 1.9).[76]

Due to the ability of these DLCs to conduct through these stacks many potential applications have arisen such as electronics,[77] light emitting diodes, [78] OLEDs[79] and solar cells.[80]

1.3.4 Alkoxytriphenylene Liquid Crystallinity

Alkoxytriphenylenes (**Tp(C_n)$_x$**; Figure 1.10) are one of the most common DLCs; their potential was first observed in 1978 by Zann *et al.*, [1] (a year after Chandrasekhar reported the first DLCs).[60]

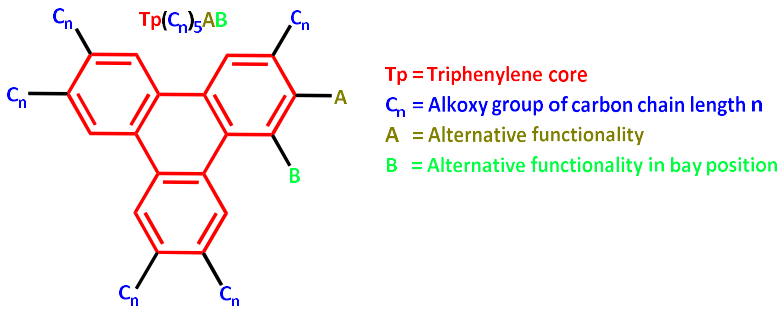

*Figure 1.10: **Tp(C_n)$_5$AB** example of how alkoxytriphenylenes (**Tp(C_n)$_x$**) will be referred to in this thesis*

The modulation of the liquid crystalline properties of the triphenylene species can be achieved by several different methods. These are outlined below.

1.3.4.1 Varying the Length of All Alkoxy Tails

Tp(C_n)$_x$ without further functionality are mesogenic when n is between three (propyl) and eleven (undecyl). Interestingly, there is a trend where the transition temperature and range of liquid crystallinity lowers with increasing chain length (Figure 1.11).

When the alkoxy groups are *n*-propyl and *n*-butyl the DLC phase is the hexagonal columnar plastic phase (Col_{hp}). The Col_{hp} phase is significantly more ordered than the Col_h phase and therefore shows higher conductivity.[81] After twelve carbons in the alkoxy chain no mesophase is observed (Figure 1.11).[3]

1.3.4.2 Bay Position Modification

The mesophase can be further modified by substituting electron withdrawing and donating groups to the bay position of the triphenylene ring. Electron donating groups such as NH_2 cause the LC temperature range of the compound to narrow.[82] Conversely electron withdrawing groups such as NO_2 cause the DLC temperature range to widen where all C3-C11 derivatives are liquid crystal at room temperature. A comparison of phase transition temperatures between **$Tp(C_n)_6$** and **$Tp(C_n)_6NO_2$** is shown below in Figure 1.11. The Col_h-I temperature range of **$Tp(C_n)_6$** is narrower than **$Tp(C_n)_6NO_2$**. Furthermore, when the chain length is greater than five **$Tp(C_n)_6NO_2$** clears to the isotropic phase at higher temperatures than the unsubstituted **$Tp(C_n)_6$**. The reason for such an effect is explained by the electron donating groups pushing electron density into the ring, the intermolecular π-π bond between the triphenylene rings weaken as there would be greater π-π repulsion between the rings. On the other hand, electron withdrawing groups remove electron density, consequently π-π repulsion is reduced, and therefore, a greater window of liquid crystallinity. This explanation is further complicated by the dipole moment the group introduces to the ring system, resulting in dipole-dipole interactions also becoming a factor in DLC intermolecular bonding.[83]

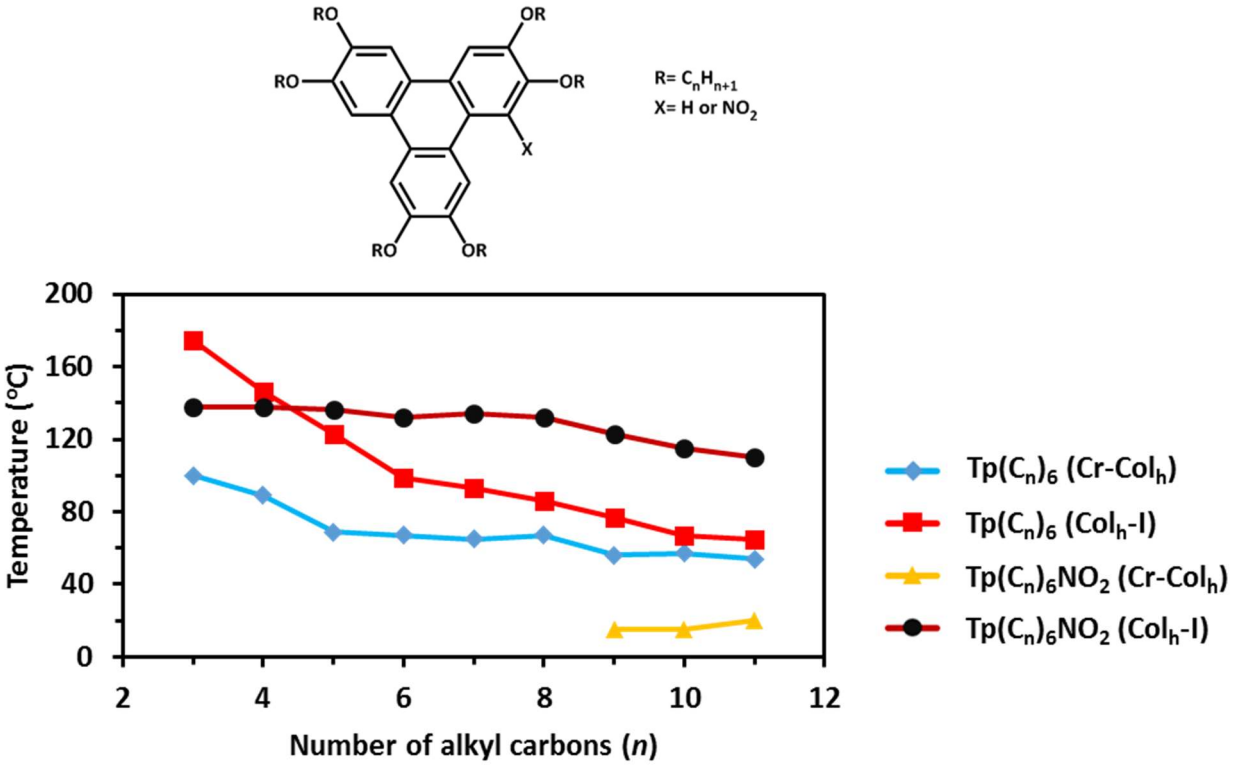

*Figure 1.11: Graph showing the transition temperature of increasing alkyl chain length of (**$Tp(C_n)_6$**) and (**$Tp(C_n)_6NO_2$**). Crystalline (Cr), hexagonal columnar (Col_h) and isotropic (I) phases are shown.* [82-87]

1.3.4.3 Single Arm Modification

In the cases above all the alkoxy arms were the same length. Trends for when there is not a homogenous R group become more difficult to extract. However, there are many examples of DLC triphenylenes with changes to one or several of the R group length and functionality (Figure 1.12).[88]

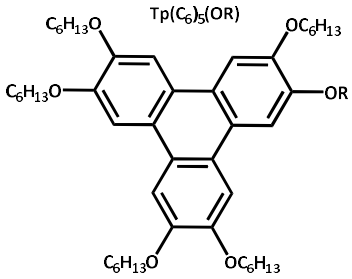

R Group	Cr-Col$_h$ (°C)	Col$_h$-I (°C)	Cr-I (°C)
H			45
Me	69	78	
C_6H_{13}	67	99	

*Figure 1.12: Alkoxytriphenylene derivative **Tp(C_6)$_5$(OR)** with R as H, Me and C_6H_{13} showing changes to liquid crystallinity.*[88-90]

Figure 1.12 displays an example of the effect of replacing one R group for a phenol or for a methyl ether. In the case of the phenol the compound does not display any DLC properties. In the case of the methyl the temperature range at which the compound is LC is reduced.

A general trend of substituting shorter chains leads to a smaller temperature range for liquid crystallinity exists. However, the converse trend does not apply. In some cases, longer chain addition greatly increases the thermal range of the DLC properties.[91]

1.3.4.4 Thioalkyltriphenylenes

Another way the DLC phase can be modified in triphenylenes is use thioethers instead of ethers. The thioether arms propagate a chiral columnic phase within the stacks, even though there is no molecular chirality.[92] The effect is suggested to be born out of competition between the attractive π-π interactions of the core and the steric repulsion between the thioether tails. The energy is minimised if the stack is at a relative rotation of 45°, thus causing the rotation (Figure 1.13). These helical stacks showed electron mobility up to 0.1 $cm^2\ V^{-1}\ s^{-1}$ (this charge transport is far greater than a typical value expected for a Col$_h$ (0.002 $cm^2\ V^{-1}\ s^{-1}$).[32] This helical phase (H) interestingly is not seen when the sulfur is replaced with selenium, where normal Col$_h$ re-emerges. The sulfur

being key to this phase was further highlighted by Cammidge *et al.* where they synthesised a variety of homologs.[4] The only examples that showed H phase contained at least two SC_6H_{11} peripheral chains was not observed with other chain lengths.[4]

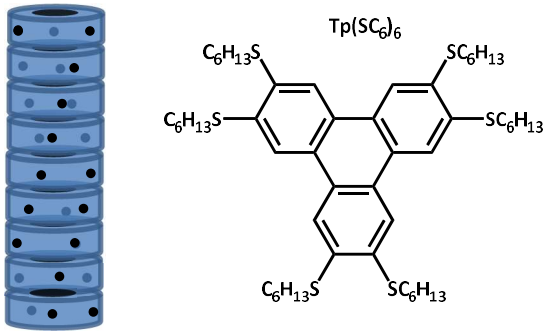

Figure 1.13: Representation of the Helical (H) phase of ***Tp(SC$_6$)$_6$*** [4]

1.3.4.5 Core Extension of Triphenylene

Another way the DLC can be modified in triphenylenes is to expand the aromatic system. Kumar *et al.* showed this in 2011 by expanding the aromatic region with an imidazole functionality (Figure 1.14). Increasing the π framework in this fashion means modifying π-π interactions, and desymmetrising the structure, and therefore, introducing a dipole, this significantly alters the DLC mesophase.[93]

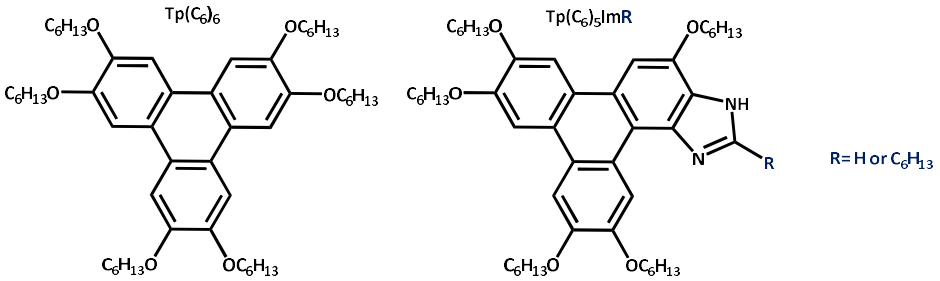

Compound	Cr-Col$_h$ (°C)	Col$_h$-I (°C)
Tp(C$_6$)$_6$	69	78
Tp(C$_6$)$_5$ImH	119	147
Tp(C$_6$)$_5$ImC$_6$	108	146

*Figure 1.14: **Tp(C$_6$)$_6$** compared to Kumar's triphenylenoimidazoles **Tp(C$_6$)$_5$ImH** and **Tp(C$_6$)$_5$ImC$_6$**. R= C_6H_{13}* [93]

When compared to the hexa-alkoxy equivalent **Tp(C$_6$)$_6$** a large difference in the temperature range of liquid crystallinity is observed (Figure 1.14). **Tp(C$_6$)$_5$ImR** is still crystalline after **Tp(C$_6$)$_6$** has entered the isotropic phase. The temperature difference is attributed to an increased ratio of rigid to flexible portions of the mesogen. The actual DLC temperature range is comparable to that of the **Tp(C$_6$)$_6$**. There is a marginal increase of 6 °C in **Tp(C$_6$)$_5$ImC$_6$** compared to **Tp(C$_6$)$_6$** (38 °C compared to 32 °C). Whereas when the R group is a hydrogen (**Tp(C$_6$)$_5$ImH**) there is an actual decrease in the DLC range by 4 °C.

Recently Cammidge *et al.* managed to fuse two triphenylenes together with a pyrazine bridge (Figure 1.15).[7]

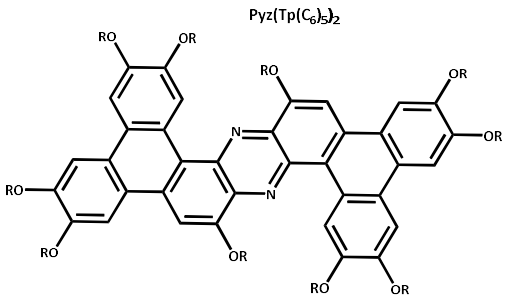

Figure 1.15: Cammidge et al. pyrazine bridge ***Pyz(Tp(C$_6$)$_5$)$_2$*** *R=C$_6$H$_{13}$* [7]

Pyz(Tp(C$_6$)$_5$)$_2$ has a large DLC temperature range of (104 °C), with the melt into the Col$_h$ phase at 123 °C and clearing at 227 °C. The high temperature of the melt can be explained again by the increased ratio of rigid to flexible portions of the mesogen. As well as DLC properties the mesogen displays a deep red colour, as well as red fluorescence.[7]

Other examples of triphenylene ring expansion show similar trends where the active liquid temperature is raised.[94]

1.4 Synthesis of Triphenylenes

This section will detail the synthetic approaches taken to synthesise triphenylene liquid crystals and their molecular modifications as highlighted in the preceding section.

1.4.1 Alkoxytriphenylenes

The synthetic strategy in synthesising alkoxytriphenylene compounds has developed rapidly over the years, from the original route shown in (Scheme 1.1).[95]

1.4.1.1 Synthesis of the Basic Hexa-Alkoxy Triphenylene core

The alkoxybenzene starting material can be prepared with a straight forward Williamson ether synthesis [96] starting from catechol and the haloalkane of desired chain length. The most commonly utilised method to form the triphenylene core is by oxidative trimerisation using $FeCl_3$ (Scheme 1.1). The reaction is an adaption of the Scholl reaction,[97] where 3 carbon-carbon bonds are made, to fuse the three catechol moieties.[98] Other Lewis acids[99] have been shown to work ($MoCl_5$ and $VOCl_3$),[100] and indeed often show better yields. However, $FeCl_3$ remains the most common trimerisation reagent, because cost is significantly lower.

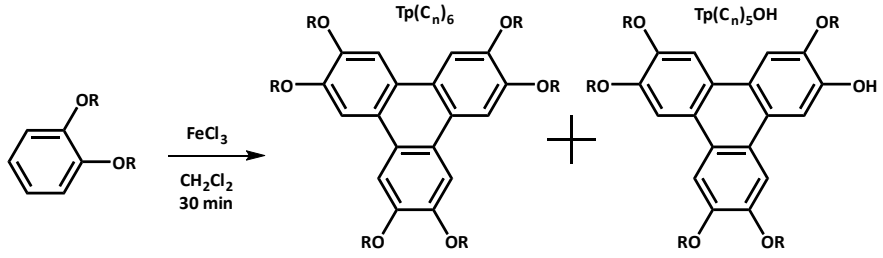

*Scheme 1.1: Typical procedure to form alkoxytriphenylene **$Tp(C_n)_6$** and **$Tp(C_n)_5OH$**, where R= alkyl chain of length n*

The reaction has many advantages in having a remarkably short reaction time, when considering three bonds are being formed, and a facile work-up. Methanol is used to quench the excess $FeCl_3$ and precipitate the alkoxytriphenylene species allowing for filtration of crude product. After this column chromatography, can be used to isolate the D_{3h} symmetric triphenylene (**Tp(C$_n$)$_6$**) in typically >40+ % yields, as well as (**Tp(C$_n$)$_5$OH**) in 10 % yields.

Modifications to this reaction have been developed, where 2% sulfuric acid is added to the mixture.[85] This increases both the yield of **Tp(C$_n$)$_6$** and **Tp(C$_n$)$_5$OH**. This route is commonly employed when the **Tp(C$_n$)$_5$OH** is the desired product.

1.4.1.2 Elaboration of Tp(C$_n$)$_5$OH

Tp(C$_n$)$_5$OH has been used in many synthetic strategies (Scheme 1.2).

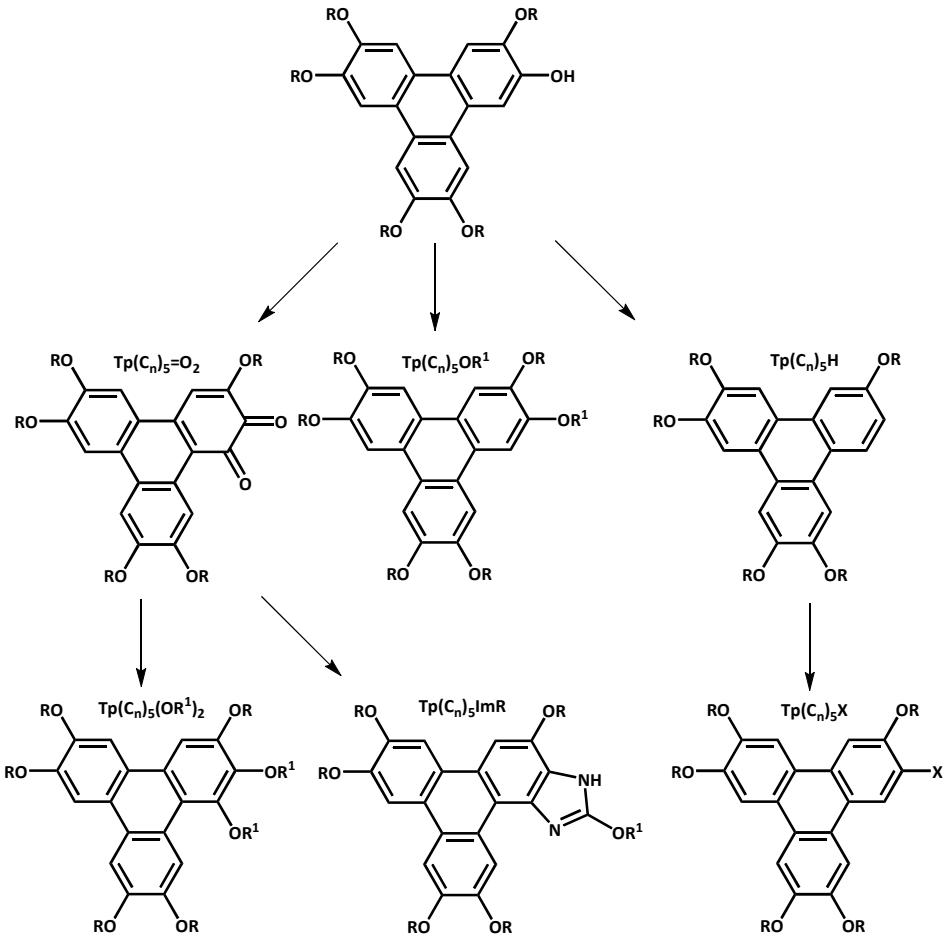

*Scheme 1.2: **Tp(C$_n$)$_5$OH** uses as a starting material, where X is an electrophile, R= alkyl chain of length n, R$_1$= alkyl of chain or ester*

Oxidation to provide the 1,2-diketone derivative can be first reduced and then alkylated to provide(**Tp(C$_n$)$_5$(OR)$_2$**).[101] Or the 1,2 diketone derivative could be used in annulation reactions to expand the aromatic core of the triphenylene (**Tp(C$_n$)$_5$ImR**) being a prime example. [93]

Tp(C$_n$)$_5$OH can simply be alkylated or converted to an ester to provide a different chain on one of the arms (**Tp(C$_n$)$_5$OR^1**), as shown in section 1.3.4 this will change the DLC thermal properties of the mesogen, or could be used for further reactions.[102]

Palladium catalysed[103] reductive removal of the OH can lead to interesting chemistry, as a previously sterically unhindered position becomes available for S_E2 chemistry. Though it should be stated other methods to form **Tp(C$_n$)$_5$H** have recently become available, for instance the **Tp(C$_n$)$_5$H** can be built into the initial triphenylene formation.[104] **Tp(C$_n$)$_5$H** has mainly been used for bromination or attack of an electrophile.[103]

1.4.1.3 Cross Coupling to Form the Triphenylene Core

Though **Tp(C$_n$)$_5$H** is useful in providing mix-tail triphenylenes, only one tail can be modified in the case of the six-tailed derivative. One way to synthesise more complicated mix-tail triphenylenes is to use the biphenyl route (Scheme 1.3).[105]

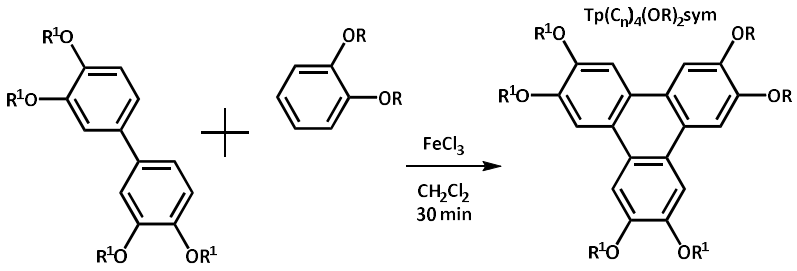

*Scheme 1.3: Biphenyl route. Providing symmetric mix-tail triphenylenes **Tp(C$_n$)$_4$(OR)$_{2sym}$**. R= alkyl of chain n, R^1= alkyl of chain ≠n*

The biphenyl starting material is made in two steps from the alkoxybenzene *via* iodination of 1,2 dialkoxybenzene, followed by heating to dimerise.[96] The coupling of the biphenyl to phenyl is performed in much the same way as the oxidative trimerisation in Scheme 1.1, with both reagents charged at 1:1 equivalents. If protecting groups like isopropyl (*i*-Pr) are used for either R or R_1 selective cleavage can be used to create either tetraphenols[106] or diphenols.[107] These can be

exploited in methods similar to **Tp(C$_n$)$_5$OH**. Furthermore, it was shown that alkylated phenols could be used instead of catechols, thus providing another route of access to **Tp(C$_n$)$_5$H**.[104]

1.4.1.4 Selective Tris Dealkylation

Tp(C$_n$)$_6$ can also be selectively dealkylated using bulky dealkylating agents such as B-bromocatecholborane (**BrBcat**) to provide tris-dealkylated products **Tp(C$_n$)$_3$(OH)$_3$sym** and **Tp(C$_n$)$_3$(OH)$_3$asym** (Scheme 1.4).[108] Due to the steric hindrance, only one chain can be dealkylated from each peripheral ring. By varying the ratio of BrBcat 1-3 alkyl chains can be removed, but never two chains from the same peripheral ring.

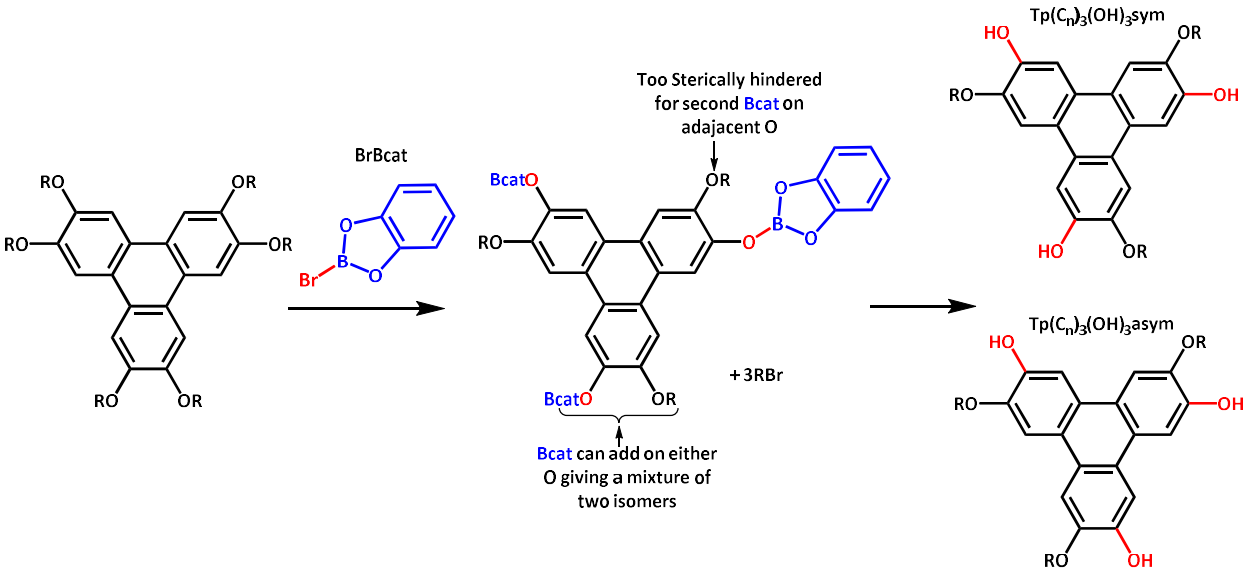

*Scheme 1.4: Selective dealkylation to provide symmetric and asymmetric **Tp(C$_n$)$_3$(OH)$_3$***

In the case shown above, purely because of statistics, **Tp(C$_n$)$_3$(OH)$_3$sym** is produced in twice the quantity as **Tp(C$_n$)$_3$(OH)$_3$asym**.

1.4.2 Modification of the Bay Position in Alkoxytriphenylenes

Literature also shows the bay position (Figure 1.10) of **Tp(C$_n$)$_6$** is rich in reactivity. Nitration,[109] bromination and[110] chlorination[111] have all been achieved using **Tp(C$_n$)$_6$** as the starting material.

Nitration of **Tp(C$_n$)$_6$** is achieved at room temperature by the use of nitric and acetic acid affording the electrophilic nitronium cation, which reacts rapidly with the electron-rich triphenylene core. Mono, bis or tris substitution is possible on different peripheral phenyl rings, by addition of more equivalents of nitric acid.[112]

The substitution pattern of the nitration is governed by the steric hindrance and electron withdrawing nature of the nitro group (Scheme 1.5).[113]

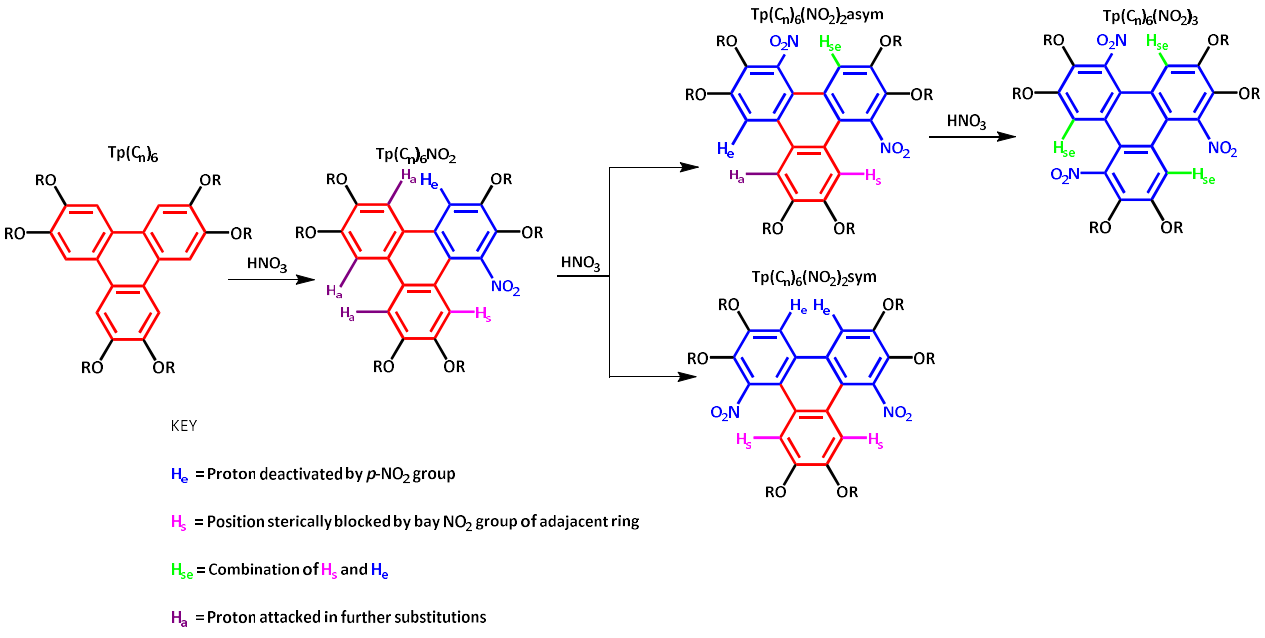

*Scheme 1.5: Nitration substitution pattern of **Tp(C$_n$)$_6$***

Scheme 1.5 shows that once a single nitro group is substituted, options for the second nitration become limited. Nitration on the same ring at H_e becomes unfavourable for S_E2 substitutions due to the electron withdrawing nature of the nitro group. The effect the nitro group has on the other rings is lessened by the small number of resonance structures where electrons migrate between the rings (see Figure 1.1), such that bis and tris nitro derivatives can still form rapidly (reaction completion within 30 minutes). H_s also becomes an unfavourable substitution position due to the steric hindrance of the nitro group.

This leaves three possible sites for further substitutions (H_a). Two out of the three substitution sites lead to **Tp(C$_n$)$_6$(NO$_2$)$_2$asym** and one out of the three sites leads to **Tp(C$_n$)$_6$(NO$_2$)$_2$sym**. The ratio between the two di-nitro compounds is 2:1, showing statistics dominates and other factors are of minimal importance. Of the two di nitro compounds only the **Tp(C$_n$)$_6$(NO$_2$)$_2$asym** can be further substituted and can be used to form **Tp(C$_n$)$_6$(NO$_2$)$_3$**. For that reason the best yield possible for **Tp(C$_n$)$_6$(NO$_2$)$_3$** is 67 %. These nitro compounds can be reduced using tin (II) chloride or sodium borohydride.[109] The resulting amine has been converted to amides, [114] azo and azide compounds.[115]

Bromination provides a different substitution pattern to nitration (Scheme 1.6). This is because the bromine is less electron withdrawing than the nitro group. Computational studies predict the bromine to provide a large enough of a steric hindrance to pucker the ring slightly.[111] Although there is no literature on the di-bromo derivative, we can assume from the yields quoted (72 %)[110] for **Tp(C$_n$)$_6$Br$_3$** that substitution occurs on the same ring as **Tp(C$_n$)$_6$Br**. Despite the withdrawing effect of the bromine, the puckering of the ring could facilitate attack for substitution.

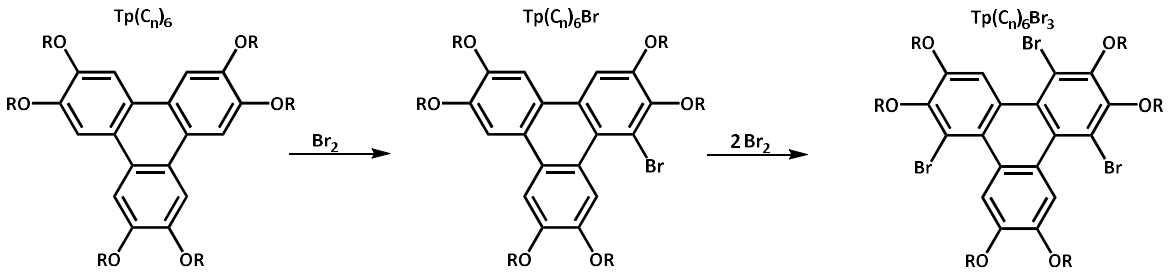

Scheme 1.6: Bromination pattern of ***Tp(C$_n$)$_6$*** [111]

The substitution pattern for Scheme 1.6 illustrates that bromination is under steric control. The bromine as well as increasing the range of liquid crystal phase, has had synthetic use and has been used for Suzuki[116] and Sonagashira[110] coupling, which ultimately leads to ring expansion.

Chlorination of **Tp(C$_n$)$_6$** has been achieved through peculiar chemistry using iodine monochloride (ICl). ICl is traditionally used as an iodinating agent of aryl substituents, because the more electronegative chlorine results in $I^{\delta+}$, and thus electrophilic behaviour of the iodine. This normally results in iodination of the aryl ring. In the case of **Tp(C$_n$)$_6$** chlorination rather than iodination occurs. The theory Bushby *et al.* provide for this odd behaviour is the large atomic radii of iodine provides too much of a steric hindrance to substitute in the bay position.[117] Chlorination occurs through a radical mechanism where one electron oxidation of **Tp(C$_n$)$_6$**, which then undergoes nucleophilic attack by the chlorine.[117] The resulting substitution pattern of chlorine is more akin to the nitro substitution, owing to the more electron withdrawing nature of chlorine when compared to bromine.[117]

Other peculiar reactions worth noting is the difference between mono nitration and bromination of **$Tp(C_n)_5H$** (Scheme 1.7). Nitration still occurs in the bay position, despite the less sterically hindered site being available. Bromination occurs in the least sterically hindered site.

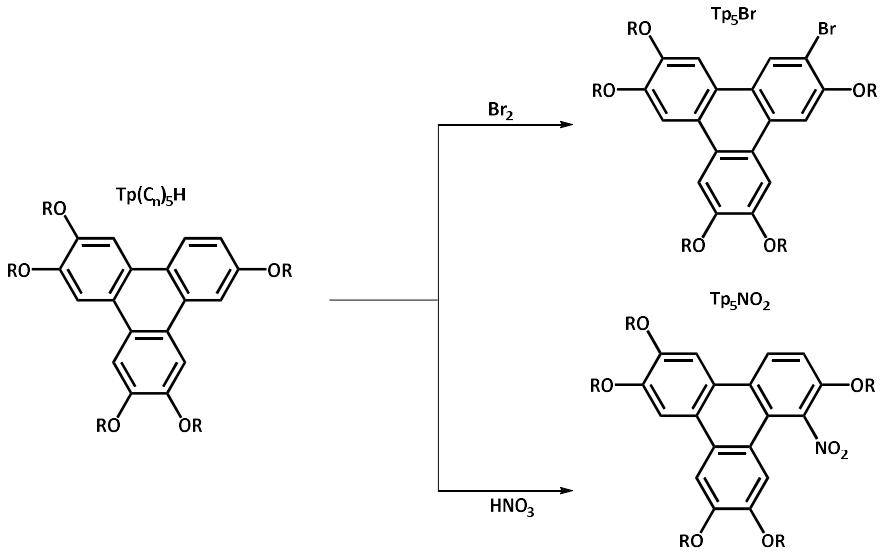

*Scheme 1.7 Mono bromination (**$Tp(C_n)_5Br$**) [103] and nitration (**$Tp(C_n)_5NO_2$**) of **$Tp(C_n)_5H$***

Nitration occurring in the more sterically hindered bay position, points towards an electrostatic driving force for this reaction.[115]

1.4.3 Synthesis of Thioether and Amino ether Triphenylenes

The strategy to synthesise triphenylene derivatives substituted with thioethers or amino groups does not work *via* the $FeCl_3$ trimerisation of 1,2, dialkyamino and sulfur analogues of catechol, as discussed earlier (Scheme 1.1). Presumably because the Lewis basicity of the amino and sulfur analogues are two great and quench the $FeCl_3$. However, a recent patent by Fujifilms has reported the hexa-thioether product by trimerisation with iron nitrate and potassium perchlorate.[118]

The most common method of synthesis of the sulfur analogue, is to begin with triphenylene and hexa-brominate with molecular bromine at 240 °C with iron powder,[119] followed by nucleophilic aromatic substitution of the bromine using an alkyl thiolate as the nucleophile Scheme 1.8).[119]

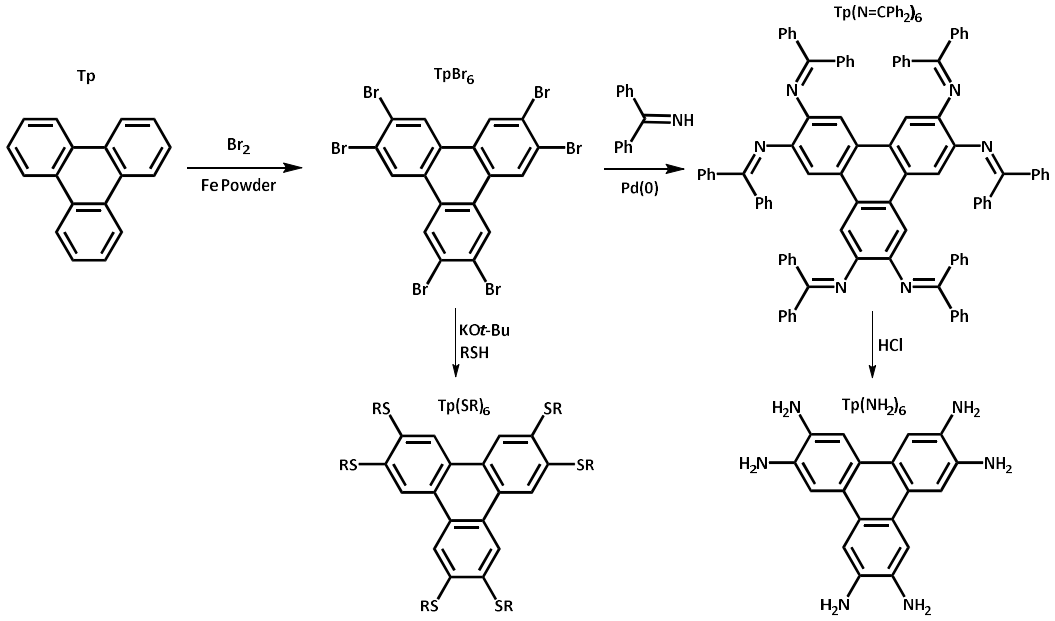

Scheme 1.8: Synthesis of thioether[119] and amino[120] substituted triphenylene, R= alkyl chain.

To synthesise the amino derivative the hexabromotriphenylene undergoes an Ullmann coupling to substitute the bromine atom, affording the hexa-imine,[120] which is converted to hexa-amine by acid hydrolysis (Scheme 1.8).[120] Alkyl tails can then be substituted by use of bromoalkanes in similar procedure to Williamson ether substitution shown before (Scheme 1.2), or by condensation with a carbonyl group. [94]

1.5 Organic Luminescent Materials

Organic luminescent molecules have become ubiquitous in the last twenty years, in technologies such as probes,[121] dyes[122] and sensors.[123] The organic fluorophores are advantageous over inorganic fluorescent complexes in certain aspects, including significantly higher quantum yields (Φ) and they are usually more facile to synthesise and cheaper.[124] Organometallics luminescence using heavy metals often benefit from larger Stokes shift.[125]

Most luminescent triphenylene derivatives owe their large Stokes shift due to a twisted internal charge transfer (TICT) mechanism.[126] Consequently, this section will first discuss the photo properties of TICT mechanisms and then show TICT luminescence with triphenylene examples.

1.5.1 Twisted Internal Charge Transfer Mechanism

TICT mechanisms are characterised by a large Stokes shift[127] (often defined as greater than 8000 cm^{-1}) and a high Φ.[128] Stokes shift is defined by IUPAC "*the difference between the spectral position of the band maxima… of the absorption and luminescence arising from the same electronic transition.*" However, literature often quote Stokes shift in general terms to refer to the difference between the absorption band excited and the emission peak emitted regardless of electronic transition.[129]

This thesis will aim to differentiate the shifts between the absorption maxima and emission maxima regardless of electronic transition as a pseudo-Stokes shift (pSS) and reference both Stokes shift and pSS as shift.

A large shift between absorption and emission is often a desired characteristic to minimise the reabsorption from the emission of the molecule.[130] TICT mechanisms are fast, with the twist and then emission happening within the pico to nanosecond time range.[131]

The reason behind the large shift is due to the difference of energy between the twisted and non-twisted excited state. Bunton *et al.* diagram of auramine's luminescent mechanism is a great example of relaxation of a twisted excited state (Scheme 1.9).[132] Auramine is a luminescent dye with a large Stokes shift. When excited, a non-planar conformation is favourable for the excited state species. By adopting this conformation, the energy of the system is lowered. After relaxation from $S_0 \leftarrow S_1$ the twisted conformation becomes unfavourable, causing relaxation into the planar ground state. The large difference in energy (365 nm and 510 nm) equates to a shift of 7790 cm^{-1}.

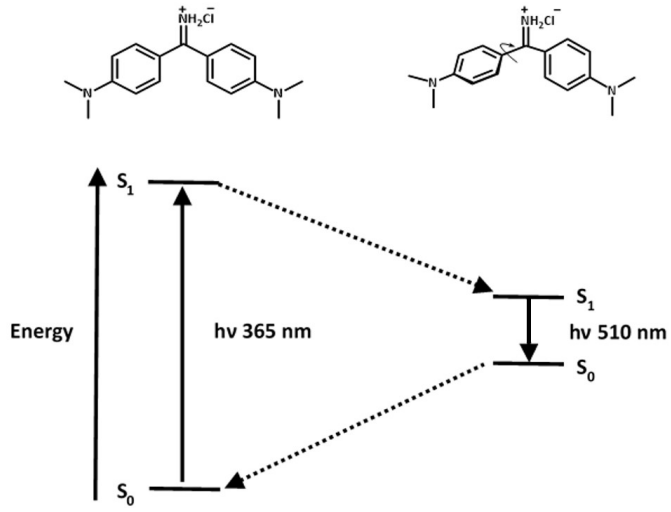

Scheme 1.9: TICT mechanism of auramine. Dashed line indicates non-radiative relaxation[132]

Bunton *et al.* exploited this mechanism to measure with great accuracy the viscosity of the medium.[132] TICT mechanisms show a square root relationship between viscosity and increasing Φ, making their use an excellent candidate in such experiments.

TICT mechanisms are also dependent upon solvent polarity,[133] with a general trend of more polar solvents result in a larger shift. The effect is caused by the more polar solvents larger dipoles align with the excited state to a higher degree, thus lowering the S_1 energy. After relaxation, the dipole alignment increases the energy of the ground state, resulting in a larger shift.[133]

Lastly the groups attached to the fluorophore can make a substantial difference to the torsion angle and electronics, and thus alter the luminescent properties of the system. Wang *et al.* study of boryl-substituted carbazoles displays the complexity of such changes.[134]

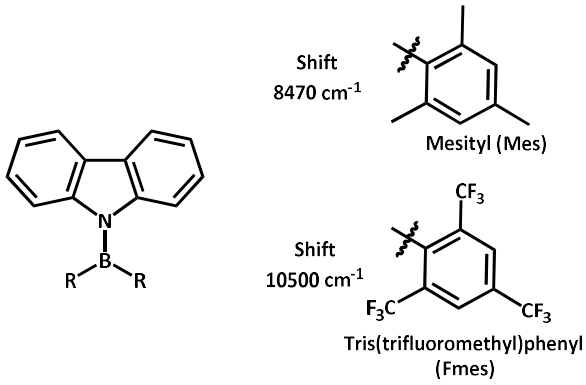

Figure 1.16: Wang et al. study of boryl-substituted carbazoles with mesityl (Mes) and Tris(trifluoromethyl)phenyl (Fmes)[134]

Figure 1.16 shows that when substituted with the electron withdrawing tris(tripfluoromethyl)phenyl (Fmes) group there is a red shift when compared to that of the mesityl (Mes). This red shift is rationalised by the Fmes better ability to stabilise the excited state. However, using time dependent density functional theory (TD-DFT) Wang *et al.* found that if the

R group of the boron was changed to hydrogen the expected Stokes shift dramatically increased. Though not experimentally confirmed, the result was ascribed in part to the ground state of the molecule being more planar than when compared to Mes and Fmes and therefore a larger relative twist than Mes and Fmes. These results show the competing factors of electronics versus sterics in TICT mechanisms.[134]

The photophysical behaviour of photoactive species can be improved by certain functional groups. Benzoxazoles and benzothiazoles have long been known to increase the Φ of substituents. The increase in Φ is thought to be due to the heterocycles increasing the rate of the radiative process. This in turn leads to a decrease in the lifetime of the transition state. [135]

Yang *et al.* used benzothiazoles to make 3 molecules which emit violet, green and orange light respectively, all with Φ of ~48 %. These were then combined using a CIE plot to make a white light LED, making the blend useful in backlight applications (Figure 1.17).[136]

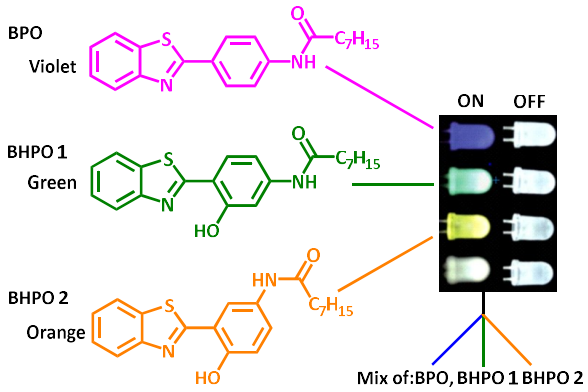

Figure 1.17: Yang et al. use of BPO, BHPO 1 and BHPO 2 as a blend to coat a UV LED and produce white light[136]

BHPO 1 and BHPO 2 emit through a different photo mechanism known as excited state intramolecular proton transfer (ESPIT), where the proton of the phenol is deprotonated in the excited state.[137]

1.5.2 Triphenylene Luminescence

Triphenylene and its derivatives often display TICT excited states and therefore a large shift between absorption and emission.[126] As a reference, unsubstituted triphenylene (**Tp**) has a small quantum yield of Φ 6 % in THF solution. The quantum yield of **Tp** can be improved by addition of alkoxy-groups, where **Tp(C$_5$)$_6$** has double the quantum efficiency.[138] Triphenylene and the **Tp(C$_n$)$_6$** derivatives have a structured emission profile and a pSS in the range of 12000 cm^{-1} depending on the medium and concentration.[139]

The luminescence mechanism of triphenylene differs slightly from the other TICT examples shown before, as absorption from $S_4 \leftarrow S_0$ followed by non-radiative relaxation to S_1 occurs.[140] Finally emission from the lowest energy excited state is observed from $S_1 \leftarrow S_0$ in accordance to Kasha's rules.[141]

The luminescence of triphenylene species vary greatly depending on concentration. Stacks occur in higher concentrations, which often reduce quantum yield.

Levell *et al.* successfully improved the quantum yield to 31 % in the solid phase by designing a twisted triphenylene derivative **TpMe$_6$** (Figure 1.18).[139] The non-planar conformation of the molecule disfavours stacking and thus prevents quenching. Furthermore, the shift of the molecule

is nearly identical in solution and solid. Whereas, **Tp** sees a noticeable red shift in the solid phase, due to stabilisation gained from the π-π stacking.[139]

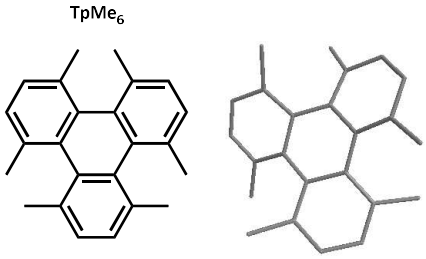

Figure 1.18: $TpMe_6$. The methyl groups in the bay position cause the molecule to be non-planar as shown in the Chemdraw 3D representation[139]

There are examples where aggregation of triphenylene leads to fluorescence enhancement. Arora *et al.* designed two triphenylene derivatives (Figure 1.19).[142] One with cyano groups on the periphery (**1**) and the other with amino groups (**2**). The aryl arms were implemented into the structure to promote packing in a slipped fashion, the bulky groups preventing π-π stacking (a similar strategy to Levell *et al.*). However, the cyano groups of **1** also promote aggregation induced emission enhancement (AIEE). The aggregation was achieved by dissolving **1** in a mixture of tetrahydrofuran (THF) and water, and then increasing water concentration. The free rotating aryl groups bonds become restricted in the aggregation, resulting in a greater proportion of radiative relaxation and thus a greater Φ. Thus, the Φ of **1** increased from 29 % in pure THF to 44 % in water-THF mix (3:7). Increasing the water concentration further caused luminescence to decrease, presumably as the stacks became too large in size.[142]

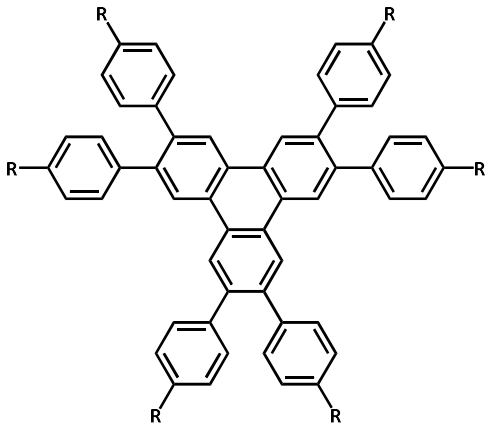

*Figure 1.19: Arora et al. triphenylene derivative. R= CN (**1**) or NH_2 (**2**)* [142]

Compound **2** proved useful as a chemo sensor in the detection of picric acid (a nitroaromatic explosive) to a 10^{-11} M concentration. The quenching caused by the formation of the ammonium salt, which made use of long range energy transfer to the picric phenolate.[142]

1.5.3 Liquid Crystal Luminescence

Recently, interest in luminescent liquid crystals (LLCs) has grown because of the potential application in LCD devices without the requirement of a backlight system, [143] or anisotropic light-emitting diodes. [144] Development is hindered by the LC state often quenching luminescence through aggregation effects. Often, the interactions of the mesomorphic units enable non-radiative relaxation through energy transfer.[145] For this reason LLC are often designed to undergo aggregation induced enhanced emission (AIEE), whereby the mesomorphic interactions enhance the luminescence effect.[146]

An example of LLC is shown by Li *et al.* chiral LLC **3** (Figure 1.20). [147]

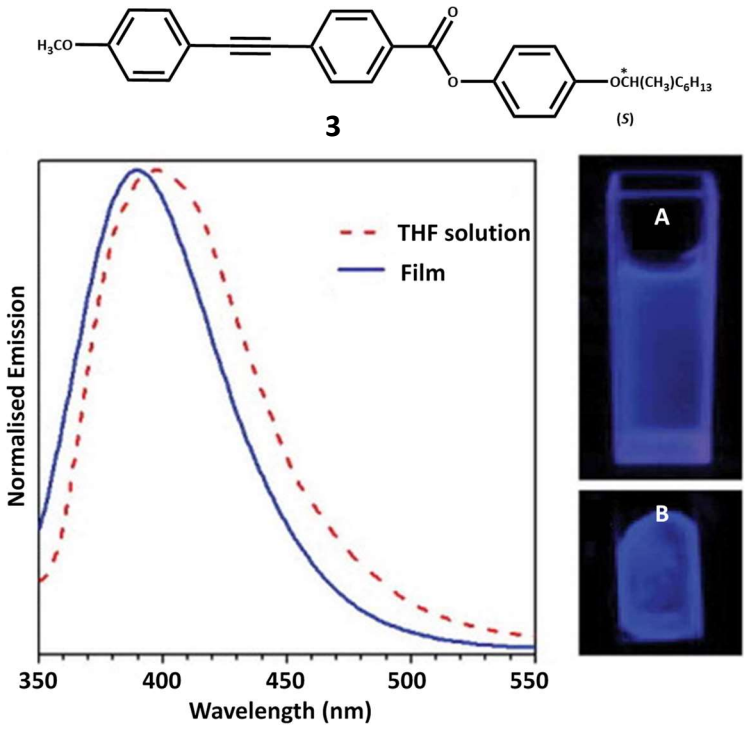

*Figure 1.20: Li et al. chiral LLC (**3**) Where A is in THF (emission max 398 nm) and B is as a film (emission max 390 nm)[147]*

Li *et al.* designed the mesogen to have a tolane base, as these are known to undergo AIEE. From here they attached a long chain, incorporating a chiral centre through an ester linkage to induce a chiral phase, which formed at 75 °C.[147]

LLC is still in its infancy, as combining luminescence and mesogenic properties, often involves overcoming aggregation induced quenching. Use of certain derivatives (like tolane), have been shown to overcome these obstacles, and it is expected for this subject to be greatly explored in the coming years.[146-148]

1.6 Conclusions

In summary, this chapter has shown examples of the different types of liquid crystalline phases and detailed their characterisation by POM, DSC and XRD analysis.

The chapter introduced thermotropic LCs- showing calamitic liquid crystals phases and citing examples of their use in current technology.

At this point, discotic LCs were introduced, with schematics showing the different 1D and 2D phases. Triphenylene then became the focal point, with synthetic methods of triphenylene cored species outlined. The effect of modifying the tails from alkyl, alkoxy, thioethers and esters was detailed, as well as changing the length of the tails.

Hybrid triphenylene structures where imidazoles and pyrazine groups were integrated to the core were discussed, and are further discussed in Chapters 3-5.

Lastly, luminescent molecules were introduced and focused largely on TICT luminescence in solution, before giving literature examples of luminescence in the liquid crystalline state.

1.7 Objective of This Thesis

Modification of the triphenylene core to extend the p-aromatic core *via* the introduction of a pyrole moiety across a bay region to generate the interesting carbazole moiety (**Tp(C_5)$_6$Cb**) and investigate it's thermal photophysical properties.

This carbazole wasn't formed, but the triphenoxazole **Tp(C_5)$_5$OxC$_4$** (Figure 1.21) was isolated. The chemistry was then further explored to introduce other appendages (**Tp(C_5)$_5$OxR^1**), and also investigate the novel triphenoxazoles thermal and photophysical properties.

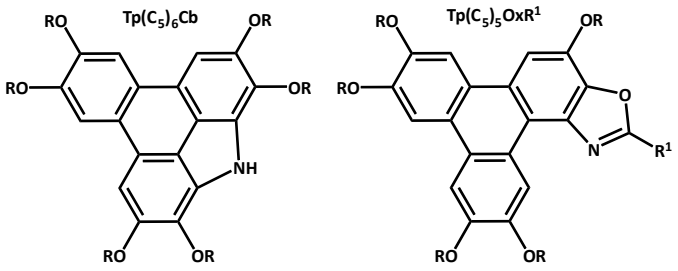

*Figure 1.21: **Tp(C_5)$_6$Cb** and **Tp(C_5)$_5$OxR^1**, where R= butyl (C_4) or phenyl*

1.8 References

[1] J. Billard, J.C. Duboisand, N.H. Tinh and A. Zann, *J. Chimie*, 1978, **2**, 535

[2] S.K. Pal, S. Setia, B.S. Avinash and S. Kumar, *Liquid Crystals*, **40**, 2013, 1769

[3] O.B. Akopova, E.V. Kurbatova and M.S. Gruzdev, *Russ. J. Gen. Chem.*, 2008, **78**, 1902

[4] A.N. Cammidge and H. Gopee, 2001, *J. Mater. Chem.*, 2001, **11**, 2773

[5] R. Shakya, P.H. Keyes, M.J. Heeg, A. Moussawel, P.A. Heiney and C.N. Verani, *Inorg. Chem.*, 2006, **45**, 7587

[6] N. Boden, R.J. Bushby and P.S. Martin, *Langmuir*, 1999, **15**, 3790

[7] W. Xiao, Z. He., S. Remiro-Buenamanana, R.J. Turner, M. Xu, X. Yang, X. Jing and A.N. Cammidge, *Org. Lett.*, 2015, **17**, 3286

[8] M. Gupta and S.K. Pal, *Langmuir*, 2016, **32**, 1120

[9] M. Faraday, *Philosophical Transactions of the Royal Society*, 1825, **115**, 440

[10] A. Kekulé, *Bulletin de la Societe Chimique de Paris*, 1865, **3**, 98

[11] T.M. Figueira-Duarte and K. Müllen, *Chem. Rev.*, 2011, **111**, 7260

[12] http://www.nasa.gov/topics/universe/features/evolution-of-cosmic-carbon-pah.html [25/09/2017]

[13] P.M. Spiecker, K.L. Gawrys, C.B. Trail and P.K. Kilpatrick, *Colloids and Surfaces A: Physicochem. Eng. Aspects*, 2003, **220**, 9

[14] J.L. Cape, P.A. Monnard and H.J. Ziock, *Astrobiology Science Conference*, 2010, 5443

[15] S.P. Tiwari, W.J. Potscavage Jr., T. Sajoto, S. Barlow, S.R. Marder and B. Kippelen, *Org. Electron.*, 2010, **11**, 860

[16] L. Zeng, C. Jiao, X. Huang, K. Huang, W. Chin and J. Wu, *Org. Lett.*, 2011, **13**, 6026

[17] M. Solá, *Front Chem.*, 2013, **1**, 22

[18] E. Clar, *The Aromatic Sextet*. New York, NY, Wiley, 1972

[19] D. Ghosh, G. Periyasamy and S.K. Pati, *Phys. Chem. Chem. Phys*, 2011, **13**, 20627

[20] C. Mannich, *Berichte der deutschen chemischen Gesellschaft*, 1907, **40**, 159

[21] N.P. McCleland and J.B. Whitworth, *J. Chem. Soc.*, 1927, **0**, 2753

[22] J. Nabar and A. Chodkowska, *J. Luminescence*, 1975, **11**, 215

[23] F. Reinitzer, Monatsh. *Chem. (Wien)*, 1888, **9**, 421

[24] S. Chandrasekhar, *Liquid Crystals*, Cambridge University Press, Cambridge [England], 1992

[25] http://www.nanotech-now.com/news.cgi?story_id=31224 [25/09/2017]

[26] M. Yan, J. Tang, H.L. Xie, B. Ni, H.L. Zhang and E.Q. Chen, *J. Mater. Chem. C*, 2015, **3**, 8526

[27] J.H. Lee, H.S. Kim, B.D. Pate and S.M. Choi, *Physica B; Condens. Matter*, 2006, **385-386**, 798

[28] J. Hoogboom, T. Rasing, A. Rowan and R.J.M. Nolte, *J. Mater. Chem.*, 2006, **16**, 1305

[29] J.A. Rego, J.A.A. Harvey, A.L. Mackinnon and E. Gatdula, *Liq. Crys*., 2010, **37**, 37

[30] http://www.tainstruments.com/wp-content/uploads/CA-2016-DSC.pdf [25/09/2017]

[31] W. Li, Y. Shen, Z. Chen, Q. Cui, S. Li and L. Chen, *Appl. Optics*, 2017, **56**, 601

[32] T. Wöhre, I. Wurzbach, J. Kirres, A. Kostidou, N. Kapernaum, J.Litterscheidt, J.C. Haenle, P. Staffeld, A. Baro, F. Giesselmann and S. Laschat, *Chem. Rev.*, 2016, **116**, 1139

[33] T. Kushida, A. Shuto, M. Yoshio, T. Kato and S. Yamaguchi, *Angew. Chem.*, 2015,**127**, 7026

[34] https://www.tester.co.uk/kern-opn-1-polarising-binocular-reflecting-microscope [25/09/2017]

[35] http://www.labx.com/item/ta-instruments-dsc-q-100-differential-scanning-calorimeter/3959326 [25/09/2017]

[36] http://www.labx.com/x-ray-analytical-xrd-xrf [25/09/2017]

[37] A. Bubnov, M. Kašpar, V. Hamplová, U. Darwin and F. Giesselmann, *Beilstein J. Org. Chem.*, 2013, **9**, 425

[38] J. Chen, W. Cranton and M. Fihn, *Handbook of Visual Display Technology*, Springer, 2012

[39] F. Araoka, M. Isoda, D. Miyajima, I. Seo, M. Oh, T. Aida and H. Takezoe, *Adv. Electron. Mater.*, 2017, **3**, 1600503

[40] I.H. Chiang, C.J. Long, H.C. Lin, W.T. Chuang, J.J. Lee and H.C. Lin, *ACS. Appl. Mater. Interfaces*, 2014, **6**, 228

[41] J. Malthe and A. Collect, *J. Am. Chem. Soc.*, 1987, **109**, 7544

[42] H.T. Nguyen, C. Destrade and J. Maltêhte, *Adv. Mater.*, 1997, **9**, 375

[43] M. Fukui, H. Orihara, A. Suzuki, Y. Ishibashi, Y. Yamada, N. Yamamoto, K. Mori, K. Nakamura, Y. Suzuko and I. Kawamura, *Jpn. J. Appl. Phys.*,1990, **29**, 329

[44] P.G. de Gennes and J. Prost, *The Physics of Liquid Crystals*, Oxford: Clarendon Press, 1993

[45] F. Araoka, K.C. Shin, Y. Takanishi, K. Ishikawa and H. Takezoe, *J. Appl. Phys.,* 2003, **94**, 67-78

[46] S.K. Ghosh, *Il Nuovo Cimento D*, 1984, **4**, 229

[47] J.A. Rego, J.A.A. Harvey, A.L. Mackinnon and E. Gatdula, *Liq. Cryst.*, 2009, **37**, 37

[48] T.J. Bunning, *Liquid Crystals Today*, 2014, **23**, 23

[49] https://acswebcontent.acs.org/prfar/2008/REPORTS/P9424.HTM [25/09/2017]

[50] https://www.hallcrest.com/color-change-basics/liquid-crystal-thermometers [25/09/2017]

[51] S.C. Jeng, S.J. Hwang, Y.H. Hung and S.C. Chen, *Optics Express*, 2010,**18**, 22572

[52] www.bmgmis.de/en/products [25/09/2017]

[53] M. Carrasco-Orozco, W.C. Tsoi, M. O'Neill, M.P. Aldred, P. Vlachos, and S.M. Kelly, *Adv. Mater.*, 2006, **18**, 1754

[54] M.A. White, *Encyclopedia of Colour Science and Technology*, Springer, 2016, 463

[55] G. Brown, *Liquid Crystals and Biological Structures*, Elsevier, 2012

[56] I. Dierking, *Symmetry*, 2014, **6**, 444

[57] materials.duke.edu/XCOURSES/ME83/lcrystals2.pdf [25/09/2017]

[58] N. Yadav, V.P. Panov, V. Swaminathan, S.P. Sreenilayam, J.K. Vij, T.S. Perova, R. Dhar, A. Panov, D. Rodriguez and P.J. Stevenson, *Phys. Rev. E*, 2017, **95**, 062704

[59] M. Sahara, S. Yano, K. Ikemoto and Z. Maejima, *Liq Cryst.*, 1993, **15**, 929

[60] S. Chandrasekhar, B.K. Sadashiva and K.A. Suresh, *J. Phys.*, 1977, **9**, 471

[61] C. Göltner, D. Pressner, K. Müllen and H.W. Spiess, *Angew. Chem., Int. Ed.*, 1993, **32**, 1660

[62] H. Bisoyi and S. Kumar, *Chem. Soc. Rev.*, 2010, **39**, 264

[63] D. Reis, E. Akpinar, A. Martins and F. Neto, *J. Phys. Chem. B*, 2013, **117**, 942

[64] S. Zhang, J. Wang, C. Zhang, H. Wu, Y. Wang, F. Hong, X. Hao, A. Zhang, and J. Pu, *Appl. Mech. Mater.*, 2015, **748**, 107

[65] T. Verbiest, S. Sioncke, A. Persoons, L. Vyklicky and T. Katz, *Angew. Chem.*, 2002, **41**, 3882

[66] J.H. Wendorff, R. Wustefield, E. Zerta and H. Ringsdorf, *Angew. Chem. Int. Ed.*, 1989, **28**, 914

[67] P.H.J. Kouwer, W.F. Jager and W.J. Mijs, *Macromolecules*, 2000, **33**, 4336

[68] R.J. Bushby and O.R. Lozman, *Curr. Opin. Colloid Interface Sci.*, 2002, **7**, 343

[69] B. Mu, X. Hao, J. Chen, Q. Li, C. Zhang and D. Chen, *Polymer Chemistry*, 2017, **8**, 3286

[70] R. Shakya, P.H. Keyes, M.J. Heeg, A. Moussawel, P.A. Heiney and C.N. Verani, *Inorg. Chem.*, 2006, **45**, 7587

[71] F. Morale, R.W. Date, D. Guillon, D.W. Bruce, R.L. Finn, C. Wilson, A.J. Blake, M. Schröder and B. Donnio, *Chem. Eur. J.*, 2003, **9**, 2484

[72] C. Tschierske and G. Ungar, *Chem. Phys. Chem.*, 2016, **17**, 9

[73] B.A. Gregg, M.A. Fox and A.J. Bard, *J. Chem. Soc., Chem. Commun.*, **1987**, 1134

[74] H. Iino, Y. Takayashiki, J.I. Hanna and R. Bushby, *Jpn. J. Appl. Phys.*, 2005, **44**, 1310

[75] P.A. Heiney, *Structure and Physical Properties of Columnar Liquid Crystals. In Handbook of Liquid Crystals, Wiley-VCH*, Weinheim, 2014, **4**, 521

[76] J.H. Lee, *Mol. Cryst. Liq. Cryst.*, 2016, **635**,133, 183

[77] S. Laschat A. Baro, N. Steinke, F. Giesselmann, C. Hagele, G. Scalia, R. Judele, E. Kapatsina, S. Sauer, A. Schreivogel and M. Tosoni, *Angew. Chem. Int. Ed.*, 2007, 4832

[78] S. Kumar, *Chem. Soc. Rev.*, 2006, **35**, 83

[79] B.R. Kaafarani, *Chem. Mater.,* 2011, **23**, 378

[80] A. Khan, M.A. Kamarudin, M.M. Qasim and T.D. Wilkinson, *Electrochimica Acta*, 2017,

244, 162

[81] S. Kumar, Chemistry of Discotic Liquid Crystals: From Monomers to Polymers, *CRC Press*, 2016, 26

[82] R. Bushby, Q. Liu, O. Lozman, Z. Lu and S. Mclaren, *Mol. Cryst Liq. Cryst.*, 2004, **411**, 293

[83] J.L. Schulte, S. Laschat, R. Schulte-Ladbeck, V. Von Arnim, A. Schneider and H. Finkelmann, *J. Organomet. Chem.*, 1998, **552** 171

[84] J.M. Warman and P.G. Schouten, *J. Phys. Chem.*, 1995, **99**, 17181

[85] H. Monobe, Y. Shimizu, S. Okamoto and H. Enomoto, *Mol. Cryst. Liq. Cryst.*, 2007, **476**, 31

[86] N. Terasawa, N. Tanigaki, H. Monobe and K. Kiyohara, *J. Fluorine Chem.*, 2006, **127**, 1096

[87] O.V. Zemtsova and K.N. Zheleznov, *Russ. Chem. Bull.*, 2004, **53**, 1743

[88] D. Stewart, G. Mchattie and C. Imrie, *J. Mater. Chem.*, 1998, **8**, 47

[89] J. Chapuzet and J. Simonet, *Tetrahedron*, 1991, **47**, 791

[90] J. Goodby, M. Hird, K. Toyne and T. Watson, *J. Chem. Soc. Chem. Commun.*, 1994, 1701

[91] Y. Hu, J. Han, L. Ge and R. Guo, *Langmuir*, 2015, **31**, 12618

[92] J. Malthête, J. Jacques, N.H Tinh and C. Destrade, *Nature*, 1982, *298*, 46

[93] S. Kumar and S.K. Gupta, *Tetrahedron Lett.*, 2011, **52**, 5363

[94] S.S. Jester, E. Sigmund, L.M. Röck and S. Höger, *Angew. Chem. Int. Ed.*, 2012, **51**, 8555

[95] J. Wei, B. Han, Q. Guo, X. Shi, W. Wang and N. Wei, *Angew. Chem. Int. Ed.*, 2010, **49**, 8209

[96] C. Zhang, J. Pu, H. Wu, S. Cheng, R. Zhang and M. Zhang, *Mol. Cryst. Liq Cryst.*, 2011, **542**, 99

[97] M. Gryzbowski, K. Skonieczny, H. Butenschön and D.T. Gryko,*Angew. Chem. Int. Ed.*,2013,

52, 9900

[98] R. Scholl and J. Mansfield, *Chem. Ber.*, 1910, **43**, 1734

[99] M.T. Allen, S. Diele, K.D.M. Harris, T. Hegmann, B.M. Kariuki, D. Lose, J.A. Preece and C. Tschierske, *J. Mater. Chem.*, 2001, **11**, 302

[100] S. Kumar and H.K. Bisoyi, *Angew. Chem. Int. Ed.*, 2007, **46**, 1501

[101] S. Kumar, M. Manickam, S.K. Varshney, D.S.S. Rao and S.K. Prasad, *J. Mater. Chem.*, 2000, **10**, 2483

[102] K.Q. Zhao, X.Y. Bai, B. Xiao, Y. Gao, P. Hu, B.Q. Wang, Q.D. Zeng, C. Weng, B. Heinrich and B. Donnio, *J. Mater. Chem.*, 2015, **3**, 11735

[103] P. Henderson, S. Kumar, J.A. Rego, H. Ringsdorf and P. Schuhmacher, *J. Chem. Soc., Chem. Commun.*, 1995, 1059

[104] S. Pan, H. Jiang, Y. Zhang, D. Chen and Y. Zhang, *Org. Lett.*, 2016, **18**, 5192

[105] Y.F. Bai, K.Q. Zhao, P. Hu, B.Q. Wang and Y. Shimizu, *Mol. Cryst. Liq. Cryst.*, 2009, **509**, 60

[106] M.K. Smith, N.E. Power-Riggs, B.H. Northrop, *RSC Adv.*, 2014, **4**, 38281

[107] R.J. Bushby and Z. Lu, *Synthesis*, 2001, 763

[108] S. Kumar and M. Manickam, *Synthesis*, 1998, 1119

[109] O.B. Akopova, M.G. Bulavkova, M.S. Gruzdev and T.V. Frolova, *Russ. J. Gen. Chem.*, 2011, **81**, 714

[110] D. Wu, H. Zhang, J. Liang, H. Ge, C. Chi, J. Wu, S. Liu and J. Yin, *J. Org. Chem.*, 2012, **77**, 11319

[111] N. Boden, R.J. Bushby, A.N. Cammidge, S. Duckworth and G. Headdock, *J. Mater. Chem.*,

1997, **7**, 601

[112] C.Y. Gan, J. Zhou, W.H. Yu, S.K. Xiang, L.C. Li, B.Q. Wang, P. Hu, K.Q. Zhao and X.Z. Chen, *Liq. Cryst.,* 2017, In Press., DOI:10.1080/02678292.2017.1306889

[113] S. Kumar and M. Manickam, *Mol. Cryst. Liq. Cryst.*, 1998, **309**, 291

[114] O.B. Akopova, E.V. Kurbatova and M.S. Gruzdev, *Russ. J. Gen. Chem.*, 2010, **80**, 268

[115] N. Boden, R.J. Bushby, A.N. Cammidge and G. Headdock, *J. Mater. Chem.*, 1995, **5**, 2275

[116] Z. Li, Z. Hu, X. Chen, Y. Zhang and J. Zhang, *Chem. Lett.*, 2012, **41**, 1588

[117] N. Boden, R.J. Bushby, A.N. Cammidge and G. Headdock, *Tetrahedron. Lett.*, 1995, **36**, 8685

[118] FujiFilm Fine Chemicals Company Limited, S. Kubo, C. Nguyen and T. Chung, JP5731346 B2, **2015**

[119] J. Cui and Z. Xu, *Chem. Commun.*, 2014, **50**, 3986

[120] A. lebkücher, C. Wagner, O. Hübner, E. Kaifer and H.J. Himmel, *Inorg. Chem.*, 2014, **53**, 9876

[121] L. Guo and D. Cao, *J. Mater. Chem. C*, 2015, **3**, 8490

[122] S. Mukherjee and P. Thilager, *J. Mater. Chem. C*, 2016, **4**, 2647

[123] H. Ma, L. Wang, J. Chen, X. Zhang, L. Wang, N. Xu, G. Yang and P. Cheng, *Daltons Trans.*, 2017, **46**, 3526

[124] P. Miluski, *Fibers*, 2017, **5**, 1

[125] F.L. Thorp-Greenwood, *Organometallics*, 2012, **31**, 5686

[126] R.D. Hall, B. Valeur and G. Weber, *Chem. Phys. Lett.*, 1985, **116**, 202

[127] A.D. McNaught and A. Wilkinson, *IUPAC. Compendium of Chemical Terminology,* Blackwell Scientific Publications, 1997, 2278

[128] Z. Zhang, R.M. Edkins, J. Nitsch, K. Fucke, A. Steffen, L. Longobardi, D.W. Stephan, C. Lambert and T.B. Marder, *Chem. Sci.*, 2015, **6**, 308

[129] X.M. Yu, G.J. Zhou, C.S. Lam, W.Y. Wong, X.L. Zhu, J.X. Sun, M. Wong and H.S. Kwok, *J. Organomet. Chem.*, 2008, **693**, 1517

[130] O. Halter, I. Fernández, H. Plenio, *Chem. Eur. J.*, 2017, 23, 711

[131] F. Yu, Y. Wang, W. Zu, Y. Huang, M. Yang, H. Ai and Z. Lu, *RSC Adv.*, 2014, **4**, 36849

[132] P. Bunton, B. Dice, J.A. Pojman, A. De Wit and F. Brau, *Phys. Fluids*, 2014, **26**, 114106

[133] V.I. Stsiapura, S.A. Kurhuzenkau, V.A. Kuzmitsky and O.V. Bouganov, *J. Phys. Chem. A.*, 2016, **120**, 5481

[134] J. Wang, Y. Wang, T. Taniguchi, S. Yamaguchi and S. Irle, *J. Phys. Chem. A.*, 2012, **116**, 1151

[135] A. Reisler, L.J. Leyshon, D. Saunders, M.V. Mijovic, A. Bright and J. Bogie, *J. Am. Chem. Soc.*, 1971, **94**, 2414

[136] F. Lu, R. Hu, S. Wang., X. Guo and G. Yang, *RSC Adv.*, 2017, **7**, 4196

[137] V.S. Padalkar and S. Seki, *Chem. Soc. Rev.*, 2016, **45**, 169

[138] D. Markovitsi, A. Germain, P. Millie, P. Lecuyer, L.K. Gallos, P. Argyrákis, H. Bengs and H. Ringsdorf, *J. Phys. Chem.*, 1995, **99**, 1005

[139] J.M. Levell, A. Ruseckas, J.B. Henry, Y. Wang, A.D. Stretton, A.R. Mount, T.H. Galow and I.D.W. Samuel, *J. Phys. Chem. A.*, 2010, **114**, 13291

[140] R.G.E. Morales and G. Traverso, *Spectroscopy Lett.*, 1982, **15**, 623

[141] M. Kasha, *Discussions of the Faraday Society*, 1950, **9**, 14

[142] H. Arora, V. Bhalla and M. Kumar, *RSC Adv.*, 2015, **5**, 32637

[143] T.E. Frizon, A.G. Dal-Bó, G. Lopez, M.M Paula and L. da Silva, *Liq. Cryst.*, 2014, **41**, 1162

[144] Y. Wang, J. Shi, J. Chen, W. Zhu and E. Baronoff, *J. Mater. Chem. C*, 2015, **3**, 7993

[145] A. Mishra, C.Q. Ma and P. Bäuerle, *Chem. Rev.*, 2009, **109**, 1141

[146] H. Lu, S. Zhang, A.X. Ding, M. Yuan, G. Zhang, W. Xu, G. Zhang, X. Wang, L. Qui, J. Yang, *New J. Chem.*, 2014, **38**, 3429

[147] Z. Cheng, Y. Zang, Y. Li, B. Li, C. Hu and H. Li, *Liq. Cryst.*, 2016, **43**, 777

[148] P. Cunningham, J. Souza, I. Fedin, C. She, B. Lee and D.V. Talapin, *ACS Nano.*, 2016, **10**, 5769

2. Characterisation of Liquid Crystals

2.1 Types of Techniques

Liquid crystals are characterised by three major techniques: differential scanning calorimetry (DSC), polarised optical microscopy (POM) and X-Ray Diffraction (XRD) these techniques are outlined below.

2.1.1 Differential Scanning Calorimetry

DSC measures as a function of temperature the difference in the amount of heat required to change the temperature of the sample compared to that of a reference. Both the sample and the reference are kept at identical temperatures, so differential changes in energy between sample and reference are related to sample phase changes.

The DSC records endothermic or exothermic events.[1] Melting requires energy to be absorbed by the system (endothermic process) this is represented by Figure 2.1. Thus, the solid to liquid transition is endothermic, as is heating from one liquid crystalline phase to another. Conversely, cooling from one phase to another is exothermic.

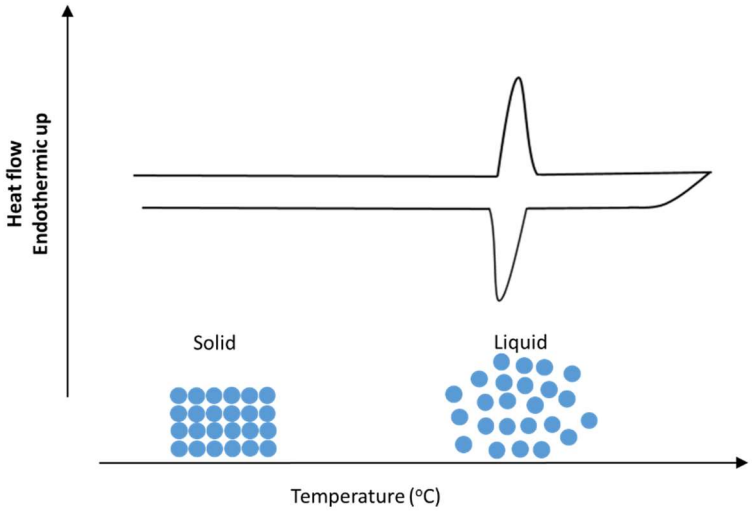

Figure 2.1: Graphic of a DSC scan on a solid to liquid phase transition

Figure 2.1 displays a DSC scan for a solid to liquid transition. In reality any enthalpic change would be detected, whether that was energy lowering of the system by reorientation of a solid or melt, thus DSC is an excellent technique for the measurements of LC transitions.

As well as finding use in the characterisation of liquid crystals, DSC is also a useful tool in other fields of research. For instance, DSC is well used to analyse the stability of a potential drug[2] and in the study of lipids and phospholipids.[3]

2.1.2 Polarised Optical Microscopy

Polarising optical microscopy is a technique which observes a sample through crossed polarisers. If the sample is isotropic the field of view will be dark. However, if the material is anistropically ordered then the material will possess two refractive indices, and the field of view will be light due to birefringence.

90 % of all solids are anistropically ordered and therefore display birefringence (Figure 2.2).[4] Birefringence results from the solid having two refractive indexes resulting from the anisotropic ordering of the molecular structures making up the solid. This results in light being refracted differently depending upon the orientation of the solid.

Isotropic liquids having one refractive index, refract light equally in all directions, are not visible under cross polarised light. Liquid crystals also possess a degree of anisotropy and thus can be visualised under POM.

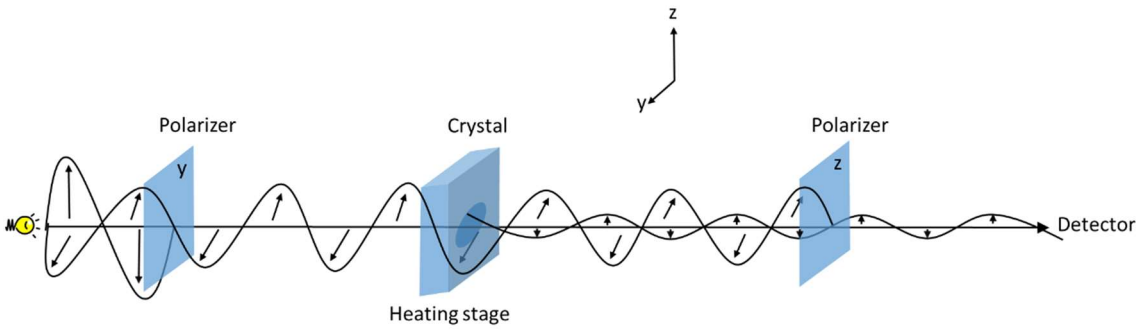

Figure 2.2: Graphic of the cross polarisation of light used in POM. Unpolarised light first travels through a polarizer which blocks light in this case the z direction. The then y polarised light refracts through the anisotropic crystal, forming a small amount of z polarised light. Finally the light travels through a z polarizer removing any light that was not refracted from the sample, allowing for detection of only anisotropic materials.

In the case of a liquid crystalline material, the liquid nature means that the material will have many liquid crystalline domains, from microns to millimetres, and the birefringence will manifest itself as a tapestry of colours, known as textures, as the light is refracted at many orientations that each domain is in.

2.1.3 X-Ray Diffraction

XRD is a powerful tool in phase identification. Unlike POM and DSC, XRD allows the user to elucidate the exact phase of a structure.[5]

Figure 2.3 shows X-rays being fired into the sample across a prespecified range of angles. The detector set at twice the incident angle (θ) from the source.

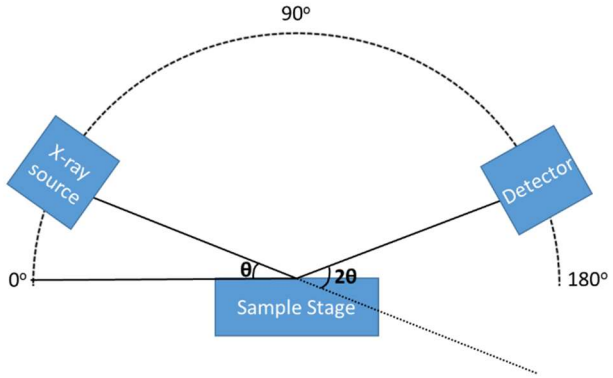

Figure 2.3: Graphic of XRD

The atoms of the material serve as an electron grating and diffract the x-rays, producing bright spots at certain angles. Measurements of where the bright spots occur; the spacing of the diffraction grating (d-spacing) can be determined using Bragg's law (Equation 2.1).[6] The d-spacing is proportional to the distance between atoms.

$$n\lambda = 2d_{hkl}sin\theta$$

Equation 2.1: Bragg's Law where n= whole integer, λ is the wavelength of the x-ray, d_{hkl} is the lattice spacing and ϑ is angle of incidence [6]

The lattice spacing is dependent upon the miller indices (hkl), which is derived from the packing of the structure.

Different LC phases have unique XRD patterns as a result of various packing arrangements. This in turn leads to phase identification. As with POM a heating stage can be attached, allowing for signature XRD peaks to appear when the LC phase is apparent.[7]

2.1.4 Examples of Data Obtained by DSC, POM and XRD

DSC and POM are often used as complementary techniques to confirm liquid crystal phases. DSC provides accurate data on the temperature of a thermal event, and POM images provides evidence of the type of what type of liquid crystal formed from the textures observed. Hartley *et al.* show a typical example of these techniques used in conjunction (Figure 2.4). [8]

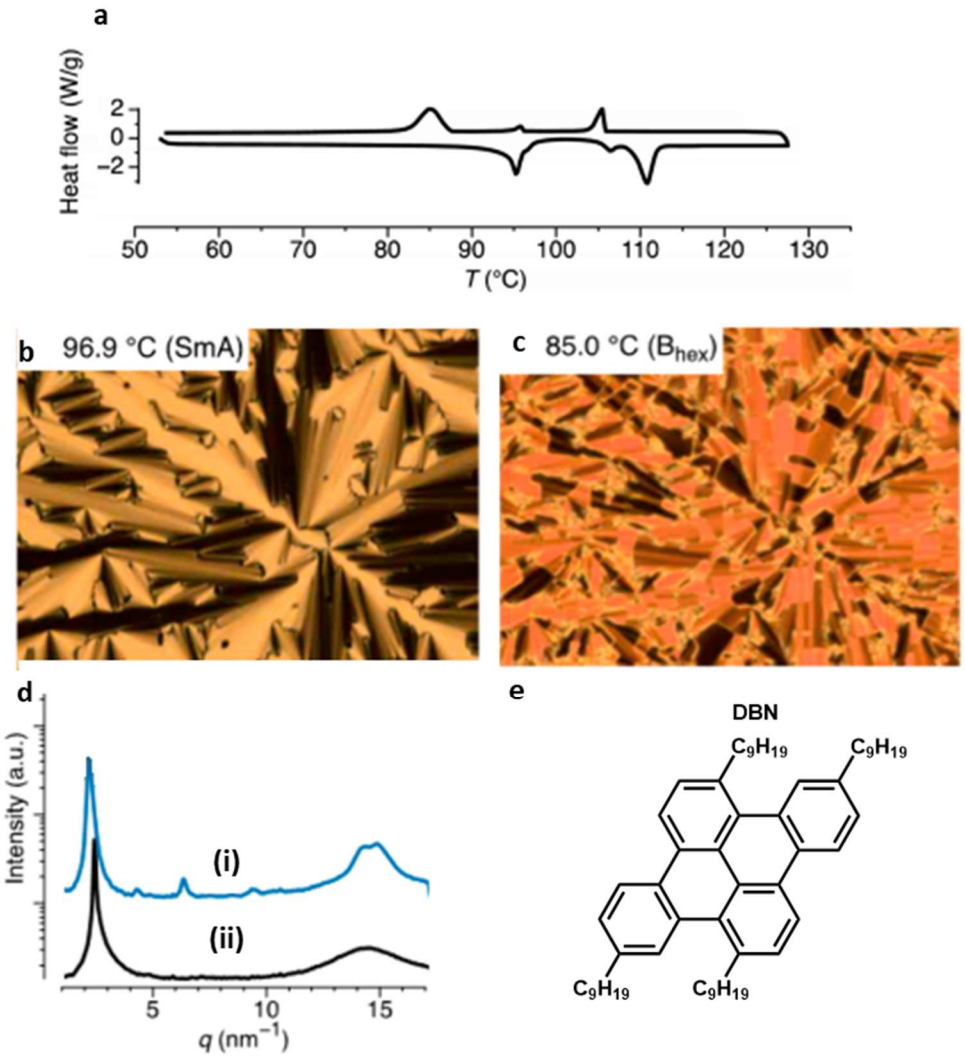

Figure 2.4: Hartley et al. use of: a) DSC, b) and c) POM and d) XRD in conjunction to analyse e) dibenzonapthacene (DBN). DSC scanning rate 5 °C min^{-1} Endothermic is up. d) (i) shows Smectic A phase at 97 °C, (ii) shows (B_{Hex}) phase at 87 °C[8]

As can be seen, the DSC (Figure 2.4a) aligns well with the POM images Figure 2.4b and c. The transition between Hexatic B (B_{hex}) and Smectic A (SmA) phase can clearly be seen. SmA is often described as having conical textures, whereas B_{hex} is identified with a mosaic texture.[8]

To identify the phase transition XRD is used to confirm. Where sharp peaks appear at 6 nm^{-1} in B_{hex} phase. The broad amorphous peak at 15 nm^{-1} is caused by the alkyl chains and is often observed in liquid crystal structures. [8]

XRD can be used to elucidate more complex data. As well as providing distinctive patterns for different liquid crystals, the number of molecules in an array and the distance the molecules are apart can be obtained.[9]

Solid state NMR is also an alternative technique used to study LCs. The technique is particularly useful for cholesteric liquid crystals, where the helix can be observed in detail. Watanbe *et al.* demonstrated this technique in studying the unwinding and winding of cholesteric liquid crystals. [10] Where the helical winding caused broadening in the NMR peaks. NMR holds advantages over XRD in being able to also to study diffusion experiments, but as a relatively new technique, it is still less commonly used.[11]

2.2 References

[1] http://www.tainstruments.com/wp-content/uploads/CA-2016-DSC.pdf [25/09/2017]

[2] G. Bruylants, J. Wouters and C. Michaux, *Curr. Med. Chem.*, 2005, **12**, 2011

[3] D. Paolino, M.L. Accolla, F. Cilurzo, M.C. Cristiano, D Cosco, F. Castelli, M. Sarpietro, M. Fresta and C. Celia, *Colloids and Surf. B*, 2017, **155**, 266

[4] www.microscopyu.com/techniques/polarized-light/polarised-light-microscopy [25/09/2017]

[5] T. Wöhre, I. Wurzbach, J. Kirres, A. Kostidou, N. Kapernaum, J.Litterscheidt, J.C. Haenle, P. Staffeld, A. Baro, F. Giesselmann and S. Laschat, *Chem. Rev.*, 2016, **116**, 1139

[6] W.H. Bragg and W.L. Bragg, *Proc. R. Soc. Lond.*, 1913, **88**, 428

[7] T. Kushida, A. Shuto, M. Yoshio, T. Kato and S. Yamaguchi, *Angew. Chem.*, 2015,**127**, 7026

[8] P.J. Repasky, D.M. Agra-Kooijman, S. Kumar and C.S. Hartley, *J. Phys. Chem. B*, 2016, **120**, 2829

[9] S. Chandrasekhar, S.K. Prasad, D.S.S. Rao and V.S.K. Balagurusamy, *PINSA*, 2002, **68**, 175

[10] K. Yamada, K. Marumo, S. Kang, K. Deguchi, T. Nakai, T. Shimizu and J. Watanabe, *J. Phys. Chem. B*, 2013, **116**, 16325

[11] K. Yamada, S. Kang, K. Takimoto, M. Hattori, K. Sharta, S. Kawuchi, K. Deguchi, T. Shimizu and J. Watanabe, *J. Phys. Chem. B*, 2013, **117**, 6830

3 The First Triphenoxazoles and Their Liquid Crystalline and Photophysical Properties

3.1 Introduction

3.1.1 Triphenylene Hybrid Molecular Structures

The combination of chemical moieties, either covalently or non-covalently has long been an interest of the chemist. The resultant (supra)molecule can show behaviour that has similarities to the individual components and behaviour that is unique to the newly created moiety.[1]

As shown in Chapter 1 (page 20) triphenylene has been covalently combined with moieties such as imidazole[2] and dimerised with a pyrazine bridge[3] creating the hybrid structures below (Figure 3.1).

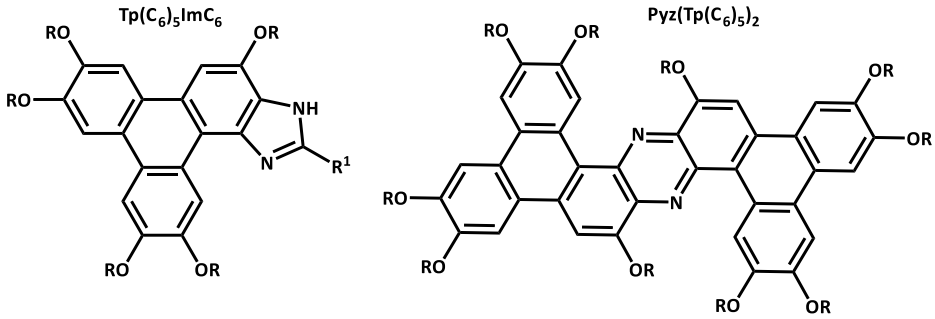

*Figure 3.1: Kumar et al. **Tp(C$_6$)$_5$ImC$_6$**.[2] and Cammidge et al. **Pyz(Tp(C$_6$)$_5$)$_2$**.[3] Where R=C$_6$H$_{13}$. R^1=C$_5$H$_{11}$*

The Preece group were interested in incorporating the carbazole moiety directly as part of triphenylene ring system, in order to produce a material which anisotropically aligns the carbazole in a less energy intensive way, than was currently used, *via* incorporation of the carbazole in a polymer, heating above the T_g, applying a relatively large electric field and cooling below the T_g.[4] Anisotropic alignment of carbazole based materials had potential application in holography, optical image storing and optical data storage.[5-6] Previous work by Manickam *et al.*

has shown that when the carbazole moiety was attached to the termini of the alkoxy arms (Figure 3.2) the resultant structure was not liquid crystalline.

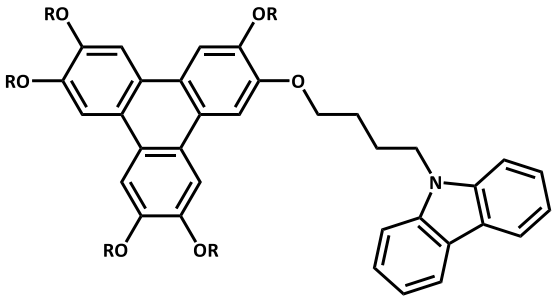

Figure 3.2: Manickam et al. triphenylene carbazole.[4] R=OC_5H_{11}

At the end of the paper Manickam *et al.* notes that the DLC phase, could potentially be restored by incorporation of the carbazole directly into the triphenylene ring, through the double insertion of a N-H into the two C-H bonds in the bay region of the triphenylene, to afford **Tp(C_5)$_6$Cb** (Figure 3.3).[4]

3.1.2 Aim of Research in This Chapter

In this chapter our initial aim was to synthesise **Tp(C_5)$_6$Cb.** The introduction of the five-membered ring would cause a loss in the planarity of the triphenylene across the four fused aromatic rings, resulting in a degree of curvature[7] of the π-system (Figure 3.3), and commensurate reduction in aromatic stabilisation. Thus, insertion of the N-H in the bay region may be non-trivial.

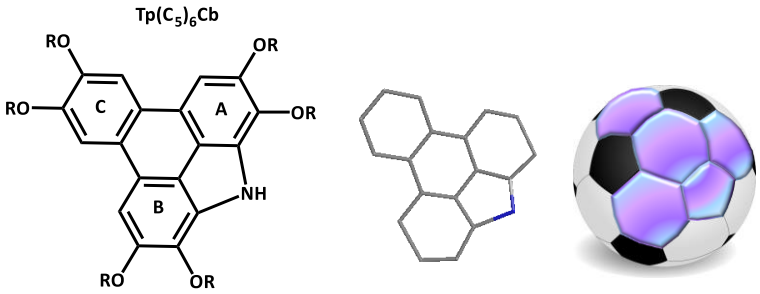

*Figure 3.3: Target compound **Tp(C5)6Cb**. R=C_5H_{11}. Chemdraw 3D model of core and **Tp(C5)6Cb** mapped onto a football*

The nitrogen attached to two adjacent rings (A and B in Figure 3.3) would increase electron density in rings A and B creating two rings that are electronically rich when compared to ring C. Another interesting feature of **Tp(C5)6Cb** is that the carbazole will cause curvature of the π-system. Therefore, the resultant electronic and photophysical properties will be modified by this molecular architecture. [8]

3.1.3 Synthetic Strategy

The synthetic strategy for the formation of **Tp(C5)6Cb** relied upon prior literature on carbazole synthesis. The most likely chance of success involves using a route where the starting materials shown (Scheme 3.1) are comparable to an alkoxytriphenylene base. An ideal scenario involves the making of a carbazole with ether chains α to the reactive sites, of a constrained aryl system.

Scheme 3.1 displays previous methods of carbazole synthesis. These methods have relied upon: building the carbazole by a C-C bond formation (Scheme 3.1a); [9] cross coupling of aryl secondary[10] (Scheme 3.1b) or primary[11] (Scheme 3.1c) amines, cross coupling of amides[12] (Scheme 3.1d), or use of an azide[13] (Scheme 3.1e).

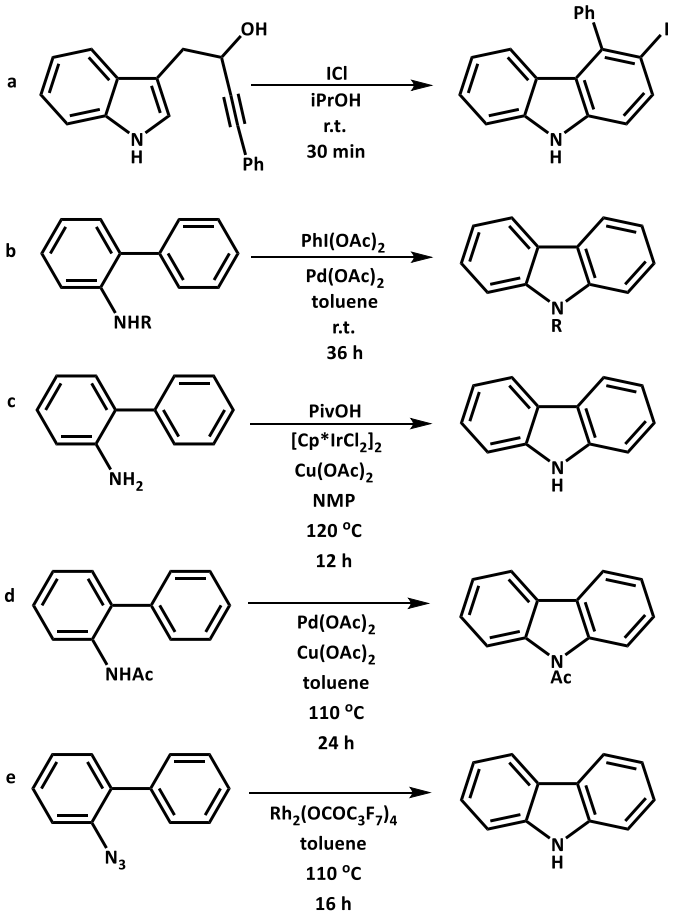

Scheme 3.1: Selected methods of carbazole synthesis (a-e). Cp= cyclopentadiene, PivOH= pivalic acid, R=H,Aryl and alkyl [9-11]

The chemistry of the carbazole synthesis in this case must be compatible with triphenylene chemistry. Synthesis of **Tp(C_5)$_6$Cb** using Scheme 3.1a would be difficult, as the triphenylene core is generally constructed first upon which further derivatisation is performed. Thus, using Scheme 3.1a chemistry would require a new multi-step synthetic strategy in which the triphenylene would be built in a very different fashion.

A better approach is likely to be where a nitrogen functionality can be introduced to the bay region of the triphenylene, followed by subsequent insertion into the adjacent C-H bond of the same bay region, as in the chemistry illustrated in Scheme 3.1b-e.

However, the chemistries shown in Scheme 3.1b-e had no examples in which there were aryl substituents. Of course, alkoxytriphenylenes have several electron rich alkoxy chains, and so are significantly electronically different to the simple 'N' functionalised biphenyls in Scheme 3.1b-e. Thus, these may not be the best synthetic routes to initially try.

A paper from 1982 by Moore *et al.*[14] describes the formation of a carbazole in a similar methodology to Scheme 3.1e.[13] Differences being, Moore made use of a sealed tube to create pressured reaction conditions, whereas in Scheme 3.1e a rhodium catalyst is used to form the carbazole. Moore's *et al.* reaction conditions though acatalytic were performed at a higher temperature and resulted in lower yields when compared to Scheme 3.1e.

That being stated, the reaction of Moore *et al.* (Scheme 3.2a) significantly resembles that of an alkoxytriphenylene. The naphthyl ring has two ethers, α and β to the azide, as with the triphenylene (Scheme 3.2b), with the C-H on to which the nitrene will insert also having an α ether.[14]

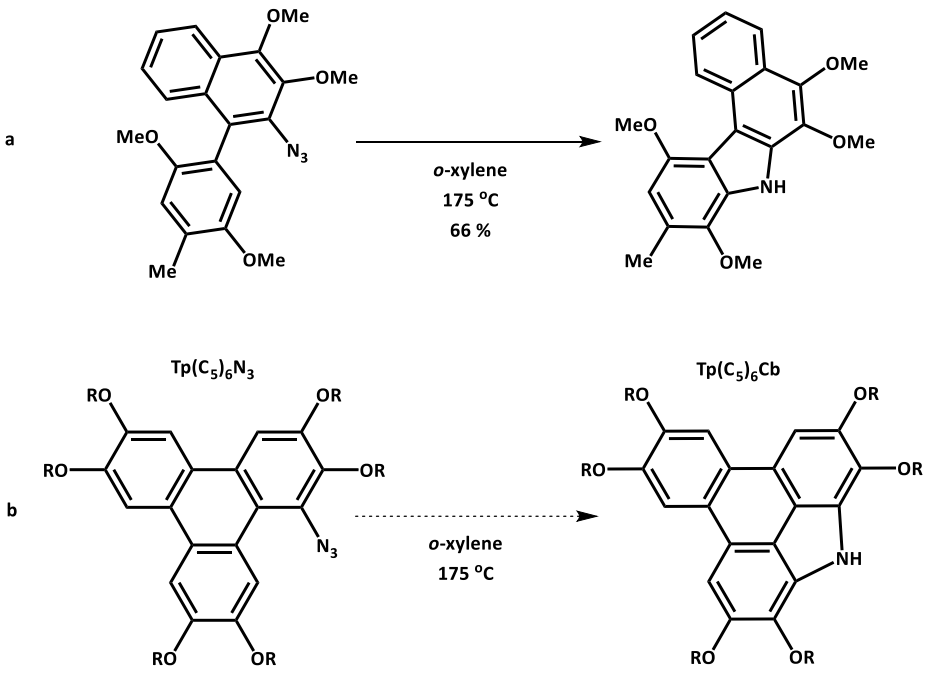

Scheme 3.2: a) Moore et al. Synthesis of Carbazole[14] and b) the envisaged triphenylene analogue ***Tp(C$_5$)$_6$N$_3$*** *(R=C$_5$H$_{11}$)*

3.2 Results and Discussion

3.2.1 Attempted Synthesis of Tp(C$_5$)$_6$Cb: Triphenoxazole Formation

Tp(C$_5$)$_6$N$_3$ has been synthesised before by Bushby *et al.*[15] The synthetic strategy to the precursor is outlined below in Scheme 3.3.

The synthesis of **Tp(C$_5$)$_6$N$_3$** was straight forward and relatively high yielding. As discussed in Section 1.4.4.2 there can be single, double and triple nitration of alkoxytriphenylenes. To minimise di and tri nitro formation, equivalents of nitric acid were kept low, at 4.5 equivalents. **Tp(C$_5$)$_6$NO$_2$** was reduced to the corresponding amine **Tp(C$_5$)$_6$NH$_2$** by use of $SnCl_2$. Later it was found that using $NaBH_4$ and $NiCl_2$ as a catalyst provided a higher yield of 89 % and an easier

work-up not involving column chromatography. Addition of $TMSN_3$ and t-Bu nitrate at 0 °C leads to quantitative conversion to **$Tp(C_5)_6N_3$**.

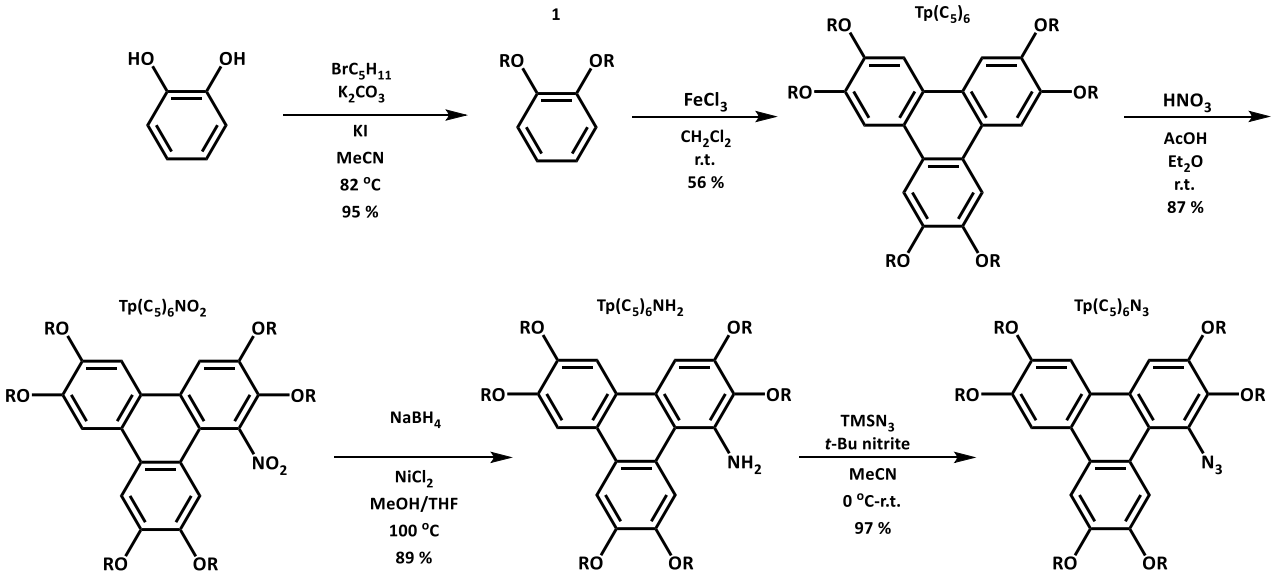

*Scheme 3.3: Synthesis of precursor **$Tp(C_5)_6N_3$**. R= C_5H_{11}*

However, the sealed tube reaction of **$Tp(C_5)_6N_3$** (Scheme 3.4) did not yield the carbazole (**$Tp(C_5)_6Cb$**) as was anticipated, and instead yielded the triphenoxazole (**$Tp(C_5)_5OxC_4$**).

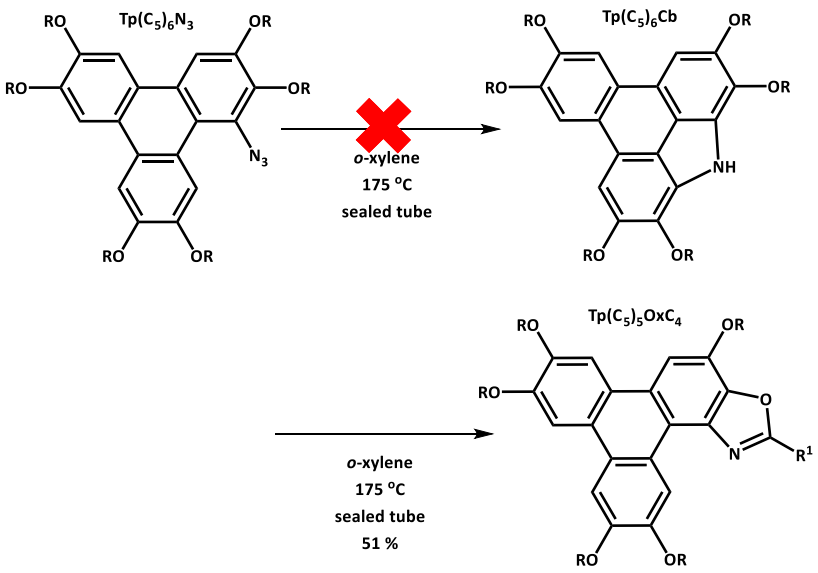

Scheme 3.4: Unexpected ***Tp(C$_5$)$_5$OxC$_4$*** *formation. R= C$_5$H$_{11}$, R^1= C$_4$H$_9$*

The proposed mechanism for the triphenoxazole formation is illustrated in Scheme 3.5, and involves nitrene formation (**Tp(C$_5$)$_6$N**) from the azide (**Tp(C$_5$)$_6$N$_3$**),[16] followed by nitrogen insertion into the C-H bond of the α-methylene of the adjacent alkoxychain to form **Tp(C$_5$)$_5$OxH$_2$C$_4$**. Finally, oxidative elimination of hydrogen leads to the triphenoxazole (**Tp(C$_5$)$_5$OxC$_4$**).

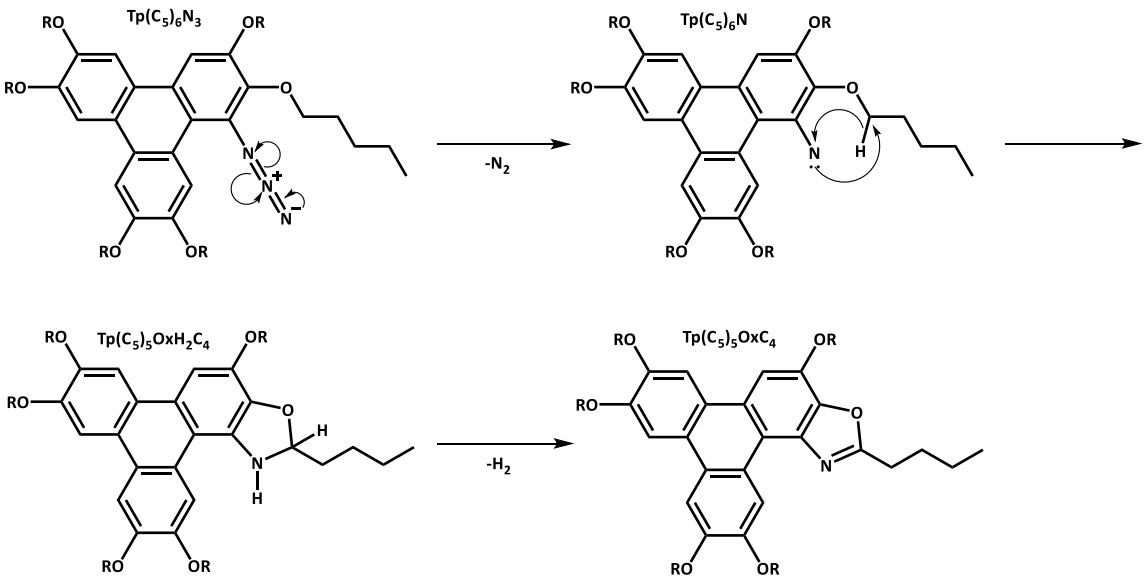

*Scheme 3.5: Proposed mechanism of **Tp(C5)5OxC4** formation. R=C_5H_{11}*

This formation of **Tp(C5)5OxC4** is synthetically remarkable for two reasons:

1) It is the first time an oxazole moiety has been fused to a triphenylene core,
2) Previous examples of oxazoles fused to aromatic moieties do not involve a direct attack of a sp^3 carbon (Figure 3.4), thus this represents a new methodology for oxazole synthesis.

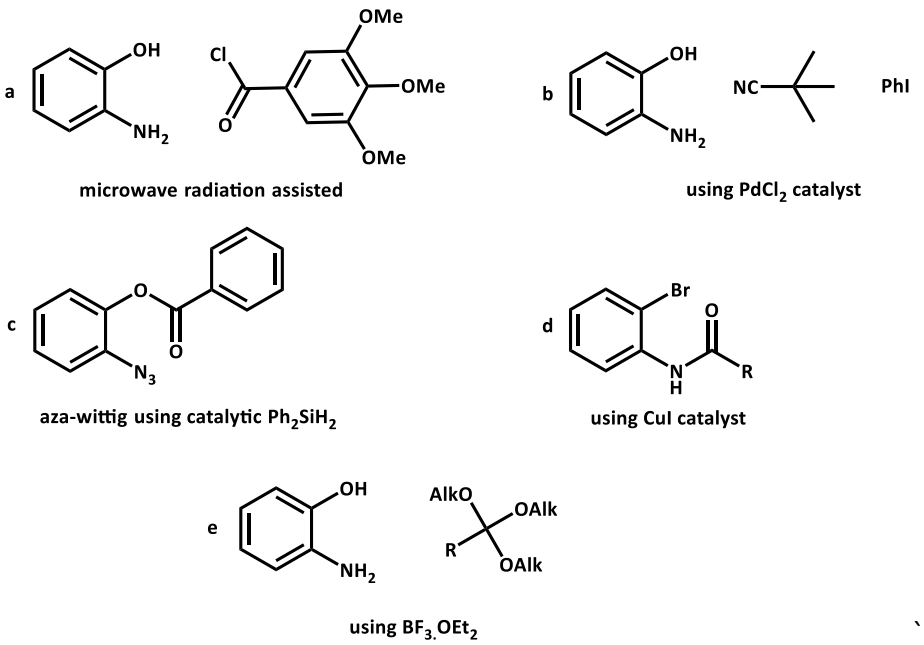

Figure 3.4: Selected examples of benzoxazole synthesis from literature; a) Campo et al.,[17] b) Suckling et al.,[18] c) van Delft et al.,[19]d) Batey et al.,[20] and e) Marko et al.[21]

There are numerous synthetic routes for the formation of the benzoxazole moiety (Figure 3.4).[17-24] Apart from Markó *et al.* who use boron to activate the carbon centre, and unmask an sp^2 centre,[21] all other reactions involve the direct use of a sp or sp^2 carbon.

The annulation reaction to form **Tp(C$_5$)$_5$OxC$_4$** is likely energetically more favoured than forming the **Tp(C$_5$)$_6$Cb.** Presumably this favouring of the triphenoxazole is due to the increased '*curvature strain*' and loss of p-orbital overlap in **Tp(C$_5$)$_6$Cb** as the N inserts across the '*biphenyl*' component of the triphenylene (Figure 3.3).

The rest of this chapter will focus on the characterising **Tp(C$_5$)$_5$OxC$_4$** by ^{1}H and ^{13}C NMR spectroscopy, modifying the synthesis for **Tp(C$_5$)$_5$OxC$_4$** and a comparison of the liquid crystal and fluorescent properties with **Tp(C$_5$)$_6$**.

3.2.2 NMR Characterisation

The protons on **Tp(C_5)$_5$OxC_4** were assigned by ^{1}H NMR and ^{13}C NMR spectroscopy (Figure 3.5) using a combination of 2D techniques including nuclear Overhauser effect spectroscopy (NOESY), heteronuclear single quantum coherence (HSQC), and heteronuclear multiple-bond correlation spectroscopy (HMBC). The aliphatic tails and carbons 11 & 16 were too similar in peak position for full assignment.

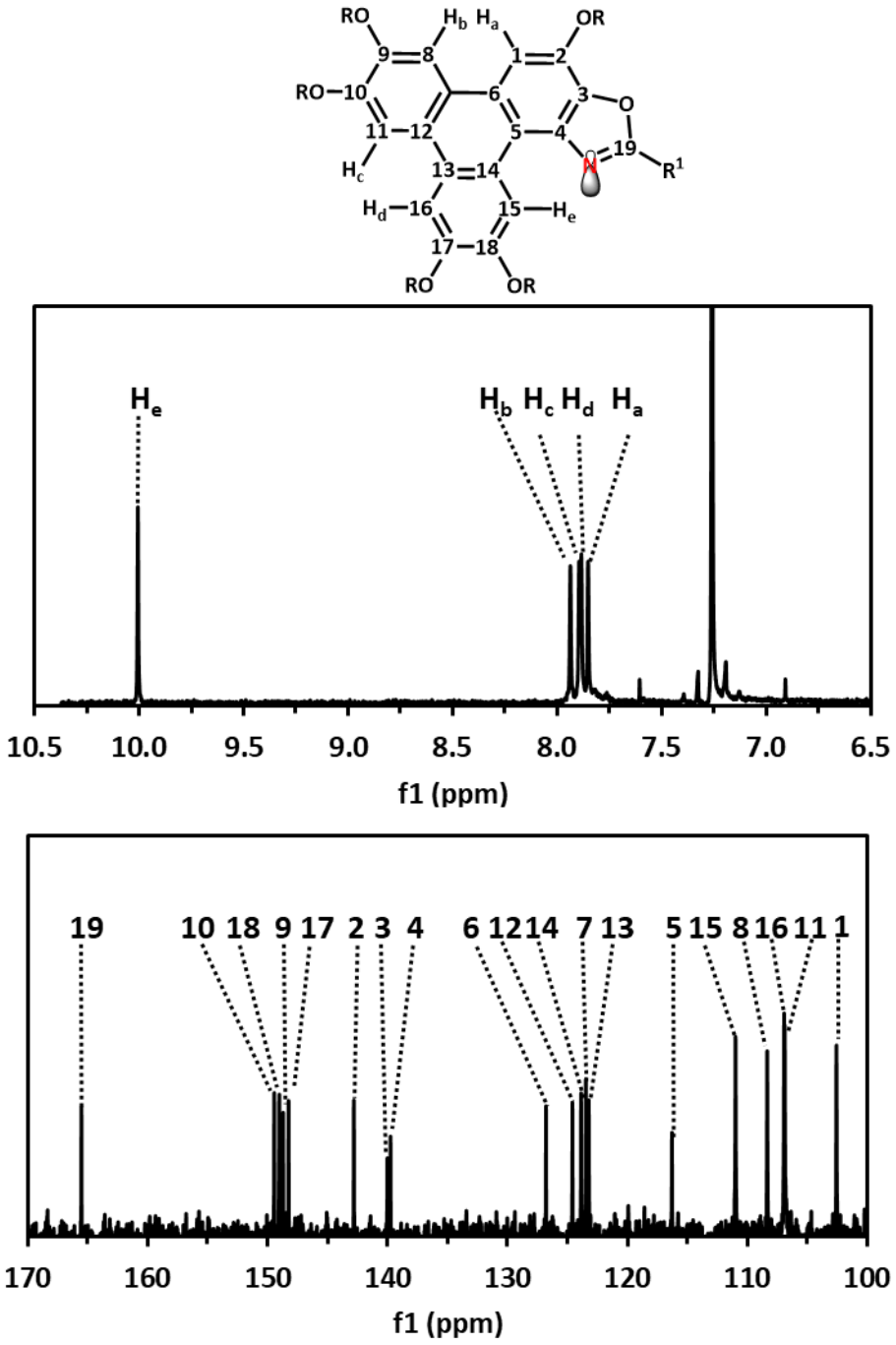

*Figure 3.5: ^{1}H NMR and ^{13}C NMR spectroscopy characterisation of **$Tp(C_5)_5OxC_4$** in $CDCl_3$ (7.26 ppm) using a Brücker AV 400 MHz spectrometer*

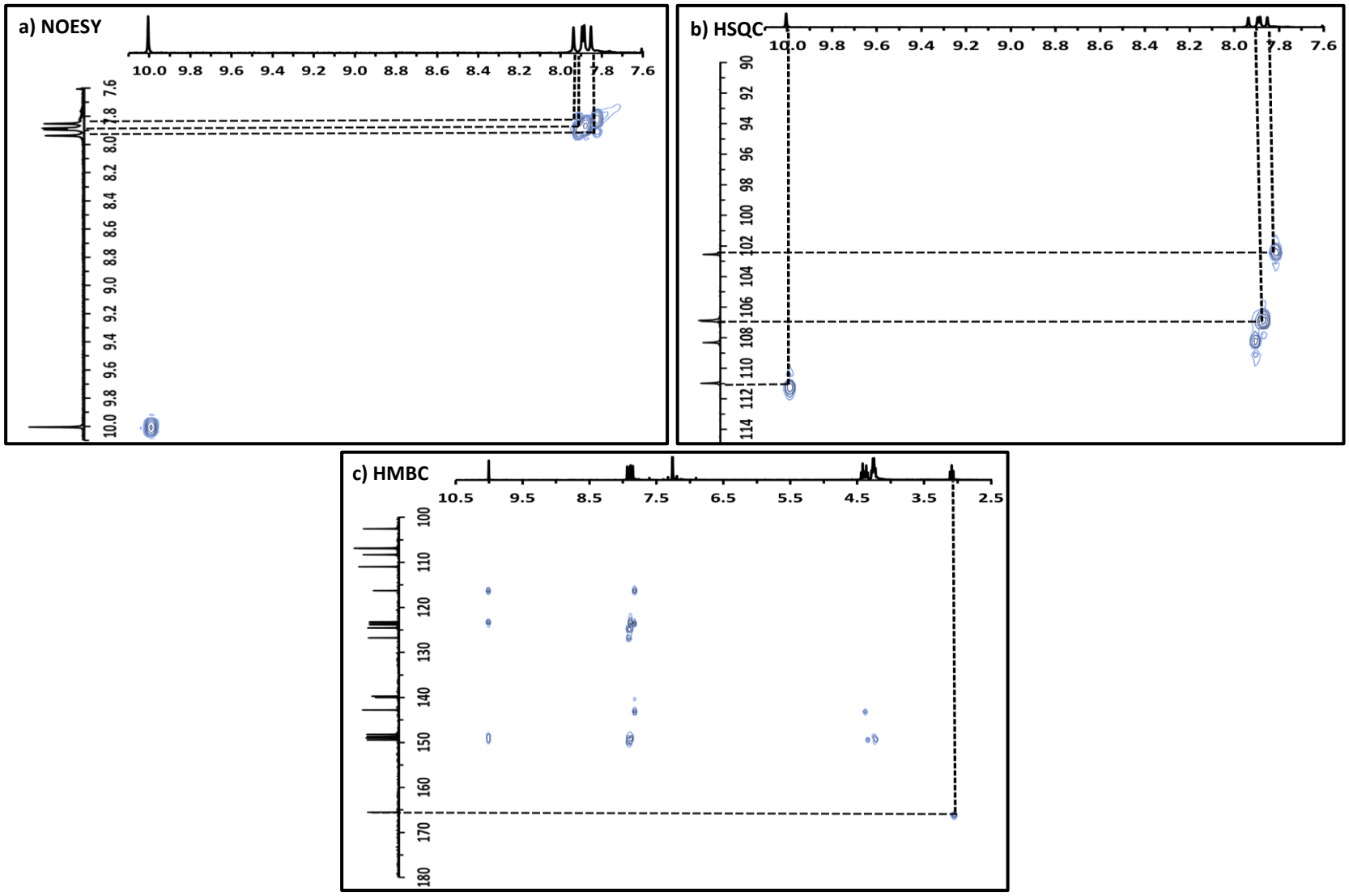

Figure 3.6: 2D NMR spectra ***Tp(C$_5$)$_5$OxC$_4$****, a) NOESY, b) HSQC, c) HMBC using a Brüker AV 400 MHz spectrometer*

NOESY (Figure 3.6a) shows that H_a interacts with H_b. H_c interacts with H_d leaving H_e with no interaction. This defined H_e as the peak at 10 ppm (downfield shifted due to the lone pair of the sp^2 nitrogen facing the proton). From here HSQC (Figure 3.6b) showed that carbon 15 connected to H_e and using this information HMBC (Figure 3.6c) was employed to assign the triphenoxazole ring. The assignment fits well with literature benzoxazoles. Carbon 19 at 165 ppm showed a connection with the first methylene group of the oxazole tail. This assignment as well as testing the validity of the structure, was useful in showing that H_e should always be considerably downfield shifted in triphenoxazoles, thus showing a signature peak, a useful feature in the synthesis of different oxazole structures.

3.2.3 Reaction Conditions Investigation:

Solvent and Temperature

The annulation reaction which led to the **Tp(C_5)$_5$OxC_4** was performed in *o*-xylene at 175 °C. High temperature reactions generate more side products.[25] Therefore it is desirable for reactions to be carried out at lower temperatures (Table 3.1).

Assuming a polar transition state polar solvents would lower the energy barrier,[26] and thus improve the efficiency of the reaction. To test this hypothesis we trialled a polar solvent acetonitrile and a non-polar solvent *n*-heptane (Table 3.1).

*Table 3.1: Comparison of yields with different solvents. 100 mg of **Tp(C$_5$)$_6$N$_3$** left for 16 h in 5 mL of solvent. Reaction performed within a sealed tube. Yield determined after purification*

Solvent	Temperature (°C)	Yield %
o-xylene	110	20
	130	28
	175	51
acetonitrile	110	17
n-heptane	110	15

All reactions performed at 110 °C showed a similar yield, indicating that the solvent properties such as dipole moment were not crucial for reaction. Reactions performed at 175 °C provided the highest yield, indicating high temperatures are necessary for reaction. To test to see if this reaction was specific to triphenylene derivatives or can be applied to other aromatic azides α to an ether centre we trialled the reaction on compound **1** (Figure 3.7).

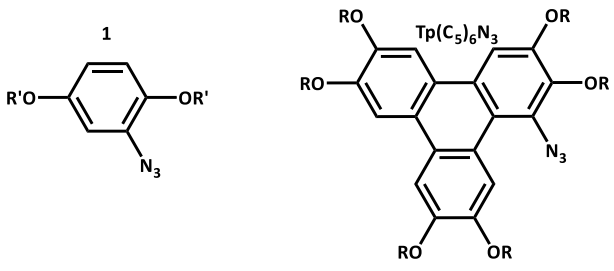

*Figure 3.7: Failed reaction of compound **1**. Where R= C$_5$H$_{11}$ R'= C$_2$H$_5$*

Compound **1** has an ether group para to the reactive centre, which allows for a rough electronic comparison between that and **Tp(C$_5$)$_6$N$_3$**. The reaction failing in the case of **1** could be for two reasons:

1) The increased aromaticity of triphenylene aids reaction;
2) The 2,5 diether substitution pattern is not conducive to oxazole formation.

Tp(C$_5$)$_6$N$_3$ remains the only molecule we have synthesised that undergoes this type of intramolecular annulation and forms an oxazole.

3.2.3.2 Photoactivation to Form Triphenoxazole

It is known that aryl-azides form nitrenes with UV light which could react to lead to a plethora of compounds.[27] Thus, it was not surprising that **Tp(C$_5$)$_6$N$_3$** spotted on a thin layer chromatography (TLC) plate blackened under a 4W 254 nm-365 nm light. To investigate this blackening an NMR sample in deuterated chloroform was irradiated for one hour with 254 nm UV light. The subsequent ^{1}H NMR spectrum revealed the identifying peak of H_e at 10 ppm for **Tp(C$_5$)$_5$OxC$_4$** (Figure 3.5) albeit in <5 % conversion by ^{1}H NMR spectroscopy. Irradiation for six hours increased the yield to ~10 % conversion by ^{1}H NMR spectroscopy. Thus, it can be concluded that the photochemical reaction rate for triphenoxazole formation is slow, at least at the wavelength and powers used here. However, in Section 3.2.7.4 it was possible to use this photoconversion reaction to produce a fluorescently patterned surface, which had a contrast between **Tp(C$_5$)$_6$N$_3$** and **Tp(C$_5$)$_5$OxC$_4$**.

3.2.3.3 Employing Catalysts for Triphenoxazole Formation

2.4.3.2.1 Rhodium Catalyst

Rhodium catalysts have long been used for catalysing azide reactions.[28] Driver *et al.* used rhodium octanoate as a catalyst to form carbazole (Scheme 3.1).[13] Thus, it seemed that this might be a route to forming the initially targeted carbazole derivate (Figure 3.3) from **$Tp(C_5)_6N_3$**. Driver *et al.* did their experiments to form carbazole at 60 °C, at this temperature **$Tp(C_5)_6N_3$** was unreactive. Elevating the temperature to 110 °C resulted in **$Tp(C_5)_5OxC_4$** being formed in quantitative yields (Scheme 3.6).

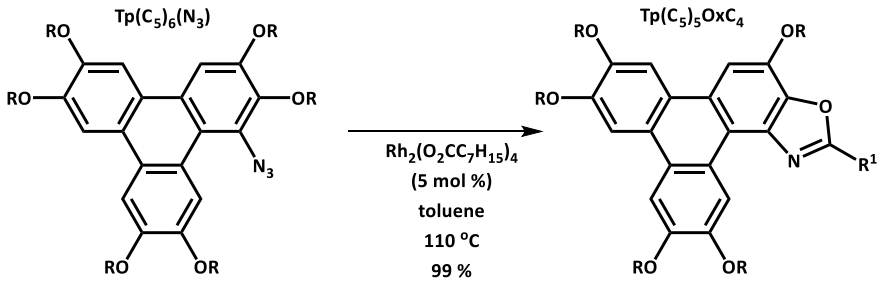

*Scheme 3.6: **$Tp(C_5)_5OxC_4$** Synthesis. R=C_5H_{11}, R^1= C_4H_9*

2.4.3.2.2 Palladium Catalysts

Gaunt *et al.*[29] used a primary or secondary amine to form a carbazole in 96 % yield, using a $Pd(OAc)_2$ catalyst (Scheme 3.7a). It seemed reasonable that **$Tp(C_5)_6NH_2$** (Scheme 3.7b) might facilitate a similar transformation to form the desired carbazole, **$Tp(C_5)_6Cb$** (Figure 3.3). Reaction of **$Tp(C_5)_6NH_2$** with the Gaunt reagents at room temperature afforded no carbazole or any other products. Upon raising the temperature of the reaction to 110 °C a highly fluorescent product was observed on the UV irradiated TLC plate. However, once again this turned out not to be the

desired carbazole **Tp(C$_5$)$_6$Cb**, nor **Tp(C$_5$)$_5$OxC$_4$**. Examination of the mass spectra revealed 42 mass units were missing, and the integration of the ^{1}H NMR spectrum was missing six protons. Both consistent with 3 methylene units missing from the structure, suggesting the butyl chain (**C$_4$**) has somehow been substituted with a methyl group (**C$_1$**) and **Tp(C$_5$)$_5$OxC$_1$** (Scheme 3.7b) had formed instead of **Tp(C$_5$)$_5$OxC$_4$**.

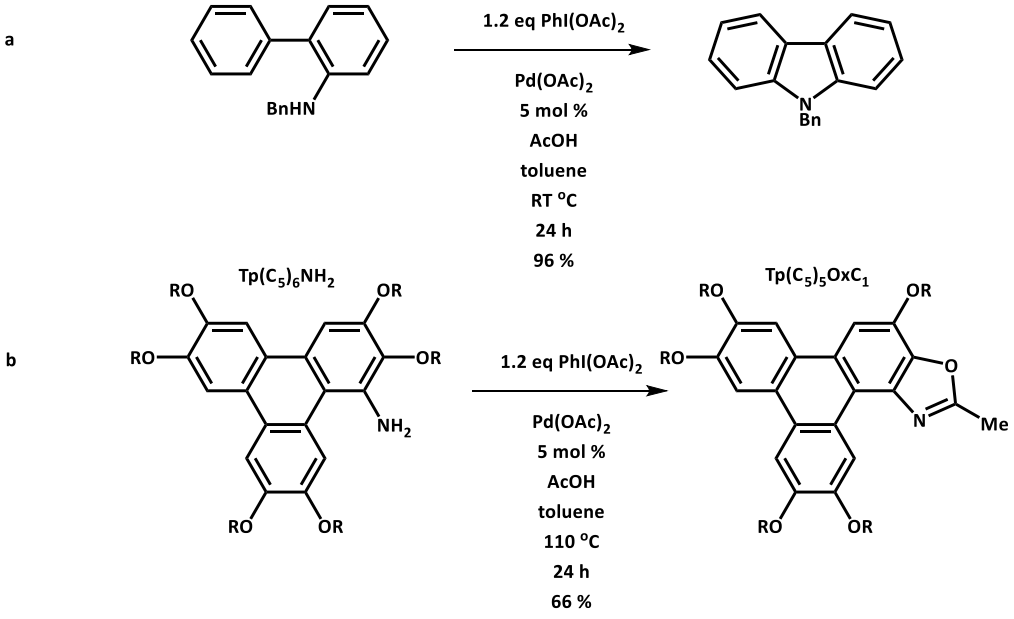

*Scheme 3.7: Gaunt et al. synthesis (a).[29] Our modified Synthesis **(b)**. R=OC$_5$H$_{11}$*

Consideration of the reagents used in the formation of **Tp(C$_5$)$_5$OxC$_1$** leads one to consider that the Me fragment has been derived from the acetyl fragments in the PhI(OAc)$_2$, AcOH or the Pd(OAc)$_2$. Given the yield is 66 % and Pd(OAc)$_2$ is present in only a catalytic quantity, it is highly probable that the PhI(OAc)$_2$ and/or AcOH is responsible for this new transformation. If this is the case then replacement of the acetate in PhI(OAc)$_2$ with other carboxylates opens the

possibility of, in principle, any organic acid being used to form $PhI(OOCR^1)_2$ leading to many different triphenoxazoles, **$Tp(C_5)_5OxR^1$** (Scheme 3.8).

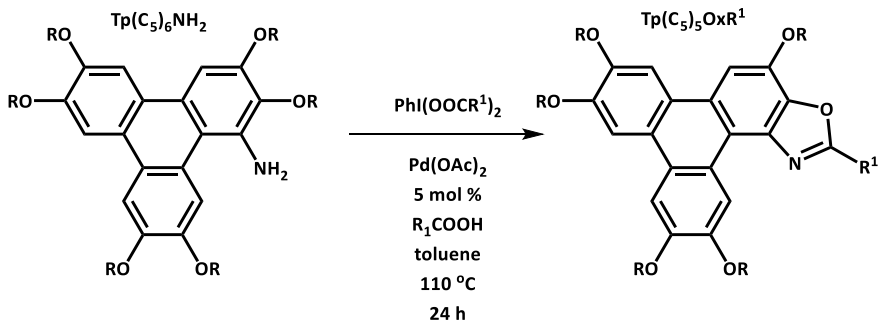

*Scheme 3.8: Generic reaction to form **$Tp(C_5)_5OxR^1$** where R^1= alkyl or phenyl*

Work by Baell *et al.* showed that $PhI(OAc)_2$ can be converted into a series of $PhI(OOCR^1)_2$, if the competing carboxylic acid has a higher boiling point than acetic acid.[30]

An example of this reaction is shown below in Scheme 3.9.

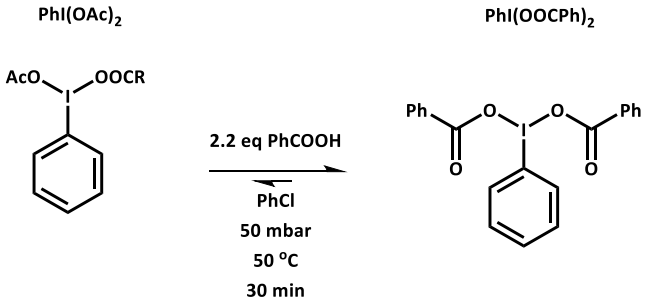

Scheme 3.9: Baell et al. Synthesis of $PhI(OOCPh)_2$[30]

The synthesis relies upon there being a dynamic equilibrium between acetic acid and the competing acid. The reaction is performed on the rotary evaporator, driving the equilibrium to the product by evaporative removal of the acetic.

Satisfyingly, exchange of $PhI(OAc)_2$ with $PhI(OOCPh)_2$ did lead to **$Tp(C_5)_5OxPh$** (Scheme 3.10).

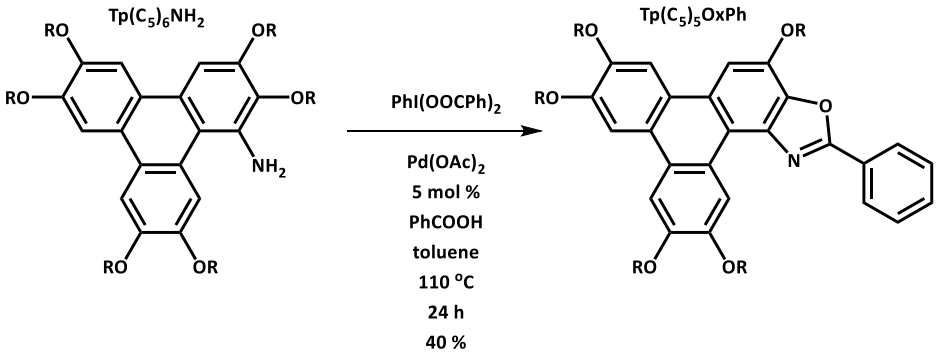

*Scheme 3.10: Synthesis of **$Tp(C_5)_5OxPh$** where $R=C_5H_{11}$*

It was found that storage of $PhI(OOCPh)_2$ for one week or more resulted in diminished yields. As such $PhI(OOCPh)_2$ had to be synthesised freshly before the annulation reaction. However, a further synthetic improvement was developed in which $PhI(OAc)_2$ and $Pd(OAc)_2$ could be reacted in the presence of 10 equivalents of RCOOH at 70 °C for 20 minutes in toluene, exploiting the dynamic equilibrium between the $PhI(OAc)_2$ and the competing acid (Scheme 3.11), pushing the equilibrium to $PhI(OOCPh)_2$ formation, to which **$Tp(C_5)_6NH_2$** is then charged, in a one-pot reaction, followed by heating under reflux for 24 hours (yield = 34 % for PhCOOH).

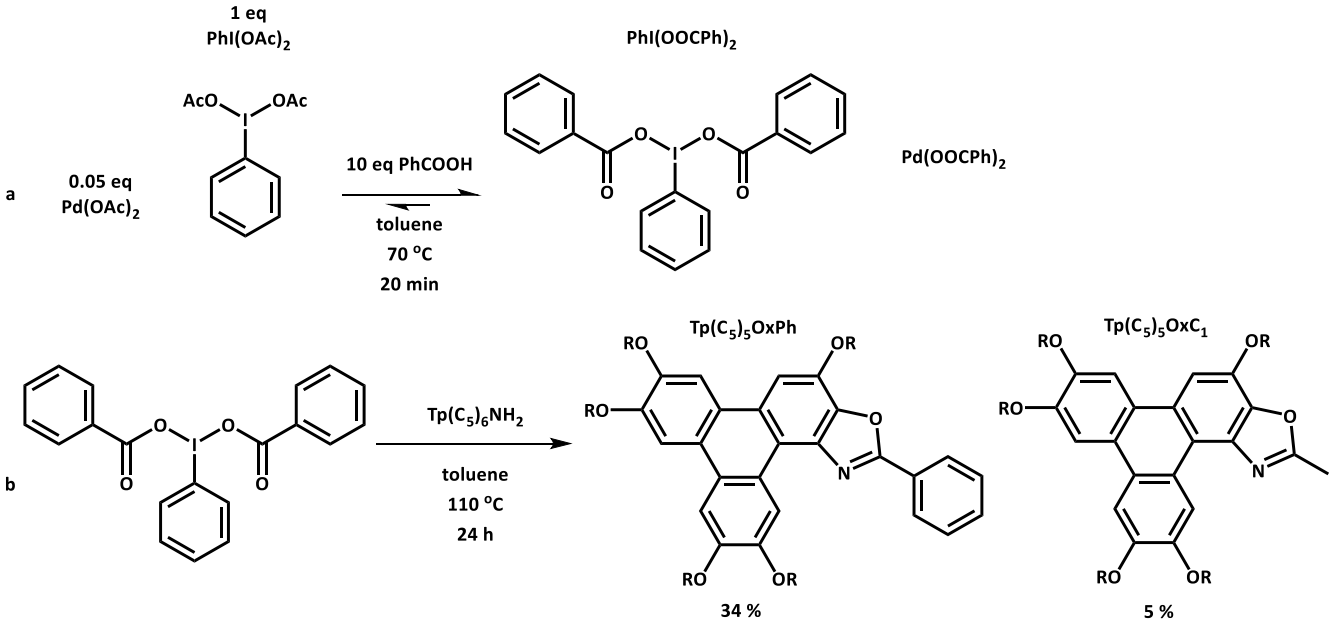

*Scheme 3.11: One-pot synthesis of **$Tp(C_5)_5OxPh$**, a) shows $PhI(OOCPh)_2$ and $Pd(OOCPh)_2$ formation in situ. b) shows **$Tp(C_5)_6NH_2$** addition to active iodine species. Where R= C_5H_{11}*

The one-pot synthesis of **$Tp(C_5)_5OxPh$** is clearly advantageous, however, ~5 % yield of **$Tp(C_5)_5OxC_1$** was also formed, but could be removed easily by column chromatography.

3.2.4 Investigation of the Triphenoxazole Formation Mechanism

In order to try and understand the mechanism of this reaction (Scheme 3.7), we trialled the reaction which formed **$Tp(C_5)_5OxC_1$** systematically excluding one reactant at a time, see (Table 3.2)

.

Table 3.2: Investigating reaction parameters on yield of triphenoxazole formation (Scheme 3.7)

Reaction Number	$Pd(OAc)_2$ mol %	$PhI(OAc)_2$ Molar Equiv.	AcOH Molar Equiv.	NaOAc Molar Equiv.	Yield %
0 (Scheme 3.7)	5	1.2	10	0	66
1	**Removed**	1.2	10	0	0
2	5	**Removed**	10	0	0
3	5	1.2	**Removed**	0	18
4	5	1.2	**Removed**	**10**	50
5	5	**5 (increased)**	10	0	0

In doing so we found that $Pd(OAc)_2$ (reaction 1) and hypervalent iodine species, $PhI(OAc)_2$ (reaction 2) were necessary for any oxazole formation.

There was a noticeable drop of yield to 18 % when acetic acid was excluded from the reaction (reaction 3). This could be for two reasons:

1) The reaction runs best in acid conditions and the acetic acid serves to maintain an acidic pH;
2) The acetic acid aids regeneration of either $Pd(OAc)_2$ or $PhI(OAc)_2$.

An experiment run using sodium acetate instead of acetic acid (reaction 4) showed an increase in yield to 50 %, indicating the acetate is regenerating either $Pd(OAc)_2$ or $PhI(OAc)_2$.

Another peculiar feature of this reaction was that when $PhI(OAc)_2$ equivalents were increased from 1.2 to 5 (reaction 5) did not yield any product. $PhI(OAc)_2$ is a mild oxidising agent and therefore could be destroying the product.

However, when **$Tp(C_5)_5OxC_1$** was solubilised with the reagents and reaction conditions for reaction 5 (Table 3.2) there was no product degradation, leading us to conclude that excess $PhI(OAc)_2$ interferes with the reaction pathway, such as poisoning the $Pd(OAc)_2$.

Finally, it is not yet understood whether the oxygen in the oxazole moiety originates from the $PhI(OAc)_2$ or from the ether in the hexaalkoxytriphenylene. A possible mechanism of the reaction where the oxygen originates from the $PhI(OAc)_2$ is shown below in Scheme 3.12.

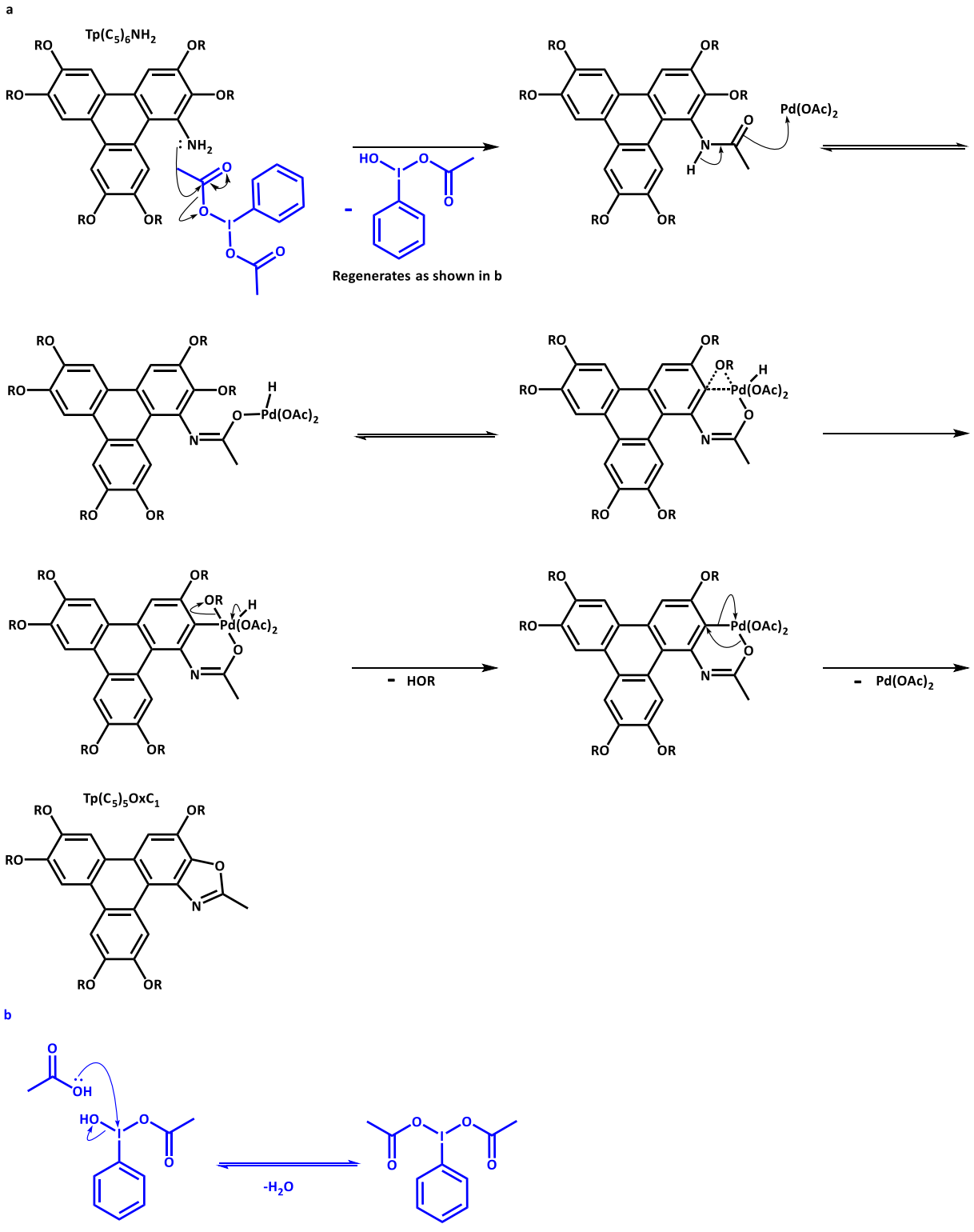

Scheme 3.12: a) Possible mechanism involving chain leaving as pentan-1-ol b) regeneration of $PhI(OAc)_2$

The mechanism in Scheme 3.12 has features similar to other mechanisms reported in the literature. A recent paper by Puddephatt *et al.* detail palladium insertion into Ar-O bonds.[31] Furthermore, it can be envisaged how large excess of $PhI(OAc)_2$ quenches the reaction, with an equilibrium set up during the palladium insertion, the $PhI(OAc)_2$ acts as a competitive inhibitor, saturating the catalytic binding sites. However, pentan-1-ol has a boiling point of 137 °C, and would be expected to be present in the crude material. Mass spectrometry of reaction samples have yet to show traces of pentan-1-ol. Using ^1H NMR spectroscopy on the crude sample would not help identify pentan-1-ol as it would be difficult to distinguish between the pentyl chains present in both starting material and product.

Isotopically labelled experiments using $Ac^{18}OH$ are planned to provide proof of whether the oxygen in the oxazole originates from the acid. Mass spectrometry of the product would show an increase in $[M+2]^+$ if the mechanism proposed in Scheme 3.12 is correct.

3.2.5 Attempted Introduction of Two and Three Oxazole Units

Attempts to form di and tri triphenoxazoles **$Tp(C_5)_4(OxC_4)_2$** and **$Tp(C_5)_3(OxC_4)_3$** through the rhodium catalysed method (Scheme 3.6) rely upon the synthesis of the bis- and tris-azide (Scheme 3.13).

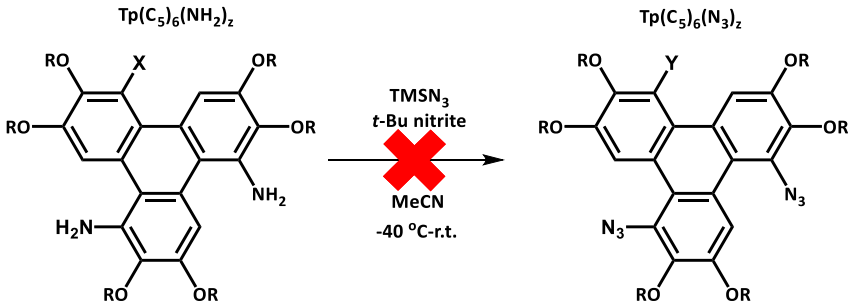

Scheme 3.13: Failed synthesis of ***Tp(C5)6(N3)2*** *and* ***Tp(C5)6(N3)3****. Where X= NH_2 or H, Y=N_3 or H and z= 2 or 3. R= C_5H_{11}*

At room temperature, no bis- or tris-azide was detected. The reaction was repeated at -40 °C, and the azides were detected by mass spectrometry. Unfortunately, side product formation dominated and as such clean di and tri triphenylene azides could not be isolated.

Furthermore, synthesis of the di and tri triphenoxazoles **$Tp(C_5)_4(OxC_1)_2$** and **$Tp(C_5)_3(OxC_1)_3$** were attempted using di and tri amine (**$Tp(C_5)_6(NH_2)_2$** and **$Tp(C_5)_6(NH_2)_3$**) shown in Scheme 3.14, where $PhI(OAc)_2$ and palladium were increased proportionately.

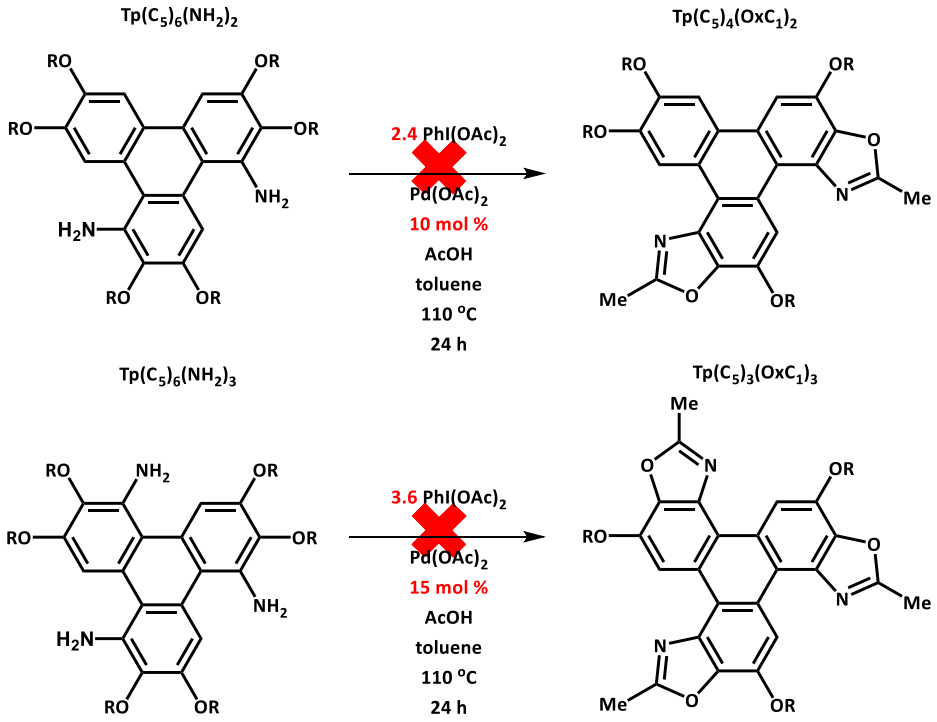

Scheme 3.14: Failed synthesis of ***$Tp(C_5)_4(OxC_1)_2$*** *and* ***$Tp(C_5)_3(OxC_1)_3$*** *where R = C_5H_{11}*

Initial explanations for the reaction failures in Scheme 3.14 was that the molar equivalents of $PhI(OAc)_2$ had been doubled or tripled from 1.2 to 2.4 and 3.6 respectively. As previously shown in Table 3.2 an increase in $PhI(OAc)_2$ led to no oxazole formation for the mono annulation.

However, when equivalents of $PhI(OAc)_2$ and $Pd(OAc)_2$ in Scheme 3.14 were halved still no product was observed. This led us to believe that the palladium gets poisoned during the reaction and as such does not form the oxazole product. This is evidenced by TLC analysis which shows a growth of a baseline spot- suggesting a palladium complex. Efforts to analyse this spot by mass spectrometry indicated many palladium species present.

The rest of this chapter will focus upon the liquid crystal and photoluminescent properties of **Tp(C$_5$)$_5$OxC$_4$** compared to the parent compound **Tp(C$_5$)$_6$**. Chapters 4 and 5 will focus upon the effect upon the liquid crystal and photoluminescent properties of modifying the triphenoxazole R group to aryl substituents, which will include **Tp(C$_5$)$_5$OxPh**.

3.2.6 Liquid Crystal Properties

As discussed in Chapter 1, a change in the ratio of rigid to flexible parts of a mesogen modifies the liquid crystal behaviour.[2] This is exemplified by Kumar's **Tp(C$_6$)$_5$ImC$_6$**, which in comparison to the parent **Tp(C$_6$)$_6$** displayed an increase in both the onset and clearing temperature of the DLC phase as well as a 6 °C increase in the DLC) range (Table 3.3).

3.2.6.1 Tp(C$_5$)$_5$OxC$_4$ Liquid Crystallinity

A study similar to Kumar *et al.* was performed here, where **Tp(C$_5$)$_5$OxC$_4$** was compared to **Tp(C$_5$)$_6$** (Figure 3.8 and Table 3.3).

Figure 3.8 shows the DSC curve of **Tp(C$_5$)$_5$OxC$_4$** and **Tp(C$_5$)$_6$**. **Tp(C$_5$)$_5$OxC$_4$** displays DLC behaviour at a significantly higher temperature to **Tp(C$_5$)$_6$**.

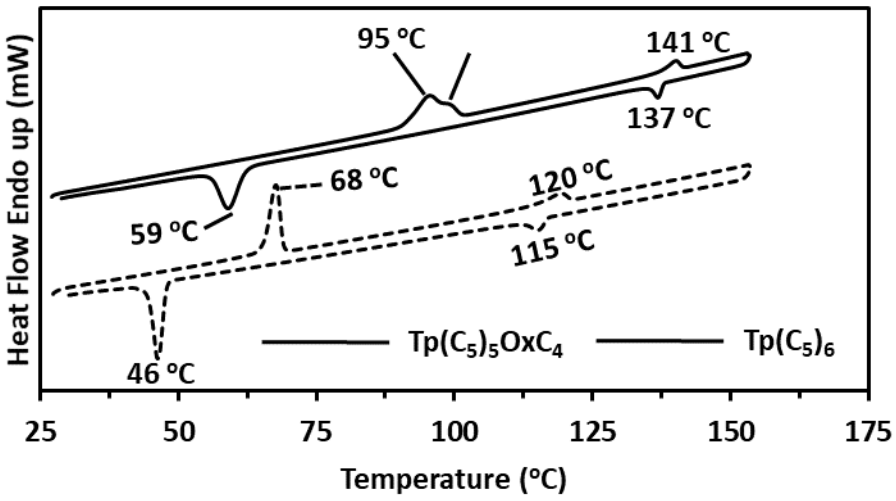

Figure 3.8: Normalised stacked DSCs (2nd heating and cooling cycle) ran at 10 °C min^{-1}

*Table 3.3: DSC summary With Kumar's **Tp(C6)5ImC6** and **Tp(C6)6** also summarised.[2] g= glass, Cr=Crystal, Col_h = hexagonal columnar, X= unknown, I= isotropic*

Compound	Heating			Cooling	
$Tp(C_5)_6$		68	120	115	46
		Cr-Col_h	Col_h-I	I-Col_h	Col_h-Cr
$Tp(C_5)_5OxC_4$	95	99	141	137	59
	Cr-X	X-Col_h	Col_h-I	I-Col_h	Col_h-Cr
$Tp(C_6)_6$ [2]		67	99	97	54
		Cr-Col_h	Col_h-I	I-Col_h	Col_h-Cr
$Tp(C_6)_5ImC_6$ [2]		108	146	141	
		g-Col_h	Col_h-I	I-Col_h	

The DSC data agrees with Kumar *et al.* **$Tp(C_6)_5ImC_6$** who attribute this to stronger intermolecular forces in the extended π system. Unlike Kumar *et al.* imidazole example the oxazole shows a decrease of 10 °C in the temperature range of liquid crystallinity during the heating cycle (42 °C compared to 52 °C). Another difference between the oxazole and the imidazole is the oxazole fully crystallises at 59 °C, missing the reverse transition seen in the heating at 95 °C. The transition at 95 °C was not visible by POM, and is assumed to be a glass phase, based on the findings of Kumar's imidazole derivative (Table 3.3). Both **$Tp(C_5)_5OxC_4$** and **$Tp(C_5)_6$** show an increase in DLC range when cooling, implying a preference for the DLC state. In a similar trend to the imidazole derivative the DLC temperature window of **$Tp(C_5)_5OxC_4$** is larger in the cooling phase when compared to **$Tp(C_5)_6$** (78 °C compared to 69 °C).

Furthermore **$Tp(C_5)_5OxC_4$** POM image showed similarities to Kumar's imidazole (Figure 3.9a and b).[2] The fan textures indicating Col_h had formed.

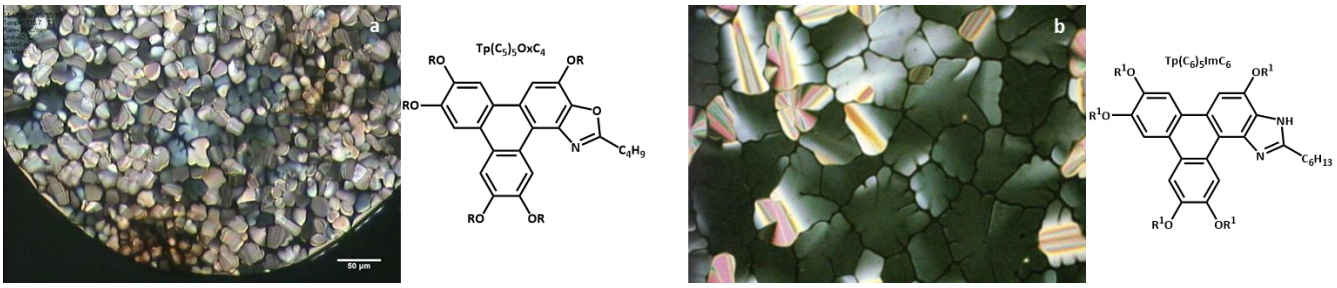

*Figure 3.9: a) POM image of **Tp(C5)5OxC4** cooling cycle (116 °C) R=C_5H_{11} compared to POM image b) Kumar's **Tp(C6)5ImC6** Col_h phase during cooling run. R^1= C_6H_{13}*

The Col_h phase of **Tp(C5)5OxC4** was confirmed by variable temperature XRD (Figure 3.10).

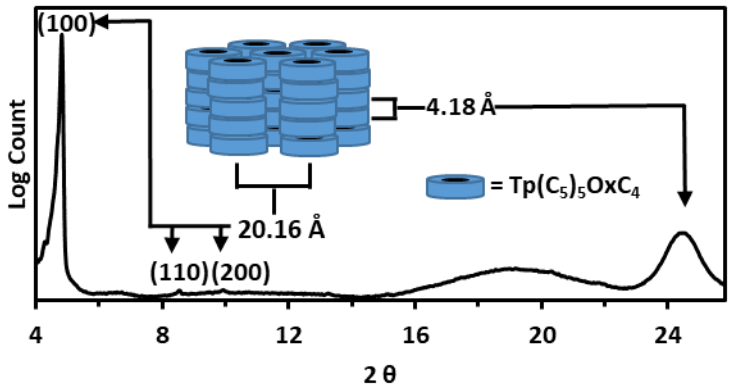

*Figure 3.10: XRD spectrum of **Tp(C5)5OxC4** cooling scan (110 °C) with cartoon diagram of structure*

Using Bragg's law and Miller indices for Col_h we found that **Tp(C5)5OxC4** has intermolecular distances of 20.16 Å and core-core separation of 4.18 Å (Figure 3.10). The intermolecular distance of **Tp(C5)5OxC4** is slightly larger than **Tp(C5)6** (18.95 Å)[32] and slightly smaller than Kumar *et al.* value for **Tp(C6)5ImC6** (21.33 Å)[2], which is expected due to **Tp(C5)5OxC4** being one carbon shorter in chain length.

3.2.7 Photophysical Properties of $Tp(C_5)_5OxC_4$

The photophysical data was gathered in three solvents (ethyl acetate, octan-1-ol and acetonitrile). These solvents were chosen for three reasons:

1) The dielectric constant of ethyl acetate, octan-1-ol and acetonitrile cover a broad range (6.0, 10.3, 37.5).[33-34] This range will show how the emission profile changes with polarity of the solvent;
2) These solvents range from non-polar aprotic, protic and polar protic. Oxazoles are hydrogen bond acceptors, so examination across these three solvents will elucidate any hydrogen bonding effects, as two are H-Bond acceptors (EtOAc and MeCN), and one is a H-Bond acceptor and donor (octan-1-ol);
3) There is a variance of viscosity. Ethyl acetate and acetonitrile have similar viscosities of 0.45 and 0.38 cP respectively, [35] whereas octan-1-ol has a much higher viscosity of 7.36 cP.[36] Lumophores that undergo twisted internal charge transfer (TICT) mechanisms generally show an increase of quantum yield with viscosity.[37]

Furthermore, the emission is also examined in the solid state.

3.2.7.1 UV Absorption in Solution

Figure 3.11 displays the UV absorption spectra of **$Tp(C_5)_5OxC_4$** and **$Tp(C_5)_6$** in ethyl acetate (1), octan-1-ol (2) and acetonitrile (3), at a concentration of 10^{-7} M, the λ_{max} and molar absorption coefficients (ϵ) are summarised in Table 3.4.

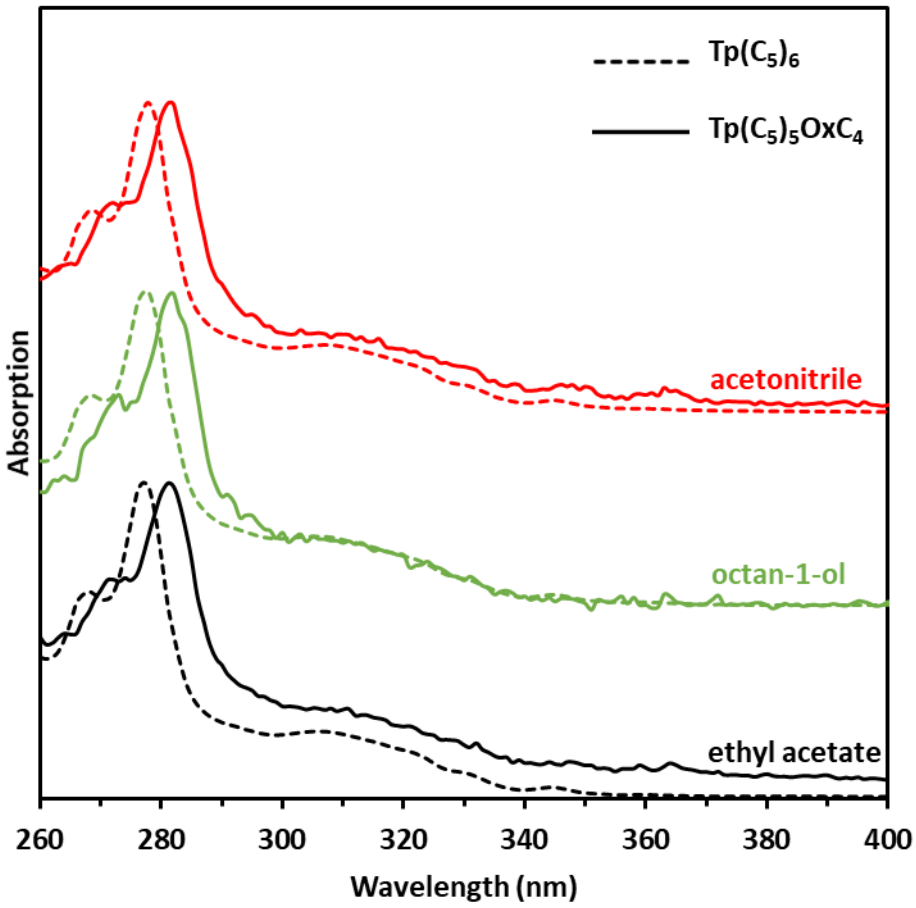

Figure 3.11: Normalised stacked UV absorption spectrum of ***$Tp(C_5)_6$*** *and* ***$Tp(C_5)_5OxC_4$***

The absorption spectra of the **$Tp(C_5)_6$** and **$Tp(C_5)_5OxC_4$** are all very similar, indicating that **$Tp(C_5)_5OxC_4$** excites through a similar pathway to **$Tp(C_5)_6$**. The UV absorption profile of **$Tp(C_5)_6$** is well understood.[38] The band at 278 nm is assigned as $S_4 \leftarrow S_0$ transition and the broad band at 310 nm is attributed as $S_3 \leftarrow S_0$ transition. **$Tp(C_5)_5OxC_4$** having a similar profile indicates that the transitions are probably the same as **$Tp(C_5)_6$**.

The absorption maxima (λ_{max}) of **Tp(C$_5$)$_5$OxC$_4$** is bathochromically shifted by 3 nm (281 nm) relative to **Tp(C$_5$)$_6$** (278nm), but there are no solvatochromic shifts.

Table 3.4: ϵ values at λ_{max} in ethyl acetate, octan-1-ol and acetonitrile. Values taken over 5 separate experiments using a Variant Cary 50 UV-Vis spectrometer and calculated using the Beer-Lambert Law.

	Tp(C$_5$)$_6$		**Tp(C$_5$)$_5$OxC$_4$**	
	λ_{max} (nm)	ϵ x 10^3 (M^{-1} cm^{-1})	λ_{max} (nm)	ϵ x 10^3 (M^{-1} cm^{-1})
Ethyl acetate	278	180 ± 15	281	160 ± 15
Octan-1-ol	278	83 ± 7	281	120 ± 12
Acetonitrile	278	170 ± 17	281	58 ± 6

The ϵ values of both **Tp(C$_5$)$_6$** and **Tp(C$_5$)$_5$OxC$_4$** across all solvents are large (where large is often quoted above >10,000 M^{-1} cm^{-1}).[39-40] The ϵ values for **Tp(C$_5$)$_6$** and **Tp(C$_5$)$_5$OxC$_4$** in ethyl acetate are similar. However, in octan-1-ol and acetonitrile there are significant and opposite solvatochromic effects, when comparing **Tp(C$_5$)$_6$** and **Tp(C$_5$)$_5$OxC$_4$**. The λ_{max} being the same across all solvents indicates no change in the molecules conformation that might result in this ϵ solvent variation.[41] Another possibility to rationalise this ϵ variation is aggregation, as aggregation leads to a reduction in ϵ,[42] as the solvent exposed p-surface area is reduced.[43] Thus, **Tp(C$_5$)$_5$OxC$_4$** might be aggregating in acetonitrile and **Tp(C$_5$)$_6$** in octan-1-ol.

Dynamic light scattering (DLS) performed upon both **Tp(C$_5$)$_5$OxC$_4$** and **Tp(C$_5$)$_6$** in acetonitrile at 10^{-7} to 10^{-6} M observed no aggregation. This does not directly rule out aggregation. DLS sensitivity drops with particle size- thus smaller particles require larger concentrations.[44] Therefore the tested solutions could be outside the sensitivity parameters of the DLS and the aggregation, if present, would involve small particle sizes.

3.2.7.2 Photoemission of Tp(C$_5$)$_5$OxC$_4$ in solution

The emission profiles (Figure 3.12) of **Tp(C$_5$)$_5$OxC$_4$** and **Tp(C$_5$)$_6$** are broadly similar, but less so than the absorption spectra, and do possess some notable differences.

Both compounds possess four solvent independent λ_{max} values at *c.a.* 365, 385, 405 and 425 nm in all three solvents (the latter 3 are vibrational overtones of the first band (V=0)), which is common for molecules with low degrees of freedom like **Tp(C$_5$)$_5$OxC$_4$** and **Tp(C$_5$)$_6$**.[41]

A noticeable difference in all three solvents is the dominant band of **Tp(C$_5$)$_5$OxC$_4$** belongs to the V=0, whereas, **Tp(C$_5$)$_6$** has a greater emission through the V=1.[45]

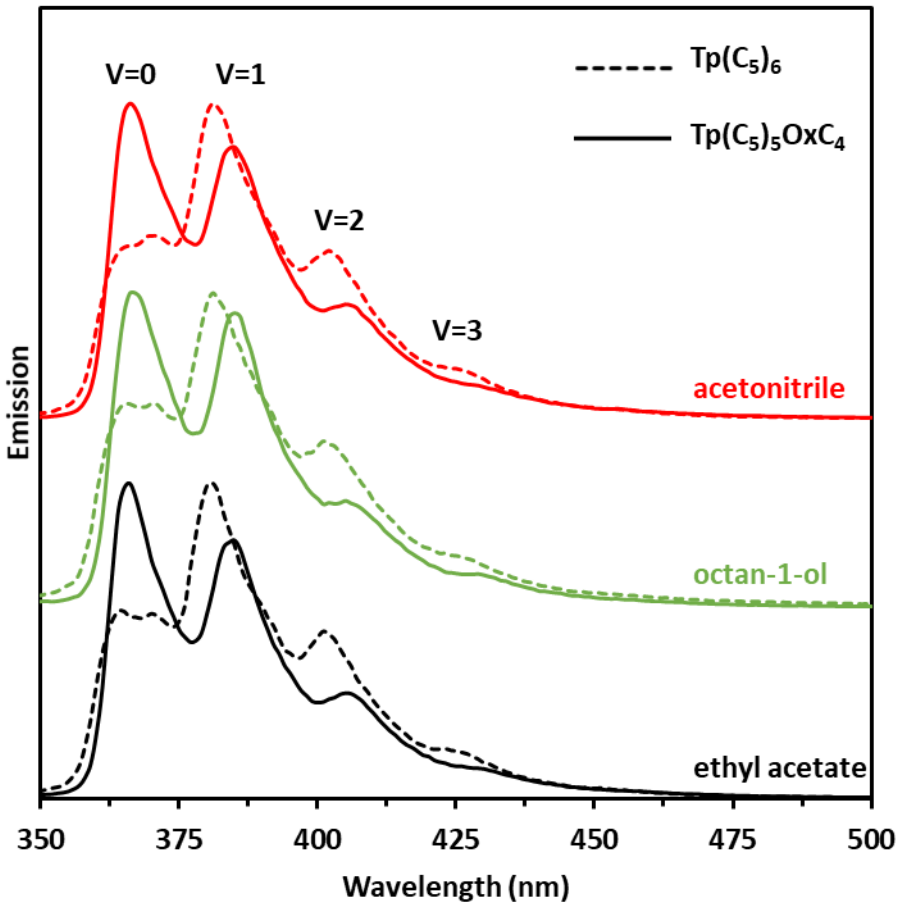

Figure 3.12: Normalised stacked UV-Vis emission spectrum: of ***Tp(C5)6*** *and* ***Tp(C5)5OxC4***

Shifts between maximum absorption (pseudo Stokes shift (pSS)) and maximum emission greater than 8000 cm^{-1} are often seen in the literature as large.[46] In that regards, both **Tp(C5)5OxC4** and **Tp(C5)6** have a large shift of 8200 cm^{-1} and 9800 cm^{-1}, respectively. **Tp(C5)6** having the larger shift due to the V=1 transition being preferred.

The quantum yield (Φ), brightness (the product of ϵ and Φ divided by 1000), pSS and steady state lifetime (τ) values of **Tp(C5)6** and **Tp(C5)5OxC4** are displayed in Table 3.5.

The Φ of both **Tp(C$_5$)$_6$** and **Tp(C$_5$)$_5$OxC$_4$** were both determined by integrating sphere. Furthermore, the Φ of **Tp(C$_5$)$_5$OxC$_4$** was also calculated using a reference ($Ru(bpy)_3Cl_2$) as a comparison.

*Table 3.5: Φ, Brightness, pSS and τ data for **Tp(C$_5$)$_6$** and **Tp(C$_5$)$_5$OxC$_4$**. X^2 for all τ data is between 1.0-1.2*

	Tp(C$_5$)$_6$				**Tp(C$_5$)$_5$OxC$_4$**				
	Integrating sphere (Φ)	Brightness	pSS (cm^{-1})	τ (ns)	Integrating sphere (Φ)	Referenced (Φ)	Brightness	pSS (cm^{-1})	τ (ns)
Ethyl acetate cP 0.45	0.09± 0.01	16 ± 2	9800	11 ± 1	0.18 ± 0.01	0.19 ± 0.02	29 ± 5	8200	6 ± 1
Octan-1-ol cP 7.36	0.17 ± 0.02	14 ± 4	9800	13 ± 1	0.30 ± 0.03	0.34 ± 0.03	36 ± 7	8200	8 ± 1
Acetonitrile cP 0.38	0.09 ± 0.01	15 ± 4	9800	11 ± 1	0.20 ± 0.02	0.20 ± 0.02	12 ± 2	8200	6 ± 1

The Φ values of **Tp(C$_5$)$_5$OxC$_4$** was found to be similar using both integrating sphere and $Ru(bpy)_3Cl_2$ reference methods for each solvent. The veracity of this result allowed us to use **Tp(C$_5$)$_5$OxC$_4$** as a Φ reference in Chapters 4 and 5.

The Φ of both **Tp(C$_5$)$_5$OxC$_4$** and **Tp(C$_5$)$_6$** are similar in ethyl acetate and acetonitrile, but is higher in octan-1-ol. As previously stated in Chapter 1, lumophores that emit *via* a TICT mechanism are

expected to have an increased Φ in viscous solvents.[37] Therefore this increase is expected, as ethyl acetate and acetonitrile have similar viscosities, and octan-1-ol has a higher viscosity.

However, octan-1-ol is a protic solvent that could potentially hydrogen bond to **Tp(C$_5$)$_5$OxC$_4$** and **Tp(C$_5$)$_6$**. Therefore, to rule out the possibility of hydrogen bonding between the solvent and solute being the source of the increase in Φ, ethanol was doped into a solution of **Tp(C$_5$)$_5$OxC$_4$** and **Tp(C$_5$)$_6$** in ethyl acetate (from 0.3-10 %w/w). If hydrogen bonding was a factor, a change in emission intensity would be expected, due to hydrogen bonding with the alcohol moiety in ethanol.[47] However, no change was observed. Therefore, octan-1-ol's high viscosity of 7.37 cP compared to ethyl acetate and acetonitrile (0.45 and 0.38 cP respectively) is seen as the dominant cause of the increased Φ.

The Φ of **Tp(C$_5$)$_5$OxC$_4$** is approximately double that of **Tp(C$_5$)$_6$** in all three solvents, which is expected as oxazoles have been shown to improve luminescent properties of molecular materials upon their covalent incorporation, by promoting luminescent relaxation.[48]

However, the brightnesses are within error the same for **Tp(C$_5$)$_6$** at ~ 15, whilst for **Tp(C$_5$)$_5$OxC$_4$** ethyl acetate are similar (within error) at ~33, whilst in acetonitrile the brightness is ~2.5 times lower (Table 3.5).

Due to superior absorptivity in ethyl acetate **Tp(C$_5$)$_5$OxC$_4$** is similarly bright in ethyl acetate as octan-1-ol and both significantly larger than **Tp(C$_5$)$_6$** in the same solvent. **Tp(C$_5$)$_5$OxC$_4$** displaying a lower ϵ in acetonitrile accounts for the lower brightness value as brightness is equal to Φ x ϵ. All values for brightness for **Tp(C$_5$)$_6$** were within error of each other.

The excited state lifetime data gathered on **Tp(C_5)$_6$** and **Tp(C_5)$_5$OxC_4** (Table 3.5) shows that both have lifetimes of 11-13 ns and 6-8 ns respectively. Typical organic singlet state emission has excited state lifetimes in between ~1-10 ns.[49] These results are concordant with literature lifetime data of **Tp(C_5)$_6$** where **Tp(C_5)$_6$** was found to have a lifetime of 9 ± 1 ns in CH_2Cl_2.[49] Furthermore **Tp(C_5)$_5$OxC_4** showing a decrease in lifetime when compared to **Tp(C_5)$_6$** is also consistent with literature on the effects oxazoles display. This is cited by Reisler *et al.* as being one of the reasons why the Φ increases, there being less time for non-radiative relaxation.[48]

3.2.7.3 Solid-State Emission

The emission spectra of **Tp(C_5)$_5$OxC_4** and **Tp(C_5)$_6$** in the solution state were significantly different: in that in the former the V=1 band dominated whilst in the latter the V=0 dominated.

Figure 3.13 illustrates the solution state and solid state spectra of **Tp(C_5)$_5$OxC_4** and **Tp(C_5)$_6$**.

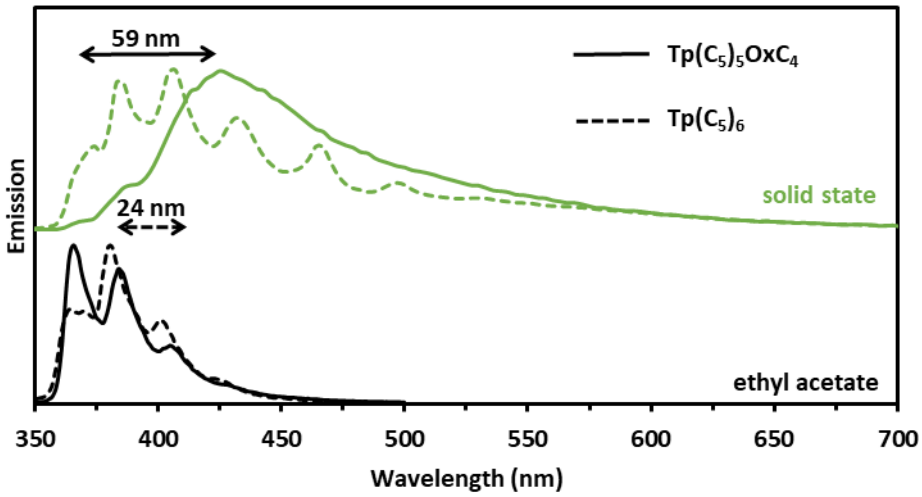

*Figure 3.13: Normalised emission spectrum: of **Tp(C5)6** and **Tp(C5)5OxC4**. Shift in peak position highlighted*

Figure 3.13 shows **Tp(C5)6** red shifted by 24 nm from solution (λ_{max} 380 nm) to solid state (λ_{max} 404 nm) and displays more structured bands. The red shift and increase in these bands is likely due to the packing of the **Tp(C5)6** where π-π interactions cause a stabilising effect of the transition state (See Section 1.5.2).[50] This is seen in other examples and discussed in Chapter 1.

Tp(C5)5OxC4 is red shifted by 59 nm from solution (λ_{max} 366 nm) to solid state (λ_{max} 424 nm) and has a continuum of energy levels in the solid state. This increased red shift when compared to **Tp(C5)6** implies that the transition state is further stabilised by the π-π interactions when compared to **Tp(C5)6**.[8] This could be put down to **Tp(C5)5OxC4** having a slightly larger aromatic area, due to the fused oxazole ring, and thus larger π-π interactions.[51] Furthermore, the continuum of energy levels shows an increase in vibrational modes[52] for **Tp(C5)5OxC4** a possible product of desymmetrising the molecule.[53]

The continuum of energy levels, shows an increase in vibrational modes for **$Tp(C_5)_5OxC_4$**, and the spectrum could also indicate a change in luminescent pathway and possible transfer of energy from one lumophore to another.[45] An experiment increasing the concentration of **$Tp(C_5)_5OxC_4$** from 10^{-5} M to 10^{-4} M (Figure 3.14) was performed to see at what concentration the spectrum begins to show similarities with the solid state spectrum.

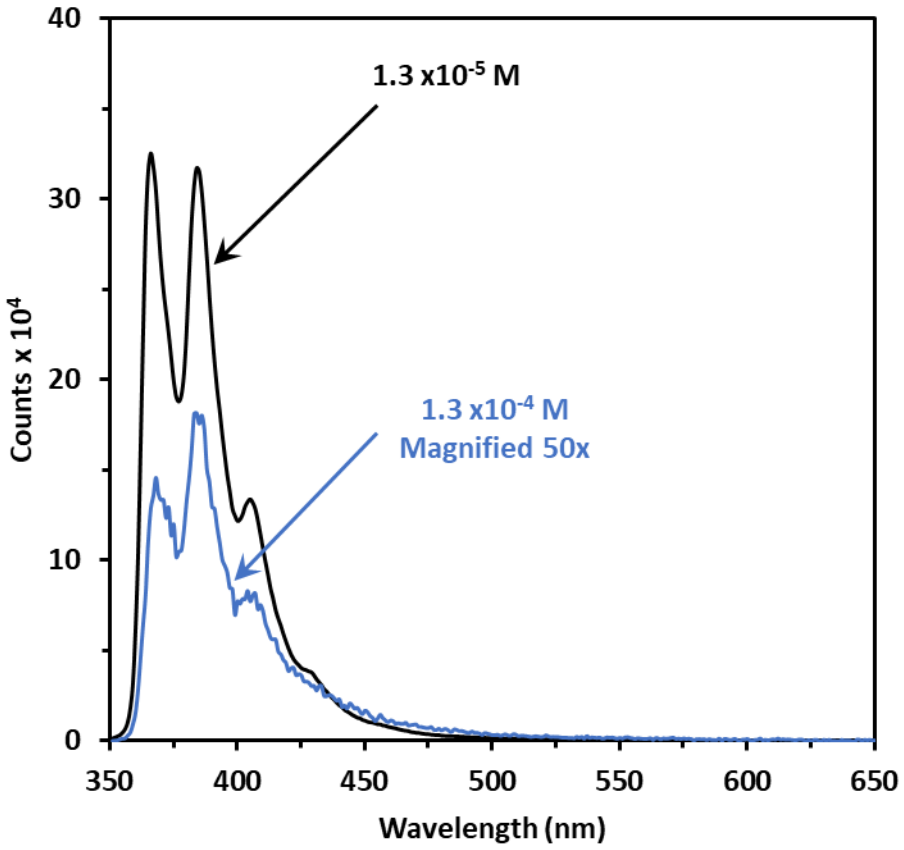

*Figure 3.14: Emission spectrums of **$Tp(C_5)_5OxC_4$** in ethyl acetate at 1.3 x10^{-5}M and 1.3 x10^{-4}M*

Figure 3.14 shows a difference in the bands as concentration increases. When concentration is increased to 1.3 x10^{-4} M the V=1 becomes the dominant band. The overall emission area becomes broader and there is a severe decrease in emission intensity due to self-quenching.

Concentration of **$Tp(C_5)_5OxC_4$** increases by a factor of 10, but emission intensity drops by a factor of 100. These changes in the spectrum show supramolecular effects are present at 1.3 $x10^{-4}$ M and that intermolecular bonding between **$Tp(C_5)_5OxC_4$** does affect emission.

3.2.7.4 Fluorescent Patterns Formed from Triphenoxazole

As can be seen from above pure **$Tp(C_5)_5OxC_4$** fluoresces much more strongly than **$Tp(C_5)_6N_3$**, and as noted in previously section 3.2.3.2 **$Tp(C_5)_5OxC_4$** can be formed in solution, slowly, from **$Tp(C_5)_6N_3$** photochemically. Thus, a solid-state photochemistry experiment was devised in which a hexagonally structured Cu TEM grid was placed over a glass surface spin-coated with **$Tp(C_5)_6N_3$**. The surface was then exposed to UV light (λ = 292 nm, 450 W) for 5 minutes. The Cu TEM grid was removed and imaged initially under:

(i) bright field mode (Figure 3.15a), where no contrast was observed between irradiated and unirradiated areas, and then

(ii) under 370 nm irradiation (Figure 3.15b) where a clear reproduction of fluorescent hexagons was observed suggesting surface conversion to **$Tp(C_5)_5OxC_4$**.

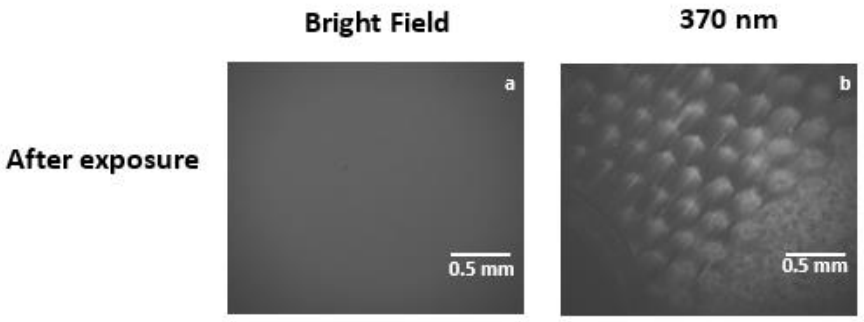

Figure 3.15: Images of a spin coated surface of ***Tp(C$_5$)$_5$N$_3$*** *exposed to 292nm light through a hexagonally structured Cu TEM grid under (a) Bright field and (b) 370 nm irradiation*

Fluorescently patterned surfaces have use in display technologies.[54] Though, this chemical system would be difficult to use due to the similar solubility characteristics **Tp(C$_5$)$_6$N$_3$** and **Tp(C$_5$)$_5$OxC$_4$** possess. However, solubilities could be markedly different by the introduction of a photoactivated polymerisable functional group into **Tp(C$_5$)$_5$N$_3$** that leads to commensurate oxazole formation and photopolymerisation.

3.3 Conclusions

In conclusion, we have shown the first synthesis of a novel fused triphenylene and oxazole ring. The chemistry, developed from existing literature on carbazole formation, exploited the molecules clear preference for oxazole, over carbazole, formation. From using rhodium octanoate as a catalyst, we formed **$Tp(C_5)_5OxC_4$** in quantitative yields.

The aromatic region of **$Tp(C_5)_5OxC_4$** was fully assigned by ^{1}H and ^{13}C NMR spectroscopy, revealing a significantly deshielded proton localised near the sp^2 nitrogen's lone pair.

$Tp(C_5)_5OxC_4$ liquid crystalline properties were examined and compared with the imidazole derivative **$Tp(C_6)_5Im(C_6)$** developed by Kumar *et al.* as well as the hexapentoxytriphenylene, **$Tp(C_5)_6$.** XRD studies revealed a Col_h phase at elevated temperatures, with similar molecular packing to Kumar imidazole. DSC and POM analysis of **$Tp(C_5)_5OxC_4$** revealed a broad range of liquid crystallinity (99- 141 °C) when heating, and a broader range when cooling (137-59 °C).

In solution, **$Tp(C_5)_5OxC_4$** displayed similar photophysical properties to **$Tp(C_5)_6$**. Showing structured bands and a large Stokes shift of 8200 cm^{-1}. **$Tp(C_5)_5OxC_4$** exhibited a superior Φ, ranging from 0.18-0.30 depending upon solvent, than **$Tp(C_5)_6$** (0.09-0.18). A result of this increase in Φ was that **$Tp(C_5)_5OxC_4$** was significantly brighter than **$Tp(C_5)_6$** in ethyl acetate and octan-1-ol. **$Tp(C_5)_5OxC_4$** showed a significant reduction in ϵ value in acetonitrile when compared to ethyl acetate and octan-1-ol (120,000 mol^{-1} cm^{-1} reduced to 59,000 mol^{-1} cm^{-1}) where aggregation of **$Tp(C_5)_5OxC_4$** is thought to have occurred. **$Tp(C_5)_5OxC_4$** emits a broad range emission in the solid state, dramatically red-shifted from 366 nm to 430 nm. This is significantly

different from **Tp(C_5)$_6$**, which emits defined structured peaks. The broad range of emission is seen as a continuum of energy levels. Variance of concentration of **Tp(C_5)$_5$OxC_4** found that at 10^{-4} M the spectrum began to change to that of the solid state. We hypothesise this as a result of intermolecular interactions between **Tp(C_5)$_5$OxC_4** units.

Further work into developing methods to make di and tri triphenoxazoles would lead to new exciting liquid crystals. Similarly, variance of chain length could be used to tweak liquid crystal transitions. Further work into why the α CH_2 is reactive should be studied perhaps through computational means.

3.4 Experimental

3.4.1 Supplementary Information

All reagents were used directly from the suppliers without further purification unless otherwise stated. All synthetic procedures were carried out under nitrogen and were magnetically stirred unless otherwise stated. All temperatures were internal flask temperatures unless otherwise stated. All solvents used were reagent grade unless otherwise stated. Heating under reflux consisted of a fitted glass condenser (water cooled). Column chromatographic separations were performed using Silica gel 120 (ICN Chrom 32-63 60 Å).

3.4.2 Analytical Techniques:

Analytical techniques used as confirmation were Electron Impact Mass Spectrometry (EIMS), Electrospray Mass Spectrometry (ES^+MS), infra-red spectroscopy and NMR spectroscopy. The NMR spectroscopic techniques used were ^1H NMR spectroscopy using the Brüker AVIII 300 spectrometer, ^{13}C NMR spectroscopy using the Brüker AVIII400 NMR spectrometer. Correlation spectroscopy (COSY), heteronuclear single quantum coherence (HSQC) and heteronuclear multiple bond correlation (HMBC) were performed on the Brüker AVIII400 NMR spectrometer.

Elemental analysis was performed on a Carlo Elba EA1110. Where the sample (1 mg) is heated to 1000 °C with a constant flow of helium. The combustion gas mixture is driven through an oxidation catalyst zone consisting of WO_3, which aids in delivering complete combustion. The

resultant mixture of components is separated by a Porapack column and detected by a thermal conductivity detector.

3.4.3 Photophysical Characterisation

UV-Vis spectroscopy data was obtained on either the Varian Cary 50 or Varian Cary 5000 spectrometer at a scan rate of 300 nm min^{-1}. Baseline corrections were performed for the appropriate solvent system and quartz cuvettes with a 1 cm path length were used.

Extinction coefficients (ϵ) were calculated by use of Equation 1, where A is absorbance maxima, c is concentration of sample and l is the path length of the cell (1 cm)

$$\epsilon = \frac{A}{cl}$$

Equation 1 ϵ calculation using Beer-Lambert Law

Emission spectroscopy data was gathered using the Edinburgh Instrument- FLSP920. Steady state measurements were obtained with a 450 W xenon arc lamp as the excitation source and the Hamamatsu R928 PMT as the detection source. A 345 nm cut off filter was used and the data was corrected using the correction file of the PMT. The F900 software was used to record the data.

Quantum yield (Φ) data was obtained on the spectrometer above. An integrating sphere was used to determine the Φ of **TpOxC$_4$** in ethyl acetate, octan-1-ol and acetonitrile. To provide accurate measurements quantum yield measurements were performed using 6 measurements

of both the reference and starting material at varying concentrations where absorbance at 286 nm did not surpass 0.2.

3.4.4 Photopatterning of $Tp(C_5)_6N_3$

Spin coating of **$Tp(C_5)_6N_3$** in chloroform (20 mg mL^{-1}) onto a quartz slide gave 300 nm thick films of good uniformity. A copper TEM grid (75 mesh) was placed gently upon the surface. The sample was then irradiated at 292 nm using the 450W Xenon arc lamp of the FLSP920 spectrometer appended with an Olympus IX71 Inverted Microscope, with a LUCPLFLN 40x0.60 NA objective for five minutes. The copper grid was removed and imaged in bright field mode and at 370 nm. Images were acquired with a Hamamatsu EM CCD C9100-13 camera.

3.4.5 Liquid Crystal Characterisation

All DSC scans were recorded using a Perkin Elmer Pyris 1. The cell is under nitrogen and water cooled. Scans take place between 25-250 °C with a scanning rate of 10 °C min^{-1}. Scans were cycled twice to confirm thermal events. Sample size of approximately 5 mg in aluminium pans with lids loosely fitted were used.

POM imaging was performed on an Olympus BX40 10x magnification lense. Capturing of images was obtained using a mounted JVC TKC1380 camera. Samples were heated using a Linkam TMS 93 mounted heating stage to 10 °C below any phase transition observed on the DSC scan. The sample was then heated 2-5 °C min^{-1} until melt, with images capturing any change.

XRD data was collected using Panalytical Empyrean. This was equipped with a positron sensitive detector and λ 1.5406 Å generated from a copper anode was used as the incident ray.

3.4.6 Synthetic Procedures

3.4.6.1 1,2-bis(pentyloxy)benzene

A solution of catechol (20.0 g; 182 mmol) in acetonitrile (650 mL) was stirred at room temperature for 20 min in a vessel fitted with a $CaCl_2$ drying tube. Potassium carbonate (87.0 g; 63.0 mmol) and potassium iodide (1.00 g; 6.02 mmol) was charged to the vessel and the resulting slurry was stirred for 15 min. The vessel was warmed to 40 °C. Neat liquid 1-bromopentane (97.0 g; 79.6 mL; 642 mmol) was added *via* syringe to the slurry over a period of 10 min. The slurry was heated under reflux for 48 h. The reaction contents were cooled to room temperature. The slurry was filtered and the resulting solid was washed with CH_2Cl_2 (3 x 30 mL). The combined filtrates were concentrated to an oil under reduced pressure. CH_2Cl_2 (100 mL) was added to the oil, which was washed with $NaOH_{(aq)}$ (100 mL; 1 M) followed by water (1.5 L). The organic phase was dried ($MgSO_4$) and filtered. The filtrate was evaporated to dryness under reduced pressure, and purified using flash chromatography (silica, 99.5 % *n*-hexane: 0.5 % ethyl acetate) to afford 1,2-bispentoxybenzene (43.3 g; 95 % yield) as a colourless oil. **^{1}H NMR** (300 MHz, $CDCl_3$) δ_H: 6.91 (4H, s), 4.01 (4H, t, *J* 6.65 Hz), 1.85 (4H, quin, *J* 6.71 Hz), 1.44 (8H, m), 0.95 (6H, t, *J* 7.10 Hz,) ppm. **^{13}C NMR** (100 MHz, $CDCl_3$) δ_C: 149.6, 121.3, 114.4, 69.6, 29.4, 28.6, 22.8, 14.4 ppm. **ES$^+$MS** *m/z*: 273.2 ($[M+Na]^+$ 50 %), 251.0 ($[M+H]^+$ 100 %), , 181.1 ($[C_{11}H_{17}O_2]^+$ 30 %), 134.1 ($[C_{11}H_{17}O_2+Na]^+$ 30 %), 111.0 ($[C_6H_6O_2]^+$ 21 %).

3.4.6.2 2,3,6,7,10,11-hexapentyloxytriphenylene $Tp(C_5)_6$

A solution of 1,2-bispentoxybenzene (19.0 g; 75.9 mmol) in anhydrous CH_2Cl_2 (100 mL) was charged to anhydrous $FeCl_3$ (37.0 g; 230 mmol). The slurry was stirred under a N_2 atmosphere for 30 min. Ice-cold MeOH(340 mL) was added slowly. Afterwards the slurry was cooled to -10 °C and left for 48 h. The slurry was filtered under vacuum and the resulting precipitate was washed with ice-cold MeOH (5 x 200 mL), and purified by flash column chromatography (silica, 99.5 % *n*-hexane: 0.5 % ethyl acetate) to afford **$Tp(C_5)_6$** (10.6 g; 56 % yield) as an off-white solid. **^{1}H NMR** (300 MHz, $CDCl_3$) δ_H: 7.84 (6H, s), 4.24 (12H, t, *J* 6.64 Hz), 2.43 (3H, quin, *J* 6.64 Hz), 1.58 (24H, m), 0.98 (18H, t, *J* 7.17 Hz) ppm. **^{13}C NMR** (100 MHz, $CDCl_3$) δ_C: 149.3, 124.0, 107.7, 70.1, 29.5, 28.8, 23.0, 14.5 ppm. **ES$^+$MS** *m/z*: 746.5 $[^{12}C_{47}{}^{13}CH_{72}O_6+H]^+$ 38 %), 745.5 ($[M+H]^+$ 100 %), 744.5 ($[M]^+$ 60 %).

3.4.6.3 1-nitro-2,3,6,7,10,11-hexapentyloxytriphenylene $Tp(C_5)_6NO_2$

Nitric acid (100 %; 0.3 mL, 6.76 mmol) was added to a solution of **$Tp(C_5)_6$** (3 g, 4.03 mmol), in glacial acetic acid (15 mL) and diethyl ether (60 mL) under a N_2 atmosphere. The solution was stirred for 20 min at room temperature and washed with water (2 x 100 mL). The organic phase was separated and evaporated to dryness *in vacuo* to leave a black solid, which was purified by flash column chromatography (silica; 70% *n*-hexane: 30 % CH_2Cl_2) to afford **$Tp(C_5)_6NO_2$** (2.77 g, 87 % yield) as a yellow solid. **^{1}H NMR** (300 MHz, $CDCl_3$) δ_H: 7.86 (1H, s), 7.76 (1H, s), 7.72 (1H, s), 7.71 (1H, s), 7.47 (1H, s), 4.25 – 4.18 (10 H, m), 4.11 (2 H, t, *J* 6.6 Hz), 1.99 – 1.85 (10 H, m), 1.83 – 1.78 (2H, m), 1.60 – 1.56 (12 H, m), 1.56 – 1.44 (12H, m), 1.02 – 0.95 (18H, m) ppm. **^{13}C NMR** (100 MHz, $CDCl_3$) δ_C: 150.5, 150.2, 149.0, 148.9, 143.8, 140.5, 126.7, 124.6, 124.4, 121.9, 119.3,

114.3, 107.7, 107.3, 107.2, 106.9, 106.4, 69.9, 69.6, 69.4, 69.3, 68.8, 29.8, 29.2, 29.1, 28.8, 28.4, 28.0, 22.6, 22.5, 14.1 ppm. **ES$^+$MS** *m/z*: 812.5 ([M+Na]$^+$ 100 %).

3.4.6.4 1-amino-2,3,6,7,10,11-hexapentyloxytriphenylene Tp(C_5)$_6$$NH_2$

Sodium borohydride (1.00 g, 27 mmol) was added in 10 small portions over a period of five minutes to a solution of nickel (II) chloride hexahydrate (2.17 g, 9.12 mmol) and **Tp(C_5)$_6$$NO_2$** (1.80 g, 2.28 mmol) in tetrahydrofuran (27 mL) and methanol (13 mL) under a N_2 atmosphere. The reaction mixture was stirred at room temperature for 3 h, and the resulting slurry was filtered under gravity and the precipitate washed with $CHCl_3$ (5 x 10 mL). The combined filtrates were evaporated to dryness *in vacuo* affording **Tp(C_5)$_6$$NH_2$** (1.54 g; 89 % yield) as a light yellow solid without need for further purification. **^{1}H NMR** (300 MHz, $CDCl_3$) δ_H: 8.82 (1 H, s), 7.84 (1 H, s), 7.80 (1 H, s), 7.78 (1 H, s), 7.38 (1 H, s), 4.62 (2H, br s), 4.25 – 4.15 (12 H, m), 1.97 – 1.90 (12 H, m), 1.57 – 1.55 (12H, m), 1.54 – 1.45 (12H, m), 1.00 – 0.96 (18H, m) ppm. **^{13}C NMR** (100 MHz, $CDCl_3$) δ_C: 150.9, 149.4, 148.8, 147.9, 147.4, 138.4, 135.4, 126.9, 124.6, 124.4, 123.9, 123.8, 113.9, 110.1, 108.3, 108.0, 106.9, 97.2, 73.1, 71.8, 69.9, 69.6, 69.3, 68.6, 30.3, 29.2, 28.5, 28.4, 22.6, 14.2 ppm. **ES$^+$MS** *m/z*: 782.5 ([M+Na]$^+$ 52 %), 760.6 ([M]$^+$ 100 %).

3.4.6.5 1-azido-2,3,6,7,10,11-hexapentyloxytriphenylene Tp(C_5)$_6$$N_3$

A solution of **Tp(C_5)$_6$$NH_2$** (100 mg; 0.13 mmol) in MeCN (10 mL) and PhMe (5 mL) was cooled to 0 °C using an ice bath under an N_2 atmosphere. After 10 mins at 0 °C *t*-butyl-nitrite (24 µL; 0.20 mmol) was added *via* syringe, through a rubber septum. After being allowed to stir for 10 mins $TMSN_3$ (35 µL; 0.26 mmol) was added *via* syringe. The resulting black solution was allowed to

warm to room temperature whilst stirring for 2 hrs. The reaction was then evaporated to dryness *in vacuo* and the solid was purified *via* flash column chromatography (Neutral alumina; 98% *n*-hexane: 2 % ethyl acetate) to afford **Tp(C$_5$)$_6$N$_3$** as a yellow solid (100 mg; 96 %). **^{1}H NMR** (300 MHz, $CDCl_3$) δ 9.32 (1H, s), 7.84 (1H, s), 7.82 (1H, s), 7.81 (1H, s), 7.74 (1H, s), 4.23 (12H, m), 1.96 (12H, m), 1.51 (24H, m) 1.01 (18H, m) ppm. **^{13}C NMR** (100 MHz, $CDCl_3$) δ 150.5, 149.8, 148.8, 148.1, 147.7, 142.9, 129.8, 126.9, 124.7, 124.3, 123.0, 122.8, 118.2, 118.1, 112.1, 108.3, 107.1, 106.8 103.5, 74.4, 69.9, 69.7, 69.5, 69.2, 68.9, 29.4, 29.2, 29.1, 29.1, 29.0, 28.5, 28.4, 28.3, 28.2, 22.6, 22.6, 14.1 ppm. **ES$^+$MS** *m/z*: 808.52 $[M+Na]^+$.

3.4.6.6 2,3,6,11,12-pentapentyloxy-8-butyl-triphenoxazole Tp(C$_5$)$_5$OxC$_4$

A solution of **Tp(C$_5$)$_6$N$_3$** (100 mg; 0.13 mmol) in dry PhMe (8 mL) was added to a flask containing rhodium octanoate dimer (8 mg; 0.01 mmol), under a N_2 atmosphere. This was then heated and held at reflux for 20 h. The reaction was cooled to room temperature and then evaporated to dryness *in vacuo,* the solid was then purified *via* flash column chromatography (silica; 95 % *n*-hexane*: 5 %* ethyl acetate) to afford **Tp(C$_5$)$_5$OxC$_4$** as a white solid (96 mg; 99 %). **^{1}H NMR** (300 MHz, $CDCl_3$) δ_H: 10.01 (1 H, s), 7.94 (1 H, s), 7.90 (1 H, s), 7.88 (1 H, s), 7.85 (1 H, s), 4.42 (2 H, t, *J* 6.7 Hz), 4.37 (2H, t, *J* 6.7 Hz) 4.29 – 4.23 (6 H, m), 3.09 (2 H, t, *J* 7.5 Hz), 2.05– 1.92 (10 H, m), 1.62 – 1.43 (24 H, m), 1.06 – 0.96 (18 H, m) ppm. **^{13}C NMR** (100 MHz, $CDCl_3$) δ_C: 165.6, 149.5, 149.1, 148.7, 148.3, 142.9, 140.1, 139.8, 124.6, 123.9, 123.5, 123.3, 116.3, 111.0, 108.3, 106.9, 106.8, 102.6, 69.9, 69.6, 69.5, 68.8, 29.2, 29.0, 28.8, 28.4, 28.3, 22.6, 22.4, 14.2, 13.9 ppm. **ES$^+$MS** *m/z*: 756.5 ($[M+H]^+$ 15 %), 778.5 ($[M+ Na]^+$ 100 %). **IR λ^{-1}** (neat): 3112w (C-H), 2953m (C-

H), 1617w (C=N), 1517w (benzene ring), 1259s (C-O), 1177s (C-O), 1159s (C-O) cm^{-1}. Elemental analysis Found: C, 76.09; H, 9.17; N, 1.95. $C_{48}H_{69}NO_6$ requires C, 76.25; H, 9.20; N, 1.85 %.

3.4.6.7 2,3,6,11,12-pentapentyloxy-8-methyl-triphenoxazole $Tp(C_5)_5OxC_1$

A slurry of **$Tp(C_5)_6NH_2$** (100mg; 0.01 mmol), $PhI(OAc)_2$ (51 mg; 0.16 mmol) and palladium diacetate (1 mg; 0.005 mmol) in a mixture of PhMe (5 mL) and acetic acid (1 mL) in PhMe (5 mL) under an N_2 atmosphere was heated and held at reflux for 72 h. The reaction was then cooled to room temperature and washed with 1M NaOH (1M; 2x10mL). The organic phase was evaporated to dryness *in vacuo*. The solid was then purified *via* flash column chromatography (60 % *n*-hexane: 40 % CH_2Cl_2) to afford the product as a white solid (64 mg; 66 %). **^{1}H NMR** δ_H: (400 MHz, $CDCl_3$) 9.94 (1H, s), 7.94 (1H, s), 7.90 (1H, s), 7.89 (1H, s), 7.85 (1H, s), 4.42 (2H, t, *J* 6.7), 4.38 (2H, t, *J* 6.8), 4.30 – 4.24 (6H, m), 2.81 (3H, s), 1.99 (10H, m), 1.65 – 1.53 (10H, m), 1.52 – 1.44 (10H, m), 1.03 – 0.96 (15H, m) ppm. **^{13}C NMR** δ_C: (100 MHz, $CDCl_3$) 162.4, 149.9, 149.4, 149.1, 148.8, 143.2, 140.8, 140.2, 127.2, 125.0, 124.2, 123.9, 123.7, 116.7, 111.6, 108.8, 107.3, 107.2, 102.9, 70.3, 70.2, 69.88, 69.40, 29.60, 29.5, 29.3, 28.8, 28.8, 28.6, 23.0, 15.2, 14.5 ppm. **MALDI** *m/z*: 714.5 ($[M]^+$ 100%).

3.4.6.8 Phenyl-λ^3-iodanediyl dibenzoate $PhI(OOCPh)_2$

A solution of benzoic acid (80 mg; 0.66 mmol) and diacetoxyiodobenzene (100 mg; 0.30 mmol) in chlorobenzene (5 mL) was mixed at 50 °C under reduced pressure of 50 mmbar for 30 minutes. The solution was then dried *in vacuo* and the solid was dissolved in CH_2Cl_2 (10 mL) and washed with NaOH (1M; 2x10mL). The organic phase was evaporated to dryness *in vacuo* to

afford **PhI(OOCPh)$_2$** as a white solid ((111 mg, 100 %). **^{1}H NMR** (300 MHz, $CDCl_3$) δ_H: 8.24 (2H, d, J=7.4 Hz) 7.93 (4H, d, *J* 7.4 Hz), 7.65-7.60 (m, 1H), 7.57-7.47 (4H, m), 7.37 (4H, t, *J* 7.4 Hz) ppm. **^{13}C NMR** (100 MHz, $CDCl_3$) δ_C: 171.3, 135.0, 132.3, 131.6, 130.9, 130.1, 129.9, 128.1, 122.2 ppm.

3.4.6.9 2,3,6,11,12-pentapentyloxy-8-phenyl-triphenoxazole Tp(C$_5$)$_5$OxPh

A slurry of benzoic acid (160 mg; 1.31 mmol), palladium diacetate (0.005 mmol) and iodobenzene diacetate (0.16 mmol) in PhMe (5 mL) was heated at 70 °C under N_2 for 20 min. **Tp(C$_5$)$_6$NH$_2$** (100mg, 0.13 mmol) in PhMe (2 mL) was added and the reaction was heated and held at reflux for 72 h. The mixture was cooled to room temperature and diluted with CH_2Cl_2 (20 mL). The mixture was washed with 1M NaOH (2 x 20 mL) and the organic phase was dried *in vacuo*. The crude black solid was purified *via* flash column chromatography (60 % *n*-hexane: 40 % CH_2Cl_2) to afford **Tp(C$_5$)$_5$OxPh** as a white solid (35 mg; 34 %). **^{1}H NMR** (300 MHz, $CDCl_3$) δ_H: 10.13 (1 H, s), 8.40 – 8.37 (2 H, m), 7.92 (1H, s), 7.88 (1H, s), 7.87 (1H,s), 7.77 (1H, s), 7.57-7.55 (1H, m), 4.48 – 4.43 (4 H, m), 4.30 – 4.23 (6 H, m), 2.12 – 1.92 (10 H, m), 1.69 – 1.54 (12 H, m), 1.53 – 1.45 (12 H, m), 1.04 – 0.96 (18 H, m) ppm. **^{13}C NMR** (100 MHz, $CDCl_3$) δ_C: 161.4, 149.5, 149.0, 148.7, 148.3, 142.9, 140.5, 140.2, 131.2, 128.9, 127.5, 127.1, 124.7, 123.8, 123.4, 123.3, 116.4, 110.9, 108.2, 106.8, 106.6, 103.8, 69.8, 69.5, 68.9, 29.2, 29.0, 28.4, 28.3, 22.6, 22.6, 14.1 ppm. **ES$^+$MS *m/z***: 775.5 ([M]$^+$ 22 %), 776.5 ([M+H]$^+$ 37 %), 798.5 ([M+Na]$^+$ 100 %). Elemental analysis Found: C, 77.46; H, 8.44; N, 1.75 %. $C_{50}H_{65}NO_6$ requires C, 77.38; H, 8.44; N, 1.80 %.

3.5 References

[1] C. Viegas-Junior, A. Danuello, V.S Bolzani, E.J. Barreiro and C.A.M. Fraga, *Curr. Med. Chem.*, 2007, **14**, 1829

[2] S. Kumar and S.K. Gupta, *Tetrahedron Lett.*, 2011, **52**, 5363

[3] W. Xiao, Z. He., S. Remiro-Buenamanana, R.J. Turner, M. Xu, X. Yang, X. Jing and A.N. Cammidge, *Org. Lett.*, 2015, **17**, 3286

[4] M. Manickam, G. Cooke, S. Kumar, P.R. Ashton, J.A. Preece and N. Spencer, *Mol. Cryst. Liq. Cryst.*, 2003, **397**, 99

[5] S. Choi , T. Wada , Y. Zhang , H. Kimura-suda , J. Kim and H. Sasabe, *Mol. Cryst. Liq. Cryst.*, 1998, **316**, 83

[6] P. Günter. and J.P. Huignardm, Photorefractive Materials & Their Applications, Springer-Verlag, New York, 1988

[7] M.D. Halling, A.M. Orendt, M. Strohmeier, M.S. Solum, V.M. Tsefrikas, T. Hirao, L.T. Scott, R.J. Pugmire and D.M. Grant, *Phys. Chem. Chem. Phys.*, 2010, **12**, 7934

[8] J.W. Levell, A. Ruseckas, J.B. Henry, Y. Wang, A.D. Stretton, A.R. Mount, T.H. Galow and J.D. Samuel, *J. Phys. Chem. A*, 2010, **114**, 13291

[9] M.J. James, R.E. Clubley, K.Y. Palate, T.J. Procter, A.C. Wyton, P. O'Brien, R.J.K. Taylor and W.P. Unsworth, *Org. Lett.*, 2015, **17**, 4372

[10] J.A. Jordan-Hore, C.C.C Johansson, M. Gulias, E.M. Beck and J. Gaunt, *J. Am. Chem. Soc.*, 2008, **130**, 16184

[11] C. Suzuki, K. Hirano, T. Satoh and M. Miura, *Org. Lett.*, 2015, **17**, 1597

[12] W.C.P. Tsang, N. Zheng and S.L. Buchwald, *J. Am. Chem. Soc.*, 2005, **127**, 14560

[13] B.J. Stokes, B. Jovanović, H. Dong, K.J. Richert, R.D. Riell and T.G. Driver, *J. Org. Chem*., 2009, **74**, 3225

[14] S.P. Lee and H.W. Moore, *Heterocycles*, 1982, **19**, 2019

[15] N. Boden, R.J. Bushby, A.N. Cammidge and G. Headdock, *J. Mater. Chem.*, 1995, **5**,

[16] G. L'Abbe, *Chem. Rev.*, 1969, **69**, 345.

[17] R.S. Pottorf, N.K. Chadha, M. Ketkevics, V. Ozola, E. Suna, H. Ghane, T. Regberg and M.R. Player, *Tetrahedron Lett*., 2003, **44***,* 175

[18] P. Boissarie, Z. Hamilton, S. Lang, J.A. Murphy and C.J. Suckling, *Org. Lett*, 2011, **13**, 6184

[19] H.A. van Kalkeren, C. te Grotenhuis, F.S. Haasjes, C.A. Hommersom, F.P.J.T. Rutjes and F.L. van Delft, *Eur. J. Org. Chem.*, 2013, 7059

[20] R.D. Viirre, G. Evindar and R.A. Batey, *J. Org. Chem.*, 2008, **73***,* 3452

[21] G. Bastug, C. Eviolitte and I.E, Markó, *Org. Lett,* 2012, **14**, 3502

[22] J.A. Seijas, M.P. Vázquez-Tato, M.R. Carballido-Reboredo, J. Crecente-Campo and L. Romar-López, *Synlett*., 2007, 313

[23] D.S. Bose and M. Idrees. *Synthesis*, 2010, 398

[24] V.P. Srivastava and L.D.S. Yadav, *Synlett*, 2013, **24**, 2758

[25] A.M. Heintz, D.J. Duffy, S.L. Hsu, W. Suen, W. Chu and C.W. Paul, *Macromolecules*, 2003, **36**, 2695

[26] P.J. Dyson and P.G. Jessop, *Catal. Sci. Technol.*, 2016, **6**, 3302

[27] https://tools.thermofisher.com/content/sfs/brochures/TR0011-Photoactivate-aryl-azides.pdf [25/09/2017]

[28] S.H. Park, J. Kwak, K. Shin, J. Ryu, Y. Park and S. Chang, *J. Am. Chem. Soc.*, 2014, **136**, 2492

[29] J.A. Jordan-Hore, C.C.C. Johansson, M. Gulias, E.M. Beck and M.J. Gaunt, *J. Am. Chem. Soc.*, 2008, **130**, 16184

[30] D.L. Priebbenow, R.W. Gable and J. Baell, *J. Org. Chem.*, 2015, **80**, 4412

[31] A. Behnia, P.D. Boyle, J.M. Blacquiere and R.J. Puddephatt, *Organometallics*, 2016, **35**, 2645

[32] M.A. Levulut, *J. Chim. Phys. Phys-Chim. Biol.*, 1983, **80**, 149

[33] http://macro.lsu.edu/HowTo/solvents/Dielectric%20Constant%20.htm [25/09/2017]

[34] http://www.stenutz.eu/chem/solv6.php?name=octanol [25/09/2017]

[35] http://macro.lsu.edu/HowTo/solvents/viscosity.htm [25/09/2017]

[36] A. Bhattacharjee and M.N. Roy, *J. Chem. Eng. Data*, 2010, **55**, 5914

[37] S. Howell, M. Dakanali, E.A. Theodorakis and M.A. Haidekker, *J. Fluoresc*, 2012, **22**, 457

[38] A. Herbaut and E. Baranoff, *CHIMIA*, 2015, **69**, 520

[39] P. Wang, C. Klein, R. Humphrey-Baker, S.M. Zakeeruddin and M. Grátzel, *J. Am. Chem. Soc.*, 2005, **127**, 808

[40] www2.chemistry.msu.edu/faculty/reusch/virttxtjml/spectrpy/uv-vis/uvspec.htm [25/09/2017]

[41] Z.R. Grabowski and K. Rotkiewicz, *Chem. Rev.*, 2003, **103**, 3899

[42] P.J. Camp, A.C. Jones, R.K. Neely and N.M. Speirs, *J. Phys. Chem. A.*, 2002, **106**, 10725

[43] J. Lakowicz, Principles of Fluorescence Spectroscopy, 3rd Edition, *Springer*, 2006

[44] J. Philo, *AAPS J.*, 2006, **8**, E564

[45] D. Markovitsi and I. Lécuyer, *J. Chem. Soc. Faraday Trans.*, 1991, **87**, 1785

[46] G. Blasse and B.C. Grabmaier, Luminescent Materials, *Springer Science & Business Media,* 2012, 121

[47] G. Guilbault, Practical Fluorescence, 2nd Edition, CRC Press, 1990

[48] A. Reisler, L.J. Leyshon, D. Saunders, M.V. Mijovic, A. Bright and J. Bogie, *J. Am. Chem. Soc.*, 1971, **94**, 2414

[49] K.J. Lee, J.H. Woo, E. Kim, Y. Xiao, X. Su, L.M. Mazur, A.J. Attias, F. Fages, O. Cregut, A. Barsella, F. Mathevet, L. Mager, J.W. Wu, A. D'Aléo and J.C. Ribierre, *Phys. Chem. Chem. Phys.,* 2016, **18**, 7875

[50] J.W. Levell, A. Ruseckas, J.B. Henry, Y. Wang, A.D. Stretton, A.R. Mount, T.H. Galow and I.D.W. Samuel, *J. Phys. Chem. A.*, 2010, **114**, 13291

[51] X. Feng, V. Marcon, W. Pisula, M.R. Hansen, J. Kirkpatrick, F. Grozema, D. Andrieko, K. Kremer and K. Müllen, *Nature Materials*, 2009, **8**, 421

[52] M. Shigeta, M. Morita and G.I. Konishi, *Molecules*, 2012, **17**, 4452

[53] www.mcgill.ca/biochemistry/files/biochemistry/404_silvius_09.pdf [25/09/2017]

[54] J. Wang, X. Wang and Y. He, *J. Polym. Sci. Part B Polym. Phys.*, 2016, **54**, 1838

4 Triphenoxazoles: Introduction of Electron-Withdrawing Substituents to Enhance the Photophysical Properties

4.1 Introduction

As discussed in Chapter 1 modifying the energy between absorption and emission is desired for multiple purposes, which include use in dyes,[1] probes[2] and sensors.[3] Organic molecules hold advantages over organometallics fluorescent complexes in certain aspects, often exhibiting a greater quantum yield and providing more facile and cheaper routes for synthesis.[4] However, organometallics which use heavy metals benefit from larger Stokes shifts, and increased life times, due to the use of an organic light harvester.[5]

A commonly employed method to synthesise molecular fluorophores is to create a molecule which have electron donating and an electron withdrawing moieties, coupled electronically through conjugation, a so-called push-pull or donor-acceptor system.[6] This molecular arrangement lowers the excited state energy, thus providing a large Stokes shift.[7] Selected examples of lumophores with this kind of system are shown below (Scheme 4.1). Thus, modifying the relative donor and acceptor properties of the push-pull system it is possible to tune the absorption and emission energies.

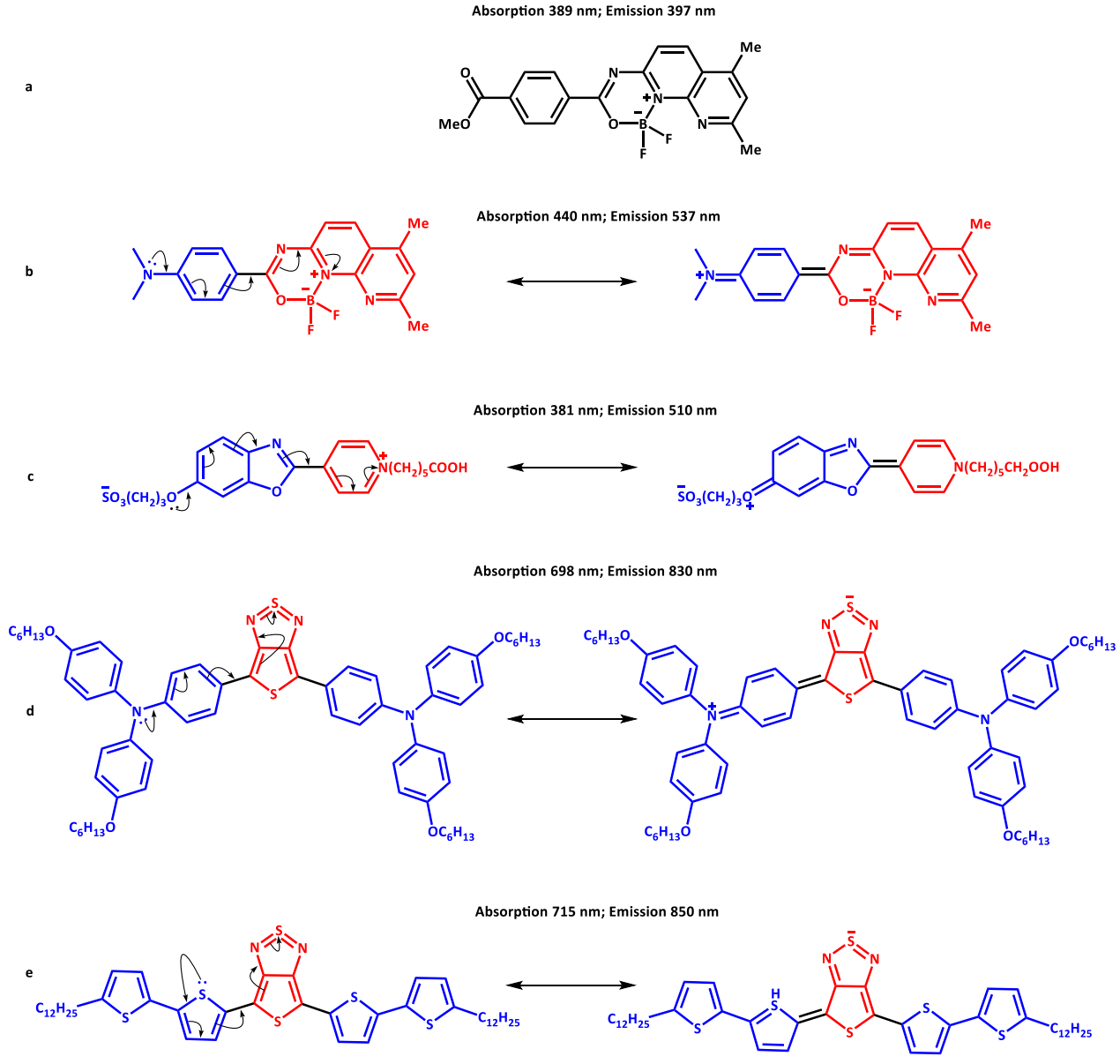

Scheme 4.1:non donor-acceptor system (a) and a selection of donor-acceptor systems (a-e). [6-8] *Donor (blue) and acceptor (red) with flow of electrons depicted*

Scheme 4.1a and b displays an excellent comparison between Wu *et al.'s* non donor-acceptor system (Scheme 4.1a) where the Stokes shift is 8 nm and a donor-acceptor system (Scheme 4.1b) where the Stokes shift is 97 nm.[6] The tertiary amine (Scheme 4.1b) can donate (push)

electrons through to the electron withdrawing (pulling) pyridinium ring, whereas the example in Scheme 4.1a, where both ends are acceptors, result in a pull-pull system and hence no lowering of the excited state energy, resulting in a significantly smaller Stokes shift.

Another push-pull system is displayed in Scheme 4.1c. The commercialised molecule[7] has an ether group which acts as the donor and the pyridinium group as the acceptor.

Scheme 4.1d-e displays Delcamp *et al.* donor-acceptor-donor examples. These are significantly different to the previous examples having a plane of symmetry, through the heteroaromatic acceptor, being flanked by two identical donor groups (triphenylamine (Scheme 4.1d) and thiophene (Scheme 4.1)).[8] Interestingly, the triphenylamine (Scheme 4.1d) has a similar Stokes shift to the thiophene (Scheme 4.1e) despite the fact the tertiary amine is a stronger donor than the thiophene.[8] Delcamp *et al.* reasoned that the triaryl amine suffers from significant steric interactions of the aryl groups, which will adopt a non-planar propeller conformation resulting in a lower degree of nitrogen lone pair conjugation than might be expected.

4.1.1 Aim of Research in this Chapter

Considering how push-pull systems can be used to modulate absorption and emission energies of organic species, examination of the substituted triphenoxazoles in Chapter 3 (**Tp(C_5)$_5$OxR**), suggests that these could simply be converted into push-pull systems: The triphenylene moiety decorated with the five electron-donating alkoxy chains will provide the 'push' moiety coupled conjugatively *via* the oxazole unit to an electron withdrawing (pull) R group

Thus, with this concept of enhancing the electron withdrawing ability of the R group in **Tp(C$_5$)$_5$OxR^1**, a series of fluorinated phenyl groups was envisaged to give **Tp(C$_5$)$_5$OxPh*x*F** (Figure 4.1), where the pK_a of the corresponding acids might correlate with the electron withdrawing power on the molecular structure, and be used to correlate with the photophysical properties.

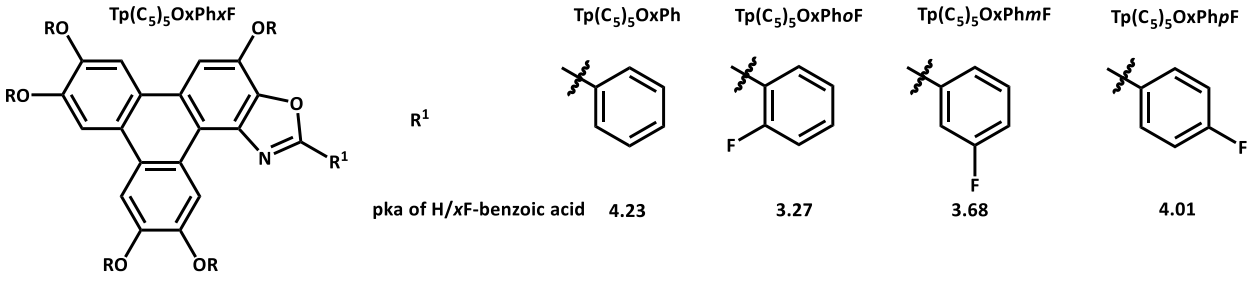

*Figure 4.1: The **Tp(C$_5$)$_5$OxPhxF** series: pka values from literature [9-10]*

4.2 Results and Discussion

4.2.1 Synthesis of the Tp(C$_5$)$_5$OxPh*x*F Series

Chapter 3 investigated in detail the methods to form triphenoxazoles **Tp(C$_5$)$_5$OxC$_4$** (Scheme 4.2a) and **Tp(C$_5$)$_5$OxPh** (Scheme 4.2b).[11] Herein the synthetic strategy is extended to introduce *o*-, *m*-, *p*-fluoro-phenyl substituents (Scheme 4.2b), *via* the 3 fluoro-benzoic acids, to form the series **Tp(C$_5$)$_5$OxPh*x*F** series.

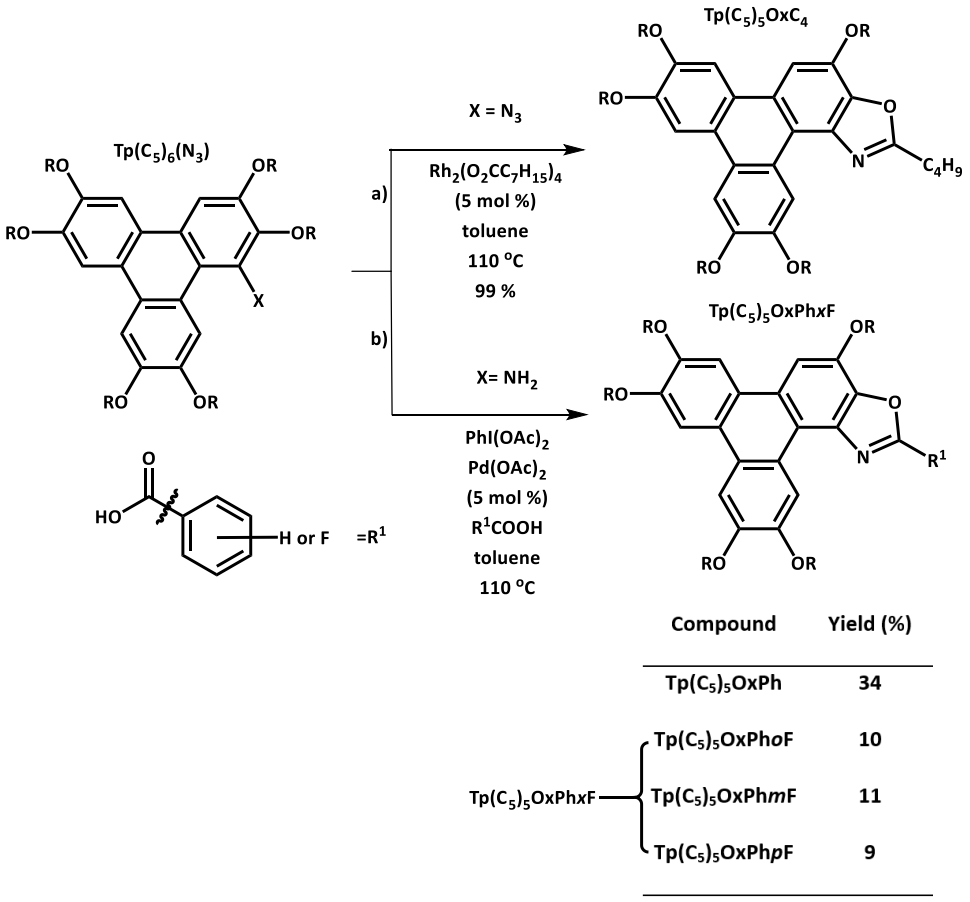

Compound	Yield (%)
$Tp(C_5)_5OxPh$	34
$Tp(C_5)_5OxPhoF$	10
$Tp(C_5)_5OxPhmF$	11
$Tp(C_5)_5OxPhpF$	9

Scheme 4.2: The synthetic routes which were used in Chapter 3 to try and form carbazole derivatives, but which led to the triphenoxazoles a) ***$Tp(C_5)_5OxC_4$*** *and b)* ***$Tp(C_5)_5OxPh$*** *and the* ***$Tp(C_5)_5OxPhxF$*** *series*

It should be noted that yields of the **$Tp(C_5)_5OxPhxF$** series (9-11 %) are lower than **$Tp(C_5)_5OxPh$** (34%). Fluorine having a similar hydrodynamic size to hydrogen ruled out steric effects, hence the electron withdrawing nature of the fluorine and reduction in pK_a, relative to benzoic acid is likely to be the cause of the loss in yield. This reasoning is in line with the mechanism proposed in Section 3.2.4 (the crucial step shown below in Scheme 4.3).

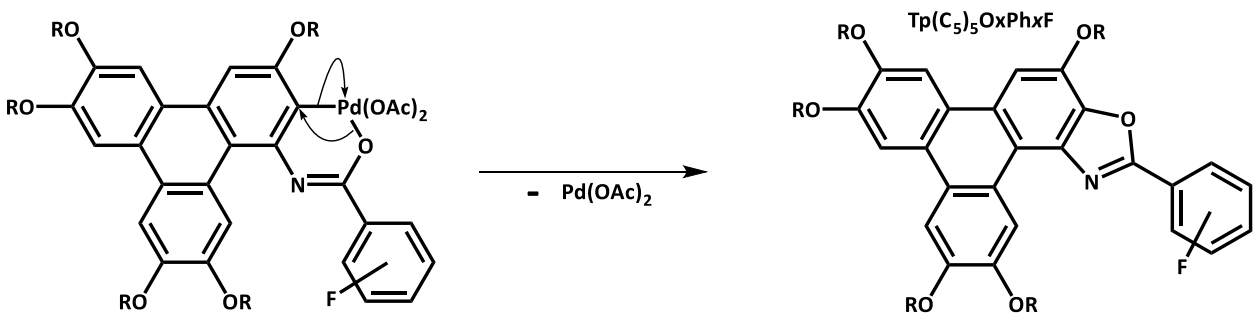

Scheme 4.3: Triphenoxazole formation step, where R= C_5H_{11}

Scheme 4.3 shows attack of the triphenylene ring and ejection of the catalyst leading to the oxazole ring formation. It is envisaged that the electron withdrawing group deactivates this attack, and thus lower the yield of product.[12]

4.2.2 Photophysical Properties of Fluorinated Aryl Triphenoxazoles

The following sections will compare the photophysical and liquid crystalline properties of the **Tp(C_5)$_5$OxPh*x*F** series to the non-fluorinated aryl triphenoxazole (**Tp(C_5)$_5$OxPh**) and the butyl derivative discussed in Chapter 3 (**Tp(C_5)$_5$OxC_4**).

The photophysical sections will focus on comparing the properties (absorption and emission) of the **Tp(C_5)$_5$OxC_4**, **Tp(C_5)$_5$OxPh*x*F** and **Tp(C_5)$_5$OxPh** as solutions in ethyl acetate, octan-1-ol, acetonitrile in order to investigate how solvent dielectric and solvent viscosity effect the properties, as well as the solid-state emission properties.

4.2.2.1 UV Absorption

The absorption spectra of the **Tp(C_5)$_5$OxPh*x*F** series are similar in terms of absorption spectra to **Tp(C_5)$_5$OxPh** (absorption maxima range 268 nm-270 nm) across all three solvents (Figure 4.2).

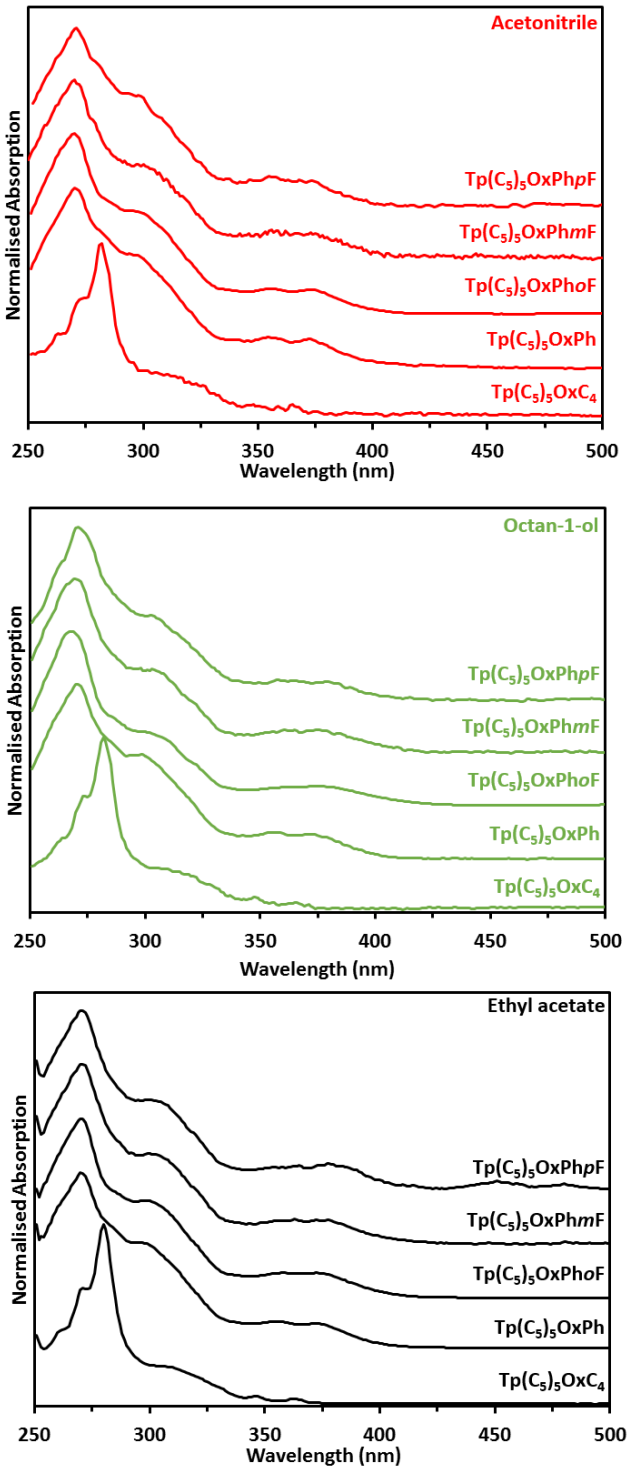

Figure 4.2: Stacked normalised absorption spectra of ***$Tp(C_5)_5OxC_4$***, ***$Tp(C_5)_5OxPh$*** *and* ***$Tp(C_5)_5OxPhxF$*** *as solution (10^{-7} M) in acetonitrile, octan-1-ol, and ethyl acetate*

The absorption data from the spectra above are summarised in Table 4.1. Relative to **Tp(C_5)$_5$OxC_4** there is a significant:

1. Blue-shift of the λ_{max} of ~10 nm, indicating an increase in energy gap between the highest occupied molecular orbital (HOMO) and lowest occupied molecular orbital (LUMO);[13]
2. Broadening of bands, caused by an increase of conjugation of the system;[14]
3. An increase in relative magnitude of π-π* absorption at 330-400 nm, also caused by an increase of conjugation of the system.[14]

*Table 4.1: molar absorptivity coefficient (ϵ) at absorption maxima of **Tp(C_5)$_5$OxC_4**, **Tp(C_5)$_5$OxPh** and **Tp(C_5)$_5$OxPhxF** series at (10^{-7} M). Values are averaged from five experiments*

	Ethyl acetate		Octan-1-ol		Acetonitrile	
	ϵ x 10^3 (M^{-1} cm^{-1})	λmax (nm)	ϵ x 10^3 (M^{-1} cm^{-1})	λmax (nm)	ϵ x 10^3 (M^{-1} cm^{-1})	λmax (nm)
Tp(C_5)$_5$OxC_4	160 ± 15	278	120 ± 12	278	58 ± 6	278
Tp(C_5)$_5$OxPh	110 ± 11	270	105 ± 10	271	66 ± 6	271
Tp(C_5)$_5$OxPh*o*F	115 ± 11	270	141 ± 14	268	114 ± 10	269
Tp(C_5)$_5$OxPh*m*F	94 ± 9	269	147 ± 14	270	145 ± 13	270
Tp(C_5)$_5$OxPh*p*F	136 ± 13	270	150 ± 15	270	134 ± 13	270

The ϵ values of the triphenoxazole species are large (where large is often quoted above >10,000 M^{-1} cm^{-1}).[15-16] Interestingly, there is a significant reduction in the molar absorptivity for **Tp(C_5)$_5$OxC_4** and **Tp(C_5)$_5$OxPh** in MeCN, relative to the fluorinated materials. An explanation

might be the increased dipole, resulting from the fluorine atoms introduction, increases the solubility of the **Tp(C$_5$)$_5$OxPh*x*F** series in the polar MeCN solvent.[17-18] This reduces the likelihood of the **Tp(C$_5$)$_5$OxPh*x*F** series aggregating, relative to **Tp(C$_5$)$_5$OxC$_4$ and Tp(C$_5$)$_5$OxPh**, which is known to lead to reductions in the molar absorptivity.[19-20] However, DLS measurements of **Tp(C$_5$)$_5$OxC$_4$**, **Tp(C$_5$)$_5$OxPh** and **Tp(C$_5$)$_5$OxPh*o*F** in acetonitrile at 10^{-6} M revealed no aggregation for any of the compounds. However, the concentrations used are probably outside the limits of detection for aggregates of the order or less than 10nm.[21]

4.2.2.2 Photoemission of Tp(C$_5$)$_5$OxPh and Tp(C$_5$)$_5$OxPh*x*F in Solution

Tp(C$_5$)$_5$OxC$_4$, as noted in the previous chapter, has a structured emission spectra with four peak emissions (~365, 384, ~410, ~430 nm) which do not display any significant solvatochromism in relation to λ_{max}. In this chapter this emissive process will be termed the *alkyl emissive mechanism* (*AlkEM*). The solution state emission of the phenyl derivatives is clearly different with a dominant broad, high intensity emission band with λ_{max} ranging from 480-520 nm (Figure 4.3), which is significantly solvatochromic in terms of λ_{max} indicating a different emissive mechanism is dominating – which will ***initially*** be termed the *phenyl emissive mechanism* (*PhEM*).

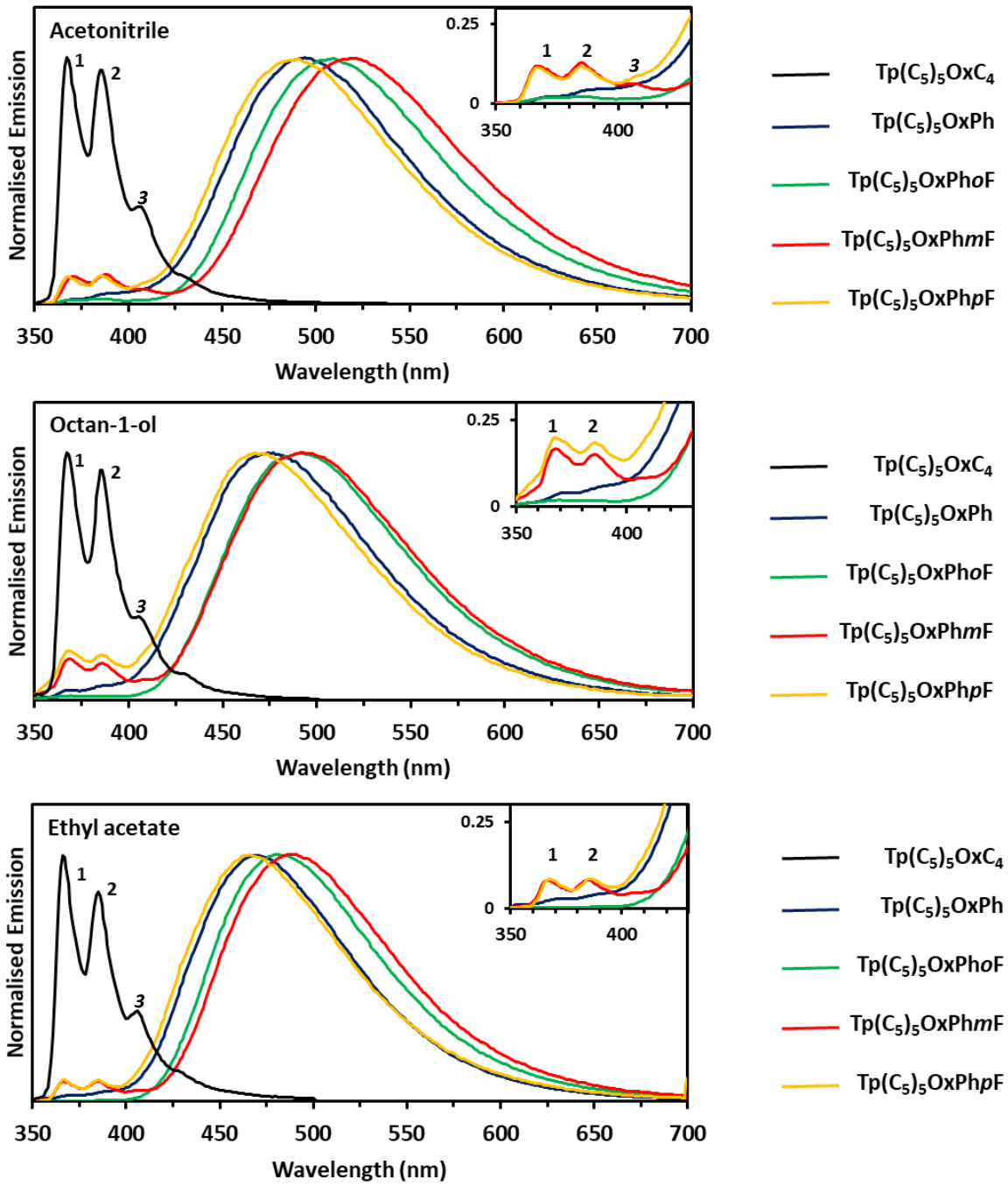

Figure 4.3: Normalised emission spectrum of ***Tp(C5)5OxC4, Tp(C5)5OxPh, Tp(C5)5OxPhoF, Tp(C5)5OxPhmF*** *and* ***Tp(C5)5OxPhpF.*** *The insets highlight the alkyl emission mechanism (AlkEM) that are operating in the phenyl derivatives*

Table 4.2 summarises the emission spectra data, revealing the solvatochromic dependence of the emissive λ_{max} for each compound (and the absorption λ_{max} from Table 4.1). When considering the Ph derivatives *PhEM* band, it is observed that relative to **Tp(C$_5$)$_5$OxPh** there is no significant shift of the emissive λ_{max} for **Tp(C$_5$)$_5$OxPh*p*F** and commensurate pseudo Stokes shift (pSS) in all three solvents. This lack of shift shows that the excited state is not further stabilised by the *p*F.

However, **Tp(C$_5$)$_5$OxPh*o*F** and **Tp(C$_5$)$_5$Ph*m*F** are redshifted up to 16 nm and 26 nm respectively, showing an increase in stability of the excited state.

*Table 4.2: Summary of solution emission of **Tp(C5)5OxC4**, **Tp(C5)5OxPh** and **Tp(C5)5PhxF** Series, where ϵ_r = dielectric constant, pSS= pseudo Stokes shift*

	Solvent			**$Tp(C_5)_5OxC_4$**	**$Tp(C_5)_5OxPh$**	**$Tp(C_5)_5OxPhpF$**	**$Tp(C_5)_5OxPhmF$**	**$Tp(C_5)_5OxPhoF$**
	ϵ_r	Viscosity (cP)						
			pK_a of acid [9-10]	4.74	4.23	4.01	3.68	3.27
Ethyl acetate	6.0	0.45	Absorption λ_{max} (nm)	281	270	270	269	270
			Emission λ_{max} (nm)	367	467	467	488	478
			pSS (cm^{-1})	8300	15600	15600	16700	16100
			Φ	0.18 ± 0.01	0.46 ± 0.04	0.49 ± 0.05	0.49 ± 0.05	0.59 ± 0.06
			Brightness (M^{-1} cm^{-1})	29 ± 5	51 ± 5	67 ± 7	46 ± 4	68 ± 7
Octan-1-ol	10.3	7.36	Absorption λ_{max} (nm)	281	271	270	270	269
			Emission λ_{max} (nm)	367	473	469	491	489
			pSS (cm^{-1})	8300	15800	15700	16700	16700
			Φ	0.30 ± 0.03	0.61 ± 0.06	0.62 ± 0.06	0.62 ± 0.06	0.70 ± 0.07
			Brightness (M^{-1} cm^{-1})	36 ± 7	64 ± 6	93 ± 9	91 ± 9	99 ± 9
Acetonitrile	37.5	0.38	Absorption λ_{max} (nm)	281	270	269	270	269
			Emission λ_{max} (nm)	367	492	490	518	508
			pSS (cm^{-1})	8300	16700	16800	17700	17500
			Φ	0.20 ± 0.02	0.46 ± 0.04	0.54 ± 0.05	0.46 ± 0.04	0.55 ± 0.05
			Brightness (M^{-1} cm^{-1})	12 ± 2	38 ± 4	72 ± 9	67 ± 7	62 ± 7

Interestingly, between 360-390 nm in the emission spectra for **Tp(C_5)$_5$OxPh*m*F** (red) and **Tp(C_5)$_5$OxPh*p*F** (yellow) (Figure 4.3). There are clearly two emissive bands at 365 nm (band 1) and 384 nm (band 2) coincident with the λ_{max} of **Tp(C_5)$_5$OxC$_4$** emissive bands, which were defined earlier as the AlkEM bands, in addition to the new large and broad emission (PhEM) centred around 500 nm. There being only two bands in the *AlkEM* visible is likely due to the *PhEM* broad band masking the third and fourth band. This is evidenced by third peak being present in acetonitrile (see acetonitrile inset Figure 4.3).

On closer inspection, these emissive bands are also present for **Tp(C_5)$_5$OxPh*o*F**, but are much less prominent. This behaviour is unusual in that one normally expects *ortho* and *para* phenyl derivatives to have similar electronic properties, and the *meta* derivative to be different, because of conjugative directing effects. Thus, this behaviour requires further examination.

These *AlkEM* bands in the phenyl derivatives relative abundance to the larger and broader *phenyl emission mechanism* band centred around 500 nm are shown in Table 4.3. Four points are of interest:

1. The largest abundance of the *AlkEM* is from the octan-1-ol solutions, which is the only solvent with a hydrogen bond acceptor;

2. The ethyl acetate and acetonitrile solutions have very similar *AlkEM* abundances, despite the much greater difference in solvent dielectric;

3. There is an enhancement of the *AlkEM* in the *meta* and *para* fluorinated phenyl rings;

4. There is a much smaller abundance of the *AlkEM* bands in the *ortho* derivative relative to the *meta* and *para* derivatives.

Thus, the system is complex, but both emission processes, *alkyl* and *phenyl emission mechanisms*, are able to operate simultaneously to various degrees in the phenyl triphenoxazole derivatives, but notably the *ortho* derivative has significantly less of the *AlkEM*.

*Table 4.3: Percentage areas of the alkyl emissive mechanism (AlkEM) (seen in **Tp(C5)5OxC4**) relative to the phenyl emissive mechanism emission for **Tp(C5)5OxPh** and the **Tp(C5)5OxPhxF** series*

	Ethyl acetate	Octan-1-ol	Acetonitrile
	% area of *AlkEM* of total emission (%)	% area of *AlkEM* total emission (%)	% area of *AlkEM* of total emission (%)
Tp(C5)5OxPh	1.5	1.9	1.1
Tp(C5)5OxPho*F*	0.1	0.7	0.6
Tp(C5)5OxPh*m*F	2.1	4.2	2.8
Tp(C5)5OxPh*p*F	2.5	5.9	2.9

To account for this discrepancy in behaviour of the *ortho* isomer, and attempt to rationalise it, one might assume that there are two limiting conformations that the phenyl ring can adopt (Figure 4.4):

1. one in which the phenyl group is cross-conjugated with the oxazole ring, in what can be referred to as the *planar conformation*, and

2. one in which the cross-conjugation is completely lost and the phenyl ring is orthogonal to the oxazole ring, in what might be referred to as the twisted-conformation.

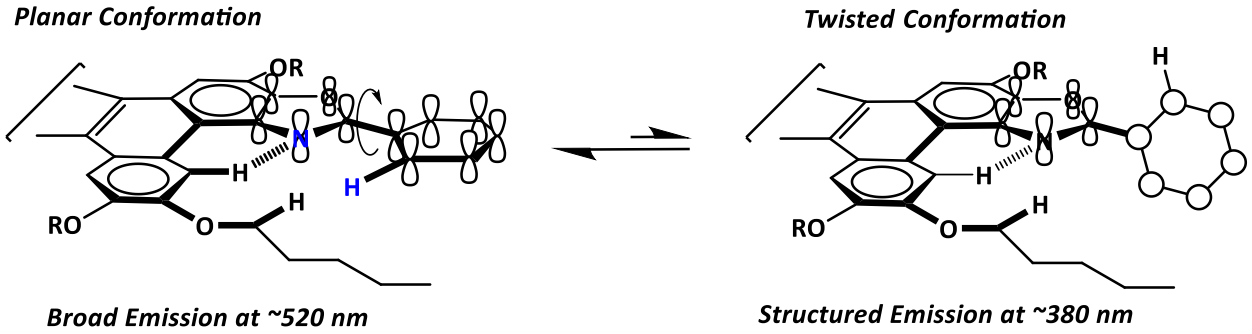

*Figure 4.4: Possible conformations of **Tp(C$_5$)$_5$OxPh**, where R=C$_5$H$_{11}$*

Considering the twisted conformation one can assume that the oxazole is not electronically coupled by conjugation to the phenyl ring, and as such the emission from such a conformation would resemble that of the **Tp(C$_5$)$_5$OxC$_4$**, with the four structured emission bands from 360-430 nm.

In contrast, the planar conformation would be fully electronically coupled and one would expect a significantly different emission profile, as the push-pull dynamics can manifests themselves, resulting in the band at ~500 nm.

Thus, turning attention to the *ortho*-fluoro-triphenoxazole **Tp(C$_5$)$_5$OxPho*F***, one has to consider why there is significantly decreased structured emission band at 360-380 nm. If the conformational hypothesis is correct, then **Tp(C$_5$)$_5$OxPho*F*** must be favouring the *planar conformation* and/or disfavouring the *twisted conformation* (Figure 4.5), resulting in

conformational equilibria biased toward the planar conformation, relative to the *meta* and *para* isomers.

Analysis of this conformation equilibria and the potential electronic effects that the *ortho* fluorine can have reveal that indeed:

1. the *planar conformation* is potential stabilised by two C-H…F hydrogen bonds between the C-H bonds of the H in the adjacent bay region, and the α-methylene of the adjacent pentoxy chain,
2. the *twisted conformation* is potentially destabilised by a fluorine lone pair being repelled by the π-electron density of the oxazole ring.

Thus, for the **Tp(C_5)$_5$OxPh*o*F** the conformational equilibria is more biased to the *planar conformation*, than it is for the other phenyl substituents, which in turn means there is less *twisted conformation* that mimics the *alkyl emission mechanism* emission band.

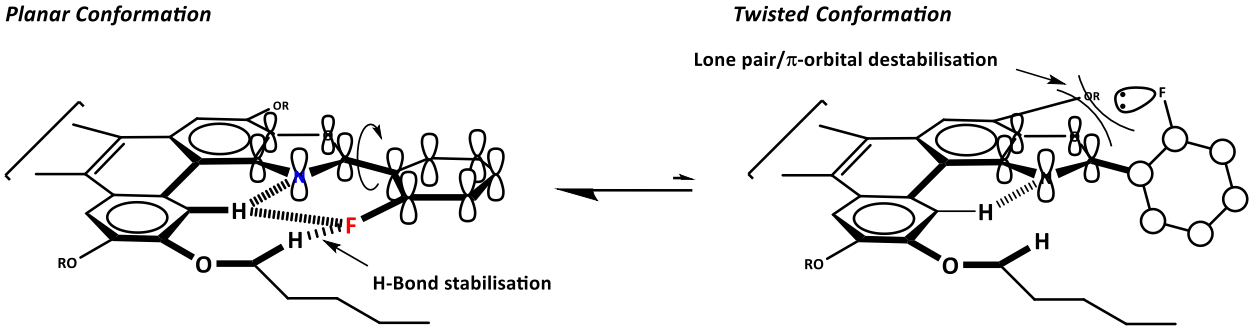

*Figure 4.5: Possible conformations of **Tp(C_5)$_5$OxPhoF**, where R=C_5H_{11}*

The enhancement of the *AlkEM* band for the octanol solutions, lend support to this hypothesis in that the octan-1-ol would be able to:

1. disrupt the hydrogen bonding in the *planar conformation* in Figure 4.5, and
2. lead to a less destabilised *twisted conformation*, through the hydrogen bonded solvation of the fluorine lone pairs.

Thus, it seems judicious at this point to rename the two emissive mechanisms for aryl related R groups to more accurately reflect the development of this hypothesis as:

a. *Planar Conjugated Emissive Mechanism* (*PCEM*) instead of the *phenyl emissive mechanism* (*PhEM*), and
b. *Twisted non-Conjugated Emissive Mechanism* (*TnCEM*) instead of the *alkyl emissive mechanism* (*AlkEM*).

A postulated mechanism of luminescence for the *PCEM* emission inspired by Bunton *et al.*[22] phenyl twist (example displayed in Section 1.7.1) is shown below in Scheme 4.4.

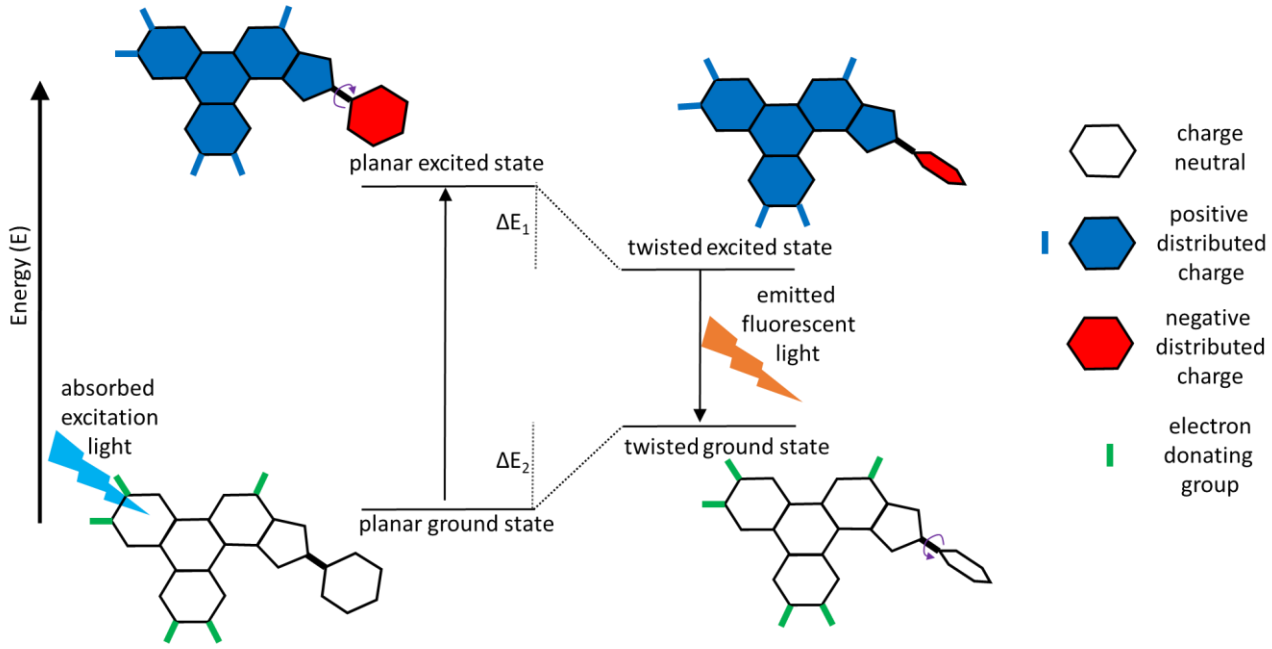

Scheme 4.4: Cartoon representation of PCEM, where skeleton aryl triphenoxazole core is excited to charge separated state, the sum of ΔE equalling the pseudo Stokes shift (pSS)

As can be seen from Scheme 4.4 upon excitation positive charge is distributed across the triphenylene core; the negative charge is distributed across the aryl substituent. The electron donating ether groups (green) aid in stabilising the positive charge by resonance effects. The molecule is stabilised by twisting the aryl substituent out of plane of the triphenoxazole core- separating the charged states. The excited state then relaxes through light emission, leaving a twisted ground state. The energy of the system is lowered by the molecule untwisting to the planar conformation. The difference in energy between the absorption and emission pseudo Stokes shift (pSS) equalling the difference in energy between the twisted and non-twisted states (the sum of $\Delta E_1 + \Delta E_2$ in Scheme 4.4).

4.2.2.2.1 Examining the Pseudo Stokes Shift

The hypothesis in this chapter was that the pSS might be increased by the introduction of electron withdrawing groups into the R group (Figure 4.1), in this case fluorine, and that the pK_a of the precursor benzoic acid and the fluorine analogues, might be a proxy for modelling the electron withdrawing nature. The plot in Figure 4.6 illustrates the relationship between the Stokes shift for each compound as a function of the pK_a, in each solvent.

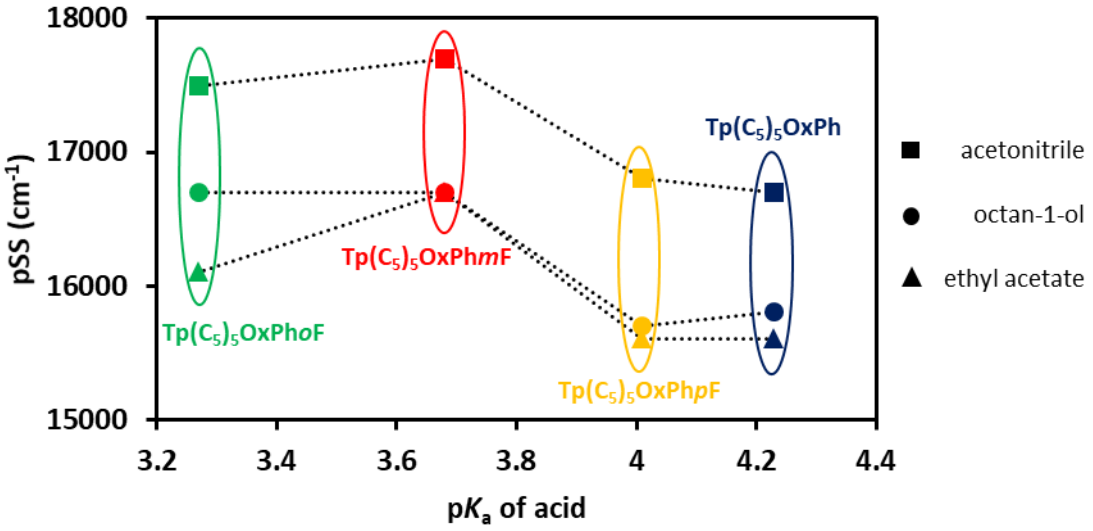

Figure 4.6: Plot of the pK_a of the acids precursors used to form triphenoxazoles versus pSS of ***Tp(C$_5$)$_5$OxPh*** *and the* ***Tp(C$_5$)$_5$OxPhxF*** *series*

Several points are noteworthy:

1) Substitution of the butyl moiety in **Tp(C$_5$)$_5$OxC$_4$** for a phenyl group in **Tp(C$_5$)$_5$OxPh** and the fluoro derivatives approximately doubles the pSS (range 15500-17700 cm^{-1}). Thus, the phenyl moieties are significantly perturbing the emission;

2) Unlike **Tp(C$_5$)$_5$OxC$_4$** (Chapter 3) there is significant solvatochromism on pSS. The pSS in acetonitrile (largest dielectric constant) are significantly higher (typically

~1000cm^{-1} wavenumbers) than those in ethyl acetate and octan-1-ol. Thus, the more polar acetonitrile is stabilising the charge separated excited state, which of course will be structure dependent, resulting in the solvatochromism of the pSS;

3) The pattern of pSS modulation in all three solvents is not linear with pK_a.

There is an argument that having greater charge stabilisation is only part of the equation for increasing the pSS. The highly electronegative fluorine would cause a change in dipole moment depending on the substituted position as shown in Figure 4.7.

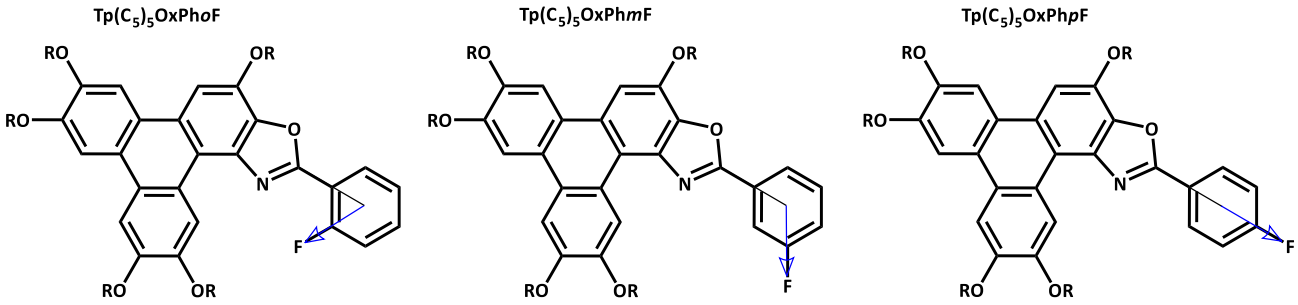

Figure 4.7: Diagram of PhxF substituent and variation upon dipole moment (Shown as arrow) depending on fluorine substitution pattern

This data highlights the complexity of functionalisation of the aryl system, and more examples of functionalisation of aryl triphenoxazoles would have to be synthesised before trends can be found.

4.2.2.2.2 Examining the Quantum Yield

The quantum yield (Φ) shows the efficiency of the luminescence relaxation pathway of the excited state.[23] A Φ of 1 would mean all molecules excited at that frequency emit light through relaxation. Conversely a Φ of 0 would mean all molecules relax through non-radiative pathways.[24] The Φ of the **Tp(C$_5$)$_5$OxPh*x*F** series was calculated with **Tp(C$_5$)$_5$OxC$_4$** as a reference using Equation 4.1.[24]

$$\Phi_x = \Phi_r \left(\frac{A_r}{A_x}\right)\left(\frac{D_x}{D_r}\right)\left(\frac{{n_x}^2}{{n_r}^2}\right)$$

*Equation 4.1: Φ calculation. Where x is unknown compound, r is the reference, A is the absorbance of the molecule at excitation, n is the refractive index of the solvent and D is the integrated area of emission peak. Φ of **Tp(C$_5$)$_5$OxC$_4$** in EtOAc is 0.18 (Chapter 3)*

Tp(C$_5$)$_5$OxC$_4$ was chosen as a reference as we had previously shown (Chapter 3) the Φ to be concordant through the two methods (integrating sphere and dilution using a Ru(bbpy)$_2$ reference). Furthermore, **Tp(C$_5$)$_5$OxC$_4$** could be excited at the same wavelength (λ = 286 nm) and allows direct comparison of results to **Tp(C$_5$)$_5$OxC$_4$.**

Graphs were plotted as a series of dilutions of **Tp(C$_5$)$_5$OxPh*x*F** and **Tp(C$_5$)$_5$OxC$_4$**, with absorbance (A) as the *x*-axis and emission area (D) as the *y*-axis (Figure 4.8). Thus, the gradient is D/A over all points. The gradient of **Tp(C$_5$)$_5$OxPh*x*F** was divided by the gradient of **Tp(C$_5$)$_5$OxC$_4$**. Absorbance values were not allowed to surpass 0.2 to avoid issues of self-quenching and all graphs showed an R^2 ≥0.99 over six points.

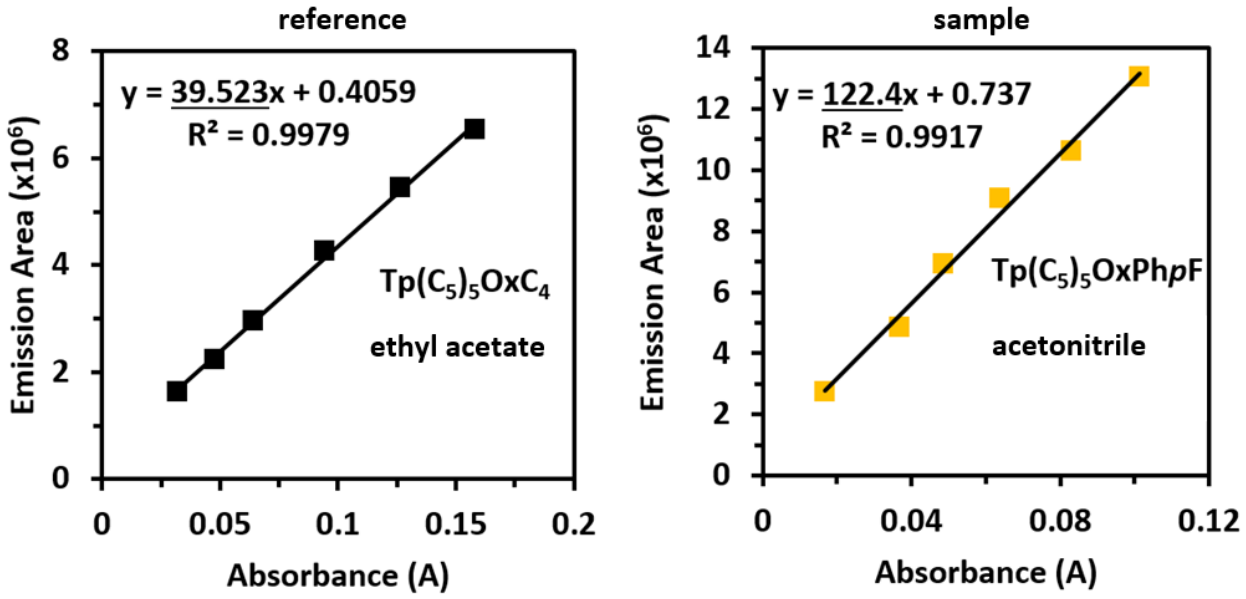

Figure 4.8: Examples of gradients used for Φ calculation where sample concentration was measured 10^{-8} to 10^{-6} M. Reference on the left, sample on the right. Gradient is underlined.

Φ data for the **Tp(C5)5OxPh*x*F** series reveal a similar Φ (0.4-0.7) to **Tp(C5)5OxPh** (Table 4.2). These values are approximately double that of **Tp(C5)5OxC4**, and show that an aromatic R-group increases the probability of luminescence relaxation. The similarity in Φ to **Tp(C5)5OxPh** shows that fluorine has little effect on the Φ.

4.2.2.2.3 Examining the Brightness

The brightness of the **Tp(C5)5OxPh*x*F** (Table 4.2) is comparable to those of the **Tp(C5)5OxAr** series (Chapter 5). All bar **Tp(C5)5OxPh*m*F** in ethyl acetate show larger brightness values than the fluorinated **Tp(C5)5OxPh** and are 2-4x brighter than **Tp(C5)5OxC4**. As Φ are similar, this increased brightness is due to increased absorptivity seen within the series. Noticeably brightness values for the **Tp(C5)5OxPh*x*F** series do not drop in acetonitrile as ϵ values remained high. The consistent high brightness when compared to commercial fluorophores[25-26] serve as an early

indication that these molecules could make an attractive proposition in applications such as fluorescent dyes,[1] and probes.[27]

4.2.3 Photoemission as a Solid

The solid-state emission profile from the **Tp(C$_5$)$_5$OxPh*x*F** series in solid state shows the broad range emission akin to that observed in solution (Figure 4.9), the *PCEM* band. One noticeable difference is the absence of the structured bands at 360-380 nm, the *TnCEM* bands.

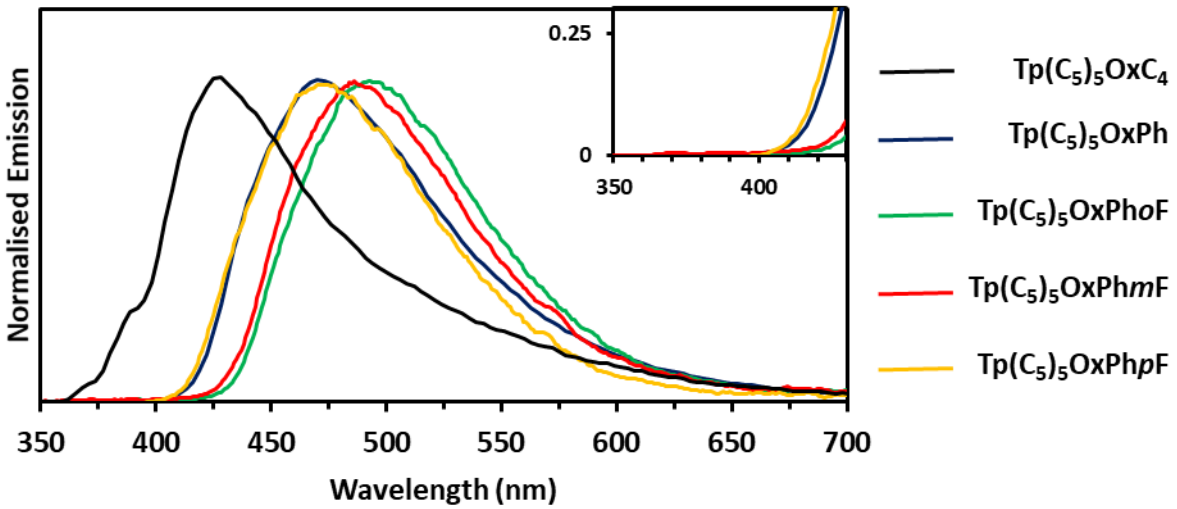

*Figure 4.9: Normalised emission spectrum in the solid state of **Tp(C$_5$)$_5$OxC$_4$**, **Tp(C$_5$)$_5$OxPh**, and the **Tp(C$_5$)$_5$OxPhoF** series*

Furthermore, the *TnCEM* band is quenched in the solid state, which according to the proposed hypothesis in relation to the *planar* and *twisted* conformations (Figure 4.4) means the aryl triphenoxazoles are biased even more to the *planar conformation* than they are in solution. Thus, one can imagine that in the solid state the packing of the triphenoxazoles is such that the phenyl moieties are all in conjugation with the oxazole, and so there is no possibility of *TnCEM*.

If this solid state-packing is controlling the conformational preference for the planar structure, then at higher solution concentrations it could be envisaged that aggregates form, leading to a planar conformational bias similar to the solid, and as such the twisted conformation would be depleted and *TnCEM* emission pathway would be reduced. To probe this hypothesis an experiment was designed to contrast the solution state emission of **Tp(C$_5$)$_5$OxPh** in ethyl acetate at 10^{-4} M and 10^{-5} M (Figure 4.10). It was found at the higher concentration (10^{-4} M) the *TnCEM* emission was significantly reduced relative to the more dilute solution (inset of Figure 4.3). Furthermore, there was also significant quenching of the broad *PCEM* emission at the higher concentration, suggesting self-quenching through aggregation,[28] further supporting the aggregation leading to *planar conformation* adoption hypothesis.

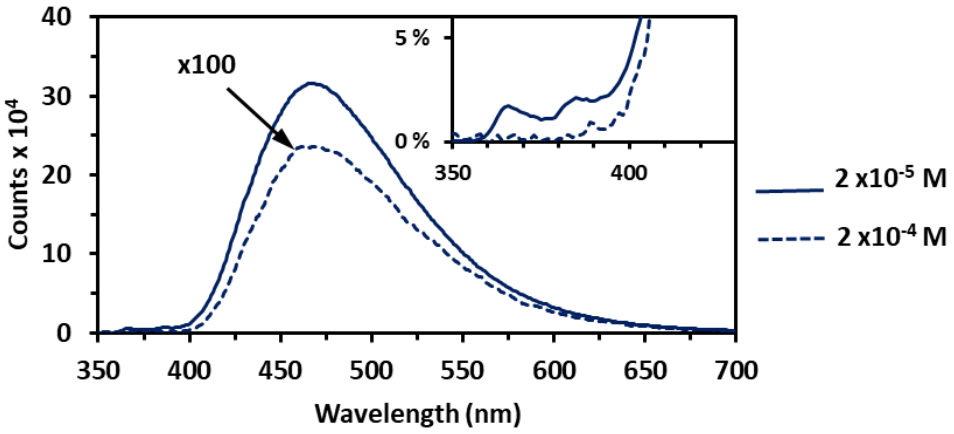

*Figure 4.10: Emission spectrum of **Tp(C$_5$)$_5$OxPh** at 2 x10^{-5}M and 2 x10^{-4} M. 2 x10^{-4} has been magnified x100*

There are notable shifts in the λ_{max} between solution and solid state of the *PCEM* emission, which are detailed in Table 4.4. There is a significant red shift of 58 nm for **Tp(C$_5$)$_5$OxC$_4$**, whilst for the phenyl derivatives the shifts are smaller, with only one significant red shift of 14 nm observed for **Tp(C$_5$)$_5$OxPhoF**. Once again, the ortho derivative has unusual behaviour,

presumably linked to the intermolecular hydrogen bonding. Some insight into this solid state behavioural difference is garnered in Section 4.2.4 when considering the significant difference in the thermal behaviour of the ortho derivative compared to the other phenyl derivatives.

*Table 4.4: Comparison of emission maxima in ethyl acetate and solid state of **Tp(C5)5OxPhxF** series*

	Tp(C5)5OxC4	**Tp(C5)5OxPh**	**Tp(C5)5OxPho*F***	**Tp(C5)5OxPh*m*F**	**Tp(C5)5OxPh*p*F**
	Emission Max (nm)	Emission Max (nm)	Emission Max (nm)	Emission Max (nm)	Emission Max (nm)
Ethyl acetate	366	467	478	488	466
Solid State	424	467	492	484	470
Δ	58	0	14	-4	4

4.2.3.1 Examining the Colour

Overall, the **Tp(C5)5OxPhxF** series displays a variation in colour (Figure 4.11) from blue to green, showing early promise that the colour of emission could be fine-tuned.

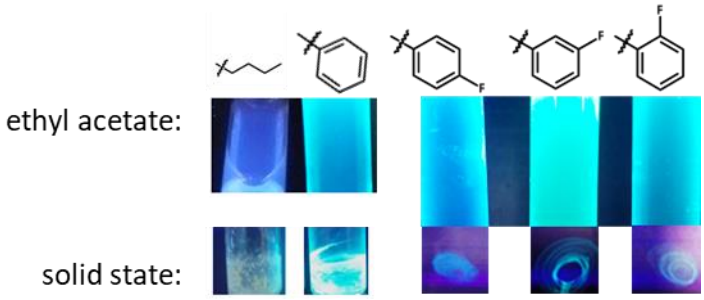

*Figure 4.11: Emission colours In ethyl acetate solution (10^{-5} M) and solid state comparison under 302 nm light (4W) of From left to right: **Tp(C5)5OxC4**, **Tp(C5)5OxPh**, **Tp(C5)5OxPhpF**, **Tp(C5)5OxPhmF** and **Tp(C5)5OxPhoF***

4.2.4 Liquid Crystallinity

Given that the parent triphenylene structure is a well-known discotic liquid crystalline material and the chemical modification of it to **Tp(C_5)$_5$OxC_4** in the previous chapter still sustained the Col_h mesophase, despite slightly increasing the π-surface area and desymmetrising the structure, it was not unreasonable to investigate the phenyl derivatives made in this chapter to see if they could still sustain a mesophase. Of course, structurally the phenyl derivatives might be thought to be less mesogenic that **Tp(C_5)$_5$OxC_4** as they have lost the butyl chain and gained the phenyl group: in simple terms, there is a reduction in components leading to the liquid state (alkyl) and an increase in the component (phenyl) leading to the crystalline state, and hence potentially disrupt the mesophase formation. However, clearly they are structurally similar enough to warrant investigation and see how the replacement of the butyl chain by the phenyl and the fluoro-phenyl isomers supported/modified, or not, a mesophase. The thermal analysis of these materials is discussed below.

4.2.4.1 DSC Thermal Analysis

Table 4.5 summarises the transition temperatures of **Tp(C_5)$_5$OxC_4**, **Tp(C_5)$_5$OxPh** and the **Tp(C_5)$_5$OxPh*x*F** series. The assignment of Col_h phases are discussed in the section below, when considering the mesophase textures obtained from polarised optical microscopy. The *meta* and *para* derivative are akin to **Tp(C_5)$_5$OxC_4** (Chapter 3), where there is an unknown thermal transition just before the mesogen enters the Col_h phase. The texture could not be identified from the POM experiment, but may be a glass phase for reasons discussed in Section 3.2.6.

*Table 4.5 Summary of transition temperatures for **Tp(C5)5OxPhxF** derivatives from 2nd cycle of DSC scan. Where Cr= Crystalline, X= unknown solid phase, Col_h= hexagonal columnar and I= Isotropic. DSC scan 10 °C min^{-1} *transition not observed on DSC scan and temperature stated from POM*

Compound	Heating (°C)			Cooling (°C)	
Tp(C5)5OxC4	95	99	141	137	59
	Cr-X	X-Col_h	Col_h-I	I-Col_h	Col_h-Cr
Tp(C5)5OxPh	103	110	189	185	78
	Cr-X	X-Col_h	Col_h-I	I-Col_h	Col_h-Cr
Tp(C5)5OxPh*o*F			99	70	60
			Cr-I	I-Col_h	Col_h-Cr
Tp(C5)5OxPh*m*F	97	108	213	212	50
	Cr-X	X-Col_h	Col_h-I	I-Col_h	Col_h-Cr
Tp(C5)5OxPh*p*F		109	183*	173*	46
		Cr-Col_h	Col_h-I	I-Col_h	Col_h-Cr

4.2.4.2 POM Thermal Analysis

Figure 4.12 displays POM images of the LC phase during the cooling cycle for the **Tp(C5)5OxPh*x*F** series and **Tp(C5)5OxC4 and Tp(C5)5OxPh** as a comparison.

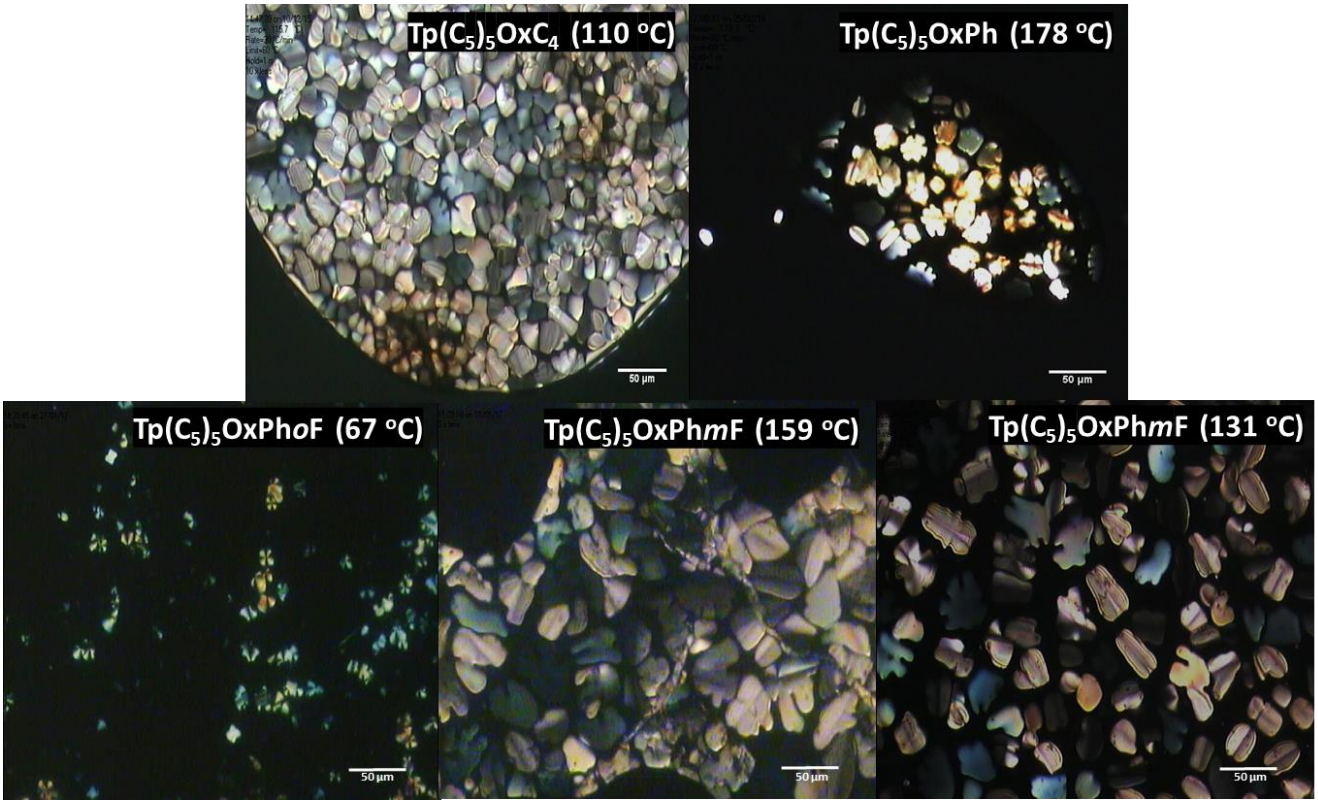

Figure 4.12 POM images (temperature included in the images) during the cooling cycle

Col_h can be assigned with reasonable confidence due to the similarity in POM image to **$Tp(C_5)_5OxC_4$**, which was shown by XRD to be a Col_h mesogen (Section 3.2.6.1). The POM images themselves show many of the characteristics of Col_h, with the broken snowflake texture and fan textures observed.[29]

Figure 4.13 graphically depicts for each compound the second heating and cooling run (DSC data) and the phases believed to be observed (POM). Several points are worth noting:

1) The replacement of the butyl group (**Tp(C_5)$_5$OxC$_4$)** by the phenyl group (**Tp(C_5)$_5$OxPh**) has not had a deleterious effect on the Col_h phase range (Cooling: phase range of 107 °C and 108 °C, respectively);

2) **Tp(C_5)$_5$OxPh*m*F** and **Tp(C_5)$_5$OxPh*p*F** have even more extended Col_h mesophase ranges (Cooling: 162 °C and 127 °C, respectively);

3) **Tp(C_5)$_5$OxPh*o*F** has an extremely short cooling Col_h mesophase range of only 10 °C in direct contrast to the *meta* and *para* isomers (and displays no mesophase on heating, in contrast to all other derivatives examined),

Once again, the *ortho* derivative stands out as the one with unusual behaviour.

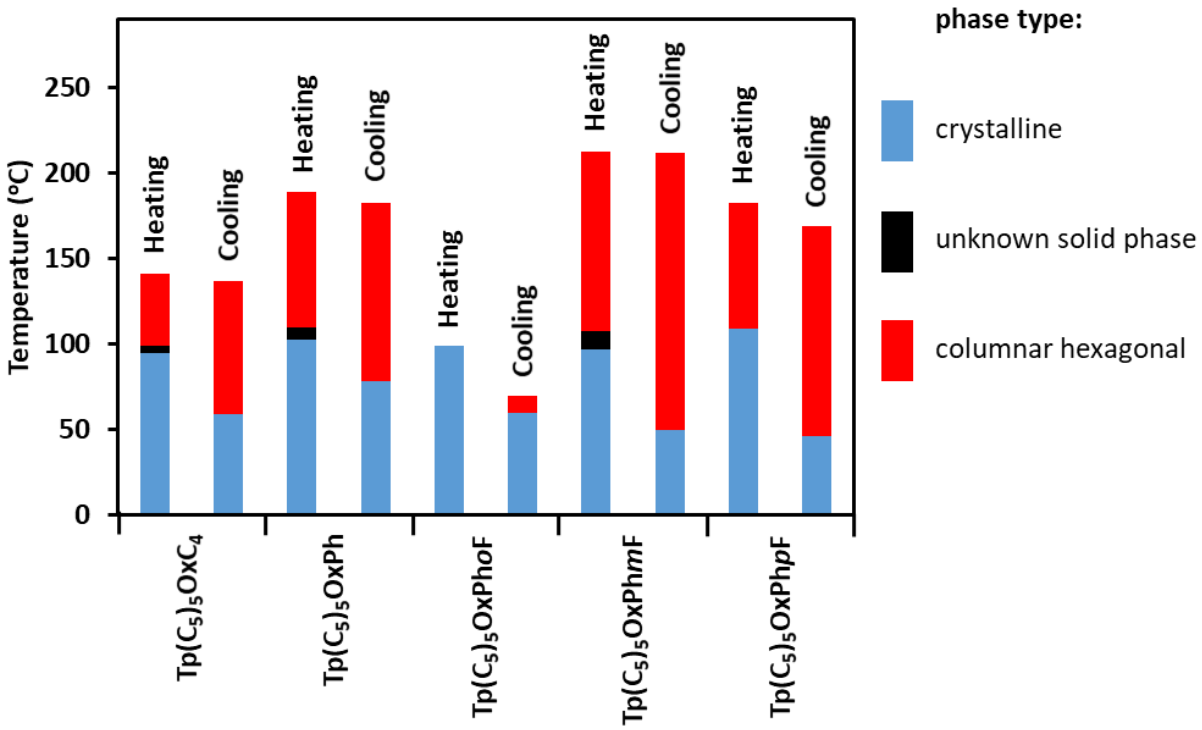

Figure 4.13: Plot of Phase type of ***$Tp(C_5)_5OxC_4$, $Tp(C_5)_5OxPh$*** *and the* ***$Tp(C_5)_5OxPhxF$*** *series*

To rationalise this anomaly with the *ortho* derivative it will be recalled when considering the photophysical data in Section 4.2.2, it was postulated that the *ortho* fluorine isomer had an intramolecular hydrogen bond which restricts the rotation around the C-C bond linking the oxazole and phenyl group, which led to different photophysical properties to the *meta* and *para* isomers. Thus, one might reason that in the liquid crystalline state this differential hydrogen bonding behaviour might manifest itself again. A hypothesis might be in the *meta* and *para* isomers the fluorine atoms are not involved in an *intramolecular* hydrogen bonding, as is the case for the *ortho* isomer (Figure 4.5), and therefore the *meta* and *para* isomers have the potential for *intermolecular* interactions, which the *ortho* isomer may not have, or at least to a lesser extent. For example, the *meta* and *para* fluorine atoms may hydrogen bond to C-H of the

aryl R groups of adjacent molecular structures in a similar manner to fluorobenzene (Figure 4.14).[30]

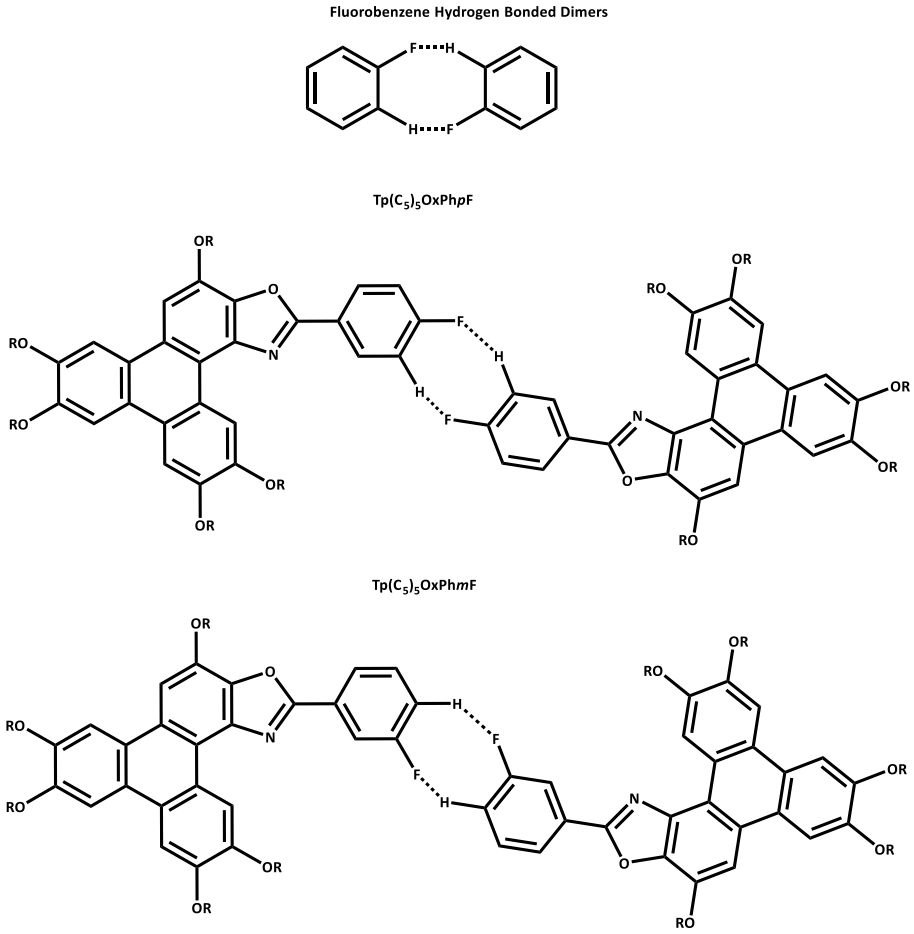

Figure 4.14: Fluorobenzene hydrogen bonding[30] and potential hydrogen bonding between aryl C-H and F-C for ***Tp(C5)5OxPhpF*** *and* ***Tp(C5)5OxPhmF*** *R=C_5H_{11}*

4.3 Conclusions

In conclusion, the intermolecular annulation to form triphenoxazoles discussed in Chapter 3 was used to create *ortho*, *meta* and *para* fluorophenyl (**Tp(C$_5$)$_5$OxPh*x*F**) and phenyl (**Tp(C$_5$)$_5$OxPh**) triphenoxazole derivatives in 9-33 % yields.

The **Tp(C$_5$)$_5$OxPh*x*F** series was studied to observe the effects of fluorination of the phenyl substituent had on the luminescent and liquid crystalline properties of the molecule.

Replacing an alkyl arm with an aryl substituent greatly improves the Φ from 0.18 to 0.40 whilst maintaining a high ϵ 90000-145000 M^{-1} cm^{-1}. The emission becomes broad, and a large pSS of 15,600 to 17800 cm^{-1} is achieved, with colours in the blue and green visible spectrum.

Unlike **Tp(C$_5$)$_5$OxPh** and **Tp(C$_5$)$_5$OxC$_4$** The **Tp(C$_5$)$_5$OxPh*x*F** series showed no reduction in ϵ when measured in acetonitrile, and thus showed improved brightness of 60 M^{-1} cm^{-1} in acetonitrile.

In solution, the aryl triphenoxazoles show two mechanisms of emission which was hypothesised to be conformationally dependent, where the aryl group is either in a planar conformation or orthogonal to the triphenoxazole leading to the broad banded emission at ~500nm (*PCEM*), or the structured bands matching **Tp(C$_5$)$_5$OxC$_4$** at ~400 nm (*TnCEM*), respectively.

Tp(C$_5$)$_5$OxPh*o*F showed much reduced *TnCEM* bands compared to the rest of the aryl triphenoxazoles, implying that this derivative had additional conformational control, giving preference to the planar conformation. Analysis of the molecular structure suggested an intramolecular CH...F hydrogen bonding network was possible to give preference to the planar

conformation, which would not be possible for the other aryl derivatives. Support to this hypothesis was derived from the experiments in octan-1-ol. This *TnCEM* emission was most prominent for **Tp(C$_5$)$_5$OxPh*p*F** in octan-1-ol and so is postulated to be a hydrogen bond effect between the fluorine and alcohol. *TnCEM* is quenched in the solid state, with only one broad band at ~500 nm (*PCEM* emission) visible in all compounds.

Interestingly, **Tp(C$_5$)$_5$OxPh*p*F** *PCEM* emission did not demonstrate any significant changes in the pseudo Stokes shift (pSS) relative to **Tp(C$_5$)$_5$OxPh**, however both fluorination in the *meta* and *ortho* position did red shift the emission band, showing an improved stabilisation effect of the excited state.

Both **Tp(C$_5$)$_5$OxPh** and the **Tp(C$_5$)$_5$OxPh*x*F** series retained liquid crystalline properties. When compared to **Tp(C$_5$)$_5$OxPh**; **Tp(C$_5$)$_5$OxPh*o*F** displayed a dramatic decrease in clearing temperature from 189 to 99 °C and a reduction in liquid crystallinity temperature range from 107 °C to 10 °C. Whereas **Tp(C$_5$)$_5$OxPh*m*F** and **Tp(C$_5$)$_5$OxPh*p*F** showed an increase in the temperature range (162 °C and 127 °C) respectively. We presume these effects are due to **Tp(C$_5$)$_5$OxPh*m*F** and **Tp(C$_5$)$_5$OxPh*p*F** ability to form intermolecular hydrogen bonds, a property that is reduced in **Tp(C$_5$)$_5$OxPh*o*F** due to a competing intramolecular hydrogen bonding with the O-CH_2 in the pendant pentyl chain and the H atom in the adjacent bay region of the triphenylene.

Further work is required to understand the detailed effects of the fluorine substitution in order to probe the CH···F intramolecular hydrogen bond hypothesis. To this end solution state variable

temperature ^{1}H NMR studies on **Tp(C$_5$)$_5$OxPh*o*F** would be able to probe the dynamics of the conformational preferences resulting from rotation around the C-C bond linking the oxazole and the phenyl moieties. Solid state NMR spectroscopy and powder XRD could elucidate information on the intermolecular hydrogen bonding of **Tp(C$_5$)$_5$OxPh*m*F** and **Tp(C$_5$)$_5$OxPh*p*F,** and the intermolecular hydrogen bonding **in Tp(C$_5$)$_5$OxPh*o*F**.

Furthermore, one can envisage looking at higher substituted fluorinated phenyl rings to explore how the photophysical and thermal properties are altered. The 1,5-difluorophenyl (in which the linking C-C bond (oxazole to phenyl)) is flanked by fluorine atoms (Figure 4.15) would be interesting as this:

1) should bias even more the conformational preference to the planar one in solution, by having two C-H…F hydrogen bonds per revolution around the C-C bond, whilst

2) allowing for an enhancement of the thermal solid state properties, by having a F atom available for intermolecular hydrogen bonding

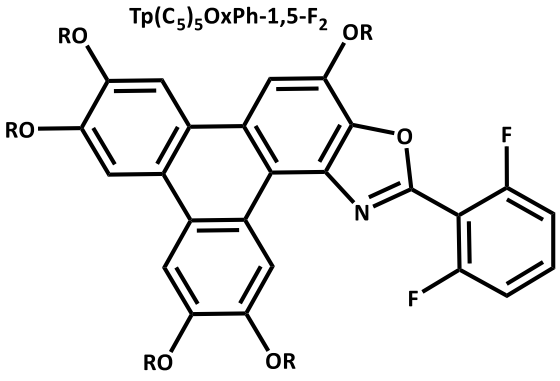

*Figure 4.15: **Tp(C$_5$)$_5$OxPh-1,5-F2** where R=C$_5$H$_{11}$*

4.4 Experimental

All reagents were used directly from the suppliers without further purification unless otherwise stated. All synthetic procedures were carried out under nitrogen and were magnetically stirred unless otherwise stated. All temperatures were internal flask temperatures unless otherwise stated. All solvents used were reagent grade unless otherwise stated. Heating under reflux consisted of a fitted glass condenser (water cooled). Column chromatographic separations were performed using Silica gel 120 (ICN Chrom 32-63 60 Å).

4.4.1 Analytical Techniques

Analytical techniques used as confirmation were matrix assisted laser desorption ionisation (MALDI), Electrospray Mass Spectrometry (ES^+MS), infra-red spectroscopy and NMR spectroscopy. The NMR spectroscopic techniques used were ^1H NMR spectroscopy using the Brüker AVIII 300 spectrometer, ^{13}C NMR spectroscopy using the Brüker AVIII400 NMR spectrometer.

Elemental analysis was performed on a Carlo Elba EA1110. Where the sample (1 mg) is heated to 1000 °C with a constant flow of helium. The combustion gas mixture is driven through an oxidation catalyst zone consisting of WO_3, which aids in delivering complete combustion. The resultant mixture of components is separated by a Porapack column and detected by a thermal conductivity detector.

4.4.2 Thermal and Photophysical Characterisation:

Thermal and photophysical characterisation procedures can be found in Chapter 3 (Sections 3.4.3 and 3.4.5).

4.4.3 Synthetic Procedures:

Synthetic procedures for **Tp(C$_5$)$_6$**, **Tp(C$_5$)$_6$NO$_2$** and **Tp(C$_5$)$_6$NH$_2$**, **Tp(C$_5$)$_5$OxC$_4$** and **Tp(C$_5$)$_5$OxPh** can be found in Chapter 3 (Sections 3.4.6.2 to 3.4.6.2.9).

4.4.3.1 General triphenylenoxazole formation:

A solution of the appropriate carboxylic acid (1.31 mmol), palladium diacetate (0.005 mmol) and iodobenzene diacetate (0.157 mmol) in PhMe (5 mL) was heated at 70 °C under N_2 for 20 min. A solution of **Tp(C$_5$)$_6$NH$_2$** (100mg; 0.131 mmol) in PhMe (2 mL) was added and and heated under reflux for 48-72 h, whilst stirring. The solution was cooled to room temperature and diluted with CH_2Cl_2 (20 mL). The organic phase was washed with aqueous NaOH (1M; 2 x 20 mL), separated and the organic phase was dried *in vacuo*. The crude black solid was purified by flash column chromatography (silica; 40 % CH_2Cl_2: 60 % *n*-hexane) to afford the desired product.

4.4.3.2 2,3,6,11,12-pentapentyloxy-8-(4-fluorophenyl)-triphenoxazole Tp(C$_5$)$_5$OxPh*p*F

Acid used was 4-fluorobenzoic acid (187 mg; 1.31 mmol) afforded an off-white solid as product (13 mg; 9 %) **^{1}H NMR** (300 MHz; $CDCl_3$) δ_H: 10.03 (s, 1H), 8.36 – 8.30 (m, 2H), 7.97 – 7.75 (m, 4H), 7.28 – 7.15 (m, 3H), 4.41 (t, *J* = 6.6 Hz, 4H), 4.26 (m, 6H), 2.06 – 1.90 (m, 9H), 1.55 (m, 22H), 1.05 – 0.95 (m, 15H) ppm. **^{13}C NMR** (100 MHz; $CDCl_3$) δ_C: 166.0, 163.5, 160.6, 149.7, 149.1,

148.9, 148.5, 143.0, 140.5, 140.3, 129.8, 129.7, 127.3, 124.8, 123.9, 123.8, 123.5, 116.5, 116.3, 116.1, 111.1, 108.4, 107.0, 106.8, 103.7, 69.9, 69.8, 69.7, 69.5, 68.9, 29.7, 29.2, 29.0, 28.5, 28.4, 28.3, 22.6, 14.2, 14.1 ppm. **^{19}F NMR** (282 MHz, $CDCl_3$) δ_F: -108.0 ppm. **MALDI$^+$** ***m/z***: 795.6 ($[M+H+1]^+$ 15 %), 794.6 ($[M+H]^+$ 55 %), 793.6 ($[M]^+$ 100 %). **IR λ^{-1}** (neat): 2952m (C-H), 2926m (C-H), 2858m (C-H), 1616w (C=N), 1517s (benzene ring), 1499m (benzene ring), 1433m (benzene ring), 1261m (C-O), 1174s (C-O) cm^{-1}.

4.4.3.3 2,3,6,11,12-pentapentyloxy-8-(3-fluorophenyl)-triphenoxazole Tp(C_5)$_5$OxPh*m*F

3-fluorobenzoic acid (182 mg; 1.3 mmol) afforded a yellow solid as product (13 mg; 11 %). **^{1}H NMR** (300 MHz; $CDCl_3$) δ_H: 10.06 (s, 1H), 8.15 (d, *J* = 7.9 Hz, 1H), 8.05 (dd, *J* = 9.0, 1.9 Hz, 1H), 7.89 (m, 4H), 7.53 (m, 1H), 7.36 – 7.16 (m, 4H), 4.45 (m, 4H), 4.33 – 4.21 (m, 6H), 2.16 – 1.90 (m, 11H), 1.71 – 1.39 (m, 24H), 1.06 – 0.93 (m, 15H) ppm.**^{13}C NMR** (100 MHz; $CDCl_3$) δ_C: 164.3, 161.8, 160.1, 160.1, 149.6, 149.1, 148.8, 148.4, 142.9, 140.3, 140.3, 130.6, 130.5, 129.6, 129.6, 127.3, 124.8, 123.7, 123.4, 123.4, 123.2, 123.2, 118.3, 118.1, 116.4, 114.6, 114.3, 110.9, 108.2, 106.8, 106.7, 103.9, 69.9, 69.8, 69.6, 69.0, 29.4, 29.3, 29.2, 28.6, 28.5, 28.4, 22.8, 14.3 ppm. **^{19}F NMR** (282 MHz; $CDCl_3$) δ_F: -111.8 ppm. **ES$^+$MS** ***m/z***: 817.5 ($[M+H+Na]^+$ 50%), 816.5 ($[M+Na]^+$ 100%), 794.5 ($[M]^+$ 55%). **IR λ^{-1}** (neat): 2952m (C-H), 2925m (C-H), 2856m (C-H), 1617w (C=N), 1518s (benzene ring), 1434s (benzene ring), 1262s (C-O), 1174s (C-O) cm^{-1}. Elemental analysis Found: C, 75.62; H, 8.25; N, 1.78 %. $C_{50}H_{64}FNO_6$ requires C, 75.63; H, 8.12; N, 1.76 %.

4.4.3.4 2,3,6,11,12-pentapentyloxy-8-(2-fluorophenyl)-triphenoxazole Tp(C_5)$_5$OxPh*o*F

2-fluorobenzoic acid (41.86 mg; 0.26 mmol) afforded a yellow solid as product (7 mg; 10 %) **^{1}H NMR** (300 MHz; $CDCl_3$) δ_H: 10.16 (s, 1H), 8.38 (m, 1H), 7.92 (m, 4H), 7.63 – 7.47 (m, 1H), 7.43 – 7.28 (m, 2H), 4.47 (m, 4H), 4.27 (m, 5H), 2.13 – 1.91 (m, 9H), 1.69 – 1.39 (m, 21H), 1.00 (m, 14H) ppm. **^{13}C NMR** (100 MHz; $CDCl_3$) δ_C: 162.4, 159.8, 157.6, 157.5, 149.7, 149.3, 148.8, 148.4, 142.9, 140.6, 140.5, 139.9, 132.9, 132.8, 130.3, 127.3, 124.8, 124.5, 123.9, 123.4, 123.4, 117.4, 117.2, 116.7, 116.0, 115.9, 110.9, 108.3, 107.0, 106.9, 104.4, 69.8, 69.5, 68.9, 29.2, 29.0, 28.4, 28.3, 22.6, 22.6, 14.1 ppm. **^{19}F NMR** (282 MHz; $CDCl_3$) δ_F: -109.1 ppm. **MALDI$^+$** ***m/z***: 795.6 ($[M+1+H]^+$ 20 %), 794.6 ($[M+H]^+$ 65 %), 793.6 ($[M]^+$ 100 %). **IR λ^{-1}** (neat): 2952m (C-H), 2925m (C-H), 2856m (C-H), 1617w (C=N), 1518m (benzene ring), 1434m (benzene ring), 1261s (C-O), 1176s (C-O) cm^{-1}. Elemental analysis Found: C, 75.92; H, 8.26; N, 1.74 %. $C_{50}H_{64}FNO_6$ requires C, 75.63; H, 8.12; N, 1.76 %.

4.5 References

[1] S. Mukherjee and P. Thilager, *J. Mater. Chem. C*, 2016, **4**, 2647

[2] L. Guo and D. Cao, *J. Mater. Chem. C*, 2015, **3**, 8490

[3] H. Ma, L. Wang, J. Chen, X. Zhang, L. Wang, N. Xu, G. Yang and P. Cheng, *Daltons Trans.*, 2017, **46**, 3526

[4] P. Miluski, *Fibers*, 2017, **5**, 1

[5] F.L. Thorp-Greenwood, *Organometallics*, 2012, **31**, 5686

[6] Y.Y. Wu, Y. Chen, G.Z. Gou, W.H. Mu, X.J. Lv, M.L. Du and W.F. Wu, *Org. Lett.*, 2012, **14**, 5226

[7] M.V. Sednev, V.N. Belov and S.W. Hell, *Methods Appl. Fluoresc.*, 2015, **3**, 042004

[8] Y. Zhang, S.A. Autry, L.E. McNamara, S.T. Nguyen, N. Le, P. Brogdon, D.L. Watkins, N.I. Hammer and J.H. Delcamp, *J. Org. Chem.*, 2017, **82**, 5597

[9] S. Boiadjiev and D.A. Lightner, *J. Phys. Org. Chem.*, 1999, **12**, 751

[10] I. Ibrahem, P. Hammer, J. Vesely, R. Rios, L. Eriksson and A. Cordova, *Adv. Synth. Cat.*, 2008, **350**, 1875

[11] B.J. Stokes, B. Jovanović, H. Dong, K.J. Richert, R.D. Riell and T.G. Driver, *J. Org. Chem.*, 2009, **74**, 3225

[12] www.mhhe.com/physsci/chemistry/carey/student/olc/ch12substituenteffects.html [25/09/2017]

[13] V. Barone and A. Polimeno, *Chem. Soc. Rev.*, 2007. **36**, 1724

[14] H. Meier, U. Stalmach and H. Kolshorn, *Acta Polymer*, 1997 **48**, 379

[15] P. Wang, C. Klein, R. Humphrey-Baker, S.M. Zakeeruddin and M. Grátzel, *J. Am. Chem. Soc.*, 2005, **127**, 808

[16] https://www2.chemistry.msu.edu/faculty/reusch/virttxtjml/spectrpy/uv-vis/uvspec.htm [25/09/2017]

[17] R. Schmid, *Monatsh. Chem.*, 2001,**132**,1295

[18] P.J. Camp, A.C. Jones, R.K. Neely and N.M. Speirs, *J. Phys. Chem. A.*, 2002, **106**, 10725

[19] Y. Xia and A. MacDiarmid, *Macromolecules*,1994, **27**, 7212

[20] Z.R. Grabowski and K. Rotkiewicz, *Chem. Rev.*, 2003, **103**, 3899

[21] J. Philo, *AAPS J.*, 2006, **8**, E564

[22] P. Bunton, B. Dice, J.A. Pojman, A. De Wit and F. Brau, *Phys. Fluids*, 2014, **26**, 114106

[23] S. Yang and K. Han, *J. Phys. Chem. A.*, 2016, **120**, 4961

[24] J.N. Demas and G.A. Crosby, *J. Phys. Chem.*, 1971, **75**, 991

[25] http://evrogen.com/protein-descriptions/TagBFP-description.pdf [25/09/2017]

[26] https://www.thermofisher.com/us/en/home/brands/molecular-probes/key-molecular-probes-products/alexa-fluor/alexa-fluor-dyes-brightest-conjugates.html [25/09/2017]

[27] M. Garland, J.J. Yim, M. Bogyo, *Cell Chem. Bio.*, 2016, **23**, 122

[28] X. Ma, R. Sun, J. Cheng, J. Liu, F. Gou, H. Xiang and X. Zhou, *J. Chem. Soc.*, **2016**, 93, 345

[29] D.J. Pesak and J.S. Moore, *Angew. Chem. Int. Ed.*, 1997, **36**, 1636

[30] V.R. Thalladi, H.C. Weiss, D. Blaser, R. Boese, A. Nangia and G. Desiraju, *J. Am. Chem. Soc.*, 1998, **120**, 8702

5 Triphenoxazoles: Introduction of Larger Aromatic Area Substituents to Enhance the Photophysical Properties

5.1 Introduction

As discussed in Chapter 1 a large difference between absorption and emission bands are desired for multiple purposes, which include use in dyes,[1] probes[2] and sensors.[3] Organic molecules hold advantages over organometallics fluorescent complexes in certain aspects, often exhibiting a greater quantum yield and usually representing a less expensive alternative.[4] Organometallics which use heavy metals benefit from larger Stokes shift due to the use of an organic light harvester and an increased life time.[5]

Chapter 4 discussed one methodology to enhance the pseudo-Stokes shift ((pSS) >18,000 cm^{-1}) and quantum yield (0.4-0.7) through the introduction of electron withdrawing π-conjugated moieties to the oxazole ring, leading to the classic push-pull electronic molecular system.[6]

Another method of creating molecular structures with a large Stokes shift is, to increase the aromatic area of either the acceptor or donor moiety, allowing greater stabilisation of the charged separated states. Nemykin *et al.* showed an example of this with their boron-coordinated benzoxazoles (Figure 5.1), where they saw a large increase in Stokes shift between the phenyl structure in Figure 5.1a to the naphthyl structure in Figure 5.1b (77 nm to 180 nm).[7] The increase in Stokes shift results from providing more stability to the excited state through having a larger π area to spread the charge in the excited state.

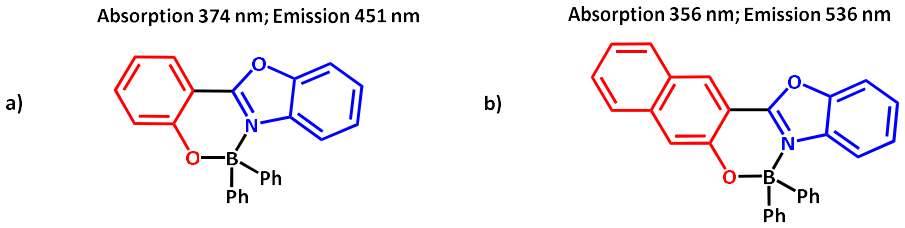

Figure 5.1: Nemykin et al. boron-co-ordinated benzoxazoles (a-b). Acceptor shown in red, donor in blue

Beverina *et al.* extended this to heteroaromatics donors attached to a perylene dye (Figure 5.2),[8] The pSS increased by 87 nm upon going from indolizine (Figure 5.2a) to carbazole (Figure 5.2b)

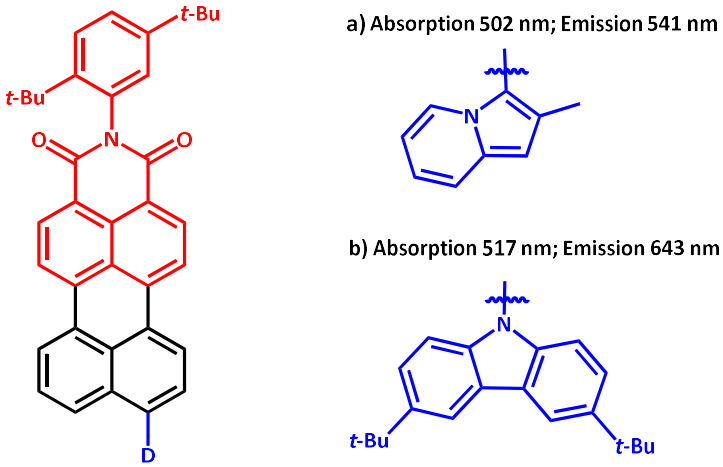

Figure 5.2: Beverina et al. perylene dyes;[8] a) indolizine and b) carbazole. D= donor, acceptor shown in red, donor in blue

5.1.1 Aim of Research in This Chapter

The aim of this chapter is to synthesise a series of triphenoxazoles in which the R moiety increases in π-surface area and substitution pattern, as illustrated in Figure 5.3. This homologous series will be examined to see how these structural effects modify the photophysical and liquid crystal properties, in a similar fashion to the investigation in Chapter 4 of the phenyl and fluoro-phenyl derivatives. In addition, in this chapter the photoconductivity of these materials will be studied.

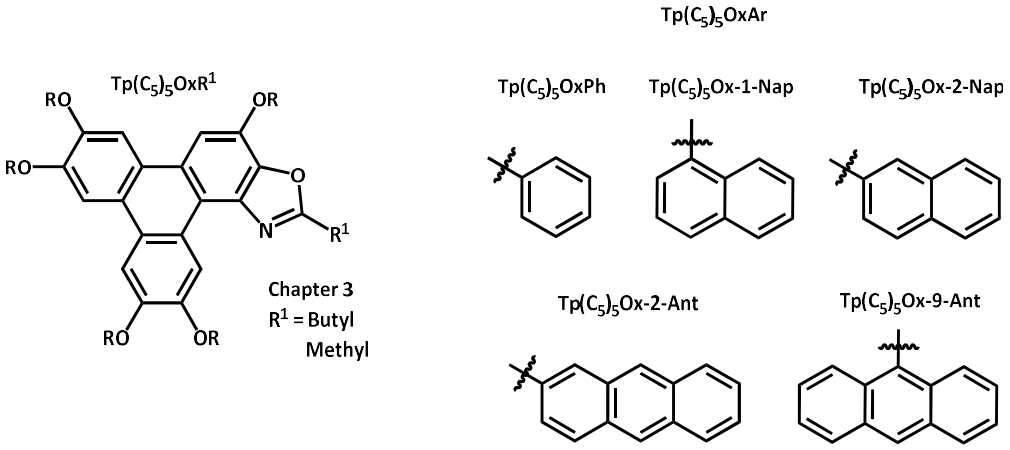

*Figure 5.3: **$Tp(C_5)_5OxR^1$** structures displaying **$Tp(C_5)_5OxAr$** series where $R=C_5H_{11}$*

Scheme 5.1 aims to integrate the work by Nemkin *et al.*[7] and Beverina *et al.*[8] with the previous work in Chapter 4 (Section 4.2.2.2) which discussed the hypothesised *PCEM* mechanism, where fluoro substituents increased stability of the excited state and therefore the Stokes shift. This time greater stabilisation of the excited state, and thus increase in Stokes shift, is achieved by incorporation of larger aromatic groups. The increase in Shift is caused by increase in resonance stabilisation of the Ar group by the additional aryl rings.

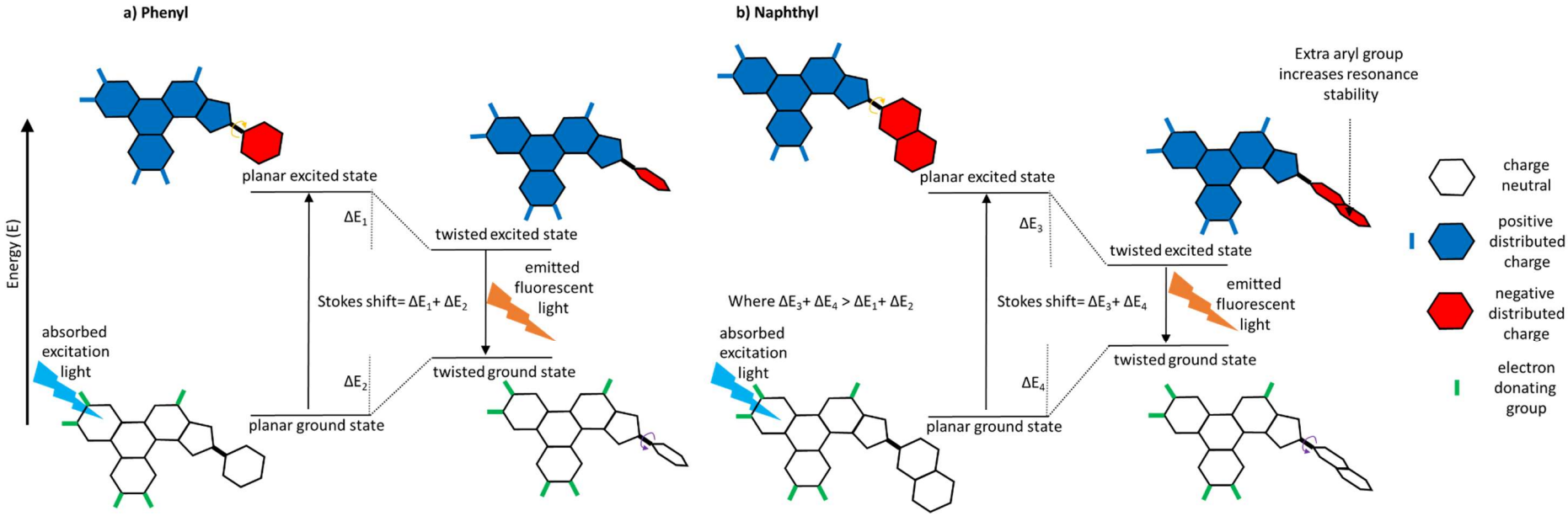

Scheme 5.1: Cartoon representation of planar conjugated emission (PCEM), where skeleton aryl triphenoxazole core is excited to charge separated state. The sum of ΔE equalling the pseudo Stokes shift (pSS). Where R group of oxazole is a) phenyl b) naphthalene

5.2 Results and Discussion

5.2.1 Synthesis of the Tp(C5)5OxAr Series

Chapters 3 and 4 showed the chemistry used to produce triphenoxazoles with different functionalised R groups. This chemistry was further exploited to form **Tp(C5)5OxAr** in 11-34 % yields (Scheme 5.2), *via* the reaction of various aromatic acids with **Tp(C5)6NH2**.[9]

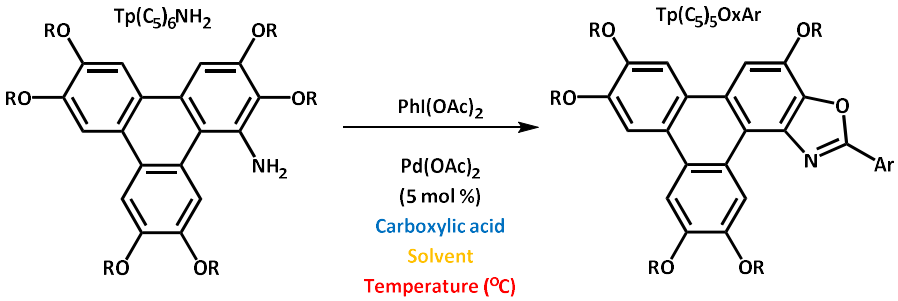

Carboxylic acid	Solvent	Temperature (°C)	Compound	Yield (%)
benzoic acid	toluene	110	$Tp(C_5)_5OxPh$	34
1-naphthanoic acid	toluene	110	$Tp(C_5)_5Ox$-1-Nap	22
2-naphthanoic acid	toluene	110	$Tp(C_5)_5Ox$-2-Nap	32
2-anthracene-carboxylic acid	toluene	110	$Tp(C_5)_5Ox$-2-Ant	20
9-anthracene-carboxylic acid	*o*-xylene	140	$Tp(C_5)_5Ox$-9-Ant	11

*Scheme 5.2: The synthesis of **Tp(C5)5OxAr**, where Ar= aromatic group arising from acids in Figure and R= C_5H_{11}*

All reaction proceeds in poor to reasonable yields in toluene, with the exception of **Tp(C5)5Ox-9-Ant**, which originally failed in toluene. Presumably the flanking of two fused phenyl rings on the central ring makes the acid too sterically encumbered relative to 1-naphthoic acid, with only one

fused ring. Furthermore, the yield of **Tp(C_5)$_5$Ox-2-Nap** is noticeably higher than that of **Tp(C_5)$_5$Ox-1-Nap**, supporting the sterically hindered argument.

However, **Tp(C_5)$_5$Ox-9-Ant** was successfully isolated when the reaction was carried out in *o*-xylene at an elevated temperature of 140 °C. The yields of the other homologues might be increased in this higher boiling point solvent.

The following sections will compare the fluorescent and liquid crystalline properties of the **Tp(C_5)$_5$OxAr** series to the butyl derivative discussed in Chapter 3 (**Tp(C_5)$_5$OxC_4**).

5.2.2 Investigating the Photophysical Properties as a Function of π-Surface Area and Substitution

This section will focus on comparing the photophysical properties (absorption and emission) of **Tp(C_5)$_5$OxC_4** and the **Tp(C_5)$_5$OxAr** series in ethyl acetate, octan-1-ol, acetonitrile, as well as the solid-state emission properties.

5.2.2.1 UV Absorption

The absorption spectra of **Tp(C_5)$_5$OxAr** (Figure 5.4) show significant changes from **Tp(C_5)$_5$OxC_4** in absorption maxima positions (253-275 compared to 280 nm) and significant changes within the series itself.

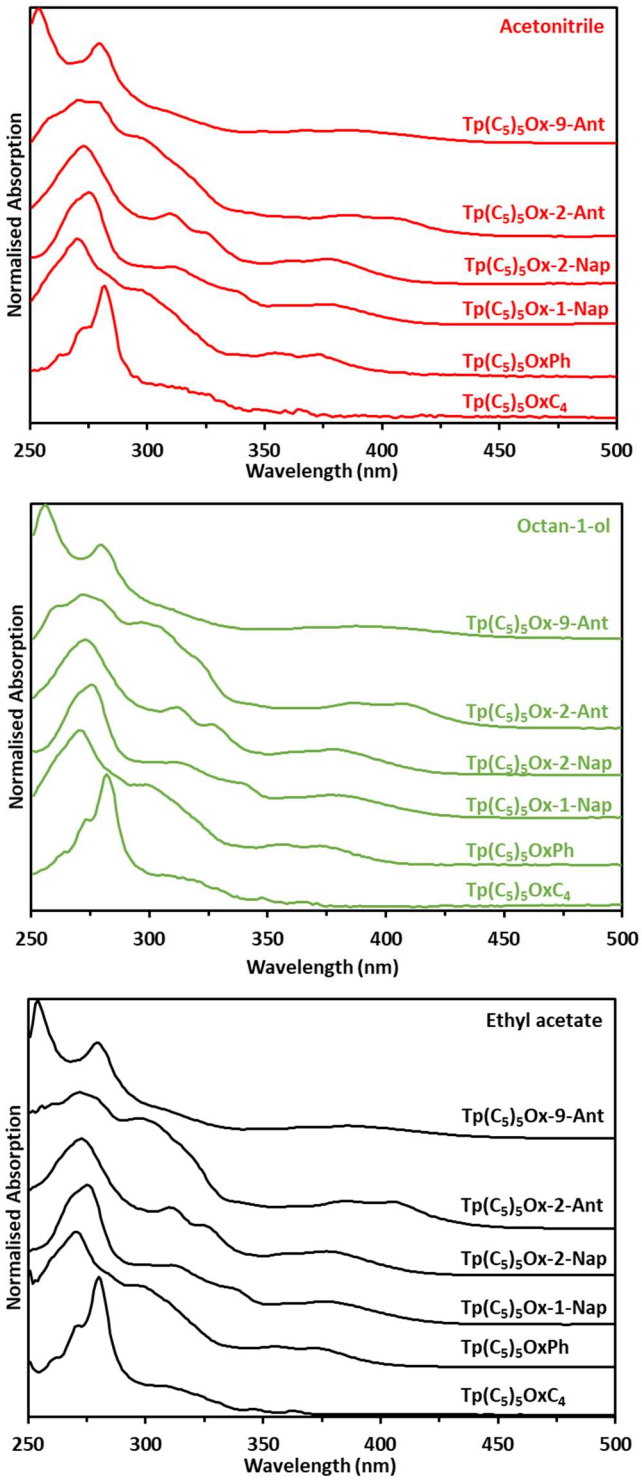

Figure 5.4: Stacked normalised absorption spectra of ***$Tp(C_5)_5OxC_4$*** *and* ***$Tp(C_5)_5OxAr$***

The absorption data from the spectra above are summarised in Table 5.1. Points to note are:

1) a general increase in relative π-π* absorption at (330- 400 nm) as conjugation is increased. **Tp(C$_5$)$_5$Ox-9-Ant** does not follow this trend, and shows the largest blue shift to 253 nm. The absorption band at 253 nm of **Tp(C$_5$)$_5$Ox-9-Ant** resembles literature regarding anthracene and 9-anthracene carboxylic acid.[10] The band at 278 nm resemble **Tp(C$_5$)$_6$** (Chapter 3) and **Tp(C$_5$)$_5$OxC$_4$**;

2) no solvatochromism between solvents in the **Tp(C$_5$)$_5$OxAr**, a trait shared with **Tp(C$_5$)$_6$**, **Tp(C$_5$)$_5$OxC$_4$** and the **Tp(C$_5$)$_5$OxPh*x*F** series (Chapter 4);

3) a shift in absorption maxima to higher energy wavelengths when compared to **Tp(C$_5$)$_5$OxC$_4$** (Table 5.1). This indicates an increase in strength of the system, as there is a requirement of higher energy light to break a bond. [11]

Furthermore, there are differences between the structural isomers within the series:

1) **Tp(C$_5$)$_5$Ox-2-Ant** displays an increased relative absorbance from 270-400 nm when compared to **Tp(C$_5$)$_5$Ox-9-Ant**. Clearly the anthracyl moiety in **Tp(C$_5$)$_5$Ox-2-Ant** relative to **Tp(C$_5$)$_5$Ox-9-Ant** is less sterically restricted with respect to rotation around the C-C bond joining the oxazole ring to the antharacene, thus when considering the extended conjugation through the oxazole to the anthracene, then this will be disrupted more in the 9-isomer and hence differences in the absorption spectrum would be expected;[12]

2) similarly, **Tp(C_5)$_5$Ox-2-Nap** shows larger relative absorbance from 280-400 nm than its **Tp(C_5)$_5$Ox-1-Nap** isomer. Presumably a similar restriction in rotation around the C-C bond as described for the anthracyl derivatives, for the 1-isomer is in effect relative to the 2-isomer.

*Table 5.1: molar absorptivity coefficient (ϵ) at absorption maxima of **Tp(C_5)$_5$OxC$_4$** and the **Tp(C_5)$_5$OxAr** series at 10^{-7} M. Values are averaged from 5 experiments*

	Ethyl acetate		Octan-1-ol		Acetonitrile	
	ϵ x 10^3 (M^{-1} cm^{-1})	λmax (nm)	ϵ x 10^3 (M^{-1} cm^{-1})	λmax (nm)	ϵ x 10^3 (M^{-1} cm^{-1})	λmax (nm)
Tp(C_5)$_5$OxC$_4$	160 ± 15	278	120 ± 12	278	58 ± 6	278
Tp(C_5)$_5$OxPh	110 ± 11	270	105 ± 10	271	66 ± 6	271
Tp(C_5)$_5$Ox-1-Nap	117 ± 12	275	122 ± 12	275	84 ± 8	275
Tp(C_5)$_5$Ox-2-Nap	164 ± 16	272	128 ± 13	272	85 ± 9	273
Tp(C_5)$_5$Ox-2-Ant	105 ± 10	272	106 ± 11	270	†	270
Tp(C_5)$_5$Ox-9-Ant	158 ± 10	253	152 ± 15	255	106 ± 11	253

† No value could be obtained because of **Tp(C_5)$_5$Ox-2-Ant** poor solubility in acetonitrile

The ϵ values of the triphenoxazole species are large (where large is often quoted above >10,000 M^{-1} cm^{-1})[13-14] with values greater than 100,000 M^{-1} cm^{-1} in ethyl acetate and octan-1-ol.

There is a reduction in all ϵ values recorded in acetonitrile across the entire series. It is hypothesised that the **Tp(C_5)$_5$OxAr** is forming aggregates in this solution, as a result of the increased π-π stacking available to the naphthyl and anthracyl derivatives, relative to the phenyl derivative, thus lowering the ϵ.[15] This is evidenced by no reduction in ϵ being observed in the

Tp(C$_5$)$_5$OxPh*x*F series (Chapter 4, Section 4.2.2.1) which due to the fluorine would have a larger dipole, and thus likely be more soluble in acetonitrile [16] and therefore less likely to form aggregates.

5.2.2.2 Photoemission in Solution

The emission spectra **Tp(C$_5$)$_5$OxC$_4$** and **Tp(C$_5$)$_5$OxAr** series are show in Figure 5.5. As discussed in Chapters 3 and 4, the phenyl and fluorophenyl derivatives had a small structured emission spectra with four peak emissions (~365, 384, ~410, ~430 nm), which were coincident with **Tp(C$_5$)$_5$OxC$_4$** and these peaks did not display any significant solvatochromism. This emission band was termed the *twisted non-conjugation emission mechanism* (*TnCEM*). In addition, there was a more dominant and broad emission band that was termed the *planar conjugation emission mechanism* (*PCEM*), which was solvatochromic in terms of λ_{max}. The extended aryl species in this chapter share these two characteristic emission profiles (*TnCEM* and *PCEM*).

Satisfyingly, the structured *TnCEM* emission bands are greater in intensity for the two naphthyl and two anthracyl derivatives, relative to the phenyl derivative, as was expected due to the increased aryl size and hence sterics, leading to a greater conformational preference for the twisted conformer. Indeed, the *TnCEM* emission from the most sterically constricted 9-anthracyl derivative is so intense it has been plotted separately in Figure 5.5d to avoid confusion with the **Tp(C$_5$)$_5$OxC$_4$** emission spectra.

In addition, the aryl derivatives have a higher intensity broad emission band, similar to the phenyl derivatives in Chapter 4, but with λ_{max} red shifted and ranging from 480-630 nm (Figure 5.5), which once again is solvatochromic, associated with the *PCEM* emission.

Table 5.2 summarises the emission spectra data (and the absorption λ_{max}), revealing the solvatochromic dependence of the emissive λ_{max} for each compound. The difference between the absorption maxima and emission maxima (pseudo-Stokes shift (pSS)) observed from **Tp(C_5)$_5$OxAr** are amongst the highest seen in the literature for organic materials.[6-17] The large shifts and position of the emission in the visible part of the spectrum makes these materials very interesting from a technological point-of-view, with opportunities in areas such as luminescent dyes and organic light emitting diodes (OLEDS).[18]

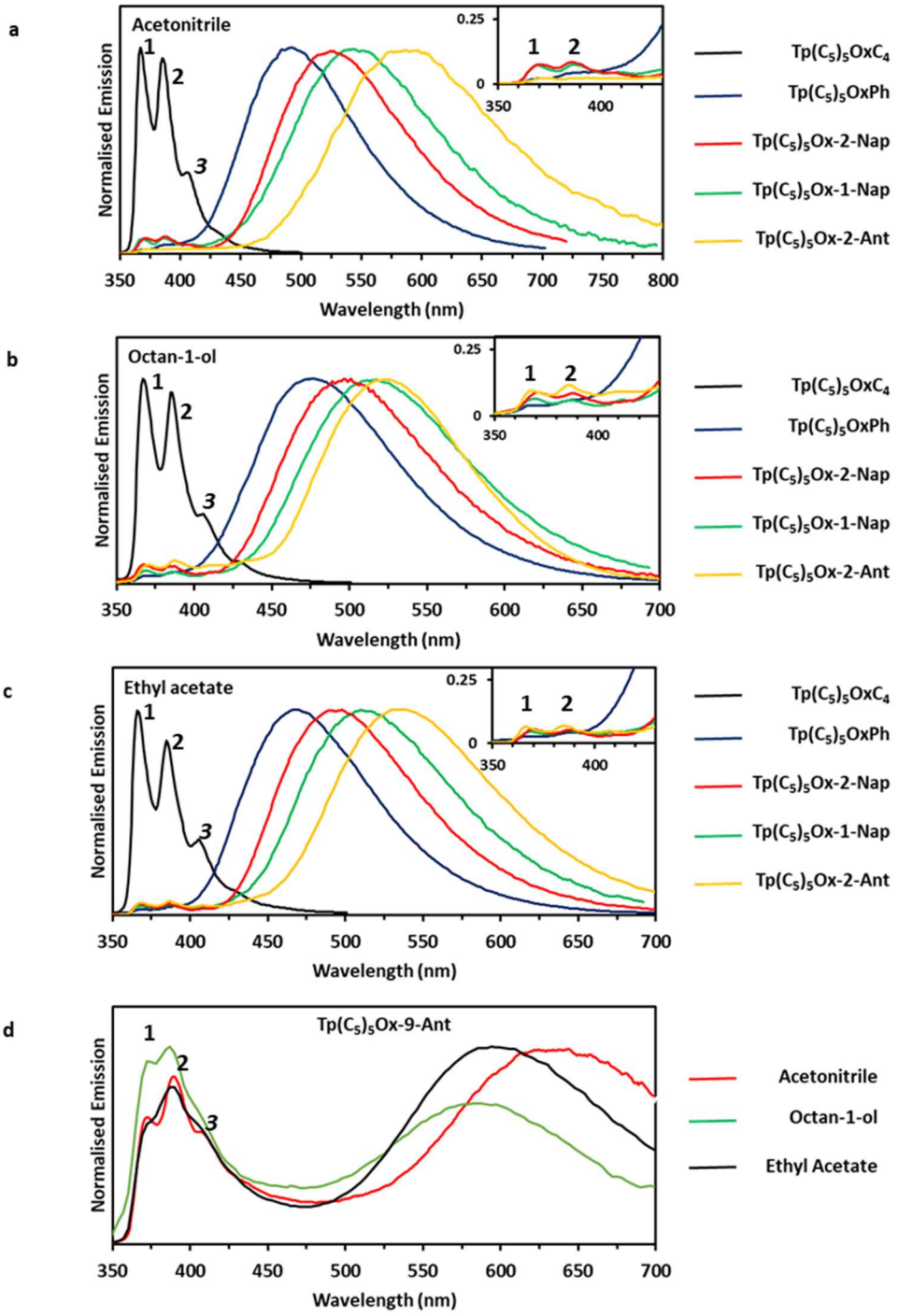

Figure 5.5: Normalised stacked emission spectrum of ***$Tp(C_5)_5OxC_4$, $Tp(C_5)_5OxPh$, $Tp(C_5)_5Ox$-2-Nap, $Tp(C_5)_5Ox$-1-Nap*** *and* ***$Tp(C_5)_5Ox$-2-Ant****, in a) acetonitrile, b) octan-1-ol, c) ethyl acetate. d) $Tp(C_5)_5Ox$-9-Ant in acetonitrile, octan-1-ol and ethyl acetate with TnCEM bands 1,2 and 3*

*Table 5.2: Summary of solution emission of **$Tp(C_5)_5OxC_4$** and the **$Tp(C_5)_5OxAr$** Series, where ϵ_r = dielectric constant, pSS= pseudo Stokes shift*

Solvent	ϵ_r	Viscosity (cP)		$Tp(C_5)_5OxC_4$	$Tp(C_5)_5OxPh$	$Tp(C_5)_5Ox$-2-Nap	$Tp(C_5)_5Ox$-1-Nap	$Tp(C_5)_5Ox$-2-Ant	$Tp(C_5)_5Ox$-9-Ant
Ethyl acetate	6.0	0.45	Absorption λ_{max} (nm)	281	270	272	275	272	253
			Emission λ_{max} (nm)	367	467	494	510	536	594
			pSS (cm^{-1})	8300	15600	16500	16800	18100	22700
			Φ	0.18 ± 0.01	0.46 ± 0.04	0.55 ± 0.05	0.48 ± 0.04	0.51 ± 0.04	†
			Brightness (M^{-1} cm^{-1})	29 ± 5	51 ± 5	92 ± 9	56 ± 5	53 ± 5	†
Octan-1-ol	10.3	7.36	Absorption λ_{max} (nm)	281	271	272	275	270	255
			Emission λ_{max} (nm)	367	473	497	515	526	384*
			pSS (cm^{-1})	8300	15800	16600	17000	18000	13200
			Φ	0.30 ± 0.03	0.61 ± 0.06	0.71 ± 0.07	0.55 ± 0.05	0.56 ± 0.05	†
			Brightness (M^{-1} cm^{-1})	36 ± 7	64 ± 6	91 ± 9	67 ± 7	50 ± 5	†
Acetonitrile	37.5	0.38	Absorption λ_{max} (nm)	281	270	273	275	270	253
			Emission λ_{max} (nm)	367	492	524	543	592	630
			pSS (cm^{-1})	8300	16700	17600	18000	20200	23650
			Φ	0.20 ± 0.02	0.46 ± 0.04	0.51 ± 0.05	0.36 ± 0.04	0.21 ± 0.02	†
			Brightness (M^{-1} cm^{-1})	12 ± 2	38 ± 4	44 ± 4	30 ± 3	‡	†

† No value could be obtained see Section 5.2.2.2.2. ‡ No value could be obtained due to poor solubility and therefore no ϵ data. **TnCEM* mechanism dominates

As noted earlier the *PCEM* emission for the extend aryl systems is more dominant than the **Tp(C_5)$_5$OxPhxF** series discussed in Chapter 4, see insets in Figure 5.5.

There are clearly two emissive bands at 367 nm (band 1) and 385 nm (band 2) coincident with λ_{max} of **Tp(C_5)$_5$OxC$_4$** emissive bands, the *TnCEM* bands. The area underneath the *TnCEM* emission band, as a percentage of total emission, is shown in Table 5.3, which reveals that **Tp(C_5)$_5$Ox-9-Ant** has a much greater (10-20 x) *TnCEM* emission than the other derivatives. One might expect this *TnCEM* emission to be larger than the other derivatives, given that the 9-anthracyl derivative will be the derivative that will find it the most difficult to adopt the planar conformation. A result of the 9-substitution pattern leading to the largest amount of steric clashes with adjacent pendant chains (Scheme 5.3), thus creating an additional bias for the twisted conformation.

However, anthracene also has emission bands in this area of the spectrum. By way of an example Figure 5.6 shows the 9-anthracene carboxylic acid spectra with its structured emission with 4 peaks at 388 nm, 411nm, 425 nm and 448 nm (λ_{max}).[19] Close examination reveals that these are distinct from the structured bands originating from the *TnCEM* emission of the triphenoxazoles, and in particular from **Tp(C_5)$_5$Ox-9-Ant**, which are at 368 nm, 389 nm and 410 nm. Thus, although one cannot rule out that there is no emission from the 9-anthracyl moiety leading to the bands observed at 368 nm, 389 nm and 410 nm, one can say that it is a low emission process and is, at least, masked by the *TnCEM* emission of the **Tp(C_5)$_5$Ox-9-Ant**. Therefore, the *TnCEM* relative emission in Table 5.3 may be overestimated.

Table 5.3: Percentage areas of TnCEM relative to the total emission

	Ethyl acetate	Octan-1-ol	Acetonitrile
	% area of *TnCEM* of total emission (%)	% area of *TnCEM* total emission (%)	% area of *TnCEM* of total emission (%)
$Tp(C_5)_5OxPh$	1.5	1.9	1.1
$Tp(C_5)_5Ox$-1-Nap	1.3	1.9	1.5
$Tp(C_5)_5Ox$-2-Nap	1.5	2.3	2
$Tp(C_5)_5Ox$-2-Ant	1.5	2.5	1.0
$Tp(C_5)_5Ox$-9-Ant†	23	28	21

†Estimated from extending the slope of the *PCEM* peak and integrating area.

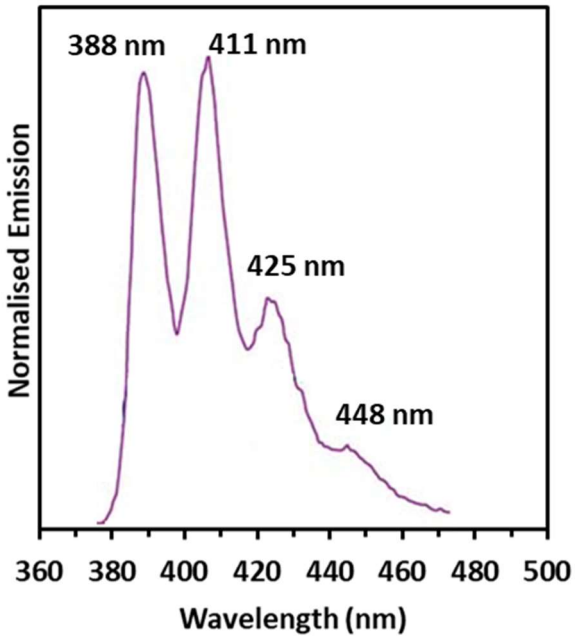

Figure 5.6: 9-anthracene carboxylic acid emission spectrum from Prough et al.[Error! Bookmark not defined.] *with λ_{max} labelled*

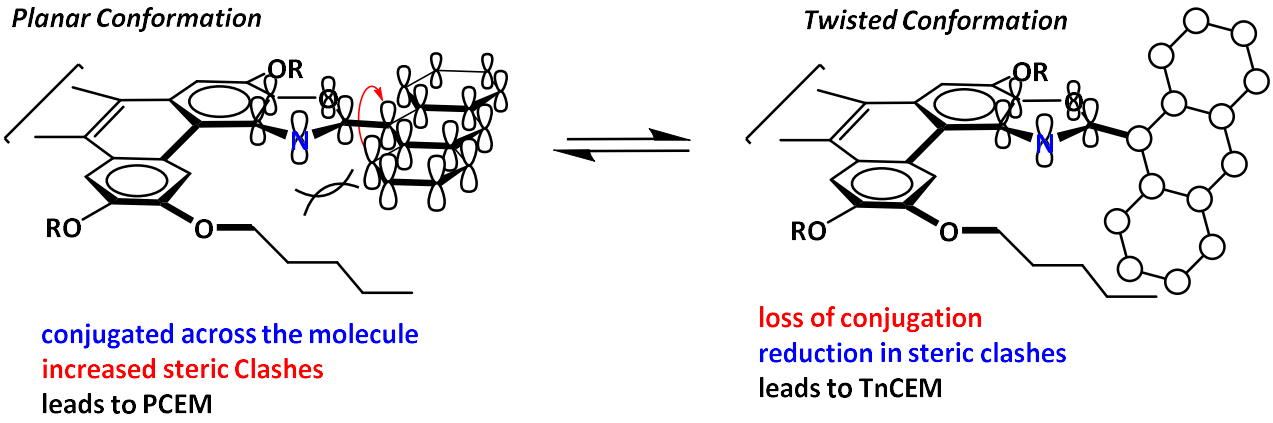

Scheme 5.3: Cartoon graphic showing the reduction of steric clashes with adjacent pendant alkoxy chains, but loss of conjugation, through adoption of the twisted conformation.

Furthermore, the reaction to form the 9-anthracyl derivative required higher temperatures than the rest of the aryl triphenoxazole series, supporting the steric hindrance hypothesis within the molecule are significantly higher than the rest of the **Tp(C_5)$_5$OxAr** series.

5.2.2.2.1 Examining the Pseudo Stokes Shift

The hypothesis in this chapter was that the pSS might be modulated and increased by the introduction of larger aryl group leading to greater resonance stabilisation of the excited state. To enable further probing of this hypothesis the emission mechanism shown in Scheme 5.1 was simplified and it was assumed that in the excited state, charge separation leads to an anionic charge, which would be stabilised by the **Ar** substituents (as the electron acceptor), and the cationic charge by the **Tp(C_5)$_5$Ox** (as the donor) moiety.

Clearly the number of resonance structures contributing to the cationic charge stabilisation will be the same for each molecule, but the number contributing to the anionic stabilisation will

increase with the π-surface area and substitution pattern of the aryl substituent. Thus, the number of resonance forms of each aryl group supporting the anionic charge was determined (Scheme 5.4) and used as a proxy for the resonance stabilisation energy (Figure 5.7a).

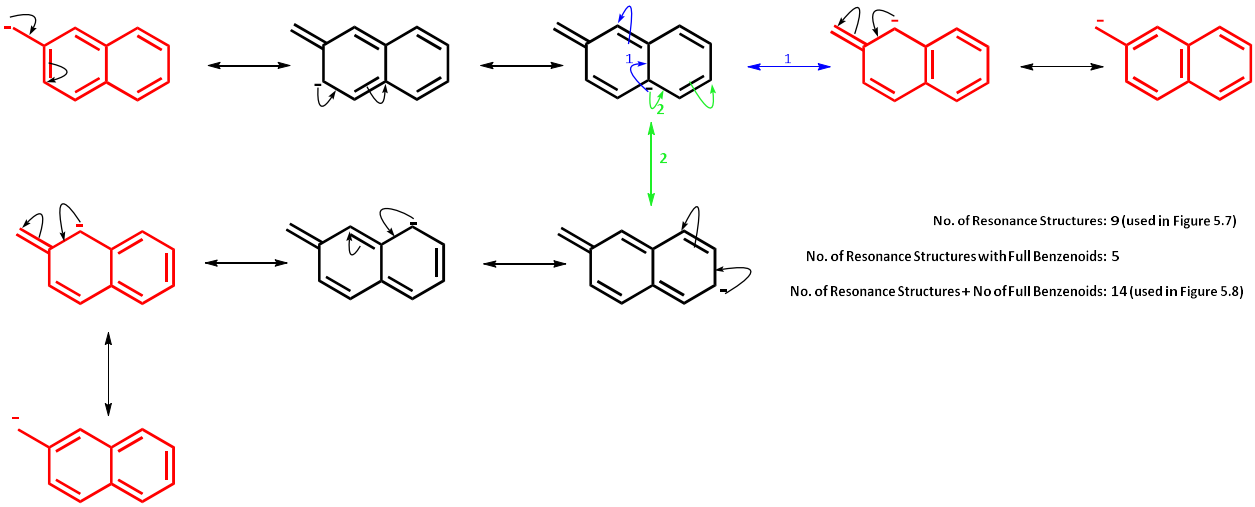

Scheme 5.4: Resonance forms of 2-Naphthyl derivative. Full benzenoids are displayed in red

Figure 5.7a is a plot of total number of resonance structures for each aryl anion (x-axis) versus pSS (y axis), which gives a reasonably straight line correlation (R^2 = 0.9399). However, on further consideration a plot of number of resonance structures, plus the number of resonance structures which contained intact benzenoid cores (Scheme 5.4), attempting to take into account the greater contribution of these resonances to the stabilisation, gave a significantly enhanced linear plot (Figure 5.7b), with an R^2 = 0.9934.

Of course, this is qualitative analysis, and computational studies are being conducted in the Johnston group in the School at present to bring a quantitative understanding to this hypothesis leading to an enhanced pSS.

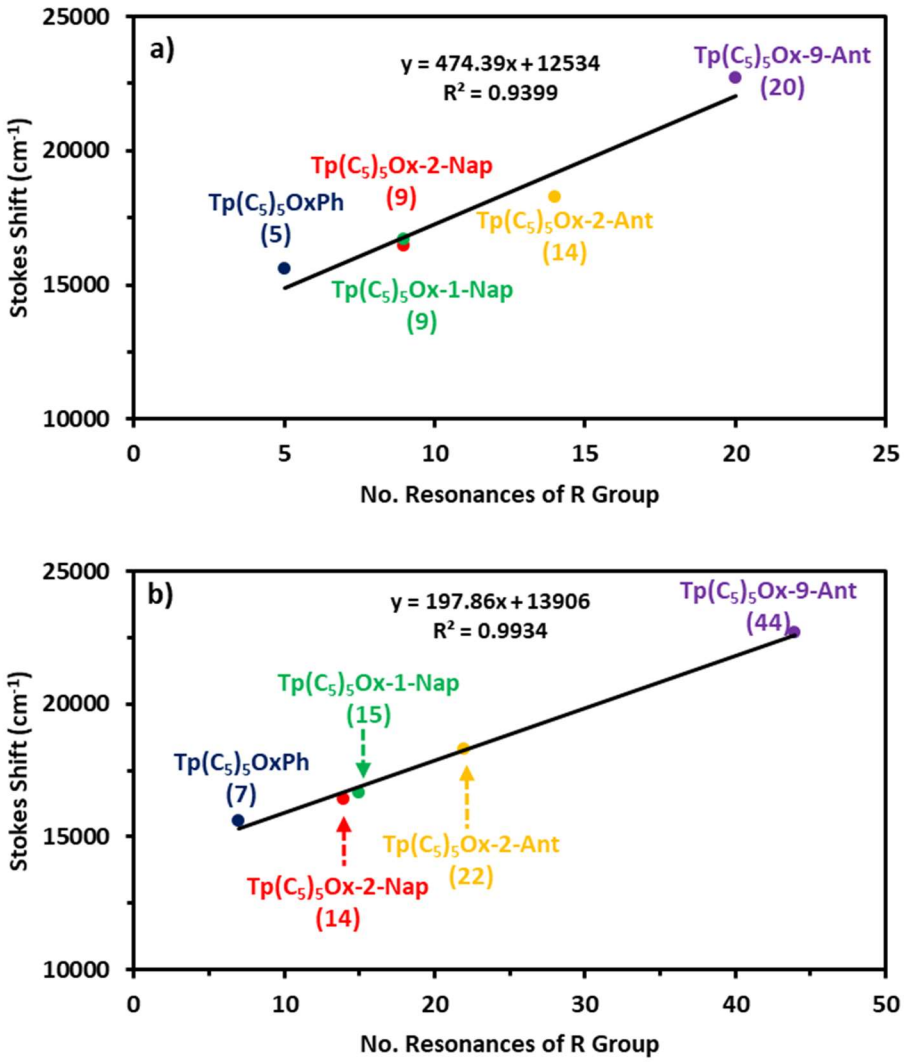

*Figure 5.7: Pseudo Stokes shift (pSS) in ethyl acetate of **Tp(C5)5OxAr** series plotted against a) the No. of Resonances of Ar Group b) the No. of Resonances of Ar Group plus full benzenoids*

Although this is a qualitative analysis it is thought to be the first time that the pSS can be pseudo-predicted by considering the resonance forms of the structure. If this relationship holds for other polyaromatic hydrocarbons (PAHs) then the molecular structure could be designed to give an emission wavelength. This prospect holds exciting possibilities for tuning the colour in the visible

part of the spectrum, for technological uses in displays. However, this hypothesis is still in development and, longer (e.g. tetracene, pentacene) and non-linear (chrysene) PAHs with varying substitution patterns need to be examined, and then quantitatively analysed using computational methods, rather than the qualitative approach of counting the resonance structures.

5.2.2.2.1.1 Effect of Solvent Polarity on the Emission Peak

The change in pSS of the *PCEM* band between ethyl acetate, octan-1-ol and acetonitrile displays a general trend that as polarity of the solvent increases so does the pSS, as illustrated in Figure 5.8.

The increase of pSS with solvent polarity is typical of twisted internal charge transfer (TICT) mechanisms[20] and demonstrates the excited state is being stabilised by the more polar solvents, thus showing red shifts as solvent polarity increases (see Section 1.5.1 for more details on TICT).

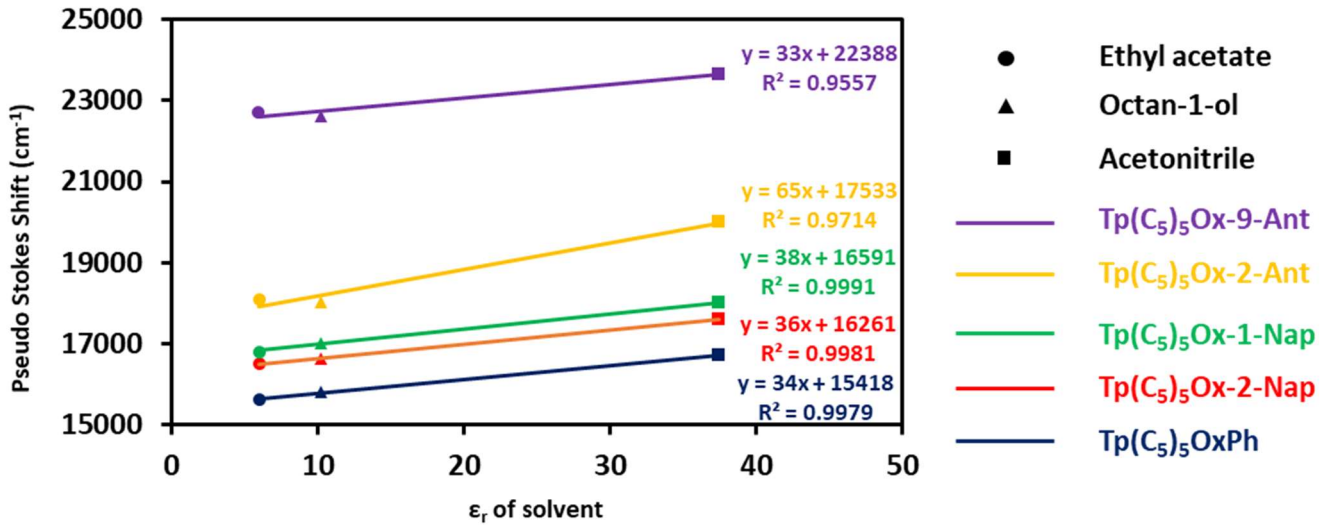

Figure 5.8: Change in pseudo Stokes shift (pSS) of PCEM across ethyl acetate, octan-1-ol (ϵ_r 10) and acetonitrile (ϵ_r 37) for ***Tp(C5)5OxAr*** *series plotted against ϵ_r of the solvent*

Tp(C_5)$_5$OxPh, **Tp(C_5)$_5$Ox-2-Nap**, **Tp(C_5)$_5$Ox-1-Nap** and **Tp(C_5)$_5$Ox-9-Ant** display a similar gradient (33-38 cm^{-1} increase of pSS for every 1 increase in dielectric constant). However, a noticeable anomaly in Figure 5.8 is that both **Tp(C_5)$_5$Ox-2-Ant** and **Tp(C_5)$_5$Ox-9-Ant** show a small decrease in pSS when in octan-1-ol (18000 cm^{-1} and 22600 cm^{-1}) compared to when in ethyl acetate (18100 cm^{-1} and 22700 cm^{-1}). Furthermore, the gradient of **Tp(C_5)$_5$Ox-2-Ant** is nearly double that of the **Tp(C_5)$_5$OxAr** series. These anomalies indicate that polarity is not the only variable to consider when predicting the pSS and more data is needed before being able to accurately predict the pSS in various solvents.

5.2.2.2.2 Examining the Quantum Yield

The quantum yield (Φ) shows the efficiency of the luminescence relaxation pathway of the excited state. A Φ of 1 would mean all molecules excited at that wavelength emit light through radiative relaxation. Conversely a Φ of 0 would show all molecules relax through non-radiative pathways.[21] The Φ of the **Tp(C_5)$_5$OxAr** series was calculated using the serial dilution method methodology described in Chapter 4 (Section 4.2.2.2.2), using **Tp(C_5)$_5$OxC_4** as a reference. The Φ values are displayed in Table 5.2.

The Φ is similar across the entire series and does not change with increasing π area. All Φ bar **Tp(C_5)$_5$Ox-2-Ant** are more than twice that of **Tp(C_5)$_5$OxC_4**, and therefore show the radiative luminescent relaxation pathway is more prominent. It is understood why the Φ of **Tp(C_5)$_5$Ox-2-Ant** is significantly reduced in acetonitrile, though it should be noted that **Tp(C_5)$_5$Ox-2-Ant** is the least soluble in acetonitrile, so the decrease could be attributed to aggregation.[22]

Unfortunately, the Φ of **Tp(C$_5$)$_5$Ox-9-Ant** was impossible to determine accurately with current equipment due to the broadness of the emission (Figure 5.9) causing the emission to extend past the range of the visible photomultiplier tube (PMT). A near infrared PMT would be needed to collect the full emission of the molecule, and future experiments are devised to use this.

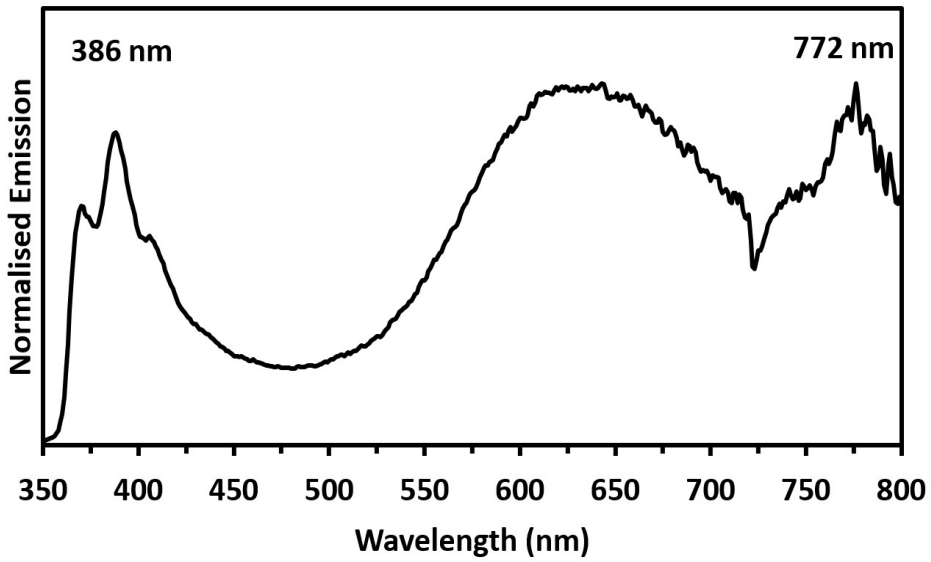

*Figure 5.9: Emission spectrum 350-800 nm of **Tp(C$_5$)$_5$Ox-9-Ant** in acetonitrile showing a large range from 350 - >800 nm*

The peak at 772 nm origin is unknown and future investigation is necessary to determine its origin.

5.2.2.2.3 Examining the Brightness

The brightness of the **Tp(C$_5$)$_5$OxAr** series up until **Tp(C$_5$)$_5$Ox-9-Ant** is tabulated in Table 5.2. Unfortunately, due to lack of Φ data for **Tp(C$_5$)$_5$Ox-9-Ant** the brightness could not be calculated and similarly the brightness of **Tp(C$_5$)$_5$Ox-2-Ant** could not be calculated as no ϵ data could be attained due to poor solubility. Table 5.2 shows brightness values 2 - 6 times more bright than **Tp(C$_5$)$_6$**. There is a noticeable drop in brightness when measured in acetonitrile compared to ethyl acetate and octan-1-ol which is theorised to be due to aggregation of the triphenoxazoles (Section

5.2.2.1) lowering the ϵ and thus the brightness. This is similar to **Tp(C_5)$_5$OxC_4**, but in the **Tp(C_5)$_5$OxPh*x*F** series no drop in ϵ when in acetonitrile was observed. This was theorised that the fluorophenyls exerted a greater dipole and thus were more likely to be soluble in the polar MeCN.[16]

The ϵ, Φ and therefore brightness displayed by the series are comparable to fluorescent dyes currently on the market. [23-24] This serves as early indication that these molecules could become an attractive proposition in applications such as fluorescent dyes[1] and probes.[25]

5.2.3 Photoemission as a Solid

The solid-state emission profile from the **Tp(C_5)$_5$OxAr** series in solid state (Figure 5.10) shows the broad range emission akin to that observed in solution (Figure 5.5). One noticeable difference is the reduction of the structured *TnCEM* bands at 360-390 nm for the series, such that for all but **Tp(C_5)$_5$Ox-9-Ant** (Figure 5.11), are not detectable, and even for the 9-anthracyl derivative they are significantly reduced to 1.5 % of the total emission peak.

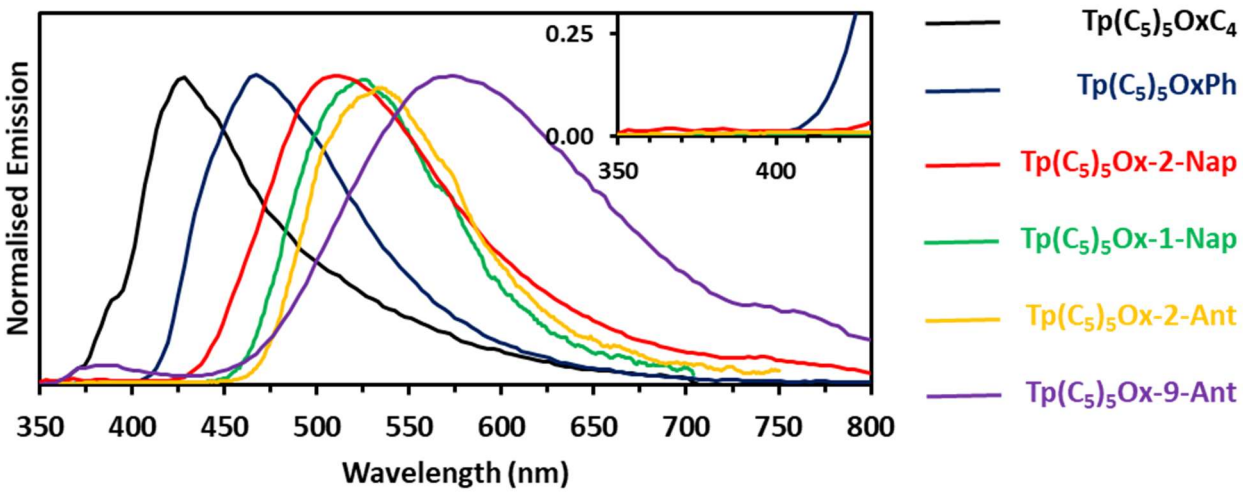

Figure 5.10: Normalised emission spectrum in the solid state of ***Tp(C5)5OxC4*** *and the* ***Tp(C5)5OxAr*** *series*

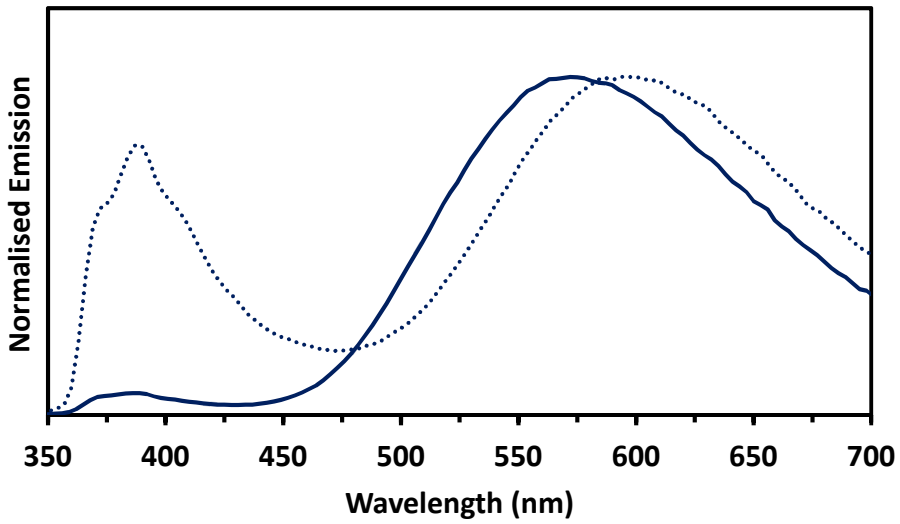

Figure 5.11: Comparison of emission spectra of ***Tp(C5)5Ox-9-Ant*** *in solution (dotted line) and solid state (solid line)*

This reduction of the *TnCEM* emission of the **Tp(C5)5OxAr** in the solid state, implies that the rotation around the aryl to oxazole C-C bond is suppressed and leaves these moieties close to a planar conformation, such that the *PCEM* emission dominates even more, when compared to the

solution state. This solid-state effect of reduction of the TnCEM emission was also observed in the **Tp(C$_5$)$_5$OxPhxF** series in Chapter 4.

Table 5.4: Comparison of emission maxima in ethyl acetate and solid state

	Tp(C$_5$)$_5$OxPh	**Tp(C$_5$)$_5$Ox-1-Nap**	**Tp(C$_5$)$_5$Ox-2-Nap**	**Tp(C$_5$)$_5$Ox-2-Ant**	**Tp(C$_5$)$_5$Ox-9-Ant**
	Emission Max (nm)	Emission Max (nm)	Emission Max (nm)	Emission Max (nm)	Emission Max (nm)
Ethyl acetate	467	508	492	537	594
Solid state	467	520	509	533	575
Δ	0	+12	+17	-7	-19

Interestingly, for the phenyl derivative there is apparently no shift in the emission λ_{max} going from the solution state to the solid state, whereas for the naphthyl derivatives there is a red shift in the solid state, and a blue shift for the anthracyl derivatives, showing that the intermolecular interactions of the solid state can have a stabilising or destabilising effect on the excited state when compared to solution.

Thus, the **Tp(C$_5$)$_5$OxAr** series display a systematic variation in colour (Figure 5.12) from blue to orange, as an apparent function of resonance stabilisation of the charged separated excited state, which allows the possibility for predictive colour tuning.

Importantly for potential display applications, the emission is not quenched in the solid state, and has the same systematic colour variation as in solution (Figure 5.12).

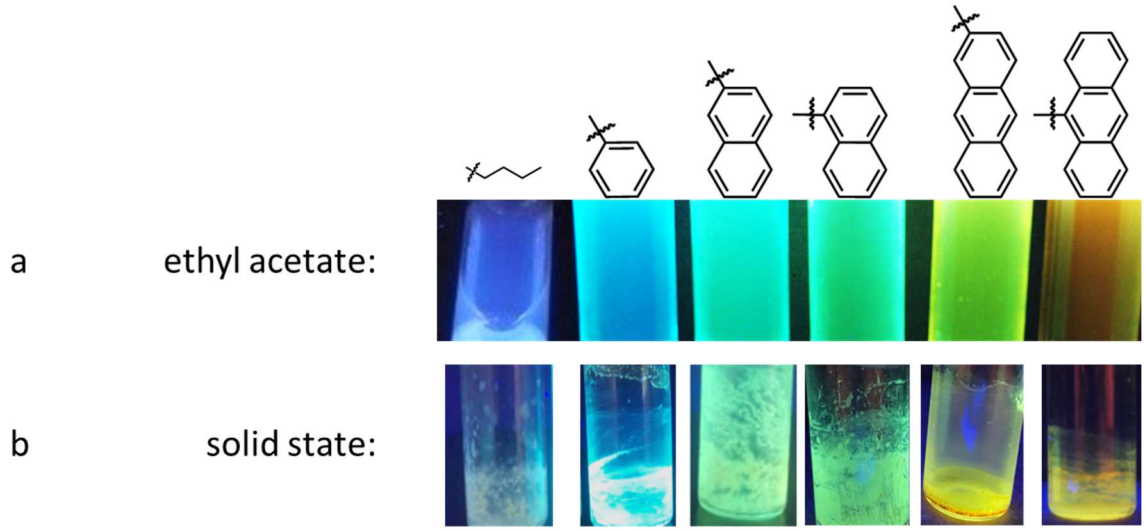

Figure 5.12: Various triphenoxazole under 302 nm UV light (4 W). a) ***Tp(C$_5$)$_5$OxC$_4$*** *and the* ***Tp(C$_5$)$_5$OxAr*** *series in ethyl acetate b)* ***Tp(C$_5$)$_5$OxC$_4$, Tp(C$_5$)$_5$OxPh, Tp(C$_5$)$_5$Ox-2-Nap*** *and* ***Tp(C$_5$)$_5$Ox-9-Ant***

5.2.4 Liquid Crystallinity

Given that the parent triphenylene structure is a well-known discotic liquid crystalline material and the chemical modification of it to the **Tp(C_5)$_5$OxPh*x*F** series in Chapter 4 still sustained the Col_h mesophase, it is not unreasonable to investigate the aryl derivatives made in this chapter to see if they could still sustain a mesophase.

Of course, structurally the **Tp(C_5)$_5$OxAr** series might be thought to be less mesogenic than **Tp(C_5)$_5$OxC_4** because

1) the aryl group is systematically increasing the π-surface area relative to the flexible alkyl chain component from phenyl through naphthyl to anthracyl, and hence modifying the balance of the molecular structural properties that are governing the state of matter,
2) the introduction of the Ar groups will have a tendency to be out of plane with the triphenoxazole moiety, as their size increases and substitution pattern varies. These two factors may inhibit the stacking of the molecular structures to support a columnar mesophase, or indeed any mesophase.

The thermal analysis of the **Tp(C_5)$_5$OxAr** series is discussed below.

5.2.4.1 DSC Thermal Analysis

Table 5.5 summarises the transition temperatures of **Tp(C_5)$_5$OxC_4** and the **Tp(C_5)$_5$OxAr** series. The assignment of Col_h and Col_x phases are discussed in the section below, when considering the mesophase textures obtained from polarised optical microscopy.

Across the series there is a general increase in LC range when cooling, which is a common trait of discotic mesogens.[26]

*Table 5.5 Summary of phase transitions for the **Tp(C5)5OxAr** series (2nd cycle of DSC scan). Where Cr= Crystalline, X= unknown endothermic event, Col_h= hexagonal columnar, I= Isotropic and Col_x= unknown liquid crystalline state. DSC scan 10 °C min^{-1}*

**transition not observed on DSC scan and temperature stated from POM*

Compound	**Heating (°C)**			**Cooling (°C)**	
Phase	Cr-X	X-Col_h	Col_h-I	I-Col_h	Col_h-Cr
Tp(C5)5OxC4	95	99	141	137	59
Tp(C5)5OxPh	103	110	189	185	78
Tp(C5)5Ox-1-Nap	86	96	168	161	43
Tp(C5)5Ox-2-Nap	88	96	197	196	152*
Tp(C5)5Ox-2-Ant		162	185	151	83
Tp(C5)5Ox-9-Ant†		**172**	**182**	**151**	**134**
		Cr-Col_x	**Col_x-I**	**I-Col_x**	**Col_x-Cr**

† **Tp(C5)5Ox-9-Ant** phase changes displayed in bold underneath the temperature

5.2.4.2 POM Thermal Analysis

Figure 5.13 displays POM images of the LC phase during the cooling cycle for the **Tp(C5)5OxAr** series and **Tp(C5)5OxC4** as a comparison.

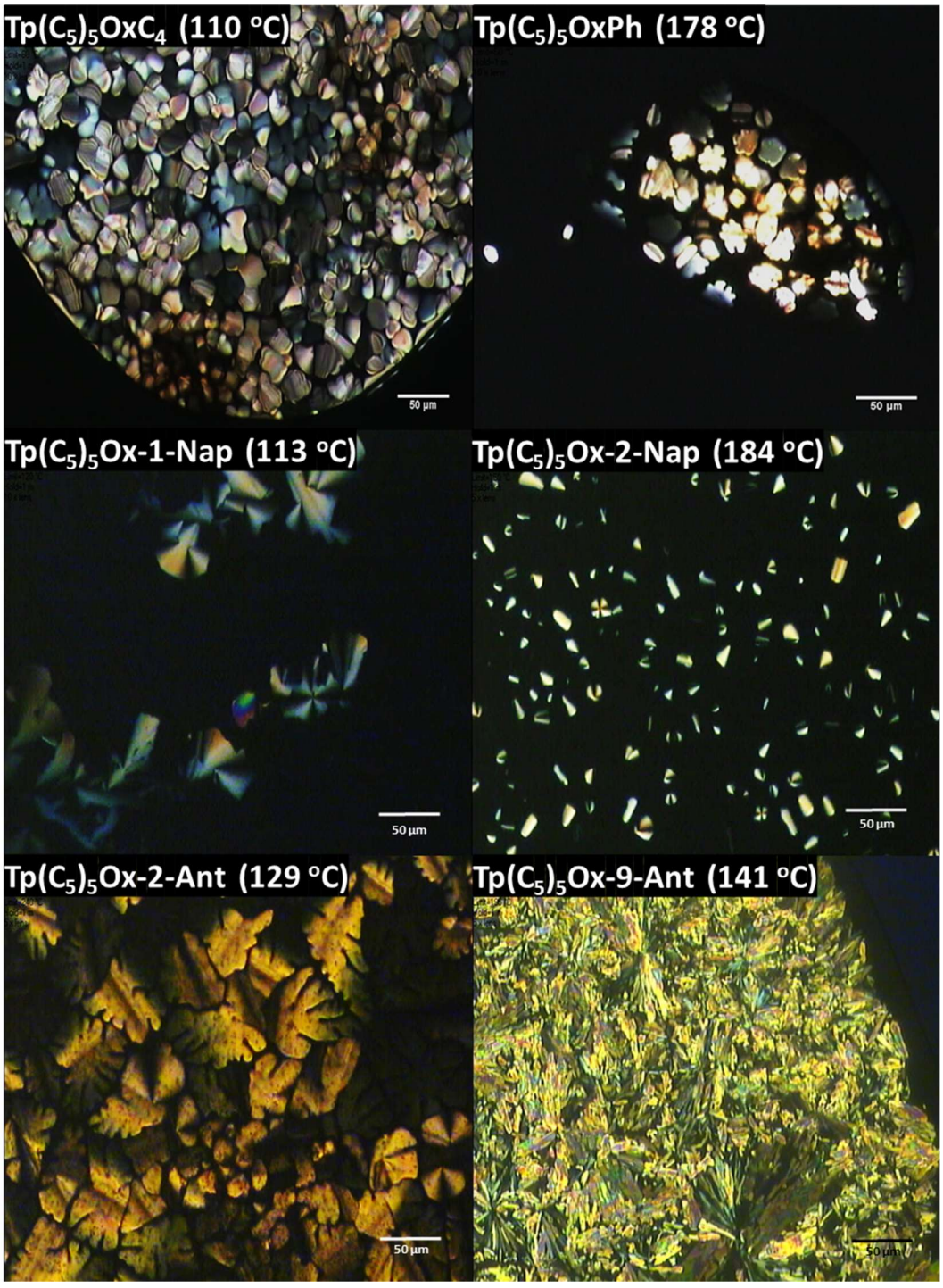

Figure 5.13: POM images (temperature included in the images) during the cooling cycle

Col_h can be assigned with reasonable confidence for all mesogens bar **$Tp(C_5)_5Ox$-9-Ant** due to the similarity in POM image to **$Tp(C_5)_5OxC_4$**, which was shown by XRD to be a Col_h mesogen (Section 3.2.6). The POM images themselves show many of the characteristics of Col_h with the broken snowflake texture and fan textures observed.[27]

The **$Tp(C_5)_5Ox$-9-Ant** sheerable texture in Figure 5.13 does not have the fans or broken snowflakes observed in the other mesogens, as such could not be defined as Col_h. The difference in texture or indeed phase could be related to the steric bulk of the 9-anthracene group causing frustration within the packing, thus preventing higher supramolecular ordering like Col_h. This rationale leads to the hypothesis of **$Tp(C_5)_5Ox$-9-Ant** might have adopted discotic nematic phase. However, the texture does not resemble that seen in the literature for discotic nematics[28-29] and as such cannot be defined. More sample is required for XRD to quantitatively define the phase.

5.2.4.3 Rationalising the Liquid Crystal Temperature Range

To investigate these DLC properties Figure 5.14 is a plot of phase changes for the triphenoxazoles discussed in this chapter. Several points are worth noting:

1) The replacement of the butyl group (**$Tp(C_5)_5OxC_4$**) by the phenyl group (**$Tp(C_5)_5OxPh$**) has not had a deleterious effect on the Col_h phase range (**$Tp(C_5)_5OxC_4$** phase range of 107 °C; **$Tp(C_5)_5OxPh$** phase range of 108 °C), as noted in Chapter 4;

2) Increasing the size of the aryl substituent has led to an increase in DLC phase range when cooling of **$Tp(C_5)_5OxPh$** (105 °C) is compared to **$Tp(C_5)_5Ox$-1-Nap** (118 °C). Or heating of **$Tp(C_5)_5OxPh$** (79 °C) is compared to heating of **$Tp(C_5)_5Ox$-2-Nap** (101 °C);

3) Conversely, increasing to larger aryl substituents has led to small DLC phase ranges for the heating of **Tp(C$_5$)$_5$Ox-1-Nap** (72 °C) and **Tp(C$_5$)$_5$Ox-2-Ant** (23 °C) when compared to **Tp(C$_5$)$_5$OxPh** (79 °C);

4) And the DLC phase range cooling of **Tp(C$_5$)$_5$Ox-2-Nap** (44 °C) and **Tp(C$_5$)$_5$Ox-2-Ant** (68 °C); is also decreased when compared to **Tp(C$_5$)$_5$OxPh** (105 °C).

These points collectively show that trends for the DLC properties are hard to identify with regards to increases in the Aryl R-group sizes and substitution pattern size.

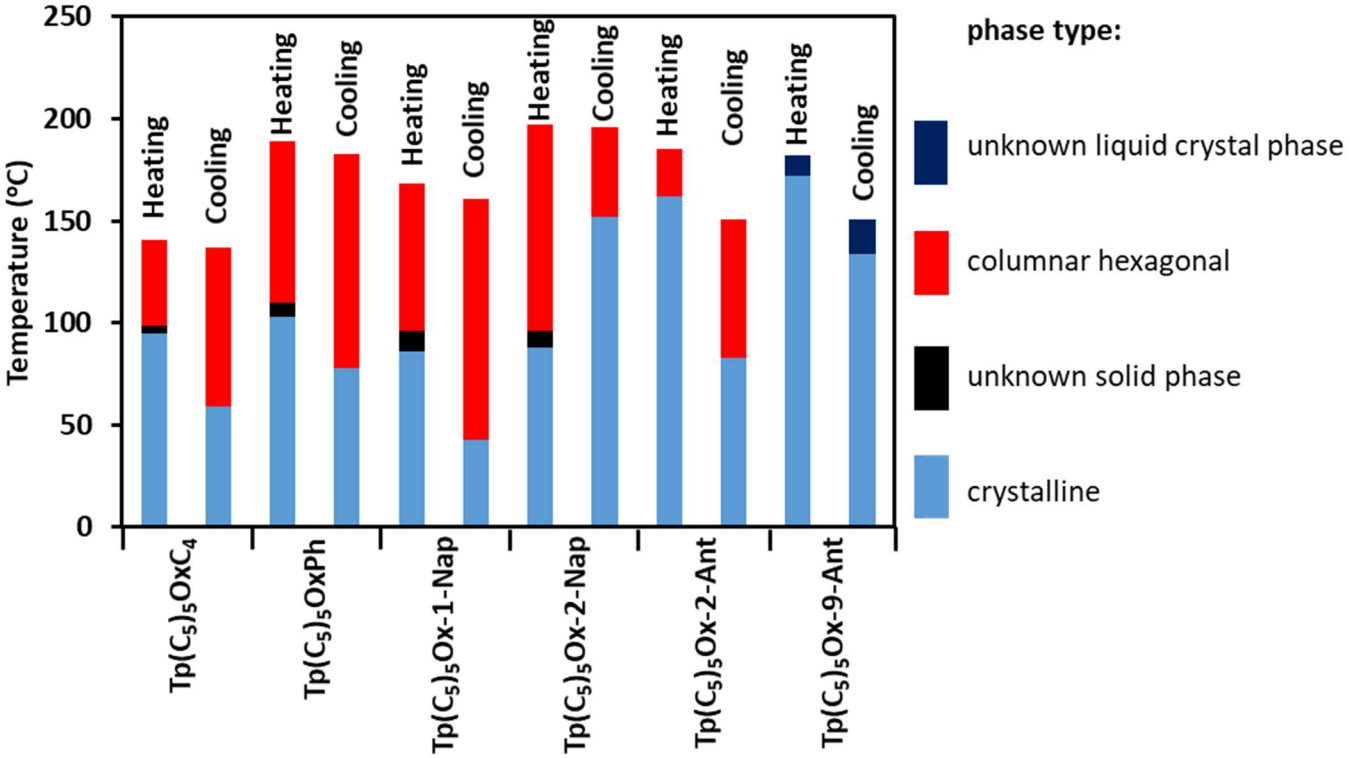

*Figure 5.14: Plot of Phase type of **Tp(C$_5$)$_5$OxC$_4$** and the **Tp(C$_5$)$_5$OxAr** series#*

However, **Tp(C$_5$)$_5$Ox-1-Nap** larger phase range when cooling compared to **Tp(C$_5$)$_5$Ox-2-Nap** (118 °C compared to 44 °C) is at first glance peculiar. **Tp(C$_5$)$_5$Ox-1-Nap** looks to be more sterically hindered than its isomer **Tp(C$_5$)$_5$Ox-2-Nap**. However, when analysing the rotation between the oxazole and the naphthyl unit it becomes clear that one conformation of the 1-naphthyl derivative would be preferred (Figure 5.15a). This less hindered conformation could lead to increased π-π stacking thus explaining the large phase range. By analysing **Tp(C$_5$)$_5$Ox-2-Nap** in the same manner, it is not clear which conformation would be preferred (Figure 5.15b).

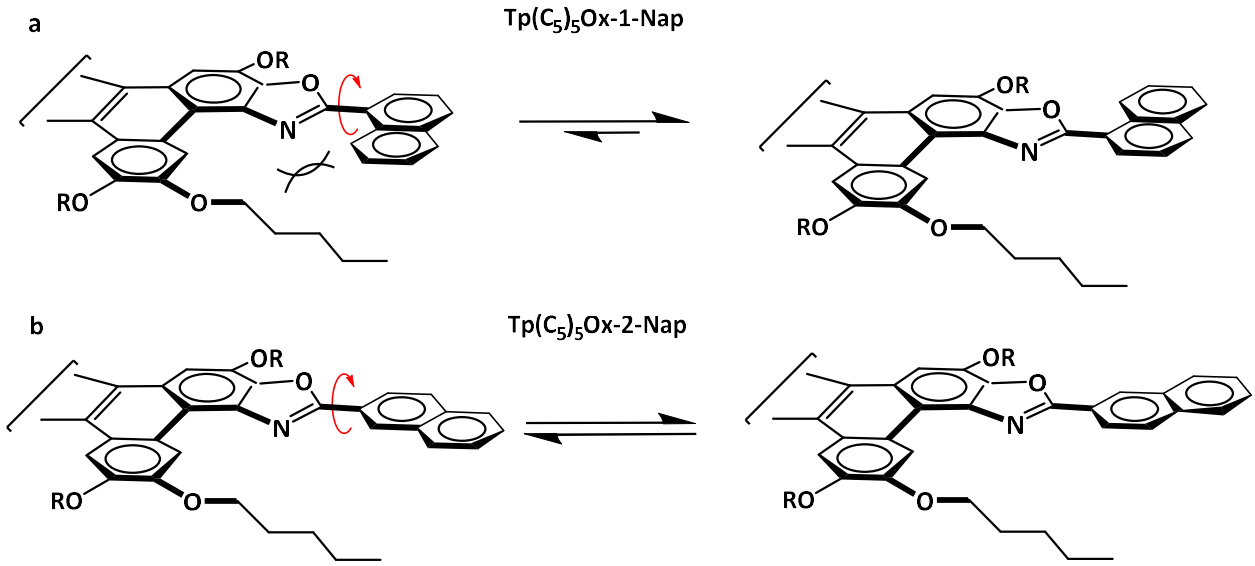

*Figure 5.15: Conformational analysis of a) **Tp(C$_5$)$_5$Ox-1-Nap** and b) **Tp(C$_5$)$_5$Ox-2-Nap***

Most of the **Tp(C$_5$)$_5$OxAr** series display DLC properties over a large temperature range of 70-118 °C, and show that modification of the triphenylene-oxazole aryl group causes drastic changes to the temperature range. One can imagine that combining the increase in size of aryl substituents with

electron withdrawing groups as shown in Chapter 4 could allow in the future for the temperature range of liquid crystallinity to be fine-tuned, as well as extending the PSS.

5.2.5 Examination of Photoconductivity of Triphenoxazoles

The ability to translate light energy into current (photoconductivity) has been of great importance in the generation of solar cells.[30] Triphenylene and related structures have been investigated elsewhere for their photoconductive properties,[31] which were found to be significant, and were thought to be related to their columnar ordering. The photoconductive properties of aryl triphenoxazoles are therefore interesting, given their enhanced photophysical properties over the parent triphenylene. The photoconductivity of these materials is described below.

5.2.5.1 Experimental Design

Experiments in this section were carried out in collaboration with the research group of Dr Alex Robinson (School of Chemical Engineering) through Karolis Virzbickas (joint PhD student with Jon Preece).

Photoconductivity was measured using a two-probe system (Figure 5.16). An input of 10 V was delivered across a 100 nm thick, 100 µm long gold underlayer, separated by 10 µm of a 300 nm thick **$Tp(C_5)_6$/$Tp(C_5)_5OxR^1$** sample. The sample was irradiated with an 8 W λ= 350 nm lamp. The current was measured with and without light irradiation (Keithley instrument) and the current was converted to conductivity using Equation 5.1.[32]

$$\sigma = \frac{Il}{VA}$$

Equation 5.1: Conversion to conductivity (in S cm^{-1}), where I= measured current (A), V= Voltage (10 V). A= cross sectional area (10 x 100 µm = 1 x10^{-5} cm^2), l= length of pathway (10 µm)

Heat was applied to the quartz wafer and measurements were carried out between 20-120 °C. Further information on this experiment can be found in the Experimental Section 5.4.4.

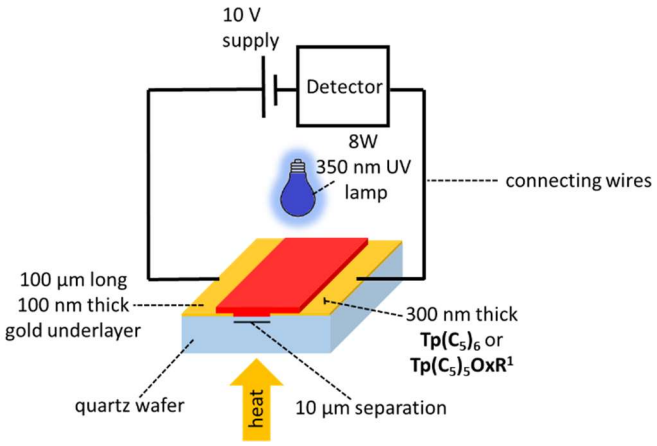

Figure 5.16: Set up to measure photoconductivity where $R^1 = C_4H_9$ or Ar

5.2.5.2 Temperature Varied Conductivity and Photoconductivity Measurements

The conductivity and photoconductivity of **$Tp(C_5)_6$** and **$Tp(C_5)_5OxR^1$** are shown in Figure 5.17 and Table 5.6. Points to note are:

1) All molecules show an increase in conductivity upon light irradiation, i.e. there is a photocurrent;
2) There is significant improvement in conductivity (which doubles), and photoconductivity (which increases by a factor of 10), when the oxazole moiety is introduced, i.e comparison of **$Tp(C_5)_5OxC_4$** with the parent hexapentyloxytriphenylene **$Tp(C_5)_6$**;
3) Compared to **$Tp(C_5)_5OxC_4$** there is a further increase in conductivity and photoconductivity for all aryl substituents with the exception of **$Tp(C_5)_5$Ox-9-Ant**;

4) As temperature increases the gap between photoconductivity and conductivity decreases for all samples;
5) The conductivity of **Tp(C$_5$)$_6$**, **Tp(C$_5$)$_5$OxC$_4$** and the **Tp(C$_5$)$_5$OxAr** series increases as a function of temperature and by 120 °C is roughly equal to photoconductivity measurements;
6) The maximum photoconductivity for the **Tp(C$_5$)$_5$OxAr** substituents seems to be irrespective of temperature, whereas **Tp(C$_5$)$_5$OxC$_4$** shows a steady increase in photoconductivity as a function of temperature;
7) Elevating the temperature to the liquid crystalline range has no step change on photoconductivity or conductivity;

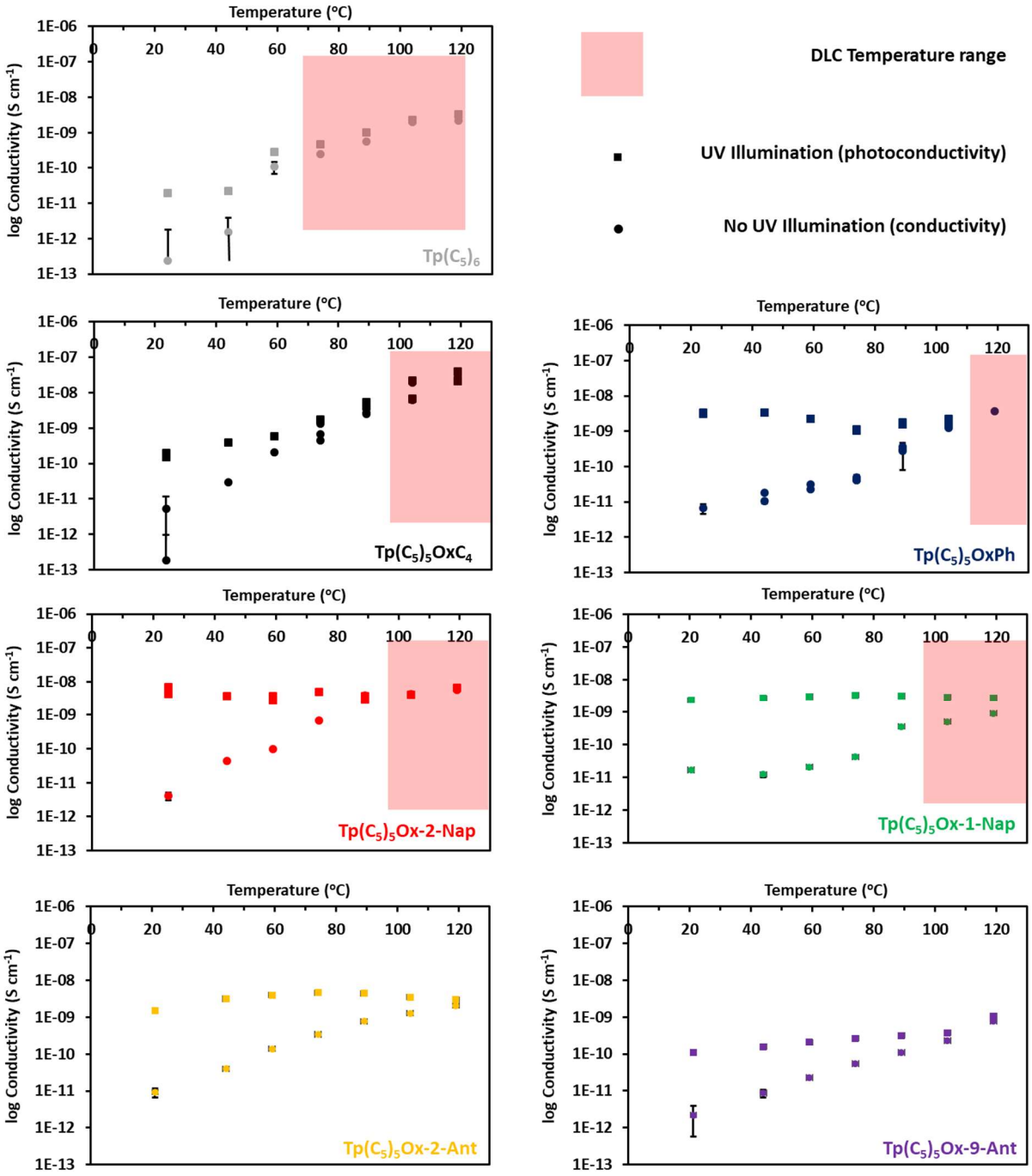

*Figure 5.17 Electrical conductivity versus temperature of 300 nm thick films of **Tp(C5)6**, **Tp(C5)5OxC4** and the **Tp(C5)5OxAr** series*

Table 5.6 and Figure 5.18 summarises the conductivity and photoconductivity of **Tp(C5)6**, **Tp(C5)5OxC4** and the **Tp(C5)5OxAr** series at room temperature. Of note is that the

photoconductivity values attained for **Tp(C_5)$_5$Ox-2-Nap** is comparable to a porphyrin derivative used in a prototype solar cells which has a photoconductivity of ~10^{-8} S cm^{-1}.[33-34]

*Table 5.6: The molar absorptivity constant (ϵ) at 350 nm in ethyl acetate, average conductivity and average photoconductivity when irradiated with λ = 350 nm at room temperature of **Tp(C_5)$_6$** and **Tp(C_5)$_5$OxR^1**. Where R^1= C_4H_9 or Ar*

Compound	(ϵ_{350nm}) x 10^3 in ethyl acetate M^{-1} cm^{-1}	Average Conductivity (S cm^{-1})	Average Photoconductivity (S cm^{-1})
Tp(C_5)$_6$	3.6	2.4 x 10^{-13}	1.98 x 10^{-11}
Tp(C_5)$_5$OxC$_4$	6.4	5.3 x 10^{-13}	2.0 x 10^{-10}
Tp(C_5)$_5$OxPh	19	6.6 x 10^{-12}	3.1 x 10^{-9}
Tp(C_5)$_5$Ox-2-Nap	26	4.1 x 10^{-12}	6.9 x 10^{-9}
Tp(C_5)$_5$Ox-1-Nap	16	1.7x 10^{-11}	2.3 x 10^{-9}
Tp(C_5)$_5$Ox-2-Ant	19	9.3 x 10^{-12}	1.5 x 10^{-9}
Tp(C_5)$_5$Ox-9-Ant	11	2.0 x 10^{-12}	1.1 x 10^{-10}

From Figure 5.18 and Table 5.6 we note that **Tp(C_5)$_5$Ox-2-Nap** is the most photoconductive, with a photoconductivity of 6.9 x10^{-9} S cm^{-1}. However, for the aryl series, **Tp(C_5)$_5$Ox-9-Ant** is the least photoconductive, with a photoconductivity of 1.1 x10^{-10} S cm^{-1}.

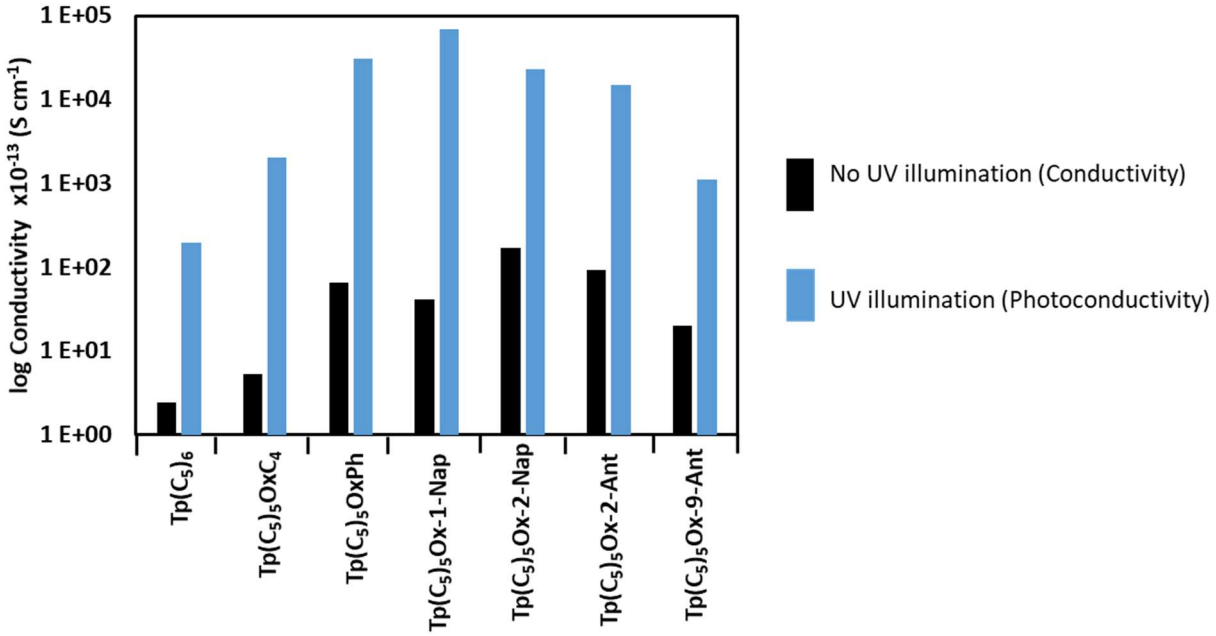

Figure 5.18: Bar chart showing at room temperature the conductivity change from no UV illumination to UV illumination for ***Tp(C5)6, Tp(C5)5OxC4*** *and the* ***Tp(C5)5OxAr*** *series*

Given the wavelength of light used to induce the photoconductivity was 350 nm a correlation was looked for that might relate to the photophysical data discussed earlier in this chapter. To this end a relationship was found for molar absorptivity coefficient (ϵ) at 350 nm (solvent: ethyl acetate) and the photoconductivity observed in **Tp(C5)6**, **Tp(C5)5OxC4** and the **Tp(C5)5OxAr** series, whereby an increase in ϵ was generally followed by an increase in photoconductivity (Figure 5.19).

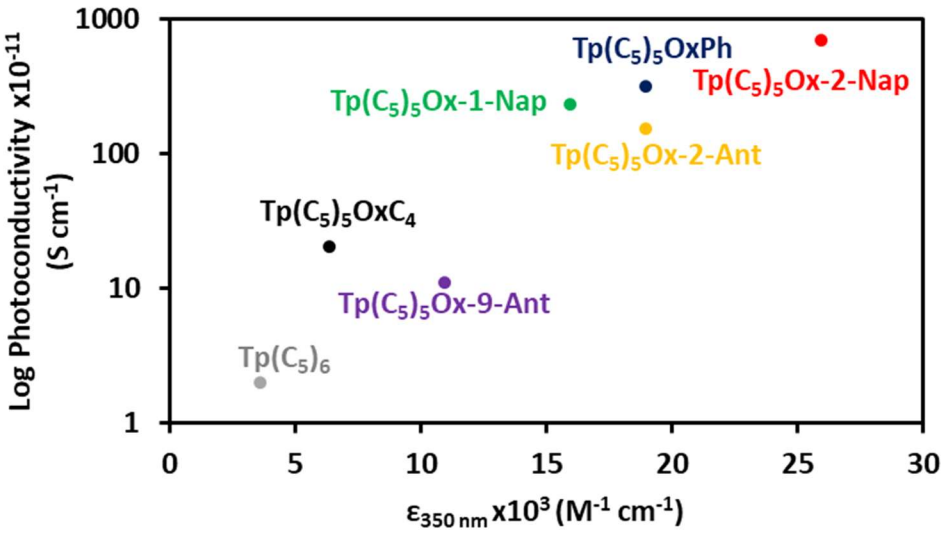

*Figure 5.19: ϵ at 350 nm of **Tp(C$_5$)$_6$**, **Tp(C$_5$)$_5$OxC$_4$** and the **Tp(C$_5$)$_5$OxAr** series compared to log photoconductivity at room temperature*

Of course, this analysis is comparing solution state data to solid state, and hence the correlation is far from perfect, as it has been shown that the solution state and solid state conformational preferences may impact on properties significantly. Thus, currently solid state molar absorptivity values are being obtained to see if the correlation is stronger.

5.2.5.3 Switching the Photocurrent On and Off

Conductivity experiments were performed at room temperature on **Tp(C$_5$)$_6$**, **Tp(C$_5$)$_5$OxC$_4$**, **Tp(C$_5$)$_5$OxPh** and **Tp(C$_5$)$_5$Ox-2-Nap**, whereby the conductivity of the samples was measured whilst irradiating with the 350 nm light for one minute and then in the dark for one minute for a total of ten minutes, as shown in Figure 5.20. Clearly, the current switches between bright and dark field states, with no apparent bleaching over the five cycles for all the materials.

Tp(C$_5$)$_5$OxC$_4$ displays a clear increase of photocurrent from **Tp(C$_5$)$_6$** (inset of Figure 5.20) and **Tp(C$_5$)$_5$OxPh** shows further increase. **Tp(C$_5$)$_5$Ox-2-Nap** shows the largest increase in photocurrent.

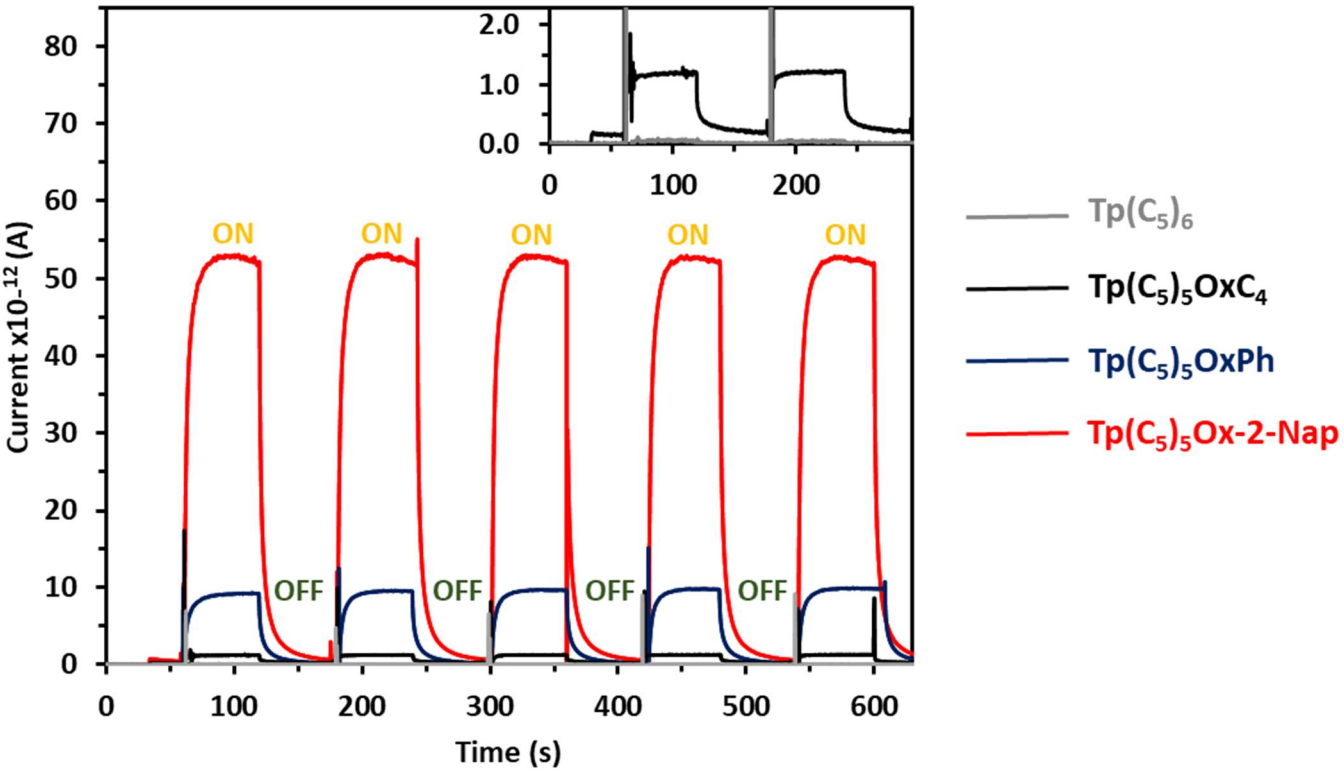

*Figure 5.20: Photocurrent switching at room temperature of **Tp(C$_5$)$_6$**, **Tp(C$_5$)$_5$OxC$_4$**, **Tp(C$_5$)$_5$OxPh** and **Tp(C$_5$)$_5$Ox-2-Nap** with λ=350 nm UV light and a supply of 10 V. Inset shows **Tp(C$_5$)$_6$** and **Tp(C$_5$)$_5$OxC$_4$***

These photoconductivity and photocurrent results represent a fascinating opportunity for this new class of molecules, where the maximum photoconductivity achieved (7 x 10^{-9} S cm^{-1}) is approximate to that of porphyrin (~10^{-8} S cm^{-1}), which is used in prototype solar cells.[34] Considering that the values in Table 5.6 are unoptimized, there is the potential for improvements to be made to the photoconductivity. For instance, modification of the oxazole R-group of the

triphenoxazole with moieties such as perylene, which have a red shift in absorption and thus a higher ϵ at 350 nm,[35] could lead to further advancement of photoconductive properties.

5.3 Conclusions

In conclusion, the novel reaction described in Chapter 3 had been used to create the extended aromatic triphenoxazole series **Tp(C_5)$_5$OxAr** in low to moderate yields ranging from 11-34 %.

Extension of the aromatic area provided mesogenic compounds that display luminescence with a large pSS of 15000-23800 cm^{-1} compared to others presented in the literature.[7-9] The large ε of 58000 – 180000 M^{-1} cm^{-1} and Φ ranging from 40-70 % make these compounds excellent candidates for future OLED devices. The potential to tune the shift by considering the resonance stabilisation energy of the excited state offers a way of tuning the emission colour.

In solution **Tp(C_5)$_5$Ox-9-Ant** showed a significant increase in the structured emission band, *TnCEM*, when compared to the rest of the aryl series. It is hypothesised that the steric bulk of the 9-anthracyl R group makes twisting out of conjugation more of a favourable conformation than the rest of the series, thus causing an increase in the *TnCEM* band. Similarly, to the **Tp(C_5)$_5$OxPh*x*F** series in the previous chapter the series displayed significant quenching of the *TnCEM* band in the solid state, thus implying that as a solid the planar conformation is more favourable.

Furthermore, DLC properties were retained within the **Tp(C_5)$_5$OxAr** series, all bar **Tp(C_5)$_5$Ox-9-Ant**, displaying the Col_h packing. It is assumed that **Tp(C_5)$_5$Ox-9-Ant** has a slightly more twisted conformation causes columnar packing to be less favourable and an unknown mesophase is formed.

Tp(C_5)$_5$Ox-1-Nap shows the widest range of liquid crystallinity, with a range of 118 °C upon cooling. This range is a significant increase from **Tp(C_5)$_5$OxPh** (107 °C), and **Tp(C_5)$_5$Ox-2-Nap** derivative (44 °C). This increase is based on the assumption that the **Tp(C_5)$_5$Ox-1-Nap** structure adopts a conformation more conducive to π-π stacking than the 2-naphthyl isomer (Figure 5.15). Computational studies to validate this hypothesis are underway.

The **Tp(C_5)$_5$OxAr** series showed increases in photoconductivity relative to the parent triphenylene. The aryl triphenoxazole derivatives enhanced photoconductivity over **Tp(C_5)$_5$OxC_4**. **Tp(C_5)$_5$Ox-2-Nap** displayed the highest photoconductivity at 7 x 10^{-9} S cm^{-1} (300x higher than **Tp(C_5)$_6$**) and within range of other organic compounds such as porphyrin (~10^{-8} S cm^{-1}) which have already been used in prototype solar cells. [34] There appears to be a trend between the solution state molar absorptivity of UV light at the excitation wavelength used in the solid state photoconductivity measurements, and the corresponding photoconductivity. However, solid state measurements are needed to test this hypothesis more thoroughly. Computational studies where the highest occupied molecular orbital (HOMO) and lowest unoccupied molecular orbital (LUMO) are currently being calculated. These values would be useful when furthering this work to create a prototype triphenoxazole solar cell.

To further understand the effect of substitution of the aryl group, a larger library of triphenoxazoles needs to be synthesised. However, the **Tp(C_5)$_5$OxAr** series combined with the **Tp(C_5)$_5$OxPh*x*F** series described in the previous chapter represent the ground work for a fascinating new library of luminescent and mesogenic compounds.

5.4 Experimental

All reagents were used directly from the suppliers without further purification unless otherwise stated. All synthetic procedures were carried out under nitrogen and were magnetically stirred unless otherwise stated. All temperatures were internal flask temperatures unless otherwise stated. All solvents used were reagent grade unless otherwise stated. Heating under reflux consisted of a fitted glass condenser (water cooled). Column chromatographic separations were performed using Silica gel 120 (ICN Chrom 32-63 60 Å).

Analytical techniques used as confirmation were matrix assisted laser desorption ionisation (MALDI), Electrospray Mass Spectrometry (ES^+MS), infra-red spectroscopy and NMR spectroscopy. The NMR spectroscopic techniques used were ^1H NMR spectroscopy using the Brüker AVIII 300 spectrometer, ^{13}C NMR spectroscopy using the Brüker AVIII400 NMR spectrometer.

5.4.1 Analytical Techniques:

Analytical techniques used as confirmation were matrix assisted laser desorption ionisation (MALDI), Electrospray Mass Spectrometry (ES^+MS), infra-red spectroscopy and NMR spectroscopy. The NMR spectroscopic techniques used were ^1H NMR spectroscopy using the Brüker AVIII 300 spectrometer, ^{13}C NMR spectroscopy using the Brüker AVIII400 NMR spectrometer.

Elemental analysis was performed on a Carlo Elba EA1110. Where the sample (1 mg) is heated to 1000 °C with a constant flow of helium. The combustion gas mixture is driven through an oxidation catalyst zone consisting of WO_3, which aids in delivering complete combustion. The resultant mixture of components is separated by a Porapack column and detected by a thermal conductivity detector.

5.4.2 Thermal and Photophysical Characterisation:

Thermal and photophysical characterisation procedures can be found in Chapter 3 (Sections 3.4.3 and 3.4.5).

5.4.3 Photoconductivity and Photocurrent Measurements:

Conductivity and photocurrent measurements were performed as follows:

2-probe chip preparation: electrodes of chrome (10 nm) and gold (90 nm) layers were sputtered upon a quartz substrate. Gold film was plasma etched using an etch mask to create electrodes with dimension of 100 µm length and 10 µm separation. The chip was cleaned using a 15 min sonication in acetone and 15 min in isopropanol followed by deionised water wash and nitrogen drying. Attention was made to make sure that substrate had no contamination that could affect measurement of electrical properties.

The sample was dissolved in chloroform (20 mg mL^{-1}) and spin coated onto the 2-probe chip shown in Figure 5.16 (Section 5.2.5.1) at 1500 rpm. This gave more than 300 nm thickness film with good uniformity. All films received post-application bake (PAB) of 75 °C for 5 min under air.

Current was measured using the Keithley 2363B source measure unit at 10 V. An 8 W UV lamp where 95 % of energy was emitted at 350 nm wavelength was used when measuring photoconductivity experiments.

Current was converted into conductivity using Equation 5.1 in Section 5.2.5.1.

5.4.4 Synthetic Procedures:

Synthetic procedures for **$Tp(C_5)_6$**, **$Tp(C_5)_6NO_2$** and **$Tp(C_5)_6NH_2$**, **$Tp(C_5)_5OxC_4$** and **$Tp(C_5)_5OxPh$** can be found in Chapter 3 (Sections 3.4.6.2 to 3.4.6.2.9).

5.4.4.1 General triphenylenoxazole formation:

A solution of the appropriate carboxylic acid (1.31 mmol), palladium diacetate (0.005 mmol) and iodobenzene diacetate (0.157 mmol) in PhMe (5 mL) was heated to 70 °C under N_2 for 20 min. A solution of **$Tp(C_5)_6NH_2$** (100mg; 0.131 mmol) in PhMe (2 mL) was added and heated to reflux for 48-72 h, whilst stirring. The solution was cooled to room temperature and diluted with CH_2Cl_2 (20 mL). The organic phase was washed with aqueous NaOH (1M; 2 x 20 mL), separated and the organic phase was dried *in vacuo*. The crude black solid was purified by flash column chromatography (silica; 40 % CH_2Cl_2: 60 % *n*-hexane) to afford the desired product.

5.4.4.2 2,3,6,11,12-pentapentyloxy-8-(naphthalen-1-yl)-triphenoxazole ($Tp(C_5)_5Ox$-1-Nap)

Acid used was 1-naphthalene carboxylic acid (225 mg, 1.31 mmol) afforded a yellow solid (24 mg; 22 %) **^{1}H NMR** (300 MHz, $CDCl_3$) δ_H: 10.15 (1 H, s), 9.82 (1 H, d, *J* 8.3 Hz), 8.59 (1 H, dd, *J* 7.3, 1.2 Hz), 8.08 (1 H, d, *J* 8.3 Hz), 8.01-7.98 (3 H, m), 7.94 (2 H, m), 7.71-7.61 (3 H, m), 4.54-4.45 (4 H, m),

4.32-4.26 (6 H, m), 2.10-1.94 (10 H, m), 1.70-1.35(20 H, m), 1.04 – 0.87 (15 H, m) ppm. **^{13}C NMR** (100 MHz, $CDCl_3$) δ_C: 161.3, 149.9, 149.6, 149.1, 148.8, 143.2, 141.0, 139.9, 134.5, 132.4, 131.0, 129.6, 129.2, 127.8, 127.5, 126.9, 126.7, 125.5, 125.0, 124.2, 124.1, 123.8, 117.0, 111.0, 108.6, 107.3, 107.2, 104.4, 70.2, 69.9, 69.1, 29.6, 29.5, 29.0, 28.8, 28.7, 23.0, 14.5 ppm. **MALDI$^+$** *m/z*: 826.7 ([M+H]$^+$ 100%). Elemental analysis Found: C, 78.49; H, 8.23; N, 1.73 %. $C_{54}H_{67}NO_6$ requires C, 78.51; H, 8.17; N, 1.70 %.

5.4.4.3 2,3,6,11,12-pentapentyloxy-8-(naphthalen-2-yl)triphenoxazole (Tp$(C_5)_5$Ox-2-Nap)

Acid used was 2-naphthalene carboxylic acid (225 mg, 1.31 mmol) afforded a yellow solid (35 mg; 32 %) **^{1}H NMR** (300 MHz, $CDCl_3$) δ_H: 10.22 (1 H, s), 8.89 (1 H, s), 8.49 (1 H, dd, *J* 8.6, 1.7), 8.05 – 7.99 (2 H, m), 7.96-7.91 (5 H, m), 7.62 – 7.59 (2 H, m), 4.54 (2 H, t, *J* 6.8), 4.51 (2 H, t, *J* 6.8), 4.32 – 4.25 (6 H, m), 2.17 – 1.93 (10 H, m), 1.76 – 1.42 (20 H, m), 1.06 – 0.97 (15 H, m) ppm. **^{13}C NMR** (100 MHz, $CDCl_3$) δ_C: 161.7, 149.8, 149.3, 149.0, 148.6, 143.2, 140.9, 140.6, 135.0, 133.4, 129.3, 128.9, 128.3, 128.0, 127.9, 127.4, 127.2, 125.0, 125.0, 124.4, 124.2, 123.7, 123.6, 116.7, 111.2, 108.5, 107.1, 107.0, 103.9, 70.2, 70.1, 69.8, 69.2, 29.6, 29.5, 28.9, 28.8, 28.7, 23.1, 23.0, 14.6, 14.5 ppm. **MALDI$^+$** *m/z*: 825.5 ([M]$^+$ 100%). **IR λ^{-1}** (neat): Elemental analysis Found: C, 78.95; H, 8.02; N, 1.83 %. $C_{54}H_{67}NO_6$ requires C, 78.51; H, 8.17; N, 1.70 %.

5.4.4.4 2,3,6,11,12-pentapentyloxy-8-(anthracen-2-yl)-triphenoxazole (Tp$(C_5)_5$Ox-2-Ant)

Acid used was 2-anthracene carboxylic acid (290 mg, 1.31 mmol); afforded a yellow solid (22 mg; 20 %) **^{1}H NMR** (300 MHz, $CDCl_3$) δ_H: 10.20 (1 H, s), 9.00 (1 H, s), 8.58 (1 H, s), 8.47 (1 H, s), 8.39 (1 H, dd, *J* 8.9, 1.6 Hz) 8.13-8.10 (2 H, m), 8.07-8.02 (2 H, m), 7.93 (1 H, s), 7.90-7.89 (3 H, m), 4.57-

4.47 (4 H, m), 4.31-4.24 (6 H, m), 2.19-1.96 (10 H, m), 1.76-1.44(20 H, m), 1.08 – 0.97 (15 H, m) ppm.**^{13}C NMR** (100 MHz, $CDCl_3$) δ_C: 161.8, 149.8, 149.4, 149.0, 148.6, 143.2, 141.0, 140.6, 133.1, 132.6, 132.3, 131.2, 129.2, 128.7 128.6, 128.2 127.4, 126.8, 126.6, 126.3, 125.0, 124.4, 124.2, 123.8, 123.6, 116.7, 111.3, 108.5, 107.1, 107.0, 104.0, 70.2, 70.1, 69.8, 69.2, 30.1, 29.6, 29.5, 28.9, 28.8, 28.7, 23.1, 23.0, 14.7, 14.5 ppm. **MALDI$^+$** *m/z*: XX ($[M+H]^+$ 100%). Elemental analysis Found: C, 79.49; H, 7.88; N, 1.51. $C_{58}H_{69}NO_6$ requires C, 79.51; H, 7.94; N, 1.60 %.

5.4.4.5 2,3,6,11,12-pentapentyloxy-8-(anthracen-9-yl)-triphenoxazole (Tp(C_5)$_5$Ox-9-Ant)

A solution of 9-anthracene carboxylic acid (290 mg; 1.31 mmol), palladium diacetate (0.005 mmol) and iodobenzene diacetate (0.157 mmol) in *o*-xylene (5 mL) was heated to 70 °C under N_2 for 20 min. A solution of **Tp(C_5)$_6$$NH_2$** (100mg, 0.131 mmol) in *o*-xylene (2 mL) was added and heated to 140 °C for 72 h. The mixture was cooled to room temperature and diluted with CH_2Cl_2 (20 mL). The mixture was washed with 1M NaOH (2 x 20 mL) and the organic phase was dried *in vacuo*. The crude black solid was purified by flash column chromatography (silica; 40 % CH_2Cl_2: 60 % *n*-hexane) to afford a yellow solid (13 mg; 11 %). **^{1}H NMR** (300 MHz, $CDCl_3$) δ_H: 10.18 (1 H, s), 8.70 (1 H, s), 8.49-8.44 (2 H, m), 8.15-8.09 (2 H, m), 8.03 (1H, s) 8.02 (1 H, s) 7.95 (1 H, s), 7.94 (1 H,s) 7.58-7.52 (4 H, m), 4.50 (2 H, t, *J* 6.7 Hz), 4.33-4.27 (6 H, m), 4.17 (2 H, t, *J* 6.7 Hz), 2.05-1.93 (8 H, m), 1.79 (2 H, p, *J* 6.7, 1.0 Hz) 1.66-1.37 (20 H, m), 1.03 – 0.92 (15 H, m) ppm.**^{13}C NMR** δ_C: (100 MHz, $CDCl_3$) 160.6, 150.0, 149.6, 149.2, 148.8, 143.5, 141.0, 140.7, 131.9, 131.7, 131.3, 129.1, 127.7, 127.6, 126.4, 125.9 124.2, 123.8, 121.1, 117.1, 111.3, 108.7, 107.3, 107.2, 104.6, 70.4, 70.3, 69.9, 69.2, 29.6, 29.5, 29.0, 28.8, 28.7, 28.6, 28.5, 23.0, 22.9, 22.6, 14.5, 14.4, 14.3 ppm. **MALDI$^+$**

m/z: 876.5 ($[M+H]^+$ 100%). Elemental analysis Found: C, 79.13; H, 7.83; N, 1.77 %. $C_{58}H_{69}NO_6$ requires C, 79.51; H, 7.94; N, 1.60 %.

5.5 References

[1] S. Mukherjee and P. Thilager, *J. Mater. Chem. C*, 2016, **4**, 2647

[2] L. Guo and D. Cao, *J. Mater. Chem. C* , 2015, **3**, 8490

[3] H. Ma, L. Wang, J. Chen, X. Zhang, L. Wang, N. Xu, G. Yang and P. Cheng, *Daltons Trans.*, 2017, **46**, 3526

[4] P. Miluski, *Fibers*, 2017, **5**, 1

[5] F.L. Thorp-Greenwood, *Organometallics*, 2012, **31**, 5686

[6] Y.Y. Wu, Y. Chen, G.Z. Gou, W.H. Mu, X.J. Lv, M.L. Du and W.F. Wu, *Org. Lett.*, 2012, **14**, 5226

[7] P. Kiprof, J.C. Carlson, D.R. Anderson and V.N. Nemykin, Daltons Trans., 2013, 42, 15120

[8] R. Turrisi, A. Sanguineti, M. Sassi, B. Savoie, A. Takai, G.E. Patriarca, M.M. Salamone, R. Ruffo, G. Vaccaro, F. Meinardi, T.J. Marks, A. Faccheitti and L. Beverina, *J. Mater. Chem. A.*, 2015, **3**, 8045

[9] B.J. Stokes, B. Jovanović, H. Dong, K.J. Richert, R.D. Riell and T.G. Driver, *J. Org. Chem*., 2009, **74**, 3225

[10] L. Li, L. Zhang, Z. Wen and D. Chen, *Chinese J. Chem.*, 2010, **28**, 171

[11] V. Barone and A. Polimeno, *Chem. Soc. Rev.*, 2007. **36**, 1724

[12] L. Giovanelli, H.L. Lees, C. Lacaze-Dufaure, M. Koudia, S. Clair, Y.P. Lin, Y. Kasari, J.M. Themlin, M. Abel and A.A. Cafolla, *J. Electron. Spectrosc. Relat. Phenom.*, 2017, **218**, 40

[13] P. Wang, C. Klein, R. Humphrey-Baker, S.M. Zakeeruddin and M. Grätzel, *J. Am. Chem. Soc.*,

2005, **127**, 808

[14] https://www2.chemistry.msu.edu/faculty/reusch/virttxtjml/spectrpy/uv-vis/uvspec.htm [25/09/2017]

[15] Z.R. Grabowski and K. Rotkiewicz, *Chem. Rev.*, 2003, **103**, 3899

[16] R. Schmid, *Monatsh. Chem.*, 2001,**132**,1295

[17] N. Lou, Y. Li and L. Gan, *Angew. Chem. Int. Ed.*, 2017, **56**, 2403

[18] F. Lu, R. Hu, S. Wang, X. Guo and G. Yang, RSC Adv., 2017, **7**, 4196

[19] I. Amunom, S. Srivastava and R.A. Prough, *Curr. Protoc. Toxicol.*, 2011, **48**, 1-4

[20] M.A. Haidekker, T.P. Brady, D. Lichlyter, E.A. Theodorakis, *Bioorg. Chem.*, 2005, **33**, 415

[21] J.N. Demas and G.A. Crosby, *J. Phys. Chem.*, 1971, **75**, 991

[22] J.L. Banal, J.M. White, K.P. Ghiggino and W.W.H. Wong, *Scientific Reports*, 2014, **4**, 4635

[23] http://evrogen.com/protein-descriptions/TagBFP-description.pdf [25/09/2017]

[24] https://www.thermofisher.com/us/en/home/brands/molecular-probes/key-molecular-probes-products/alexa-fluor/alexa-fluor-dyes-brightest-conjugates.html [25/09/2017]

[25] M. Garland, J.J. Yim, M. Bogyo, *Cell Chem. Bio.*, 2016, **23**, 122

[26] S. Kumar and S.K. Gupta, *Tetrahedron Lett.*, 2011, **52**, 5363

[27] D.J. Pesak and J.S. Moore, *Angew. Chem. Int. Ed.*, 1997, **36**, 1636

[28] J. Ban, S. Chen and H. Zhang, *RSC Adv.*, 2014, **4**, 54158

[29] J. Ban, L. Mu, L. Chen, S. Chen and H. Zhang, *RSC Adv.*, 2016, **6**, 38790

[30] K.P. Regan, J.R. Swierk, J. Neu and C.A. Schmuttenmaer, *J. Phys. Chem. C.*, 2017, 121, 15949

[31] Y. Wang, C. Zhang, H. Wu and J. Pu, *J. Mater. Chem. C*, 2014, **2**, 1667

[32] J.D. Bronzino and D.R. Peterson, *Biomedical Engineering Fundamentals,* CRC Press, 2006

[33] A. Aziz, L. Narasimhan, N. Perisamy and N.C. Maiti, *Philos. Mag. B*, 1999, **79**, 993

[34] T. Higashino and H. Imahori, *Dalton Trans.*, 2015, **44**, 448

[35] H. Jiang, G. Hershtig, S. Richter and R. Jelinek, *J. Phys. Chem. Lett.*, 2016, **7**, 1628

6 Chapter Summary and Further work

In conclusion, triphenoxazoles, a new class of alkoxytriphenylene derivatives have been described.

Chapter 3 displayed two routes to form these compounds, both exploiting existing chemistry which formed carbazoles: [1-2]

1) route a) used a rhodium catalyst and **$Tp(C_5)_6N_3$** to form **$Tp(C_5)_5OxC_4$** *via* an intramolecular step in quantitative yields. However, the chemistry was limiting in that if further chemistry was explored the product would always be **$Tp(C_n)_5OxC_{n-1}$**;

2) route b) used R^1COOH, $PhI(OAc)_2$ and palladium acetate catalyst to form **$Tp(C_5)_5OxR^1$** where R^1=aryl was discussed in this thesis. This intermolecular chemistry was lower yielding (yields 10 - 34 %) but offered the advantage in the potential to form a large family of compounds.

The chapter went onto assign in detail the aromatic hydrogens and carbons of **$Tp(C_5)_5OxC_4$** by ^1H and ^{13}C NMR spectroscopy, revealing a significantly deshielded proton located near the sp^2 nitrogen's lone pair.

$Tp(C_5)_5OxC_4$ liquid crystalline properties were examined and compared with the imidazole derivative **$Tp(C_6)_5Im(C_6)$** [3] developed by Kumar *et al.* as well as the hexapentoxytriphenylene, **$Tp(C_5)_6$.** XRD studies revealed a Col_h phase at elevated temperatures, with similar molecular packing to Kumar imidazole. DSC and POM analysis of **$Tp(C_5)_5OxC_4$** revealed a broad range of liquid crystallinity (99- 141 °C) when heating, and a broader range when cooling (137-59 °C).

The chapter went onto describe the fluorescence of T**p(C$_5$)$_5$OxC$_4$**, which in solution, displayed similar photophysical properties to **Tp(C$_5$)$_6$**. Showing structured bands and a large pseudo Stokes shift (pSS) of 8200 cm^{-1}. The quantum yield (Φ)of **Tp(C$_5$)$_5$OxC$_4$** was measured using an integrating sphere and using a serial dilution method. Where **Tp(C$_5$)$_5$OxC$_4$** displayed a superior Φ, ranging from 0.18-0.30 depending upon solvent, to **Tp(C$_5$)$_6$** (0.09-0.18). A result of this increase in Φ was that **Tp(C$_5$)$_5$OxC$_4$** was significantly brighter than **Tp(C$_5$)$_6$** in ethyl acetate and octan-1-ol. **Tp(C$_5$)$_5$OxC$_4$** showed a significant reduction in ϵ value in acetonitrile when compared to ethyl acetate and octan-1-ol (120,000 mol^{-1} cm^{-1} reduced to 59,000 mol^{-1} cm^{-1}) where aggregation of **Tp(C$_5$)$_5$OxC$_4$** is thought to have occurred.

In the solid state **Tp(C$_5$)$_5$OxC$_4$** emits a broad range emission, dramatically red-shifted from 366 nm to 430 nm. This is significantly different from **Tp(C$_5$)$_6$**, whose emission is defined structured peaks. The broad range of emission is seen as a continuum of energy levels. Variance of concentration of **Tp(C$_5$)$_5$OxC$_4$** found that at 10^{-4} M the spectrum began to change to that of the solid state. We hypothesise this as a result of intermolecular interactions between **Tp(C$_5$)$_5$OxC$_4$** units.

It was suggested at the end of the chapter that further work into developing methods to make di and tri triphenoxazoles could lead to exciting liquid materials. Similarly, it was suggested that variance of chain length could also be used to tweak liquid crystal transitions and finally further work into why the α CH_2 is reactive should be studied perhaps through computational means.

Chapter 4 and 5 further explored the intermolecular annulation chemistry described in Chapter 3 and exhibited two series of aryl triphenoxazoles (**Tp(C_5)$_5$OxPh*x*F**, Chapter 4) and (**Tp(C_5)$_5$OxAr**, Chapter 5).

Both sets of compounds were designed to form new luminescent materials by having the oxazole R group as the acceptor and the triphenylene as the donor. The **Tp(C_5)$_5$OxPh*x*F** derivatives aimed to modulate the colour by increasing the strength of the acceptor by substituting in fluorophenyls with the ascribed chemistry from Chapter 3. [4]

Whereas, the **Tp(C_5)$_5$OxAr** derivatives aimed to modulate the colour by using larger aromatic areas to stabilise the excited state.[5]

Both were synthesised in low to moderate yields of 9-33 % and showed similar luminescent and mesogenic properties. As such will be summarised together below.

It was found that replacing an alkyl arm with an aryl substituent greatly improves the Φ from 0.18 to 0.40 in ethyl acetate whilst maintaining a high ϵ of 60000-145000 M^{-1} cm^{-1}. The dominant emission band was broad, and a large pSS of 15,600 to 17800 cm^{-1} (**Tp(C_5)$_5$OxPh*x*F** series) and 15,600 to 23,600 cm^{-1} (**Tp(C_5)$_5$OxAr** series) was achieved. Colours ranged from the blue to green (**Tp(C_5)$_5$OxPh*x*F** series) and blue to orange (**Tp(C_5)$_5$OxAr** series) of the visible spectrum, with **Tp(C_5)$_5$Ox-9-Ant** showing the largest pSS.

One noticeable difference between the **Tp(C_5)$_5$OxPh*x*F** and the **Tp(C_5)$_5$OxAr** series was that the fluoro derivatives saw no loss in ϵ when in acetonitrile. Whereas, the **Tp(C_5)$_5$OxAr** series had a

drop in ϵ to ~60,000 M^{-1} cm^{-1}. This was assumed to be a result of an increase in solubility of the fluoro substituents when in acetonitrile.

In solution, the aryl triphenoxazoles showed two mechanisms of emission which was hypothesised to be conformationally dependent, where the aryl group is either in a planar conformation or orthogonal to the triphenoxazole leading to the broad banded emission at 500-630 nm depending on the compound (planar conjugated emission mechanism; *PCEM*), or the structured bands matching **Tp(C_5)$_5$OxC$_4$** at ~365 nm (twisted non-conjugated emission mechanism; *TnCEM*), respectively.

Tp(C_5)$_5$OxPh*o*F showed no *TnCEM* bands compared to the rest of the aryl triphenoxazoles, implying that this derivative had additional conformational control, giving preference to the planar conformation. Analysis of the molecular structure suggested an intramolecular CH···F hydrogen bonding network was possible to give preference to the planar conformation, which would not be possible for the other aryl derivatives.

Conversely, **Tp(C_5)$_5$Ox-9-Ant** showed substantial enhancement of the *TnCEM* band (up to 28 % of total emission area). **Tp(C_5)$_5$Ox-9-Ant** is more sterically hindered than any of the other aryl triphenoxazoles, so it is hypothesised a reduction in planarity to ease steric clashes leads to the high *TnCEM*.

TnCEM is quenched in the solid state, with only one clear band visible in all compounds bar **Tp(C_5)$_5$Ox-9-Ant** which shows substantial reduction in the band, implying a more planar conformation is preferred in the solid state.

Interestingly, the para fluorinated phenyl (**Tp(C_5)$_5$OxPh*p*F**) *PCEM* emission did not demonstrate any significant changes in the pseudo Stokes shift (pSS) to **Tp(C_5)$_5$OxPh**, whereas both fluorination in the *meta* and *ortho* position did red shift the emission band, showing an improved stabilisation effect of the excited state.

The aromatic series showed a general trend of increasing pSS with the number of resonances available to stabilise the excited state. This is the first time to our knowledge that a '*resonance count*' has been used to trend the pSS with the number of resonances of a substituent.

Both the **Tp(C_5)$_5$OxPh*x*F** and the **Tp(C_5)$_5$OxAr** series retained liquid crystalline properties to varying degrees, where all bar **Tp(C_5)$_5$Ox-9-Ant** showed Col_h DLC behaviour.

The **Tp(C_5)$_5$OxPh*x*F** series showed a large variance of mesogenic behaviour, where **Tp(C_5)$_5$OxPh*o*F** showed a small mesogenic phase range of 10 °C when cooling, whereas the isomers **Tp(C_5)$_5$OxPh*m*F** and **Tp(C_5)$_5$OxPh*p*F** displayed an increase in DLC temperature range of 162 °C (the largest across both series) and 127 °C respectively. We presume these effects are due to **Tp(C_5)$_5$OxPh*m*F** and **Tp(C_5)$_5$OxPh*p*F** ability to form intermolecular hydrogen bonds, a property that is reduced in **Tp(C_5)$_5$OxPh*o*F** due to steric hindrance and competing intramolecular hydrogen bonding with the O-CH_2 of the pendant pentyl chain.

Extension of the aromatic area also retained DLC behaviour. It is assumed that **Tp(C_5)$_5$Ox-9-Ant** has a slightly more twisted conformation causes columnar packing to be less favourable and an unknown phase change occurs. Variable temperature XRD is recommended to elucidate the exact phase of the structure.

Tp(C_5)$_5$Ox-1-Nap shows the widest range of liquid crystallinity, with a range of 118 °C when cooling. This is a significant increase from **Tp(C_5)$_5$OxPh** (107 °C), and **Tp(C_5)$_5$Ox-2-Nap** derivative (44 °C). This increase is based on the assumption that the **Tp(C_5)$_5$Ox-1-Nap** structure adopts a conformation more conducive to π-π bonding than the 2-naphthyl isomer (Figure 5.15). Computational studies to validate this hypothesis are underway.

Finally, the **Tp(C_5)$_5$OxAr** series underwent preliminary testing for use in photovoltaics. It was shown that the aryl triphenoxazole moiety enhanced photoconductivity from **Tp(C_5)$_5$OxC_4**. **Tp(C_5)$_5$Ox-2-Nap** displayed the highest photoconductivity at 7 x 10^{-9} S cm^{-1} (300 x higher than **Tp(C_5)$_6$**) and within range of other organic compounds such as porphyrin (~10^{-8} S cm^{-1}) which have already been used in solar cells. [6] There appears to a be a trend between the absorption of UV light at the excitation wavelength and the corresponding photoconductivity. However, solid state measurements are needed to test this hypothesis more thoroughly. Computational studies where the highest occupied molecular orbital (HOMO) and lowest unoccupied molecular orbital (LUMO) are currently being calculated. These values would be useful when furthering this work to create a prototype triphenoxazole solar cell.

To further understand the effect of substitution of the aryl group, a larger library of triphenoxazoles needs to be synthesised. Further work should be applied to synthesising di (**Tp(C_5)$_4$(OxAr)$_2$**) and tri (**Tp(C_5)$_3$(OxAr)$_3$**) triphenoxazoles. The molecules described showed many avenues for potential research. These include and are not limited to: luminescent dyes,[7] OLEDs[8] and solar cells.[6]

6.1 References

[1] B.J. Stokes, B. Jovanović, H. Dong, K.J. Richert, R.D. Riell and T.G. Driver, *J. Org. Chem*., 2009, **74**, 3225

[2] J.A. Jordan-Hore, C.C.C. Johansson, M. Gulias, E.M. Beck and M.J. Gaunt, *J. Am. Chem. Soc.*, 2008, **130**, 16184

[3] S. Kumar and S.K. Gupta, *Tetrahedron Lett.*, 2011, **52**, 5363

[4] Y. Zhang, S.A. Autry, L.E. McNamara, S.T. Nguyen, N. Le, P. Brogdon, D.L. Watkins, N.I. Hammer and J.H. Delcamp, *J. Org. Chem.*, 2017, **82**, 5597

[5] P. Kiprof, J.C. Carlson, D.R. Anderson and V.N. Nemykin, *Daltons Trans.*, 2013, **42**, 15120

[6] T. Higashino and H. Imahori, *Dalton Trans.*, 2015, **44**, 448

[7] S. Mukherjee and P. Thilager, *J. Mater. Chem. C*, 2016, **4**, 2647

[8] F. Lu, R. Hu, S. Wang, X. Guo and G. Yang, *RSC Adv.*, 2017, **7**, 4196

7 Appendix

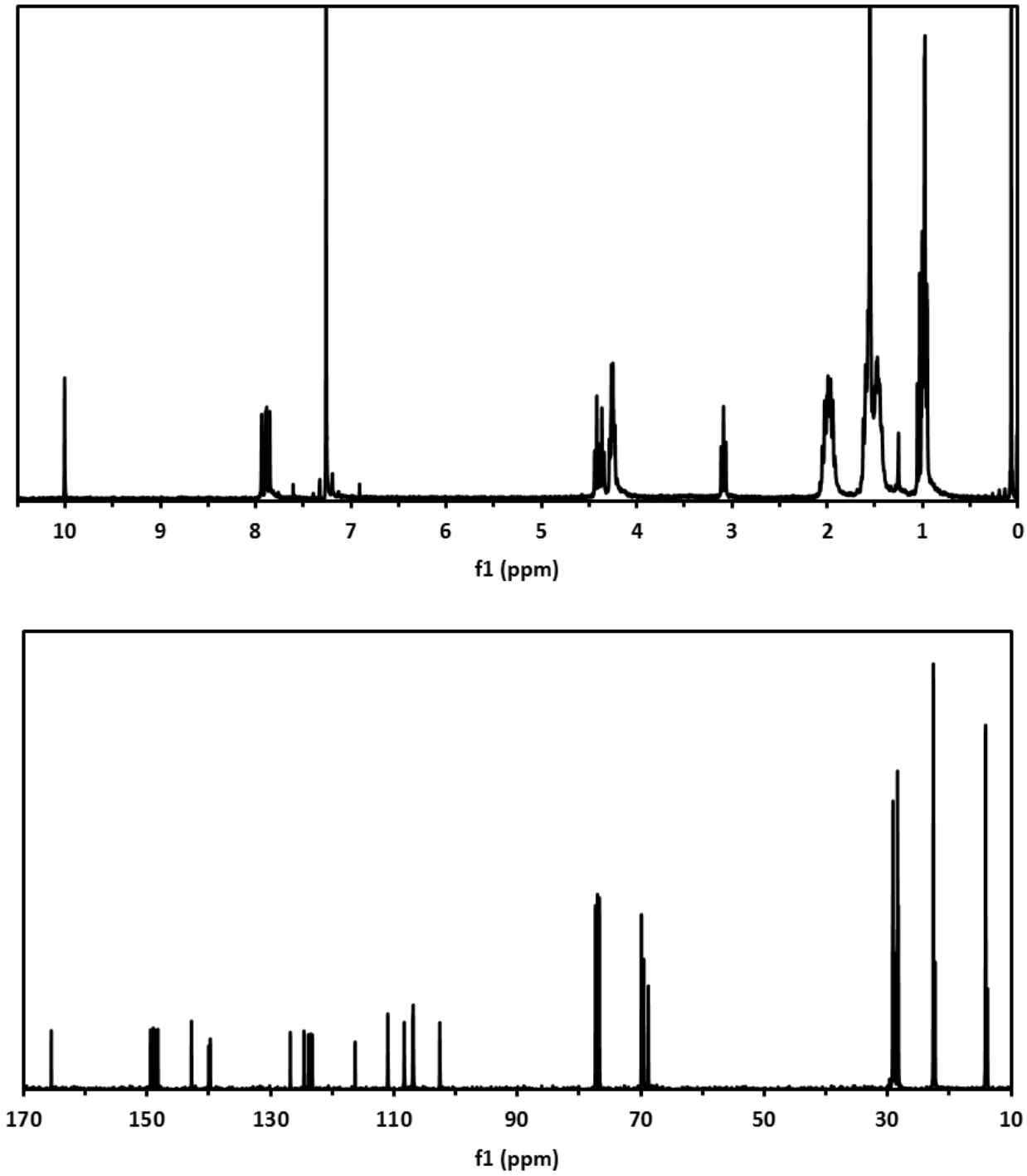

*Figure 7.1: **Tp(C$_5$)$_5$OxC$_4$** ^{1}H and ^{13}C NMR spectra*

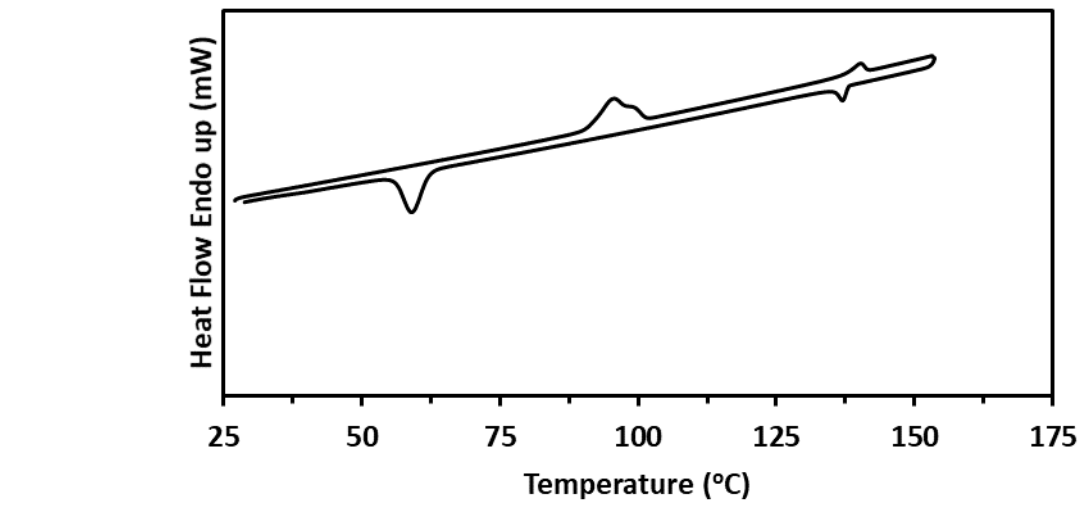

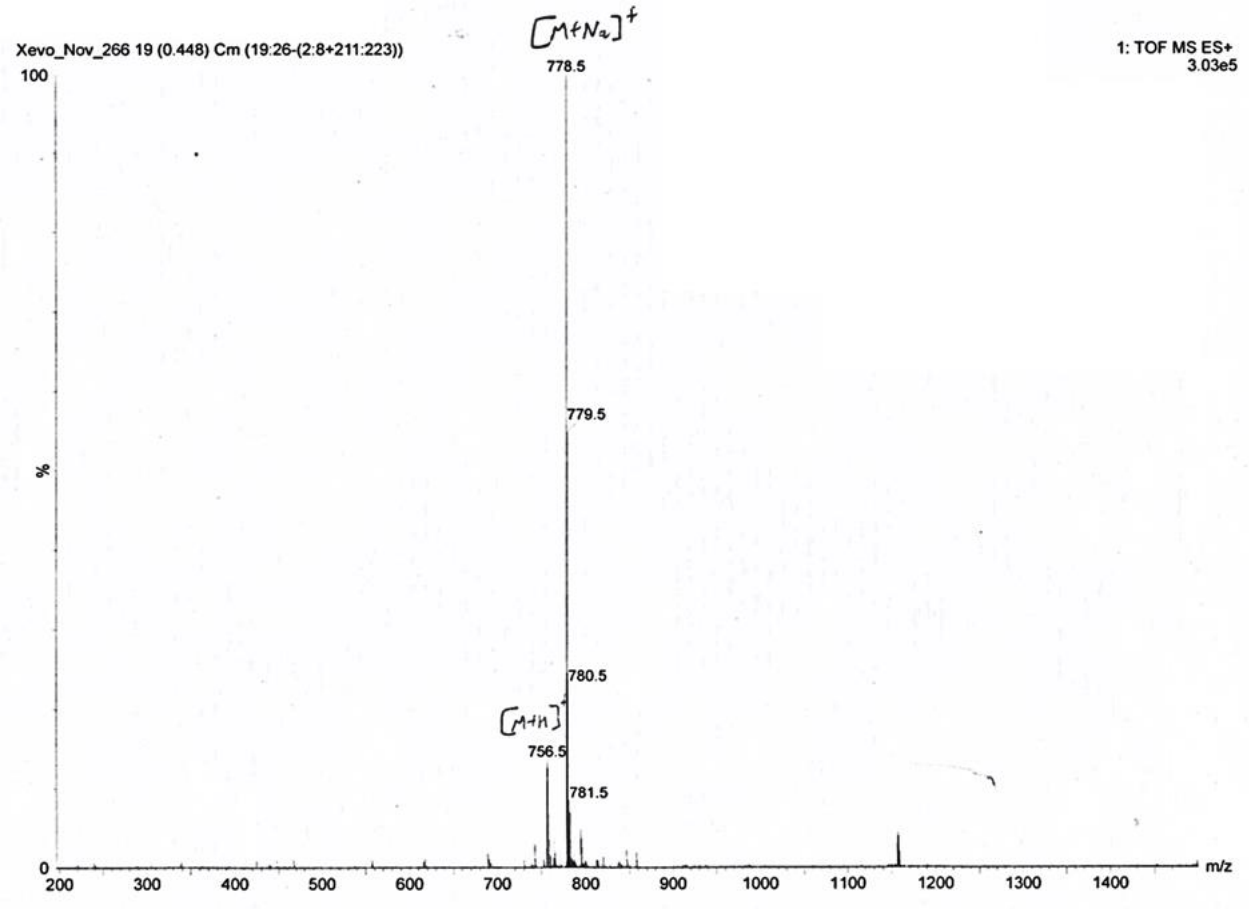

*Figure 7.2: **Tp(C_5)$_5$OxC_4** DSC (2nd Scan) and mass spectrum*

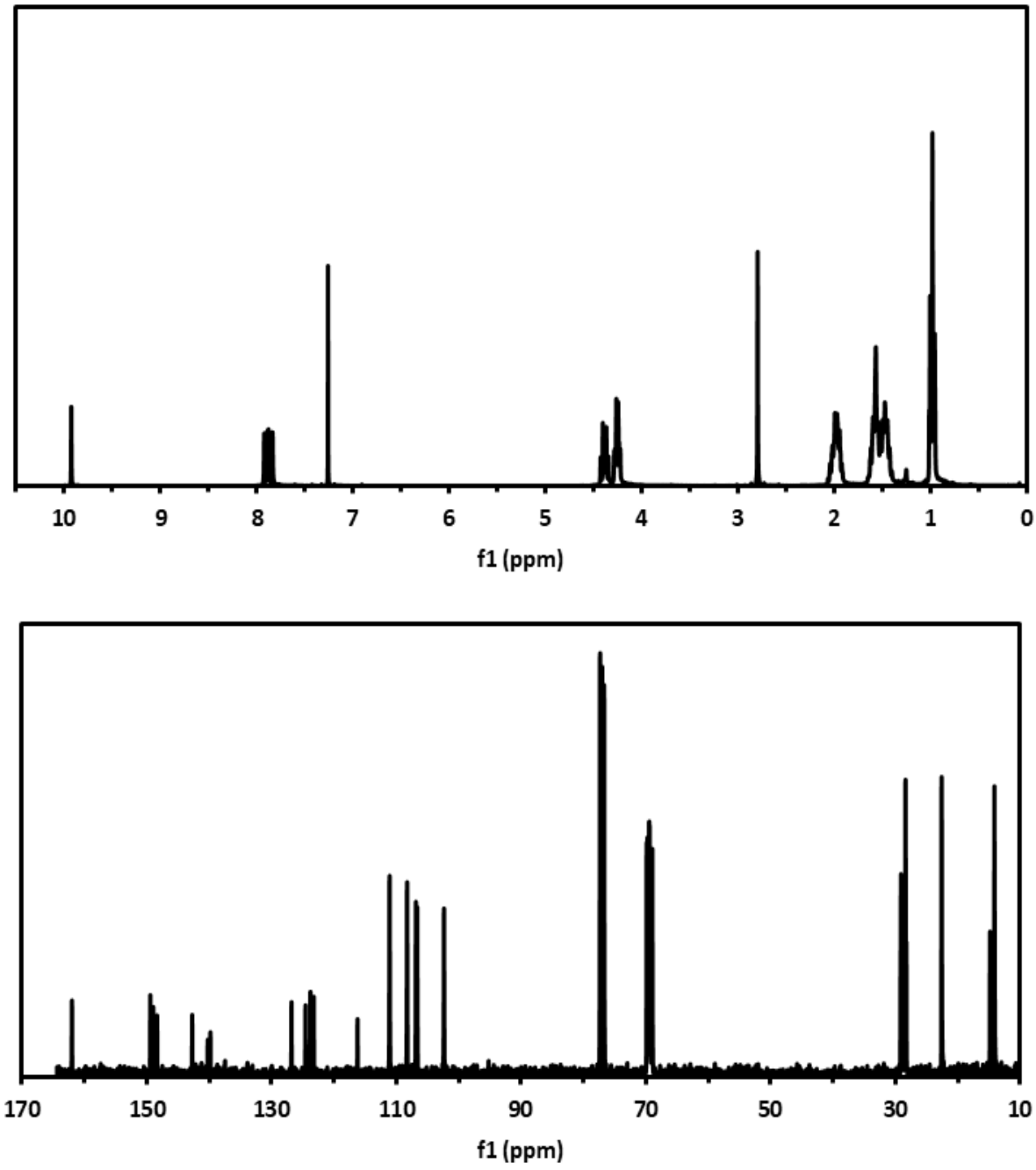

Figure 7.3: ***Tp(C$_5$)$_5$OxC$_1$*** *^{1}H and ^{13}C NMR spectra*

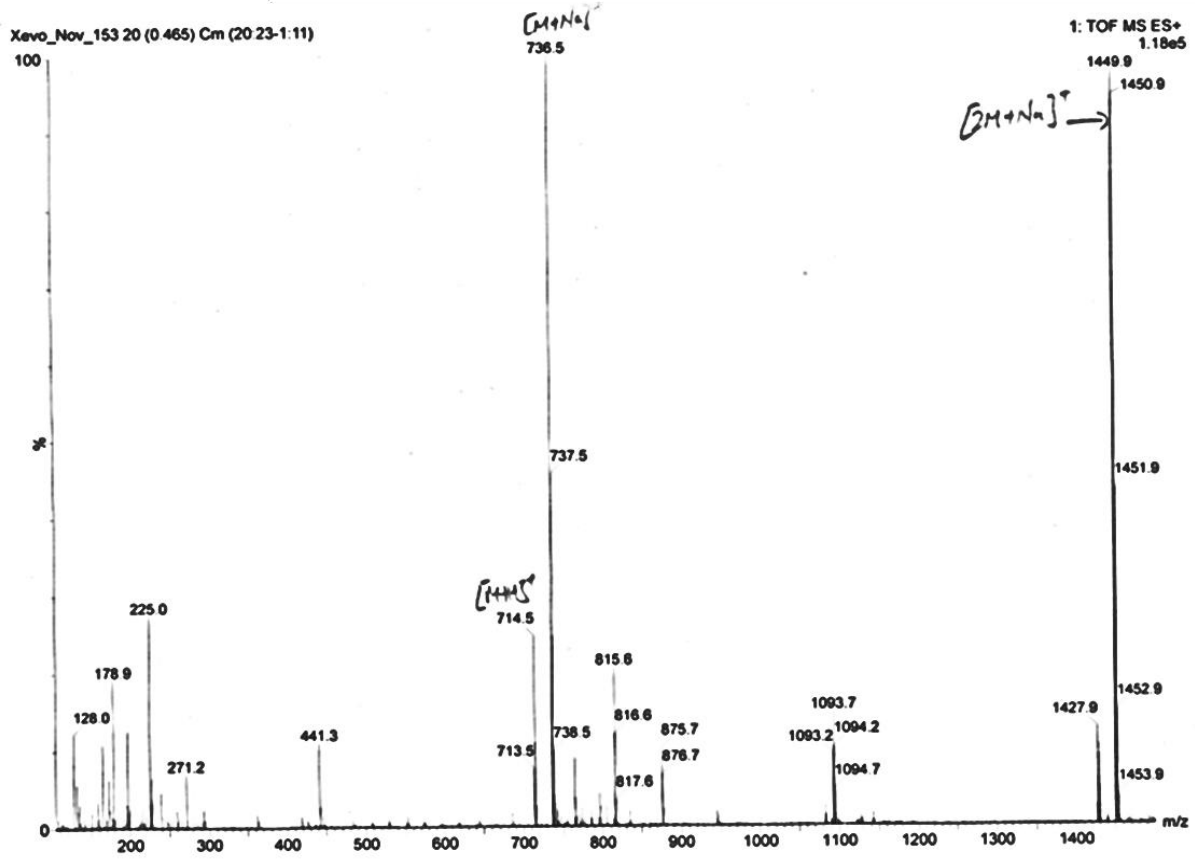

*Figure 7.4: **$Tp(C_5)_5OxC_1$** mass spectrum*

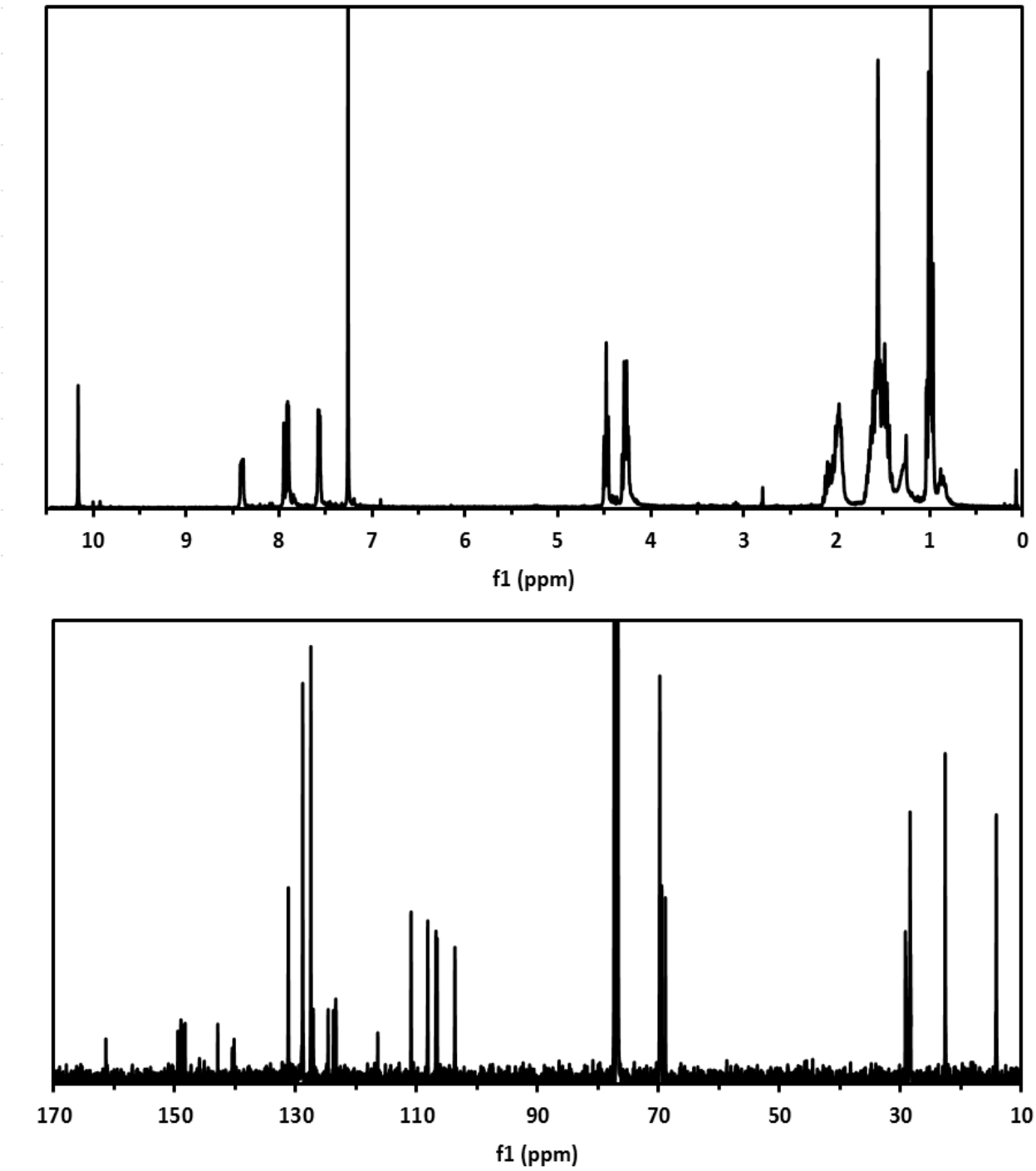

*Figure 7.5: **Tp(C5)5OxPh** ^{1}H and ^{13}C NMR spectra*

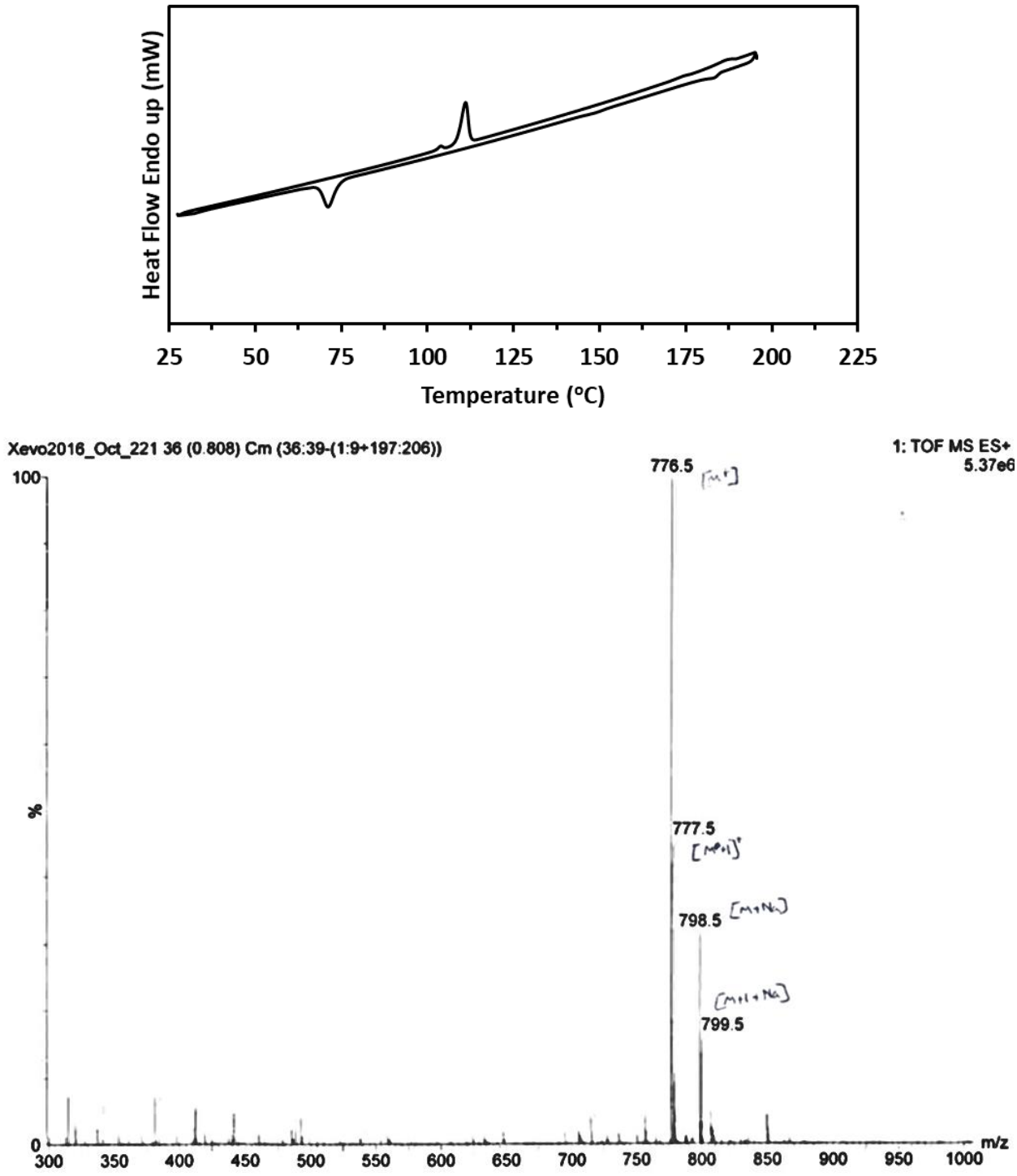

*Figure 7.6: **Tp(C_5)$_5$OxPh** DSC (2nd Scan) and mass spectrum*

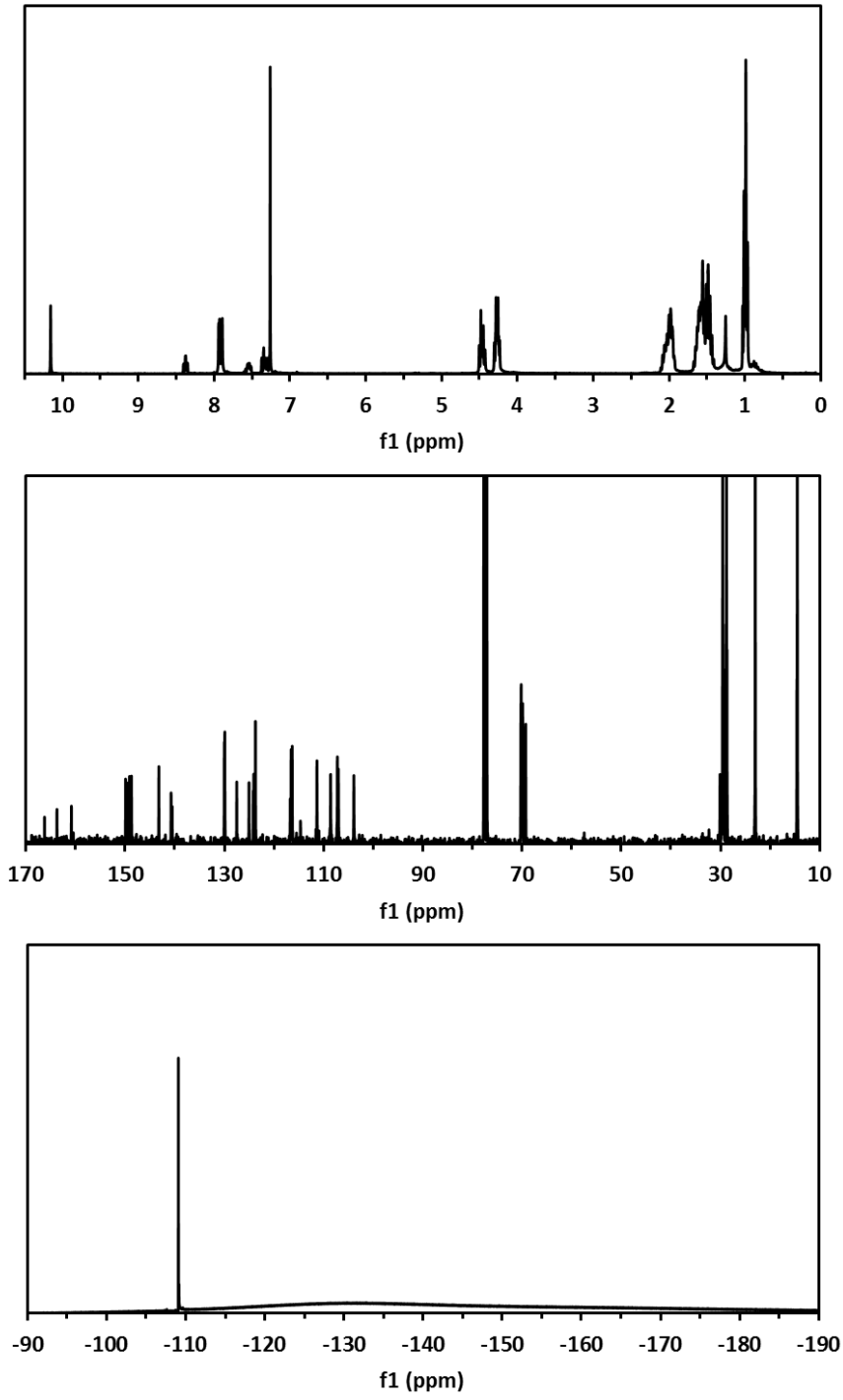

Figure 7.7: ***Tp(C$_5$)$_5$OxPhoF*** *^{1}H, ^{13}C and ^{19}F NMR spectra*

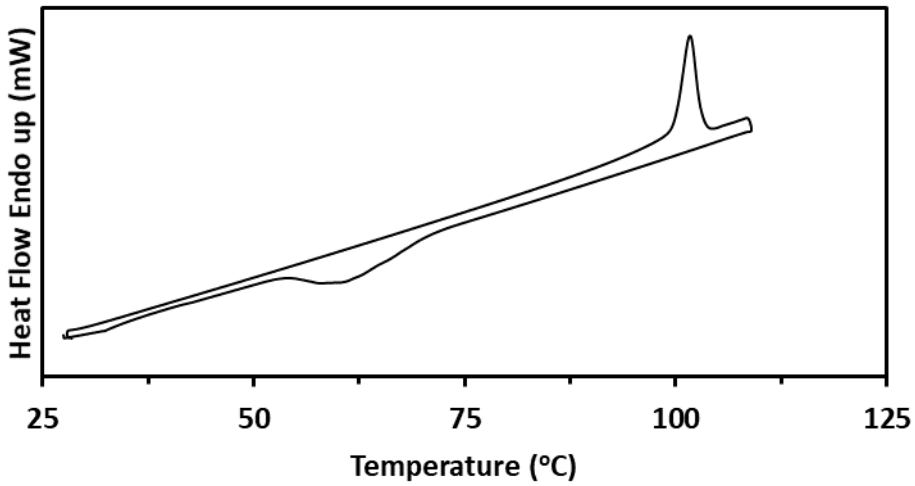

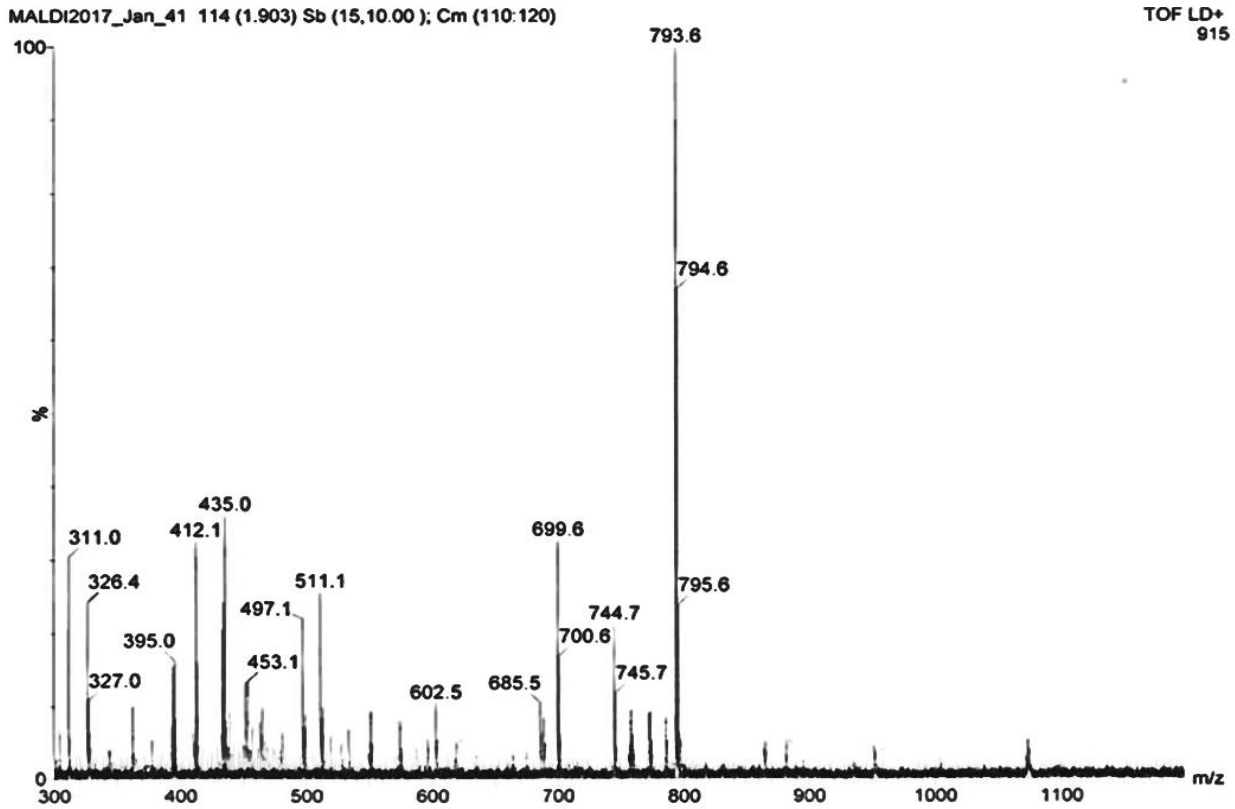

Figure 7.8: ***Tp(C5)5OxPhoF*** *DSC (2nd Scan) and mass spectrum*

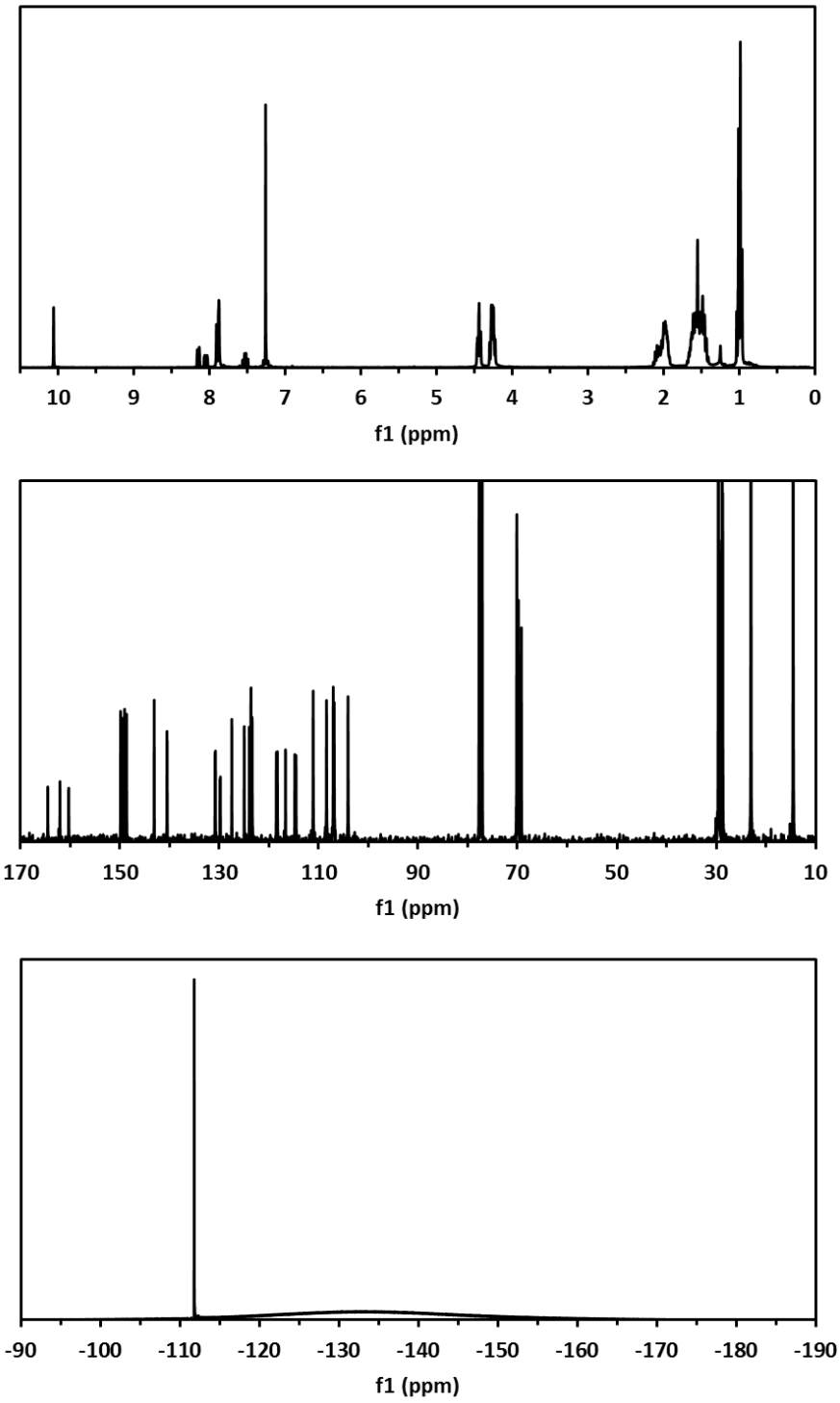

*Figure 7.9: **Tp(C_5)$_5$OxPhmF** ^{1}H, ^{13}C and ^{19}F NMR spectra*

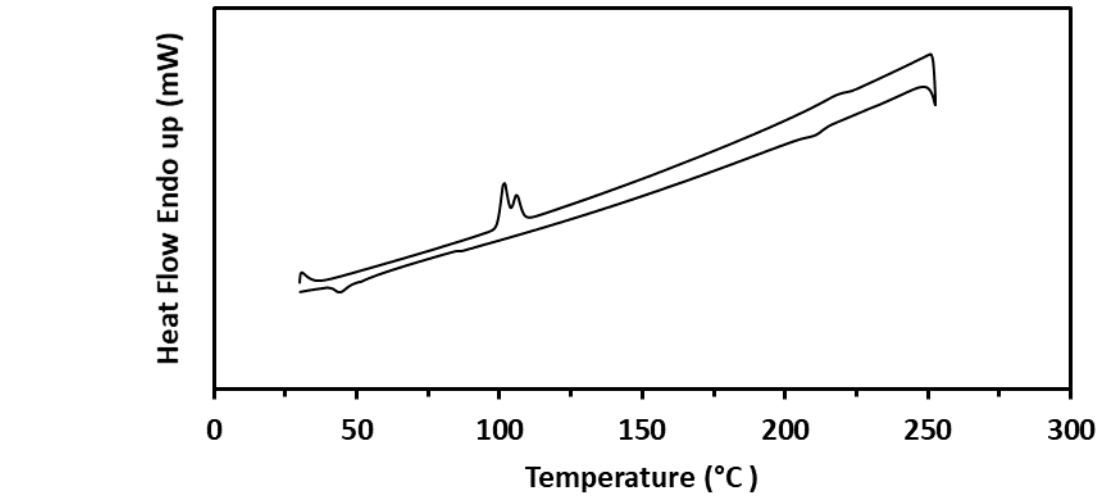

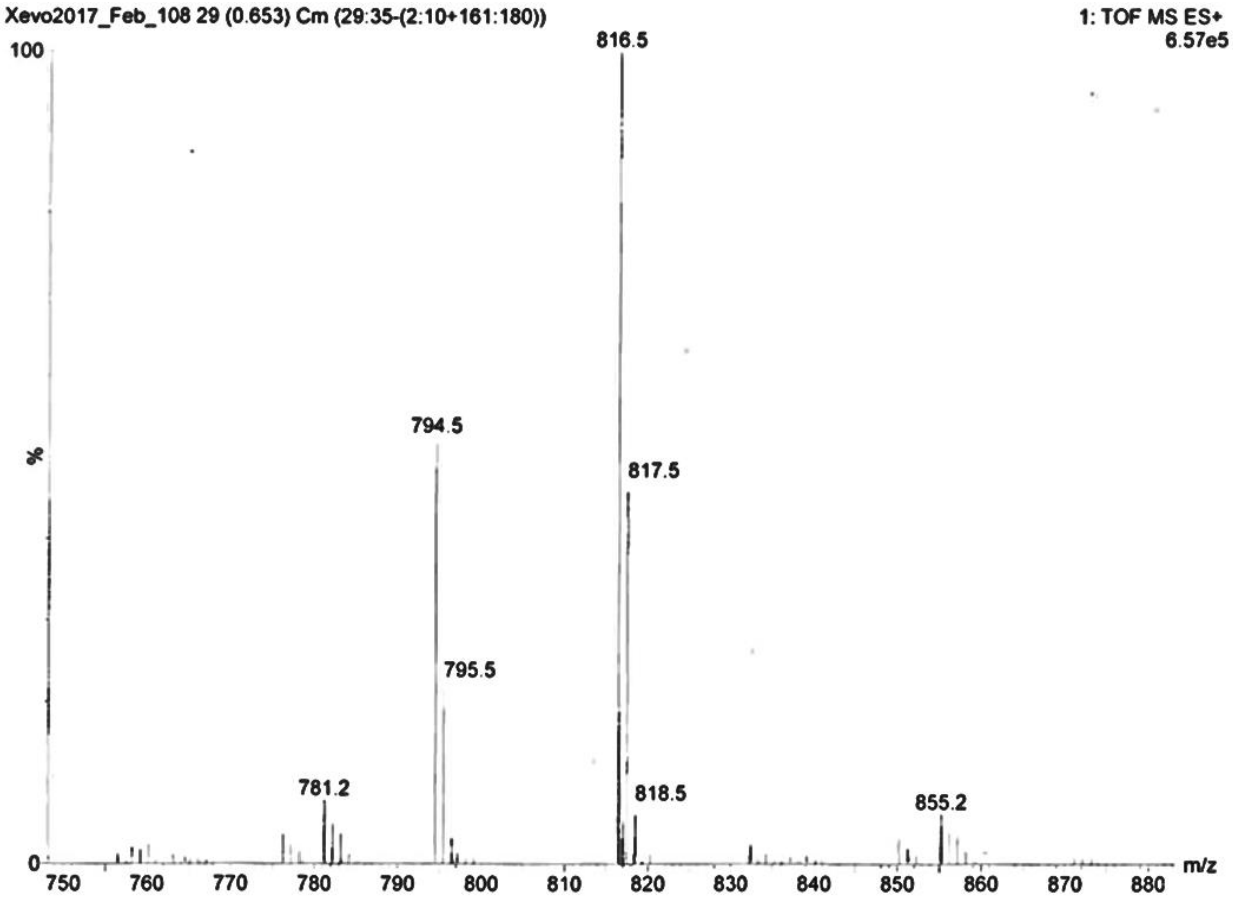

Figure 7.10: ***Tp(C_5)$_5$OxPhmF*** *DSC (2nd Scan) and mass spectrum*

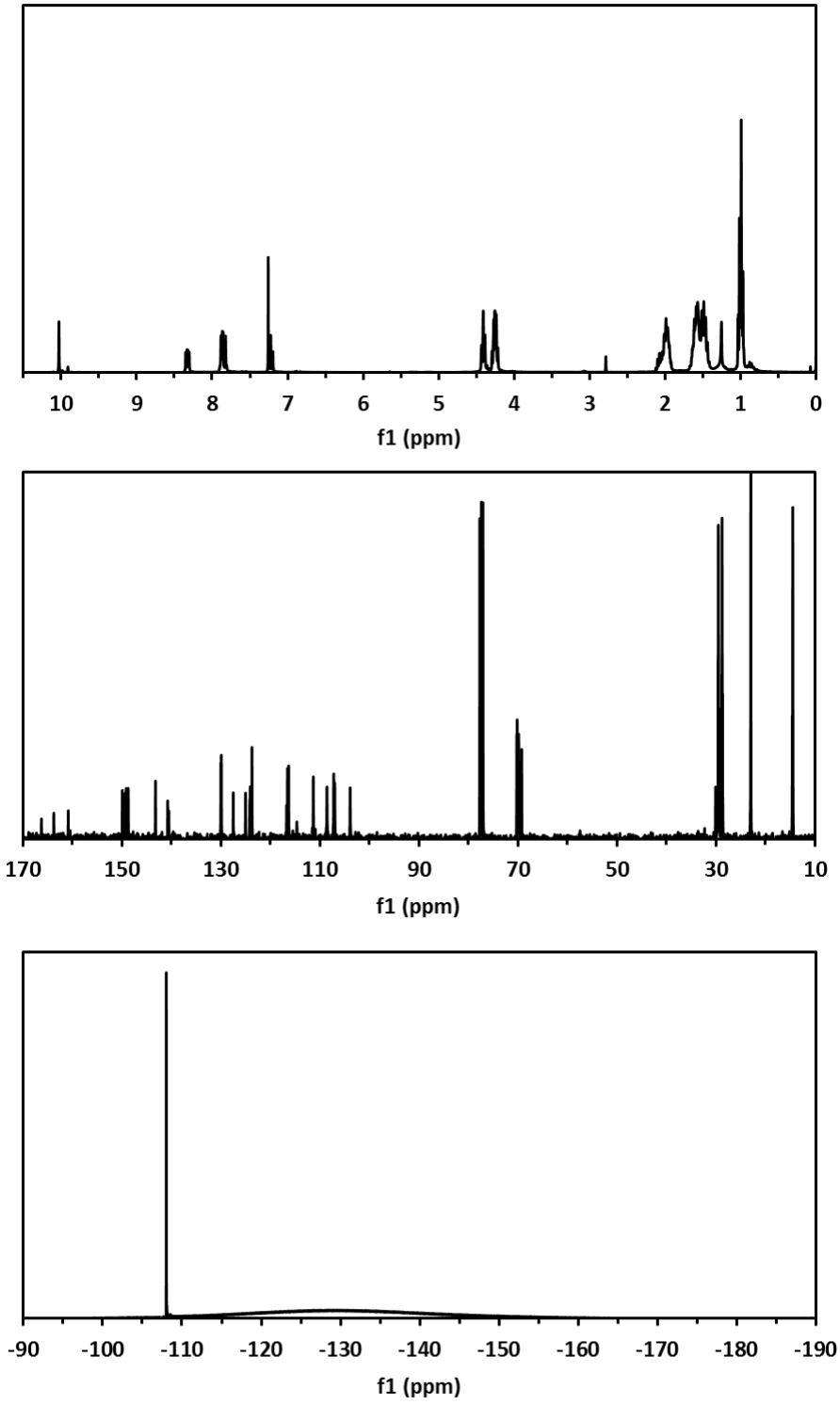

*Figure 7.11: **Tp(C$_5$)$_5$OxPhpF** ^{1}H, ^{13}C and ^{19}F NMR spectra*

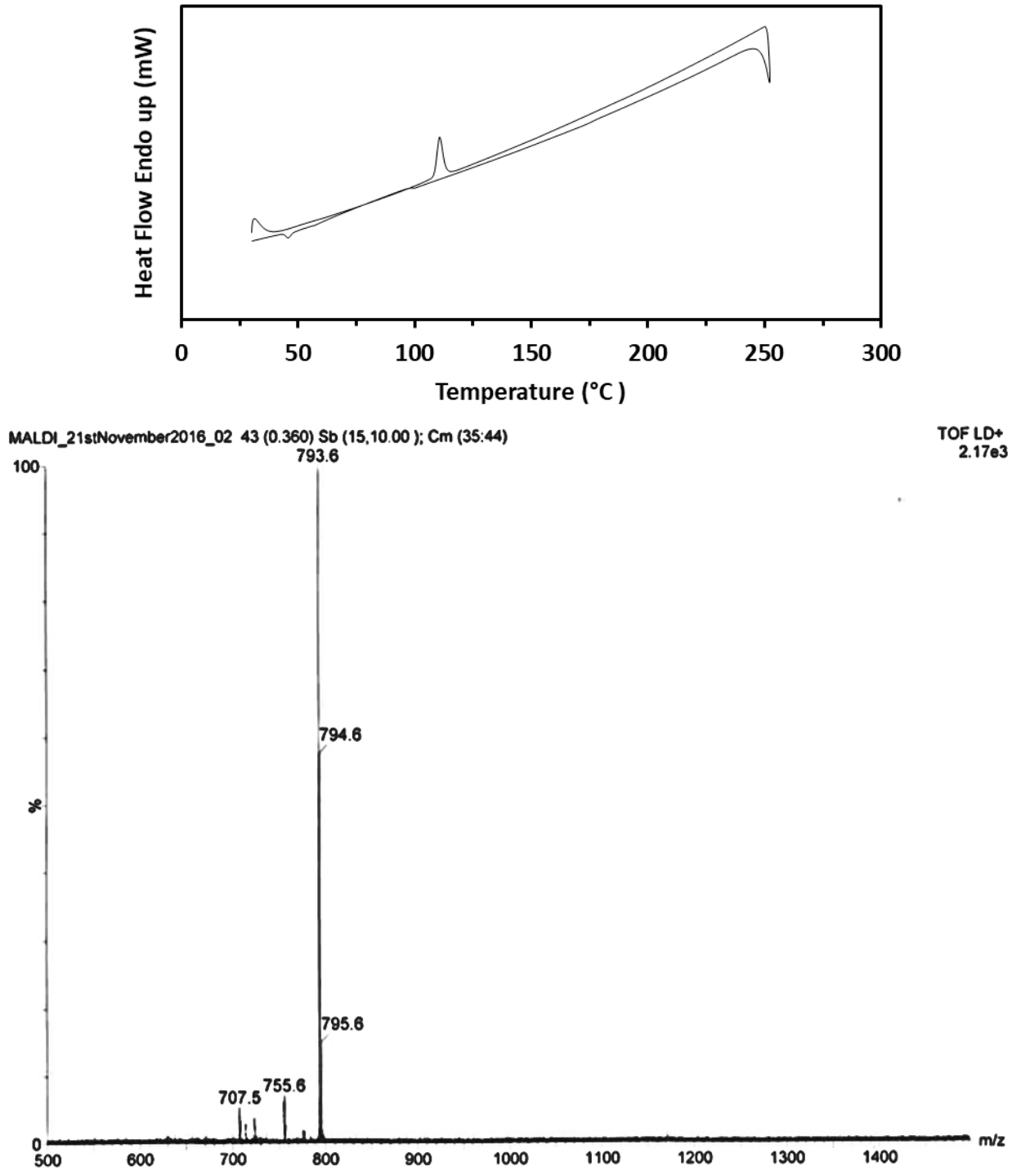

*Figure 7.12: **Tp(C$_5$)$_5$OxPhpF** DSC (2nd Scan) and mass spectrum*

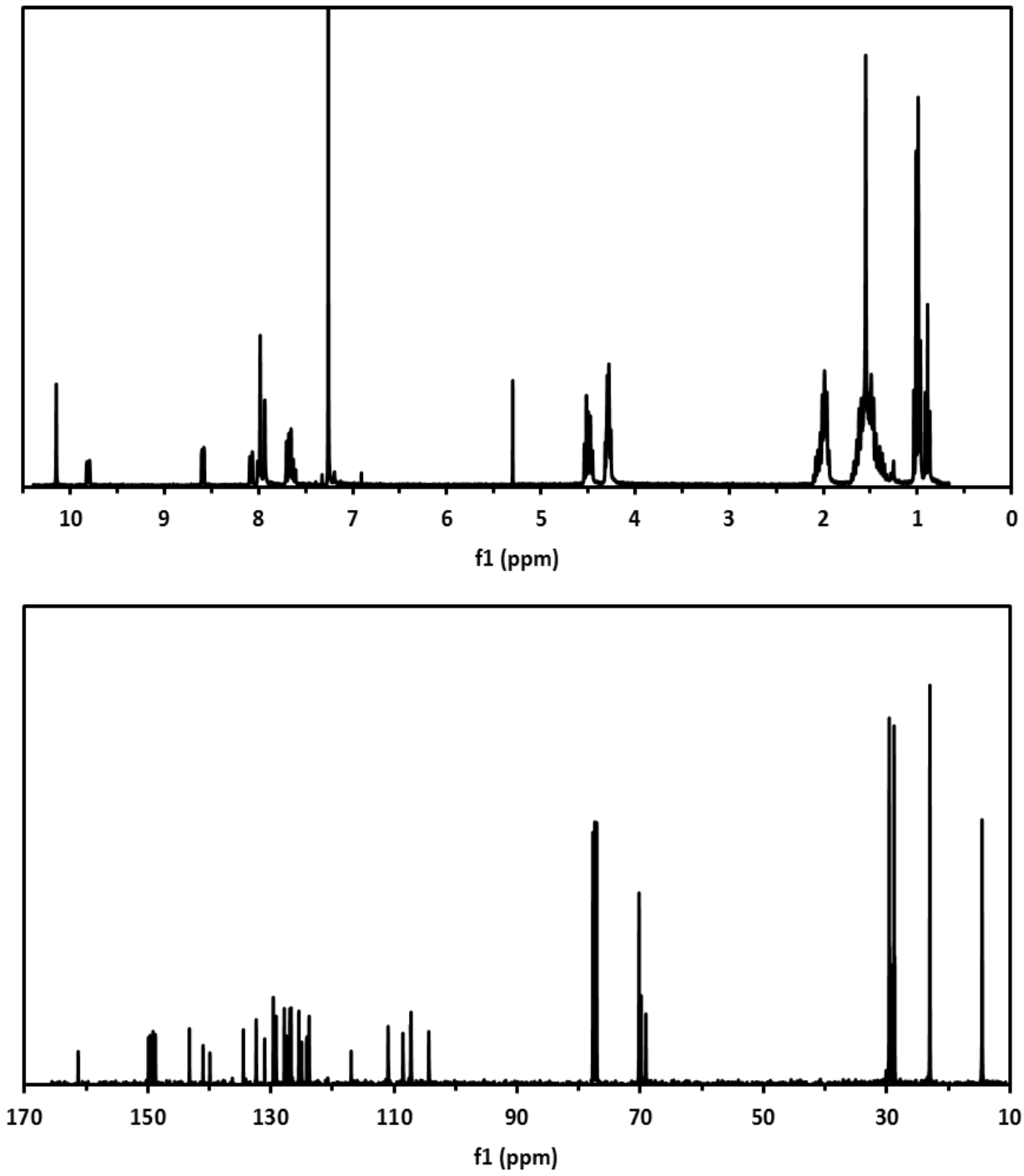

Figure 7.13: ***Tp(C$_5$)$_5$Ox-1-Nap*** *^{1}H and ^{13}C NMR spectra*

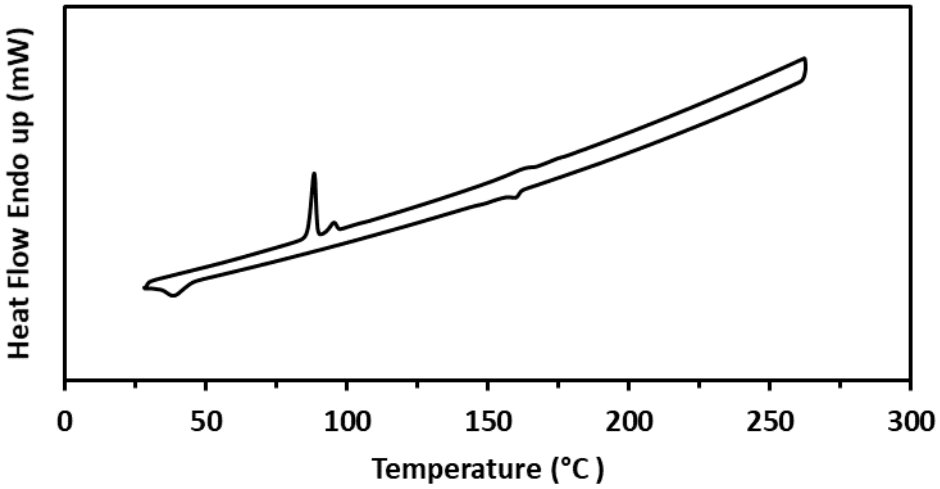

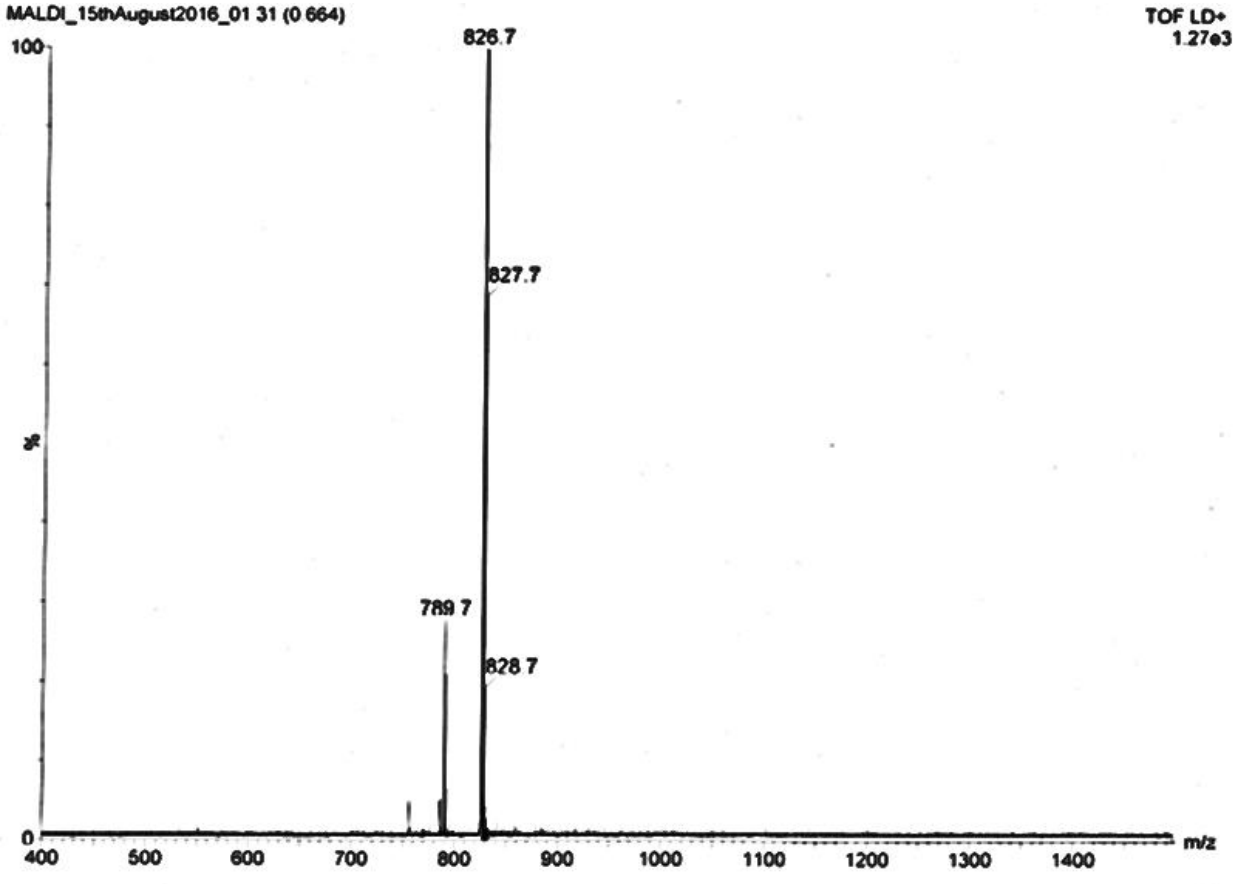

*Figure 7.14: **Tp(C$_5$)$_5$Ox-1-Nap** DSC (2nd Scan) and mass spectrum*

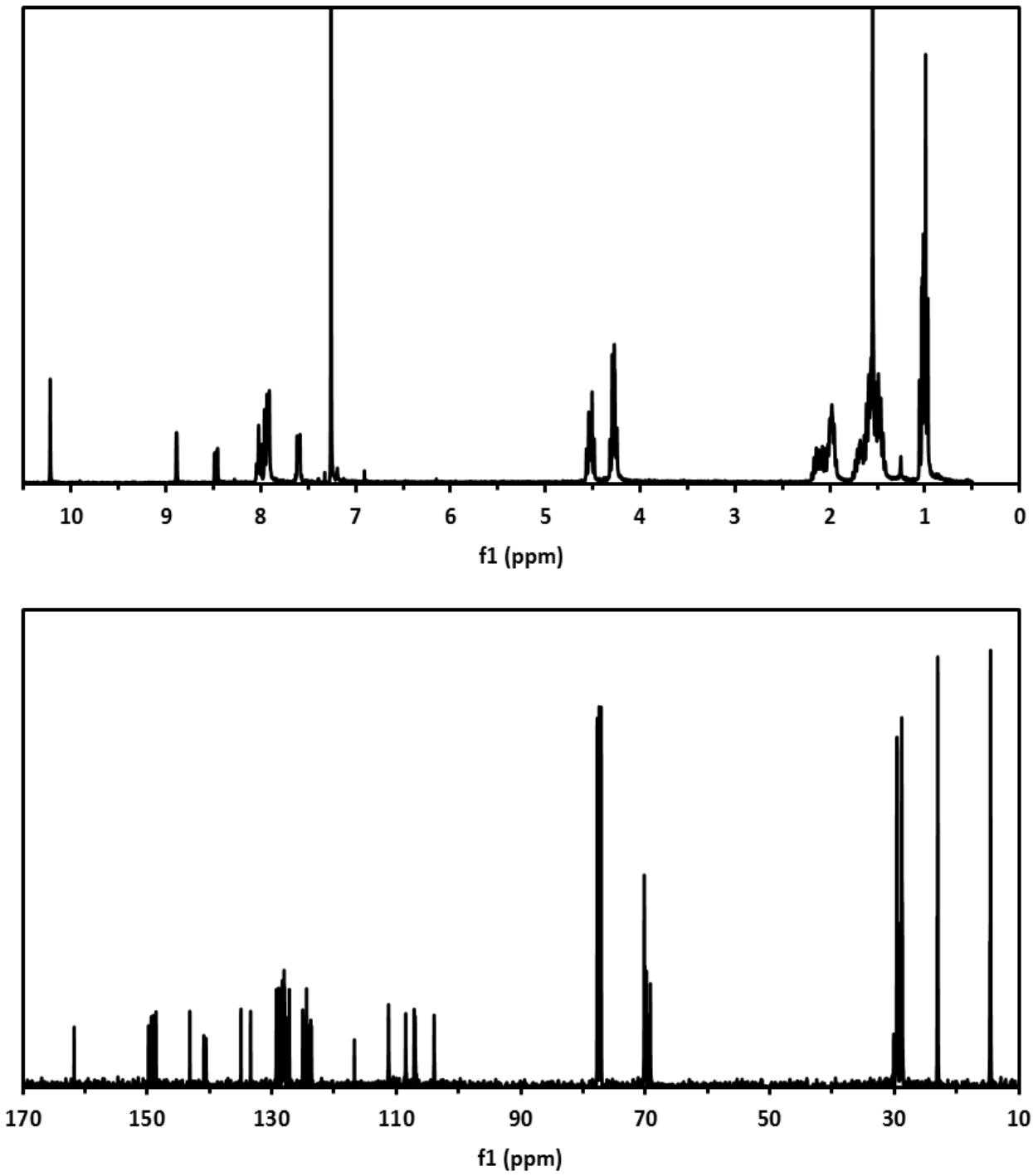

Figure 7.15: ***Tp(C$_5$)$_5$Ox-2-Nap*** *^{1}H and ^{13}C NMR spectra*

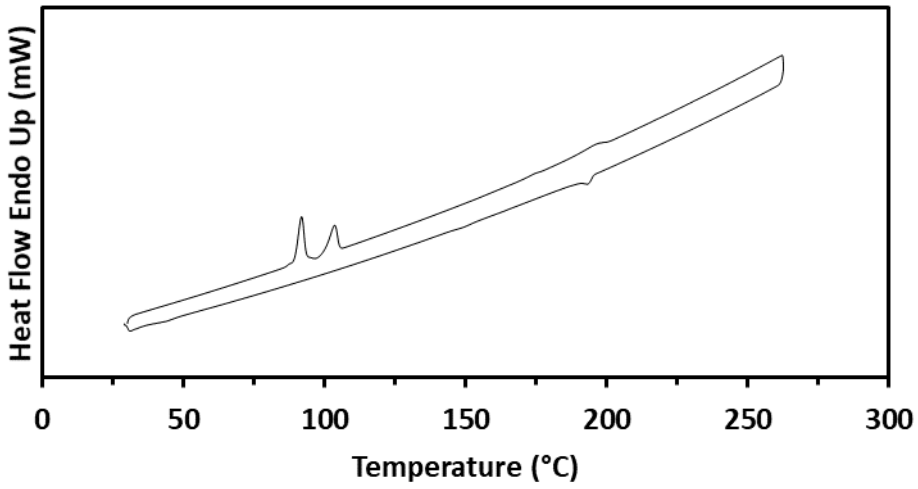

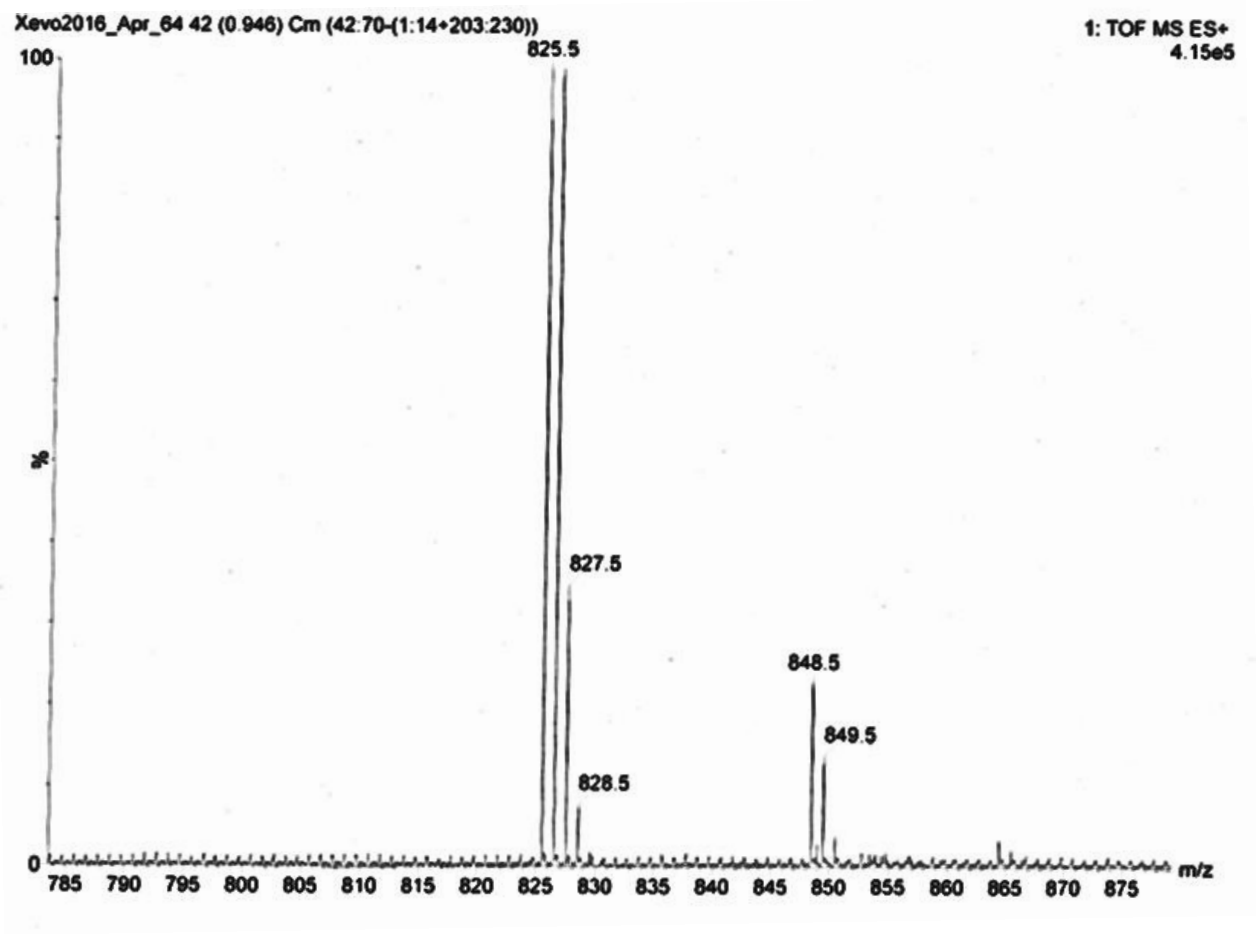

*Figure 7.16: **Tp(C$_5$)$_5$Ox-2-Nap** DSC (2nd Scan) and mass spectrum*

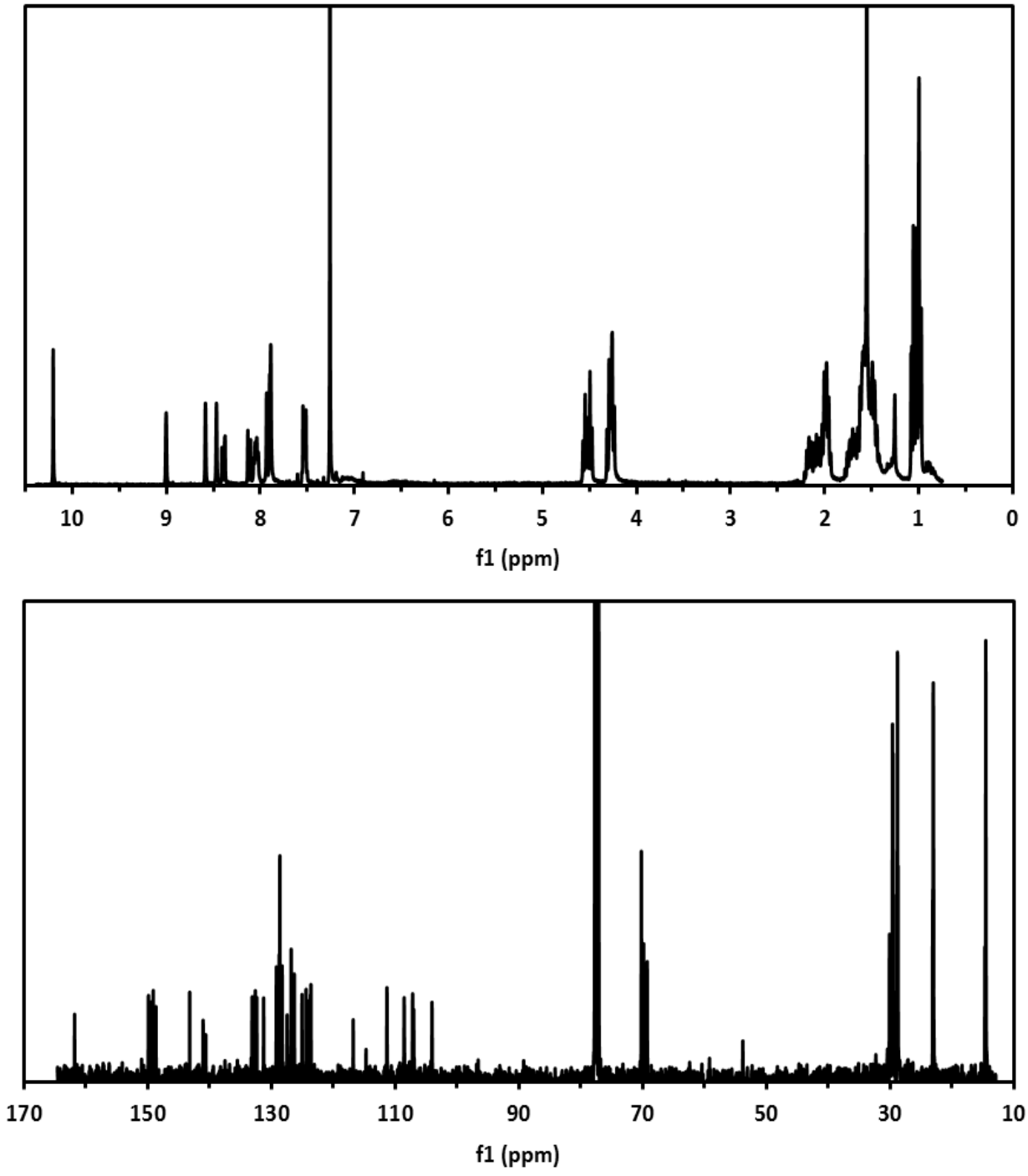

Figure 7.17: ***Tp(C$_5$)$_5$Ox-2-Ant*** *^{1}H and ^{13}C NMR spectra*

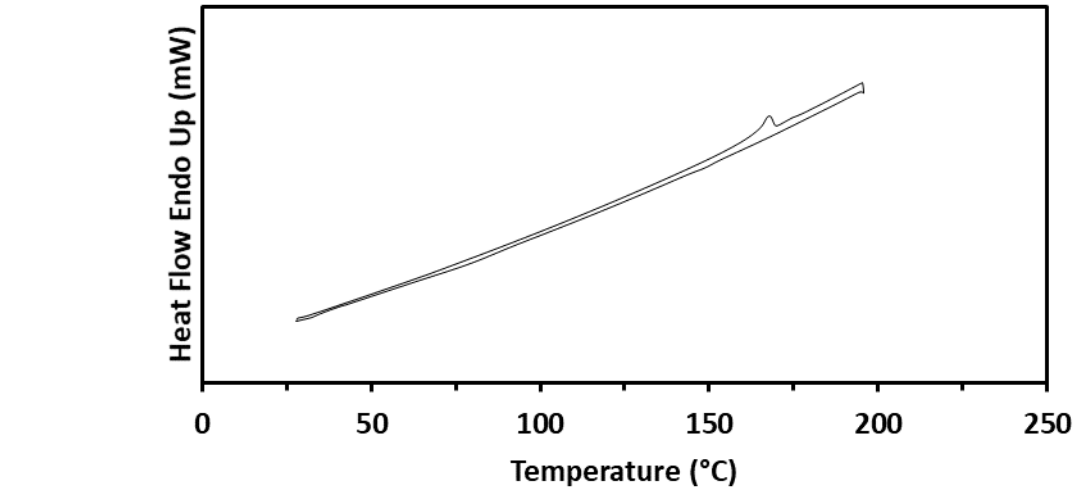

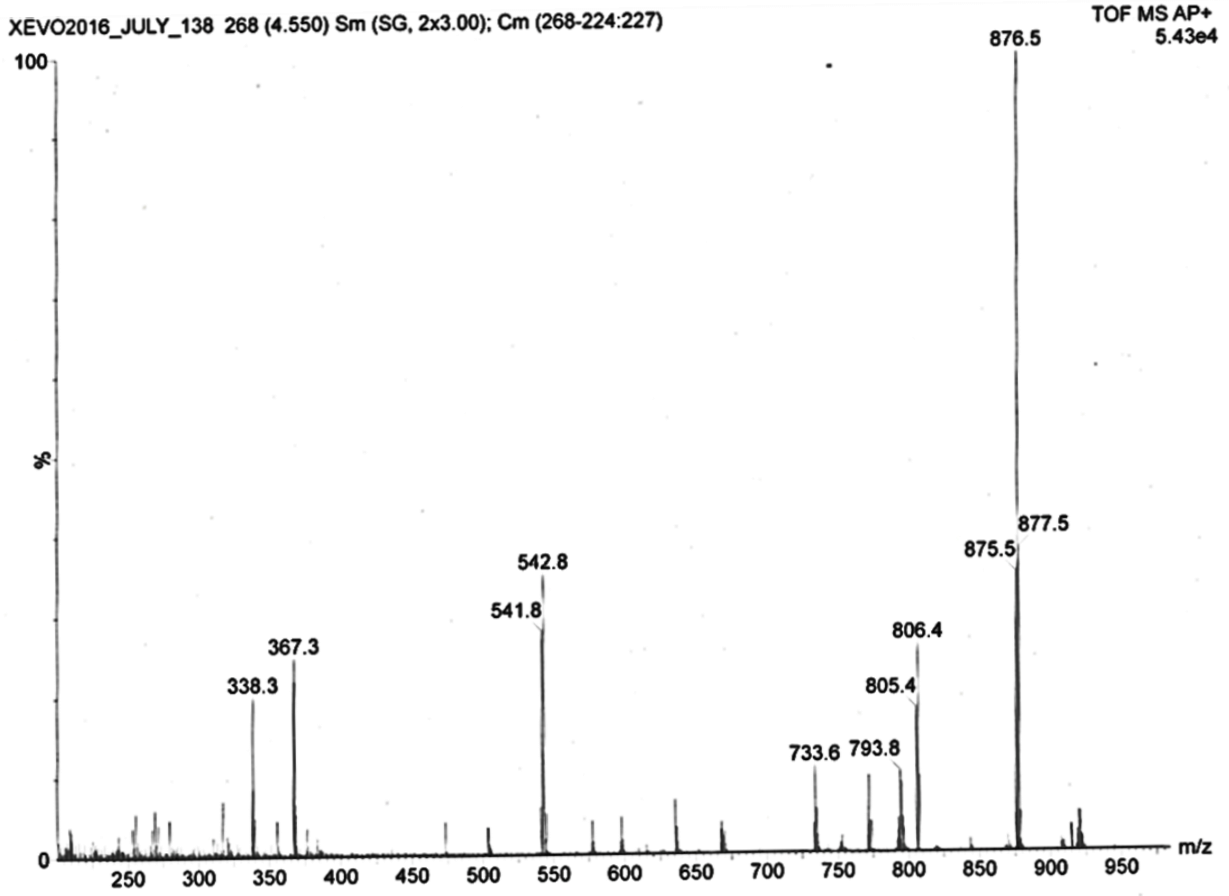

*Figure 7.18: **Tp(C5)5Ox-2-Ant** DSC (2nd Scan) and mass spectrum*

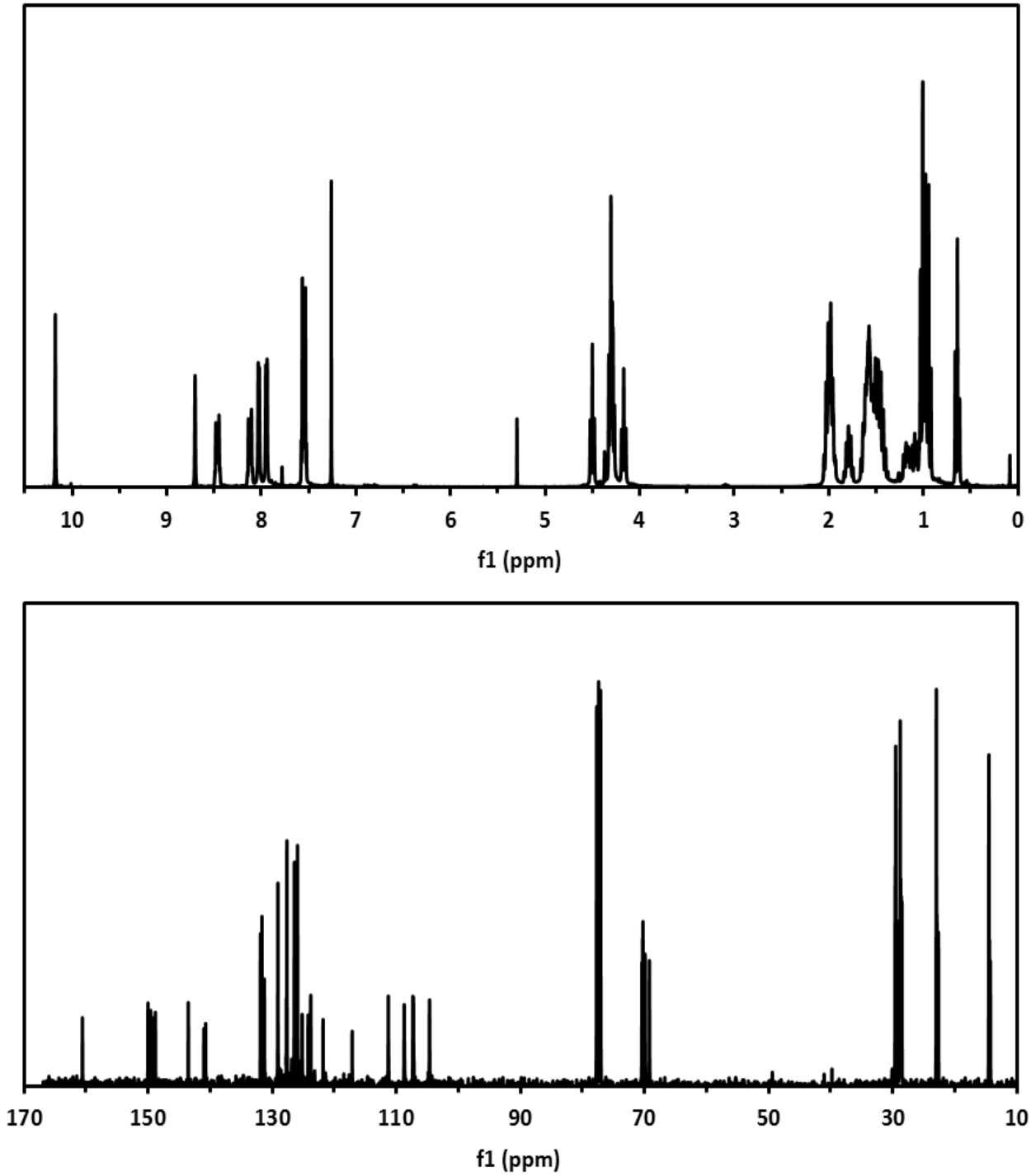

Figure 7.19: ***Tp(C5)5Ox-9-Ant*** *^{1}H and ^{13}C NMR spectra*

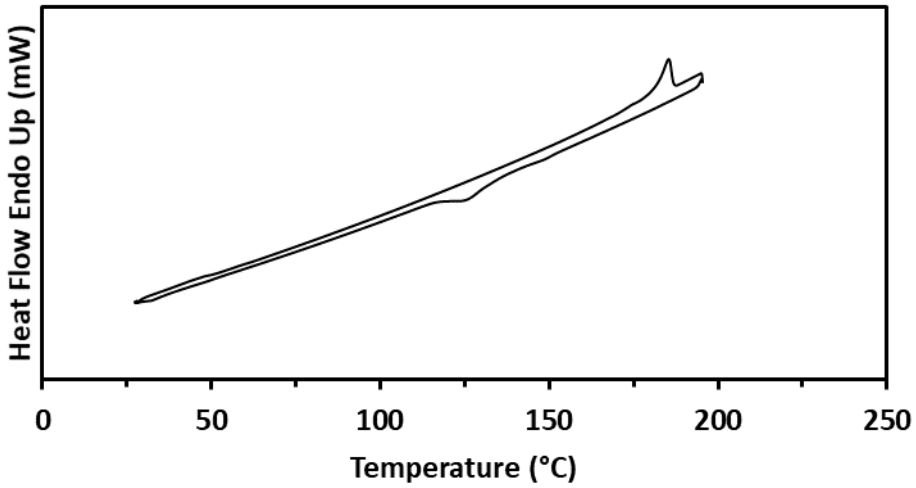

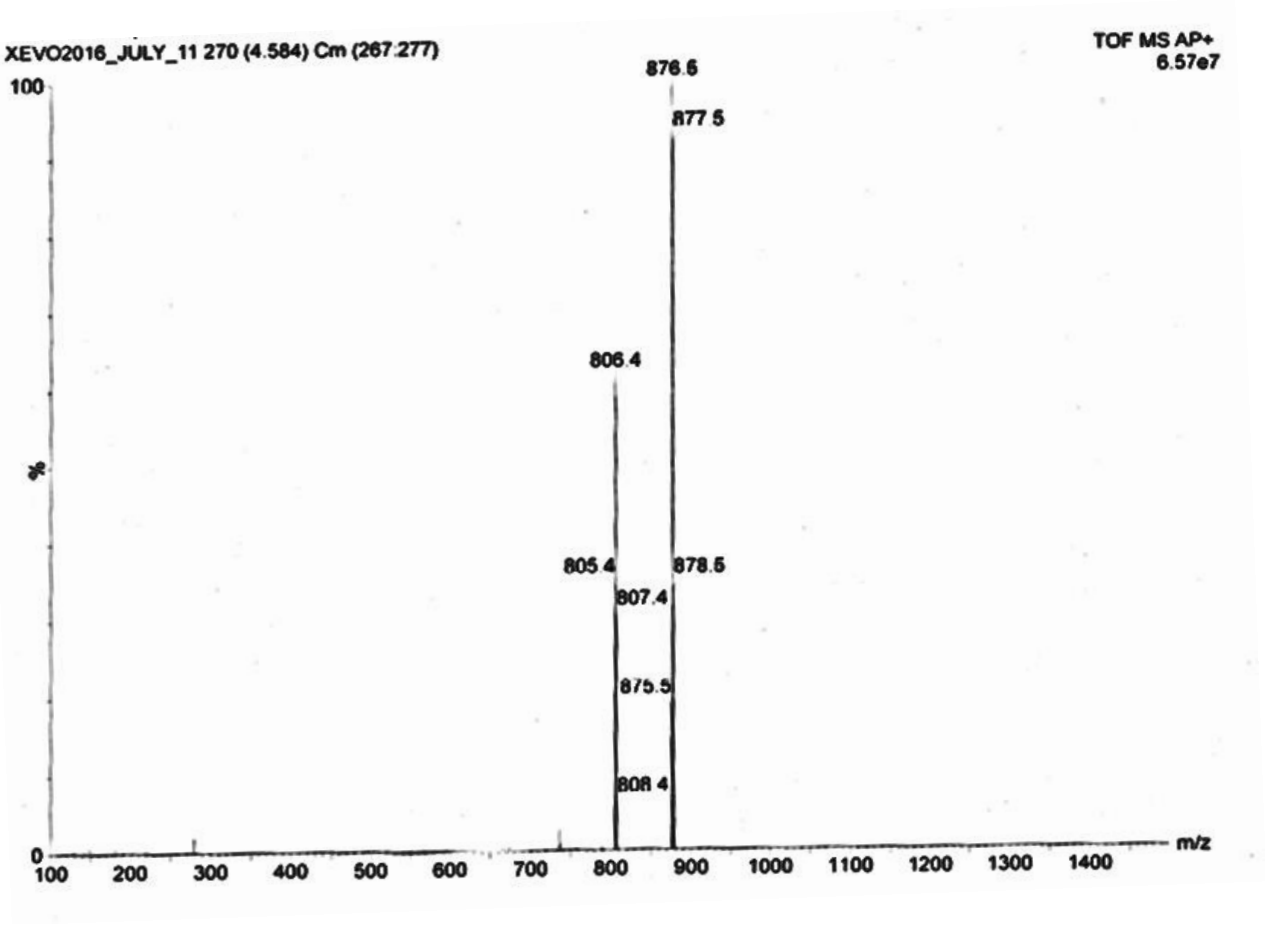

Figure 7.20: ***Tp(C$_5$)$_5$Ox-9-Ant*** *DSC (2nd Scan) and mass spectrum*